New Ruthenium tach Complexes as Water-Soluble Chemotherapy Agents

Sham Wali Arkawazi

Doctor of Philosophy

University of York

Chemistry

August 2017

Abstract

Ruthenium complexes are currently attracting much attention in the field of medicinal chemistry as they provide numerous properties which make them an appropriate candidate for drug design. Recently, a series of ruthenium tach complexes with extremely high *in vitro* activity and high solubility have been developed. *Cis*-1,3,5-triaminocyclohexane (tach) provides a hydrogen bond donor through amine groups, which aids both solubility and interaction with biomolecules.

The chemistry of the ruthenium tach complexes was developed in order to understand their activity in a biological environment. The parent compound, tach **[2]** was modified by the incorporation of a new functional group (benzyl) into the coordination sphere of the ligand and synthesis a new tach analogue, tachmb **[3]**. The coordination chemistry of **[3]** was performed with a range of different ruthenium precursors to yield [Ru(tachmb)(DMSO)Cl_2] **[5]**, [Ru(tachmb)(PPh_3)Cl_2] **[7]**, and [Ru(tachmb)(dppb)Cl]Cl **[9]**. The anti-proliferative activity of the modified tach **[3]** and the complexes were evaluated with *in vitro* tests against A549 (human lung cancer) and A2780 (human ovarian cancer) cell lines. The activity of **[3]** showed mild activity in comparison to the non-toxic tach, **[2]**. Both complexes **[7]** and **[9]** showed high activity; in particular, the activity of **[9]** was found to exceed that of cisplatin in both cell lines.

Two new analogues of ruthenium tach complexes tagged with fluorescent ligands were synthesised and fully characterised, [Ru(tach)(FL-I)Cl]Cl **[10]** and [Ru(tach)(FL-II)Cl]Cl **[13]**. Two previously reported complexes were also prepared; one complex with high cytotoxic activity ([Ru(tach)(dppp)Cl]Cl, **[11]**) and one complex with light sensitive behaviour ([Ru(tach)(phen)(DMSO)], **[12]**). The interactions of these complexes with Calf Thymus DNA (CT-DNA) and bovine serum albumin (BSA) were examined spectrophotometrically. The results show intercalation behaviour of **[10]** and **[12]** towards DNA while complex **[11]** instead exhibits high binding affinity towards BSA. The cytotoxicity of the complexes indicates that proteins may be the potential biological targets of ruthenium tach anti-cancer drugs.

Table of contents

Figures, Tables and Equations

Acknowledgements

This thesis would not have been possible without the inspiration and support of a number of wonderful individuals — my thanks and appreciation to all of them for being part of this journey and making this thesis possible.

Firstly, I would like to express my sincere gratitude to my supervisors Paul Walton and Jason Lynam for the continuous support of my PhD study, for their patience, motivation, and immense knowledge. Their guidance helped me in all the time, during the research and writing of this thesis. I could not have imagined having better advisors and mentors for my PhD study.

I also want to thank the members of the Walton and Lynam group… it was great sharing laboratory with all of you during last four years.

I am forever thankful to my colleagues; Luisa " 3rd supervisor", who taught me most of the things needed in my project especially cell culture technique, she has made available her support in a number of ways, especially towards the completion of this thesis. Lucy you are wonderful and always happy to help when there were any problems, heartily thank.

I am thankful to and fortunate enough to get constant encouragement, support and guidance from Naser and Eman, both scientifically and personally over the last four years.

Also, I would like to extend sincere esteems to all staff in laboratory for their timely support.

A special thanks to my big family for their continuous and unparalleled love, help and support. Words cannot express how grateful I am to my mother and father for all of the sacrifices that you've made on my behalf. Your prayers for me was what sustained me thus far. I am grateful to my sisters for always being there for me as a friend and supported me in writing, and incented me to strive towards my goal. At the end, I would like express appreciation to my beloved husband Omar, the man who has made all the

difference in my life and was always my support in the moments when there was no one to answer my queries. Without his patience and sacrifice, I could not have completed this thesis. Last but by no means least, I appreciate my little girl Yara for abiding my ignorance and the patience she showed during my thesis writing. Words would never say how grateful I am to both of you. I consider myself the luckiest in the world to have such a lovely and caring family, standing beside me with their love and unconditional support.

Sham Wali Arkawazi

Declaration

The research presented in this thesis was carried out at the University of York (2014-2017). This work is, to the best of my knowledge, original and my own, except for the following:

- ESI-MS experiments were performed by Mr Karl Heaton;
- Elemental analyses were performed by Dr Graeme McAllister;
- 500 MHz NMR spectra were recorded by Dr Naser Jasim;
- X-ray crystallography was performed by Dr Jason Lynam, data was collected by Miss Rachel Bean and structures solved by Dr Adrian Whitwood/ Miss Rachel Bean;
- The fluorescent ligands FL-I and FL-II were synthesised by the group of Professor Paul Pringle (University of Bristol);
- The cell culture technique and MTT assay were performed by myself in York Structural Biology Laboratory (YSBL), University of York, after training from Dr Luisa Ciano.

Chapter 1

Introduction

1 Introduction

1.1 General facts about cancer

Cancer is the leading cause of death across the world and has a major impact on society.[1] Globally, cancer was responsible for 8.8 million deaths in 2015, which equals to nearly 1 in 6.[2] Nearly, 70% of deaths from cancer occur in low- and middle-income countries, and the number of new cases is expected to increase by about 70% over the next two decades.[2]

Cancer, medically termed as malignant neoplasm, is regarded as an evolutionary process that results from the build-up of somatic mutations within the progeny of a regular cell, leading to a selective growth advantage within the mutated cells and in the long run to uncontrolled proliferation.[3] Among the different tissues present in the human body, the most frequent human cancers arise in epithelial tissues inclusive of the pores and skin, colon, breast, prostate or lung, and collectively result in numerous deaths within 12 months.[4] Cancer cells differ from normal cells in many ways. Normal cells divide and increase their number in a process called mitosis (to replace lost cells or to repair injuries) then stop dividing.[5] Instead, cancer is an abnormal mass of cells which continue to grow when no longer needed and may grow into adjacent tissue or spread to distant parts of the body. This indefinite growth ends in the formation of a tumour. [6]

The uncontrolled growth takes place if there are mutations to DNA which cause an alteration to the genes involved in cell division, and some of these mutations can prevent the correction of the DNA damage and apoptosis. The end result of the accumulations of a series of such mutation is uncontrollable cell growth.[7, 8]

The tumour microenvironment is heterogeneous, containing mixtures of cells which are exposed to various concentrations of nutrients and oxygen.These variable levels of oxygen and nutrients can have an effect on the expression of genes and select for a

more aggressive phenotype inside regions of the microenvironment. Therefore, new blood vessels are required to provide nutrients for tumour cell proliferation (termed angiogenesis). Cells that are further away from the blood source are poorly oxygenated (hypoxia) and are generally slower growing or nonproliferative,[9, 10] whilst poor clearance of cell breakdown products, such as lactic and carbonic acid, results in a low pH region.[10] These features, together with the high interstitial pressures, make diffusion (in preference to convection) the dominant mechanism of extravascular delivery of nutrients and drugs in tumors.[9, 11, 12]

The cell growth in the normal tissues is a carefully controlled process, regulated by several 'checkpoints' throughout the cell cycle. The two main steps of the cell cycle are; 1) interphase, where the cell prepares itself for replication and 2) mitosis, wherein the division of the cell's nucleus takes place.[13] Therefore, for replication to take place, the cell has to pass through the various checkpoints. The deregulation of the normal cell cycle through loss of any checkpoint control (normally the p53-dependant checkpoint) leads to a decreased genetic stability and uncontrolled, unstructured and unregulated cellular growth, facilitating tumour developments. [13, 14]

Normally, there are several options of therapies available when a tumour is detected. This could be either surgical removal of a solid tumour followed by radiation therapy, or radiation therapy/chemotherapy, when surgery is not possible.[15]

The hypoxic property of tumour cells also leads to a resistance to many chemotherapeutic treatments; thus, limitation of drug delivery has occurred as a result of the relatively long distance diffusion of chemotherapeutic agents. An additional reason for resistance is that several anticancer agents take effect through anti-proliferative mechanisms of the malignant cells that have a greater proliferative rate than healthy cells such as drug target alteration, activation of prosurvival pathways, cell death inhibition or any combination of these mechanism .[16]

For potential drug development, the targeting of these mutations is a common objective in anti-cancer research. Indeed, there is much interest in the development of anticancer drugs which are able to be cytotoxic only when in the hypoxic environment of a tumour region to decrease the cytotoxicity of the drugs to the normal tissues.[17, 18]

1.2 Platinum Anticancer Agents

1.2.1 Cisplatin and its derivatives

Cis-diamminedichloridoplatinum(II) and its *trans* analogue were first described by Peyrone in 1845.[19] In 1893 Werner used these compounds as the first example of isomers in coordination chemistry. The anticancer properties were not discovered until 1965, when Rosenberg realized that the generation of cisplatin at a platinum electrodes used in one of his experiments affected bacterial cell growth of *Escherichia coli*.[20]

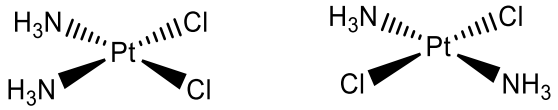

Figure 1.1: Chemical structure of cis and trans-diamminedichloridoplatinum(II).

The world's highest selling anticancer drug, cisplatin, has opened the door to the use of metal-based compound for cancer treatment.[21] Cisplatin clinical trials on solid tumours in humans followed rapidly and the Phase I clinical trials started in 1971,[22] receiving Food and Drug Administration (FDA) approval in 1978 under the name 'Platinol'.[23] Cisplatin displays great efficacy against solid tumour types, such as testicular, ovarian, head, and neck cancers, and against small-cell lung cancer,[24] with a cure rate rising to 90%.[25]

1.2.2 Mode of action

The mechanism of action of cisplatin involves several steps (Figure 1.2).[26] Once it is injected into the bloodstream, cisplatin binds to blood plasma proteins, foremost to albumin. The presence of high extracellular concentration of chloride ions (104 mM) prevents hydrolysis of the complex and maintains the drug in its neutral form.[27] Although the mechanism of cellular uptake of cisplatin has remained unclear, early research showed that passive diffusion is the main mechanism[28, 29] although more recent work has indicated the involvement of active transport mechanisms such as active copper transport proteins.[30, 31] After the compound crosses the cell membrane, cisplatin becomes activated and undergoes hydrolysis due to the higher concentration of water and lower chloride concentration (4-20 mM) to produce $[Pt(NH_3)_2Cl(OH_2)]^+$ and $[Pt(NH_3)_2(OH_2)_2]^{2+}$ These aqua products are potent electrophiles that can form numerous adducts with a nucleophile, including the sulfhydryl groups on proteins and nitrogen donor atoms on nucleic acids.[26, 32, 33]

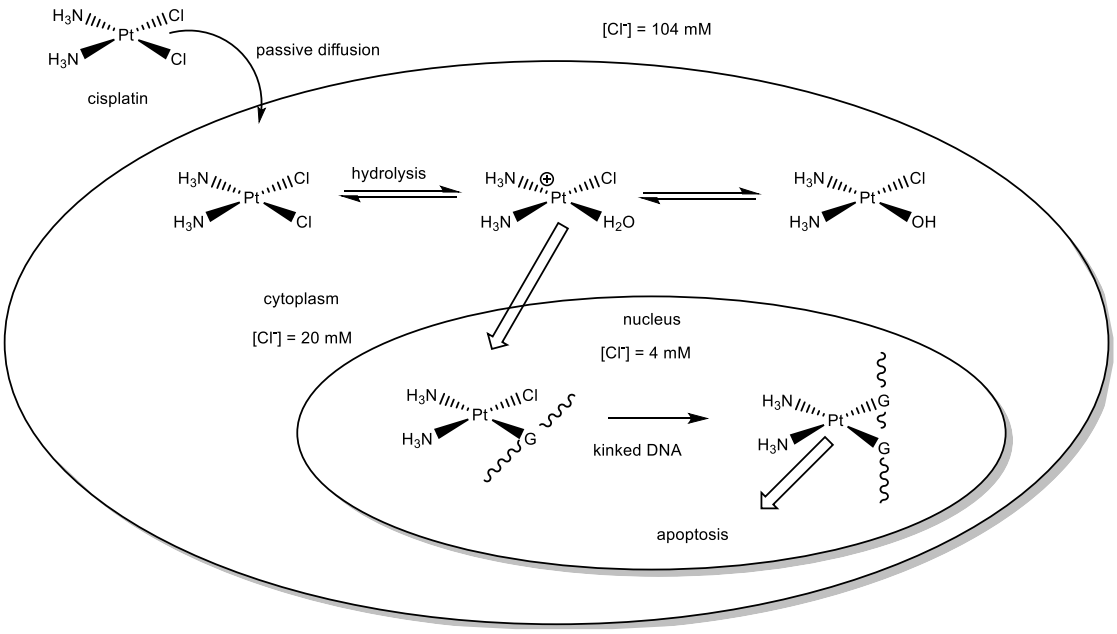

Figure 1.2: Cisplatin mechanism and DNA binding in cells.

The ready interaction of platinum aqua complexes with many endogenous nucleophiles, such as glutathione (GSH), methionine, metallothionein, and protein, is a result of a relatively high intracellular concentration of the tripeptide glutathione GSH (0.5 –10 mM)[34] and high affinity of the drug for sulfur. However, binding of cisplatin to intracellular components is consider to be disadvantageous for its anticancer activity and is often associated with cisplatin toxicity and resistance.[35] Ultimately, only a small percentage of the drug reaches the DNA of the genome which is the main cellular target for cisplatin.[35]

The most favoured site for the platinum aqua complex to bind under physiological conditions is the N7 (the most nucleophilic positions on DNA) atoms of the purine residue guanine (Figure 1.3). Binding to adenine is less favoured and the other potential binding positions in DNA nucleobases are either protonated or involved in DNA base pairing at physiological pH (7.2 –7.4).[36] Cisplatin binds with DNA in two steps; first, the monofunctional adduct with N7 guanine and mono-aquated species $[Pt(NH_3)_2Cl(H_2O)]^+$ is formed, and then further binding with guanine or adenine forms a broad spectrum of intra- and inter strand crosslinks. The great majority of products are 1,2-intrastrand d(GpG) crosslinks which represent 60-65% of all the adducts formed, or 1,2-intrastrand d(ApG) adducts which account for 20-25% of adducts. Minor adducts include 1,3-intrastrand and interstrand crosslinks (Figure 1.4).[26, 37-39]

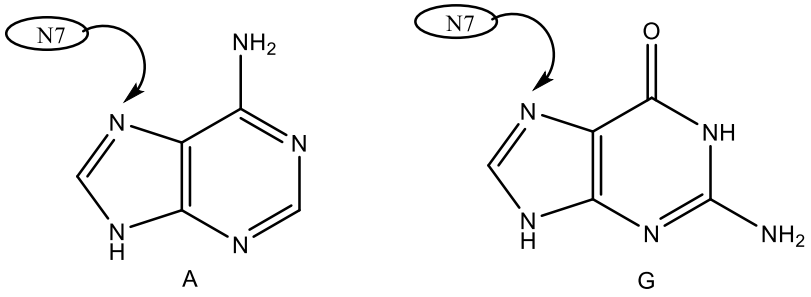

Figure 1.3: Platinum binding at the N7 sites of adenosine (A) and guanosine (G).

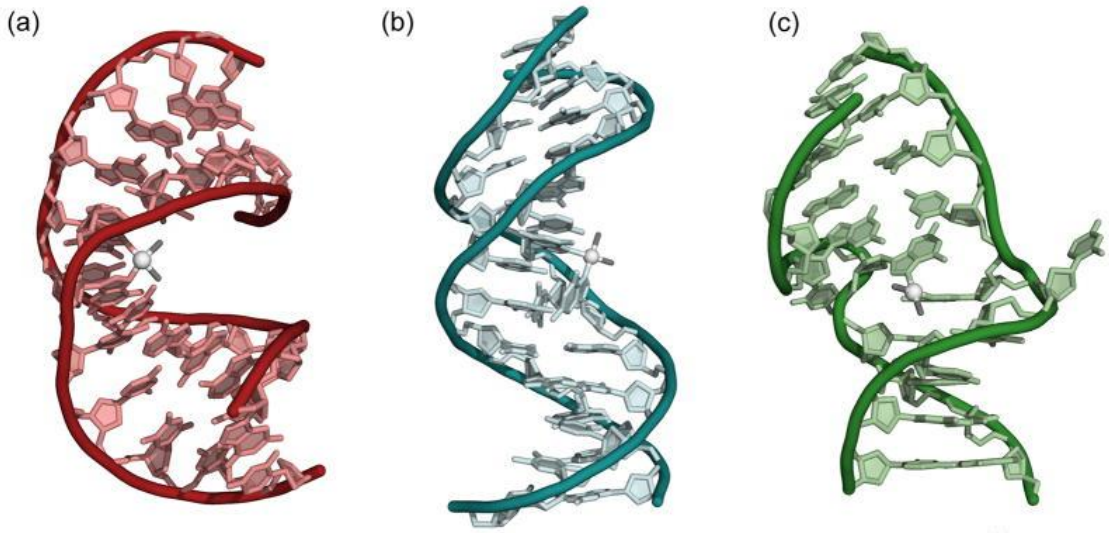

Figure 1.4: Double stranded DNA distortions from a) intrastrand cross-link 1,2 d(GpG) (60–65 %), b) intrastrand cross-link 1,3 d(GpG) (2–3 %) and c) interstrand cross-link 1,2 d(GpG) (1–5 %). Intrastrand 1,2 d(GpA) (20–25 %) not shown.[40]

The DNA platination cause a structural distortion of the double helix.[41] In intrastrand 1,2-d(GpG) adducts, platination causes a bend towards the major groove of DNA of 40-70° and also causes partial unwinding of the double helix up to 23° (Figure 1.4).[42] On the other hand, the 1,3-d(GTG) adducts induce a kink on DNA of 27-33° towards the major groove[43] and interstrand adducts cause a bend of the double helix towards the minor groove (20-40°) and a high degree of DNA unwinding (approximately 80°).[43, 44]

The bending and unwinding of the double helix affects essential cellular processes. Several proteins are known to recognize the DNA bending induced by specific cisplatin adducts.[41] For example, high mobility HMG-domain proteins (e.g. HMG1 and HMG2) which are non-histone chromosomal proteins involved in gene regulation and chromatin structure are known to recognize cisplatin-DNA adducts.[45] The protein HMG binds with high selectivity to the DNA lesions structurally distorted by 1,2-d(GpG) crosslinks.[46] Two mechanisms have been suggested to interpret how HMG proteins might control cisplatin cytotoxicity. The first mechanism postulates that HMG proteins

act as a shield and protect cisplatin-DNA crosslinks from recognition by the DNA repair mechanism of the cell known as "repair shielding model".[47] The other model, the "hijacking model", proposes that HMG binding modulates cell cycle pathways by inhibiting the nucleotide excision repair NER proteins,[48] and it has been connected to mismatch repair MMR proteins, p53 activity (a tumour suppressor protein) and MARK pathway.[49, 50] The recognition of 1,2-intrastrand adducts by these proteins may be responsible for the cytotoxic effects of cisplatin,[51, 52] Finally, all the attempts to repair the damage in DNA leads to a programmed cell death known as apoptosis.[26, 36, 53, 54]

Since transplatin is not able to form these adducts, it was considered initially as inactive in comparison to the cisplatin, however several platinum compounds with *trans* geometry have been proven to be antitumor active,[55] such as [*trans*-$PtCl_2$(pyridine)$_2$].[56] Recently, single *trans* isomers of bis-picolinamide ruthenium(III) diiodide complexes showed high activity and selectivity with IC_{50} values in the nanomolar range.[57]

It was found that *trans* compounds are also capable causing DNA structural distortions. Therefore, it is hypothesised that the inactivity of this compound is due to a greater kinetic instability, leading to increased deactivation of the compound.[56, 58]

1.2.3 Cisplatin side effects

Whilst cisplatin has had obvious success, there are several drawbacks with its clinical use that reduces the efficiency. Various studies confirmed that cisplatin induces the formation of Reactive Oxygen Species (ROS) accountable for several side effects such as organ toxicities. These include nephrotoxicity, ototoxicity, hepatotoxicity, cardiotoxicity and neurotoxicity.[59] These problems are coupled to the general side effects which result from cell damage such as nausea, vomiting, immunosuppression (decreased response of the immune system to infection), decreased blood cell and myelosuppression (platelet production in bone marrow).[60, 61]

In addition to these serious side effects, the resistance of some tumours cells to cisplatin is a common issue in cancer chemotherapy[34, 62] For example, colorectal cancer and non-small cell lung cancer are inherently insensitive to cisplatin (intrinsic resistance).[63] Other cancer cells, for instance, testicular and ovarian cancer, respond initially to the treatment but resistance then develops after repeated administrations of cisplatin (acquired resistance).[64, 65]

All these side effects have triggered an intensive search for new platinum-based anticancer drugs to overcome or, to some extent, diminish the side effects.[66]

1.2.4 Second and third generation platinum drugs

New platinum-based anticancer drugs have been developed in order to overcome cisplatin side effects. However, from over 3000 complexes screened for antitumor activity, only a few compounds have entered clinical trials (Figure 1.5).[67]

The second-generation platinum drug, carboplatin, was one of the first complexes introduced into cancer therapy in 1989 with a reducing and non-overlapping toxicity in comparison with cisplatin. The replacement of the unidentate chloride ligands of cisplatin by a chelating cyclobutanedicarboxylate ligand of carboplatin (Figure 1.4) provides the complex with a reduced rate of aquation, good aqueous solubility and greater stability which leads to diminished side effects.[68, 69] Carboplatin can be applied in higher doses in the treatment of several types of cancer such as ovarian cancer that exceeds the dosage of cisplatin. The main drawback is that carboplatin did not overcome the cross-resistant mechanism.[70]

The cisplatin and carboplatin cross-resistance was first overcome by oxaliplatin (1*R*,2*R*-diaminocyclohexane)oxalatoplatinum(II).[71, 72] It has less cross-resistance and a more favourable toxicity activity due to a different carrier ligand, diaminocyclohexane. Oxaloplatin is effective against colorectal cancer when used in combination with 5-

fluorouracil and folinic acid.[73] The main reason for the lower cross-resistance is thought to be because of different adduct formation with DNA; the drug forms GpG intrastrand adducts with the bulky hydrophobic diaminocyclohexane ligand pointing into the DNA major groove and preventing DNA binding.[74] Furthermore, the oxalate ligand is also known to reduce the severity of side effects in comparison with cisplatin.[72, 75] Nedaplatin is also a second-generation cisplatin analogue with greater water solubility and significantly less nephrotoxicity than both cisplatin and carboplatin. It was approved for clinical in 1995 and it possesses good antitumor activity against non-small cell lung cancer, small cell lung cancer, esophageal cancer, head and neck cancers with fewer side effects.[76]

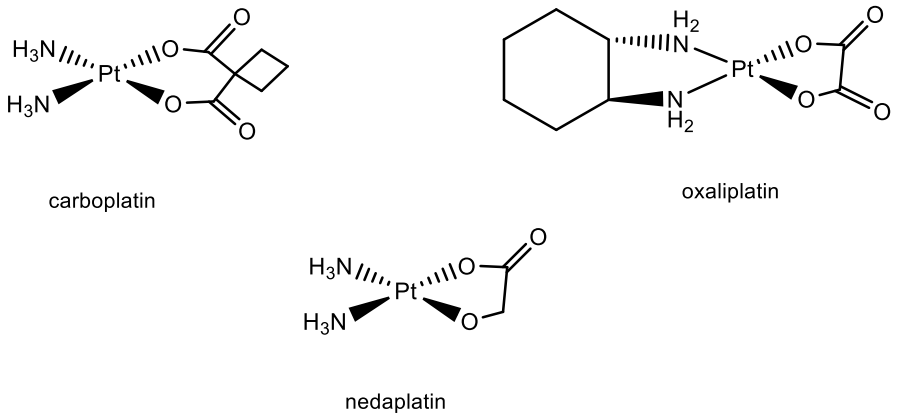

Figure 1.5: Second-generation platinum(II) complexes that are approved for clinical use include carboplatin, oxaliplatin and nedaplatin.

As discussed above, the second-generation platinum-based anticancer compounds have lower renal toxicity whilst retaining antitumor activity due to the replacement of the amine or chloride by more stable chelating ligands. However, the first and second generation are not orally bioavailable, which influenced research to develop these drugs by minimizing their side effects, resulting in the syntheses of third generation platinum drugs (Figure 1.6).[77] Not all of these attempts, however, have been successful. Although satraplatin, a Pt(IV) octahedral centre, exhibits some activity in cisplatin resistant tumour

cell lines and showed increasing oral bioavailability, it has been unsuccessful in clinical trials.[78]

Lobaplatin[79] and heptaplatin[80] are two third generation drugs that gained approval for the treatment of cancer in certain regions of the world, and each of them shows some activities that are not established by cisplatin.[81, 82]

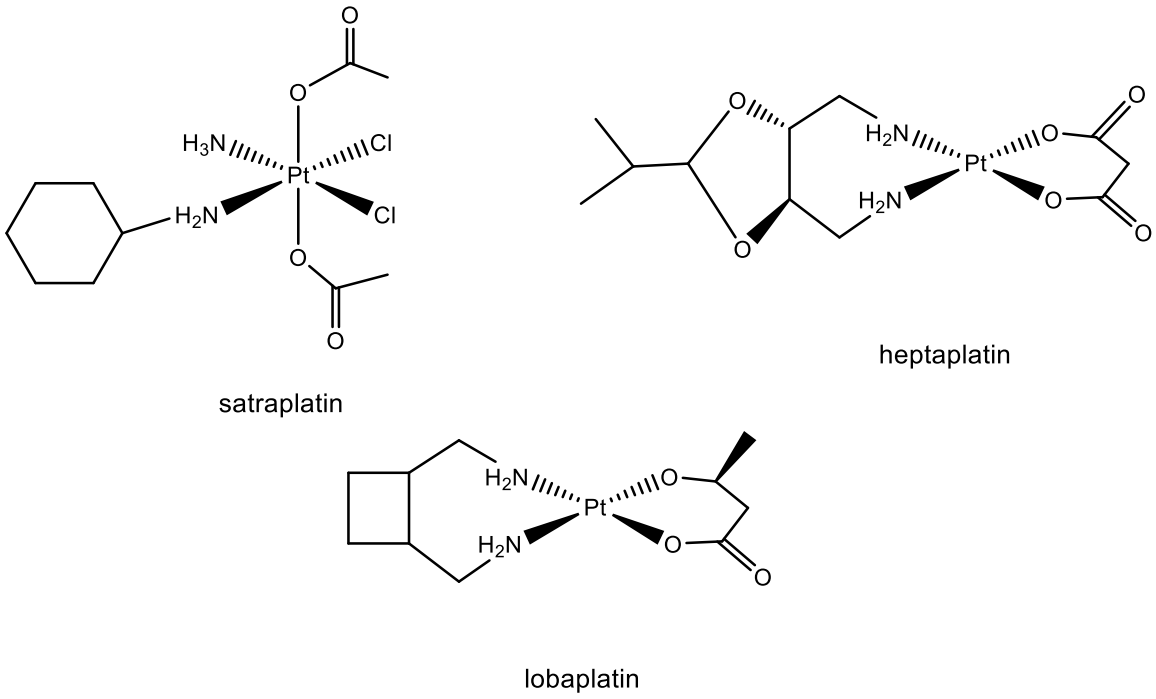

Figure 1.6: Third-generation platinum(II) complexes that are approved for clinical use include satraplatin, heptaplatin, and lobaplatin.

In all of the examples discussed above, the fact remains that many of these complexes are toxic to all tissues (cancer and healthy cells), are mutagenic, have severe side effects and act against a limited number of cancers. As a result, research directions have turned toward the exploration of other active transition metal complexes for the treatment of cancers that deviate in reactivity and mechanism of platinum-based anticancer drugs.[83]

1.3 Non-platinum anticancer agents

Platinum is not the only metal used in anti-tumour drugs. There are various examples of other metals (Figure 1.7) incorporated into anticancer drugs.[84]

Compounds of ruthenium, gallium, or titanium have already been tested in clinical phase I and phase II trials, whilst complexes of iron, gold, or cobalt have shown interesting results in preclinical research.[85]

Figure 1.7 shows the most common compounds used as anticancer drugs. Many gallium complexes have been prepared with promising anticancer properties such as the metallodrug, KP46 (*tris*(8-hydroxyquinolinato)gallium(III)).[86] The simplest and first gallium complex that stimulated further research in the field is gallium nitrate $Ga(NO_3)_3$ and it is consider as a standard against which newer gallium complexes should be compared due to its high activity. $Ga(NO_3)_3$ is approved for the treatment of hypercalcemia of malignancies by reducing the elevated Ca^{2+} levels in the blood.[87, 88]

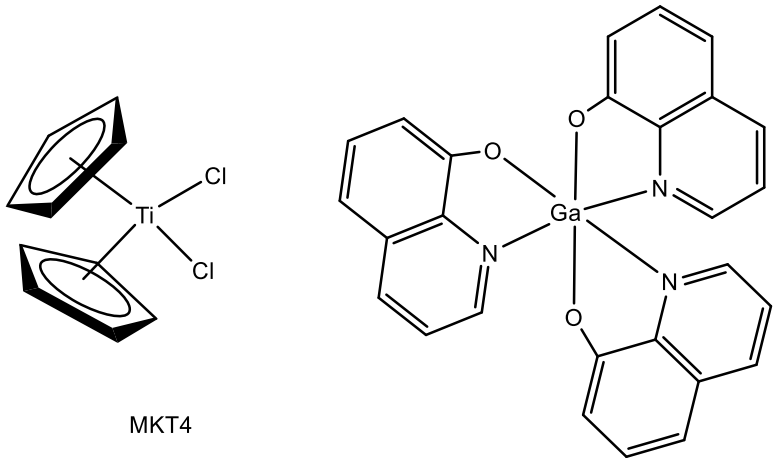

Figure 1.7: The most promising anticancer compounds, KP4 and MKT4.

Titanium metal became very important in the field of antitumor metallodrugs since the discovery that titanocene dichloride $[TiCl_2Cp_2]$ or MTK4 is an active anticancer drugs

against breast and gastrointestinal carcinomas.[89] The activity of this compound was supposed to be in the same manner as cisplatin with DNA as the main target, but the aqeuous chemistry of MTK4 showed that DNA is not considered as a site of action. Instead, the inhibition of collagenase type IV activity, which is involved in regulation of cellular proliferation, protein kinase C and DNA topoisomerase II activities, seems to contribute to the biological activity of this compound.[85, 90] Since this discovery there has been extensive research by Tacke, McGowan, Valentine, Meléndez, and Tshuva on many titanium compounds, many of which show promising anticancer activity.[90]

In conclusion, it is clear that platinum is not the only metal that offers a high activity in the chemotherapy field, since many other metals (including gallium, titanium and ruthenium) have been used in the further development of metallotherapeuticals.

1.4 Ruthenium complexes with anticancer properties

One of the new strategies for the design of new anticancer drugs is finding an alternative metal centre to platinum that possesses new structures and modes of action to overcome the drawbacks associated with cisplatin therapy.[85] Ruthenium complexes turn out to be the most promising metal in the field of anticancer compounds.[91] Ruthenium complexes show similar ligand exchange kinetics to platinum under physiological conditions, which in both cases is slow.[92, 93] Furthermore, ruthenium compounds are less toxic than platinum drugs.[92] This low toxicity is supposed to relate to the redox potential of ruthenium complexes under physiological conditions that allows the administration of inert Ru(III) drugs which are activated by reduction to Ru(II) in diseased tissues (as cancer cells have a more chemically reducing environment than healthy cells owing to their lower oxygen concentration).[94] The lower toxicity is also believed to be due to the ability of ruthenium to mimic iron in binding to many biomolecules, such as transferrin or albumin, which causes higher drug concentrations in cancer cells in comparison to healthy cells.[95] This aids ruthenium complexes to be selectively activated in cancer tissues.[92, 96] All of these

features, in combination with the ability of ruthenium to forms hexacoordinated complexes (which is markedly different to the well-known platinum drugs where the metal usually has a square planar geometry), makes ruthenium compounds suitable for use in biological applications. Ruthenium-based drugs do not mimic cisplatin and its analogues in their mode of action.[97]

1.4.1 Development of ruthenium(III) complexes

Ruthenium compounds were first tested successfully for biological activity by Dwyer and coworkers in 1950.[98] The complex *fac*-$[RuCl_3(NH_3)_3]$ was one of the earliest types of Ru(III) species and found to inhibit the growth of *Escherichia coli* cells in 1978, at similar concentrations to cisplatin[99] Then, in 1980 cis-$[RuCl_2(NH_3)_4]$ was also observed by Clarke and coworkers to exhibit anticancer properties.[100] The main concern with these two complexes was their poor water solubility that prevented their formulation as drugs.[101]

To overcome solubility issues, highly water soluble $[Ru(DMSO)_4Cl_2]$ was explored. Surprisingly, when the *cis* and *trans* isomers were investigated for anticancer activity, the *trans* isomer was much more cytotoxic than the *cis* isomer.[102, 103] This behaviour is in stark contrast to the relative activities of the Pt(II) isomers, which pointed to the possibility of differences in the mechanisms of action of Ru(II) and Pt(II) complexes.[104]

The search for more biologically active complexes related to *trans*-$[Ru(DMSO)_4Cl_2]$ led to the development of *trans*-$[RuCl_4(Im)(DMSO)](ImH+)$, NAMI-A by Alessio (Figure 1.8).[105] This drug has been one of the most promising candidates, having completed Phase I clinical trials and also showing encouraging results in Phase II clinical trials, especially in colon, head, liver and neck and endometrial cancers.[106, 107] NAMI-A has a negligible effect on the primary tumour; instead, it is known to be effective against tumour metastases, not only in preventing the formation of metastases but also in inhibiting their growth once established, particularly in the lungs.[106] This is a very important activity since treating secondary metastases is still a clinical challenge. The

exact mechanism of action of NAMI-A remains to be elucidated. Although NAMI-A is capable of binding to DNA, such binding is not believed to be relevant to their biological action,[108] hence this drug undergoes aquation and hydrolysis within minutes at pH = 7.4 in aqueous solution[109] and has non-cytotoxic behaviour in common cancer cell lines. The interactions with actin-type proteins on the cell surface,[110] or with collagens of the extracellular matrix,[111, 112] result in reduced mobility of invasive cancer cells and migration. These were suggested as possible mechanisms of anti-metastatic action of NAMI-A.[113, 114]

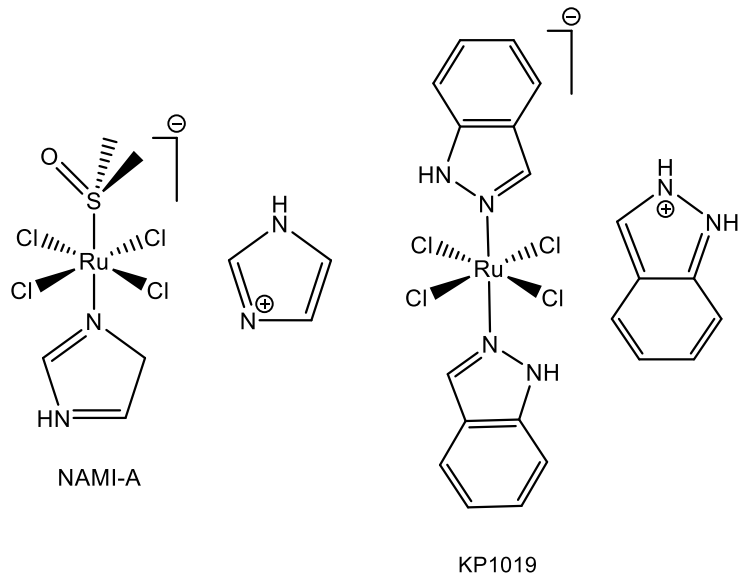

Figure 1.8: Two ruthenium(III) complexes in clinical trials, NAMI-A and KP1019.

KP1019, [IndH][trans-$RuCl_4(Ind)_2$] (Ind = indazole) (Figure 1.8), developed by Keppler, was the second ruthenium anticancer drug to pass Phase I clinical trials.[115] It is effective against cisplatin, resistant colorectal cancer, the second common type of cancer.[116] Although KP1019 largely resembles NAMI-A in chemical properties, it has different behaviour *in vivo* due to the ability to induce cell apoptosis (programmed cell death), which is attributed to the different protein binding interactions of the two complexes.[114, 117] KP1019 can bind to iron pockets in transferrin, with two ruthenium

moieties residing in each iron binding site which results in the high accumulation of the drugs in tumour tissue due to the high iron requirement of tumour cells.[114] Then apoptosis is induced via depolarization of mitochondrial membranes and activation of caspase-3 as well as down-modulation of the antiapoptotic factor bcl-2.[118] The cell death by KP1019 drugs was found to be independent of the p53 status of tumour tissues, indicating that DNA is not the primary target and that DNA strand breaks may possibly contribute to the formation of reactive oxygen species in tumour cell lines.[114]

1.4.2 Redox activation of ruthenium-based prodrugs as a hypothesis

Ruthenium(III) drugs may remain in the same oxidation state until they reach the tumour site or partial reduction in biological media is sometimes possible.[119] Drugs administered as inert Ru(III) complexes may be activated, once inside the cell, by a process called "activation by reduction".[120, 121] Increased amounts of *in vivo* reduction is expected to take place within cancer cells due to the lower oxygen (more hypoxic) content and the acidic environments due to insufficient formation of new blood vessels.[122] Compared to healthy cells, cancer cells tend to be more dependent on glycolysis for their energy and an excess of lactic acid is produced; this in turn lowers the pH of the local environment[123] which favours the production of Ru(II) intermediates from the Ru(III) precursors. Thus Ru(III) complexes are considered as pro-drugs.[121, 124]

The biologically active Ru (II) species are more reactive to chlorido loss than the Ru(III) prodrugs. This is because reduction from Ru(III) to Ru(II) fills the d_{π} orbitals, causing π-donor ligands such as chloride to dissociate more readly.[121, 125]

Activation by ligand substitution in Ru(III) prodrugs is thought to be important for both NAMI-A and KP1019 drugs and the hypothesis that Ru(II) rapidly coordinates to biomolecules leads to generate an interest towards compounds that have a stable Ru(II) oxidation state, such as the organometallic Ru(II) arene complexes.[126, 127]

1.4.3 Ruthenium-arene complexes as anticancer agents

In the field of modern medicinal chemistry, a new class of ruthenium(II) compounds featuring the η^6-arene ligand have attracted much attention for use as anti-cancer agents.[126, 128]

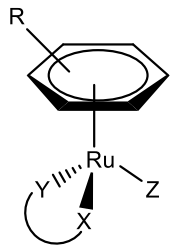

Figure 1.9: General structure of piano-stool ruthenium(II) arene complexes.

The "half-sandwich" ruthenium(II) arene compounds are also referred to as "piano-stool" complex, and were developed by Sadler and co-workers of a general formula [Ru(η^6-arene)(XY)(Z)], (Figure 1.9) where XY is a bidentate chelating ligand and Z is monoanionic labile ligand.[129] Structure-activity relationships have determined that a chelating ligand (XY) can provide stability towards aquation by controlling the ligand exchange kinetics of the complexes, and ligand XY also influences the p*K*a of the compounds and selectivity of binding to the nucleobases. The nature of the arene, with three *fac*-coordination sites acting as a π-acceptor, can confer stability to the +2 oxidation state. Finally, the monodentate leaving group (Z), such as halide, allows activation of the compound by providing a vacant coordination site for biomolecules.[128, 129]

The first ruthenium(II) arene complex with identified cytotoxic activity was [Ru(η^6-C_6H_6)(DMSO)Cl_2]. The complex shows strong inhibition of topoisomerase II activity, which play an important role in structural organization of the mitotic chromosomal scaffold during cell replication process.[130] Replacing the DMSO ligand with 3-aminopyridine, *p*-aminobenzoic acid or aminoguanidine ligands shows enhanced

efficacy of topoisomerase II inhibition and higher cytotoxicity against colon and breast cancer cells in comparison to the parent complexes (Figure 1.10).[131]

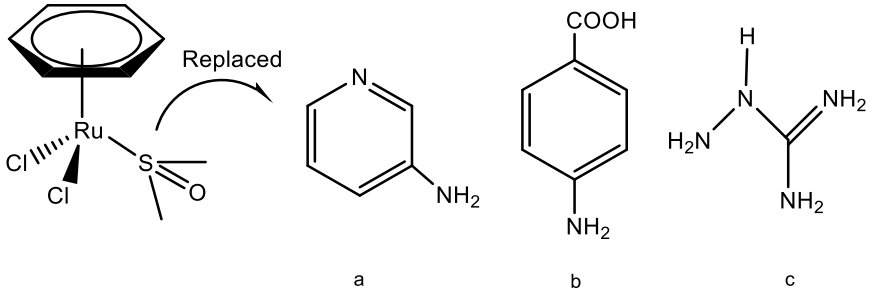

Figure 1.10: Chemical structures of the [Ru(η⁶-C₆H₆)(DMSO)Cl₂] and replacement of DMSO by a) 3-aminopyridine b) p-aminobenzoic acid or c) aminoguanidine.

Since then, many Ru(II)-arene complexes containing chelating nitrogen ligands such as ethylenediamine (en) or N-ethylethylenediamine (en-Et), some of which are given in Table 1.1, were developed by Sadler and co-workers in 2001[128] in order to exhibit desirable physical, chemical and biological properties. These ethylenediamine-based complexes were evaluated against the human ovarian cancer cell line A2780 and the obtained results show high *in vitro* and *in vivo* anticancer activities, some of them as potent as cisplatin and carboplatin.[132] Some structure–activity relationships have been established (Table 1.1). Initially, complexes with extended hydrophobic arenes such as $[(\eta^6\text{-tetrahydroanthracene})Ru(en)Cl]^+$ were found to be active with IC_{50} values equipotent with cisplatin (0.5 μM). This revealed the importance of the identity of the arene ligand and the increased hydrophobicity was assumed to increase the ability of the complex to passively diffuse through the cell membranes.[126, 133]

The importance of the chelating ligand (Table 1.1) (**R_2-R_2**) for moderating anticancer activity was indicated when the chelating ligand (en) was substituted by relatively labile monodentate ligands such as $[(p\text{-cymene})Ru(CH_3CN)_2Cl]^+$ and [(*p*-

cymene)Ru(isonicotinamde)$_2$Cl]$^+$. This led to less cytotoxic complexes (IC_{50} values > 100 μM) compared to the chelated ligand-containing complexes which exhibited high activity (9 μM).[128] The lack of activity was attributed to the high reactivity of the monodentate complexes which lead to inactivation of the complexes before reaching their target .[134]

Other evidence of the importance of the ethylenediamine chelating ligand comes from comparison of the activity of [Ru(*p*-cymene)Cl(en)]$^+$ with its monodentate analogue [Ru(*p*-cymene)Cl(NH_3)$_2$]$^+$ The presence of two ammonia ligands instead of ethylenediamine showed loss of cytotoxicity in the three cell lines A549 (non-small cell lung carcinoma), CH1 (ovarian carcinoma), and SW480 (colon carcinoma). This lack of activity may be related to instability of the non-chelating analogue which leads to rapid hydrolysis of both Cl and NH_3 ligands and formation of the [({*p*-cymene}Ru)$_2$(μ-OH)$_3$] $^+$ species, as found in the solid state.[135]

Substitution of chloride by bromide or iodide has only a marginal effect on the cytotoxicity of ethylenediamine complexes. This was hypothesised to be due to the high intercellular chloride concentration, which leads to the exchange of any halogen ligand with chloride.[136]

Table 1.1: IC_{50} values of Ru(II) arene complexes $[(R_1)Ru(R_2\text{-}R_2)(R_3)]^+$, carboplatin and cisplatin in A2780 human ovarian cancer cells after 24 h drug exposure.

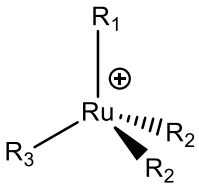

R_1	R_2— R_2	R_3	IC_{50} A2780(μM)	Ref.
benzene	En	Cl	17	128, 134
p-cymene	En	Cl	10	128, 134
biphenyl	En	Cl	5	128, 134
Dihydroanthracene	En	Cl	2	128, 134
Dihydrophenanthrene	En	Cl	1	137
Tetrahydroanthracene	En	Cl	0.5	128, 134
arene	En	Cl	1	138
arene	En	Br	5	138
arene	En	I	9	138
p-cymene	En	I	9	126
p-cymene	En	Cl	10	126
biphenyl	en-En	Cl	6	128, 138
p-cymene	2(Isonicotinamide)	Cl	>100	128
p-cymene	$(CH_3CN)_2$	Cl	>100	128
p-cymene	Diamino benzene	Cl	11	126
biphenyl	Diamino benzene	Cl	5	126
Carboplatin	-	-	6	134
cisplatin	-	-	0.6	134

Overall it appears that a more hydrophobic arene ligand and a single ligand exchange site, with the two other sites occupied by a bidentate chelating ligand *N,N*- result in high cytotoxicity.[126]

Using a σ-donor / π-donor oxygen chelating ligand *O,O*-, such as acetylacetonate (acac) instead of a dinitrogen σ donor *N,N*-, results in a change to the reactivity of the ruthenium arene complexes (Figure 1.11). The activity depends upon the size of arene in the following order: *p*-cymene > biphenyl > dihydroanthracene > benzene, the changing in arene size leads to change the activity against A2780 ovarian cancer cells from an IC_{50} 70 µM to 11 µM and the most potent complex is achieved with [(*p*-cymene)Ru(PhCOCHCOPh)Cl].[126] It was hypothesised that the acac complexes hydrolyse rapidly and have poor solubility. Also the steric bulk around the metal centre in case of p-cymene and biphenyl appears to enhance the activity of these acac complexes because rotating components can shield the metal centre and protect the chelating ligand from displacement.[126, 139]

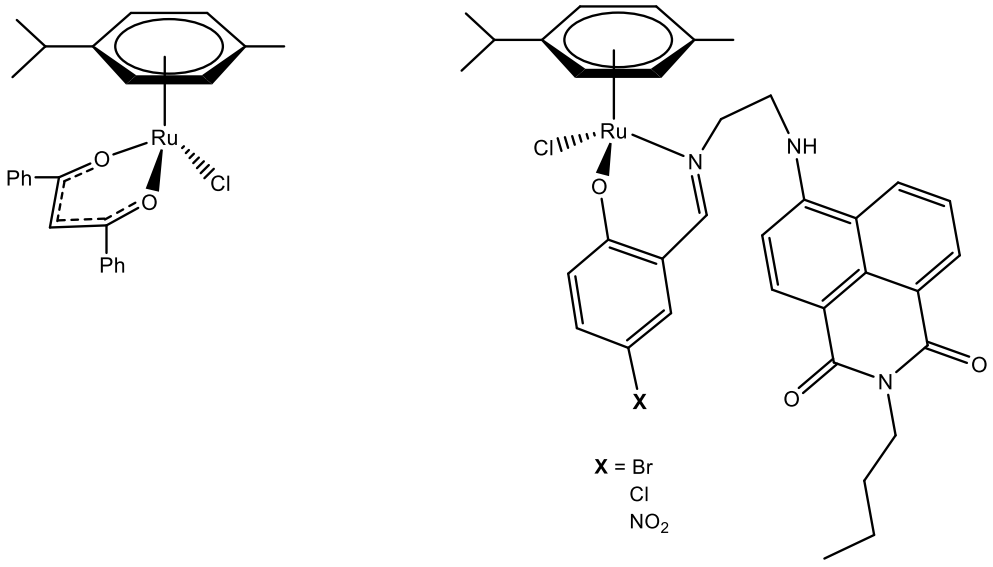

Figure 1.11: Structure of ruthenium(II)-cymene complexes with N,O- chelating ligand [Ru(p-cymene)Cl(N,O)] where: N,O = 4-[N-(2-((2-hydroxy-5-Xphenyl)methyl imino)ethyl)]-N-butyl-1,8-naphthalimide (right) and O,O- chelating ligand [(p-cymene)Ru(PhCOCHCOPh)Cl] (left).

The *N,O*- chelating complexes of the type [(*p*-cymene)Ru(N,O)Cl] such as glycine, L-alanine, O-alanine, L-phenylalanine, and 8-hydroyxquinoline have been found to be inactive towards the ovarian cancer cell A2780.[126] Recently, a new family of ruthenium(II) arene complexes with naphthalimide conjugated chelating ligands of the general formula [Ru(*p*-cymene)Cl(**N,O**)] where: **N,O** = 4-[N-(2-((2-hydroxy-5-Br phenyl)methylimino)ethyl)]-N-butyl-1,8-naphthalimide, 4-[N-(2-((2-hydroxy-5-Cl phenyl)methylimino)ethyl)]-N-butyl-1,8-naphthalimide, and N-butyl-4-[N-(2-((2 hydroxy-5-NO_2-phenyl)methylimino)ethyl)]-N-butyl-1,8-naphthalimide, Figure1.11 were synthesised and these complexes exhibit significant antiproliferative activities against the CRL8678 human melanoma skin cancer, with IC_{50} values in the ranges (0.70-0.89 μM).[140]

1.4.4 Mechanism of action

During the past decades, much research has been carried out exploring the mode of action of ruthenium (II) arene complexes. The studied complexes show remarkable activity against cisplatin-resistant cell lines, which may imply a different mode of action than that of cisplatin.[141]

Activation through hydrolysis may be important for the mechanism of cytotoxic action of Ru(II) arene complexes and their chemical behaviour in aqueous media has been extensively studied. For example, hydrolysis of [Ru(η^6-arene)Cl(en)]$^+$ is largely suppressed in the blood where high chloride concentrations are found (104 mM), whereas in the cytoplasm and nucleus, the chloride concentration is significantly lower than the extracellular concentration (20, 4 mM), respectively. Thus, under physiological conditions, the generated hydrolysis products (Ru–OH_2/OH species) are likely to increase from about 30% in the cytoplasm to about 70% in the nucleus.

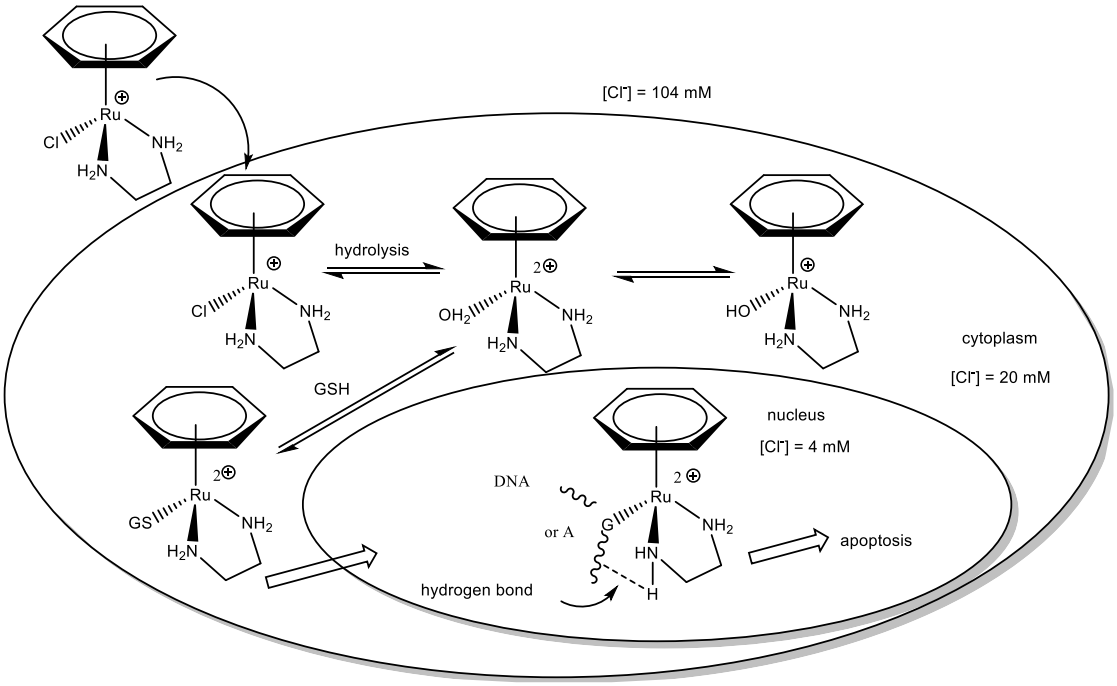

Figure 1.12: Proposed mechanism and DNA binding for ruthenium arene complexes.

The hydroxo and aqua species will exist in varying ratios within a range of pH values. If the pK_a of the aqua complex (Ru-OH_2) is too low, the inactive hydroxo Ru-OH species will predominate (Figure 1.12). The deprotonated Ru-OH species is less reactive due to the less labile hydroxide ligand compared to water, which will not be displaced easily by biomolecule targets. Thus, ideally the pK_a values of aqua complexes should be (>7.7) so that the deprotonation of the aqua products is negligible at physiological pH. Furthermore, the equation kinetics of ruthenium (II) arene complexes have also been studied since it is considered as an activation step for the complex for potential binding to DNA or other possible cellular targets, and it appear to be rapid about twenty times faster than that of cisplatin.[142]

The main cellular target for Ru(II) arenes, as for many metal-based drugs, is believed to be DNA. It is found that the aqua species has a high affinity for the N7 position of guanine (G) base, with different mode of binding to DNA, as the ruthenium arene complexes can form only monofunctional adducts while cisplatin forms bifunctional adducts.[143] This behaviour has been verified by a comparative study with various DNA bases in aqueous solution. The reactivity of the various binding sites of nucleobases towards arene ruthenium ethylenediamine at neutral pH decreases in the order G(N7) > T(N3) > C(N3) > A(N7), A(N1), and binds very weakly to N(3) of cytidine and almost no binding to adenosine was observed.[144]

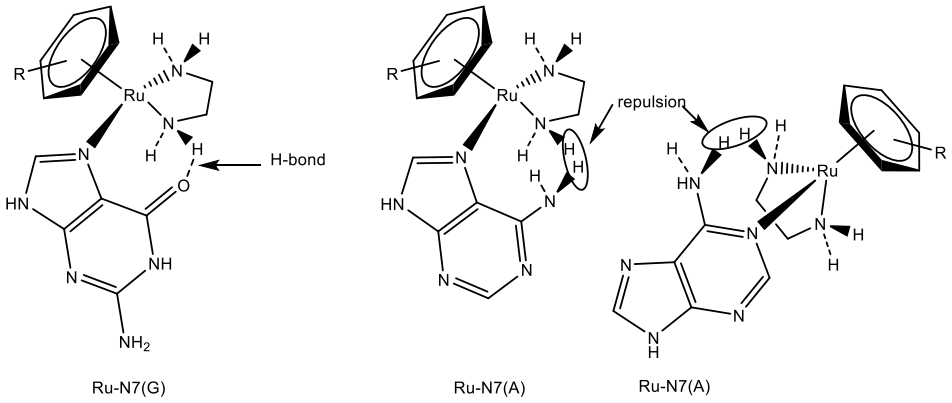

Figure 1.13: Ruthenium(II) arene interactions within guanine (G) and adenine (A) adducts.

The observed base selectivity can be justified in terms of hydrogen bonding attractions/repulsions. The ethylenediamine NH_2 groups were found to form hydrogen bonds with exocyclic oxygens C_6 of the guanine system whereas repulsive and non-bonding interactions towards exocyclic amino groups of the nucleobases such as C_6 of adenine system were observed (Figure 1.13).[96, 128, 145] In addition, when bearing an extended arene ligand such as dihydroanthracene, and tetrahydroanthracene, the complexes nucleotide binding was promoted by hydrophobic arene-purine base π-π stacking interactions, therefore enhancing the cytotoxicity of those derivatives.[99, 145]

The experimental data in both the solid (X-ray crystal structures) and solution (NMR) state are in good agreement with Density Functional Theory (DFT) calculations on these complexes with isolated nucleobases.[145] However, the affinity for adenine was found to be greater than guanine in case of ruthenium (II) arene complexes with *O,O*-chelating ligands which is believed to be due to specific hydrogen-bond recognition of the complex by the bases.[144]

Overall, these complexes are cytotoxic to several cancer cell lines,[126] including cisplatin resistant strains, while $[Ru(\eta^6\text{-biphenyl})(en)Cl]^+$ shows high activity against the MCa mammary carcinoma, reducing both the growth of the primary tumor and growth of lung metastases.[146] These promising activity has led to further efforts to develop ruthenium(II) arene complexes.

1.4.5 Second class of organometallic ruthenium (II) complexes

A series of Ru-organometallic complexes of formula $[Ru(II)(arene)Cl_2(PTA)]$, known as RAPTA compounds have been developed by Dyson and co-workers.[147] The piano-stool structure of RAPTA compounds are based on arene moieties and PTA ligands where PTA is 1,3,5-triaza-7-phosphatricyclo[3.3.1.1.]decane (Figure 1.14). The monodentate PTA ligand is the distinguishing feature of the RAPTA structure that differentiates this family of complexes from other ruthenium(II)-arene compounds evaluated for their anticancer activity. This sterically undemanding ligand increased aqueous solubility of the RAPTA complexes depending on the nature of the co-ligands.[147, 148]

The first complex reported as a potentially interesting biological active agent is RAPTA-C, as when it was incubated with supercoiled pBR322 DNA it exhibited pH-dependent DNA damage. DNA damage was observed at pH 7.0 and below but not at physiological pH (pH ≥ 7.5), which provided a means to target cancer cells, since they exhibit reduced pH (hypoxic cells).[149]

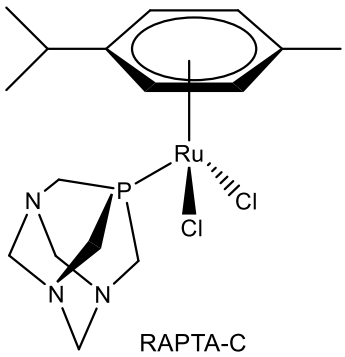

Figure 1.14: Structure of RAPTA-C complex as anti-metastatic agent.

Despite the obvious difference between RAPTA compounds and NAMI-A in oxidation state, ligand, and geometry, their behaviour *in vitro* and *in vivo* is very similar.[149] These compounds show excellent inhibition of metastases growth in addition to high selectivity and a very low general toxicity.[150] This remarkable activity of RAPTA-C has prompted the study of a large number of RAPTA analogues with a range of properties,[149, 151] (Figure 1.16).

1.4.6 Mechanism of action and structure development

The RAPTA-C complex has been shown to undergo rapid hydrolysis in pure water, over 20 minutes faster than both cisplatin and Sadler ruthenium arene complexes, and at a physiological concentration of 100 mM NaCl, the hydrolysis is suppressed.[147] On the basis of these results, many studies have been done to highlight the activation steps of these complexes. Under physiological conditions of low chloride concentration (5 mM) the major species in solution is the mono-aqua adduct of the RAPTA complex, $[Ru(\eta^6\text{-arene})Cl(H_2O)(PTA)]^+$, along with lesser amounts of $[Ru(\eta^6\text{-arene})(OH)(H_2O)(PTA)]^+$ and $[Ru(\eta^6\text{-arene})Cl_2(PTA)]$ also present. Equilibrium was reached after 20 min (Figure 1.15),[152] assuming that *in vivo* the drug, like cisplatin, is activated by hydrolysis in a low

chloride environment. However, another study revealed that the rate of hydrolysis does not support the mode of action as the replacement of the two chloride ligands by a chelating ligand such as oxalato (oxalo-RAPTA) leads to a decrease in the rate of hydrolysis, whereas reactivity towards a single stranded oligomer and *in vitro* activity remain unchanged.[153] Furthermore, it was later found that this complex has a p*K*a of 3.13, indicating that this complex is unlikely to be protonated under physiological conditions.[147]

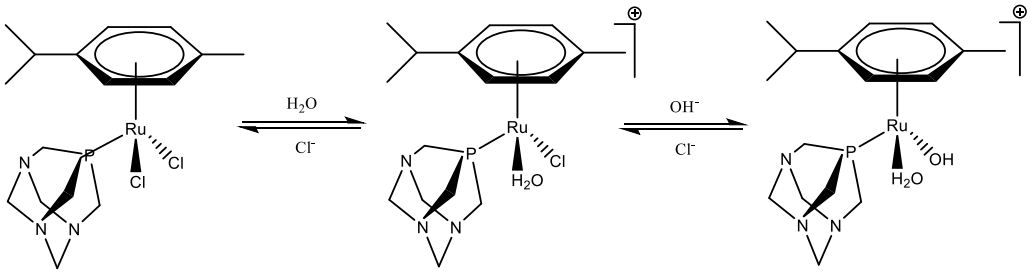

Figure 1.15: Hydrolysis of RAPTA-C under physiological conditions.

After the initial report of the ability of RAPTA-C to damage DNA, three close analogues, [Ru(*p*-cymene)X_2(PTA)] (X = Cl, Br, I, NCS), were evaluated. These RAPTA compounds possessed a degree of antibiotic activity. The level of observed activity against a particular microbe was related to the nature of the leaving group ligand (X), while *in vitro* DNA-damaging property of a particular RAPTA compound did not correlate with the observed antimicrobial activity, suggesting a non-DNA-based mechanism of action.[154]

On the other hand, a study of incubation of RAPTA-C with *E. coli*, followed by the extraction and separation of intracellular proteins, then using laser ablation inductively coupled mass spectrometry (LA-ICP-MS) for examination, the results specified the formation of protein-ruthenium interactions, implying protein-binding may be a major influence in the activity of these complexes and indicating a non-classical mechanism for the cell killing mechanism of RAPTA-C and their analogues.[155]

In view of this, protein interactions of RAPTA compounds are extensively studied.[99, 155, 156] A study of the RAPTA compound with low molecular weight proteins or peptides mimicking the active sites of albumin and transferrin residues was performed using mass spectrometric analysis which demonstrated that a histidine residue is the major binding model and cysteine is also engaged in the binding but to a lesser extent.[157] It is clear that the affinity of RAPTA-T for albumin and transferrin is higher than that of cisplatin, supposedly due to the direct reaction of RAPTA compounds with biomolecular targets without aqua adduct formation.[155]

1.4.7 Structure-Activity Relationship (SAR) development of the RAPTA structure

Promising antitumor activity of some of the original RAPTA structures, in particular RAPTA-B, RAPTA-C, and RAPTA-T (Figure 1.16) prompted further investigations on the effect of modulating individual structural substituents of the RAPTA scaffold to achieve structure-activity relationships to achieve more active compounds.

In order to investigate the effect of PTA ligand, RAPTA-C and RAPTA-T were modulated with PTA-Me^+ ligand shown in Figure 1.16, which lead to reduced selectivity compared to the original complexes. This supposedly confirmed the hypothesis that RAPTA complex activity originates from protonation of its PTA ligand.[147]

Further indication of a different mechanism of action in RAPTA compounds activity resulted from introducing hydrogen bonding groups to the arene ligand, for instance, RAPTA-OH, RAPTA-N1 and RAPTA-N2 Figure 1.16, which are assumed to promote reactivity towards oligonucleotides. However *in vitro* they proved to be less active and selective, correlated to reduced uptake of these modified complexes into the cell.[158]

A series of structural modifications of the PTA moiety were carried out to yield a series of RAPTA analogues with a chelating PTN (3,7-dimethyl-7-phospha-1,3,5

triazabicyclo(3.3.1)nonane) ligand in place of the PTA ligand (Figure 1.16). The chelate complexes were highly water soluble and strongly resistant to hydrolysis in addition to demonstrating little reactivity towards DNA. However, their *in vitro* activities are comparable to or better than those of their PTA analogues with high affinity for model protein ubiquitin.[159] This finding was a clear indication that the interactions of RAPTA compounds with proteins play a greater role on the antitumor activity of these compounds.

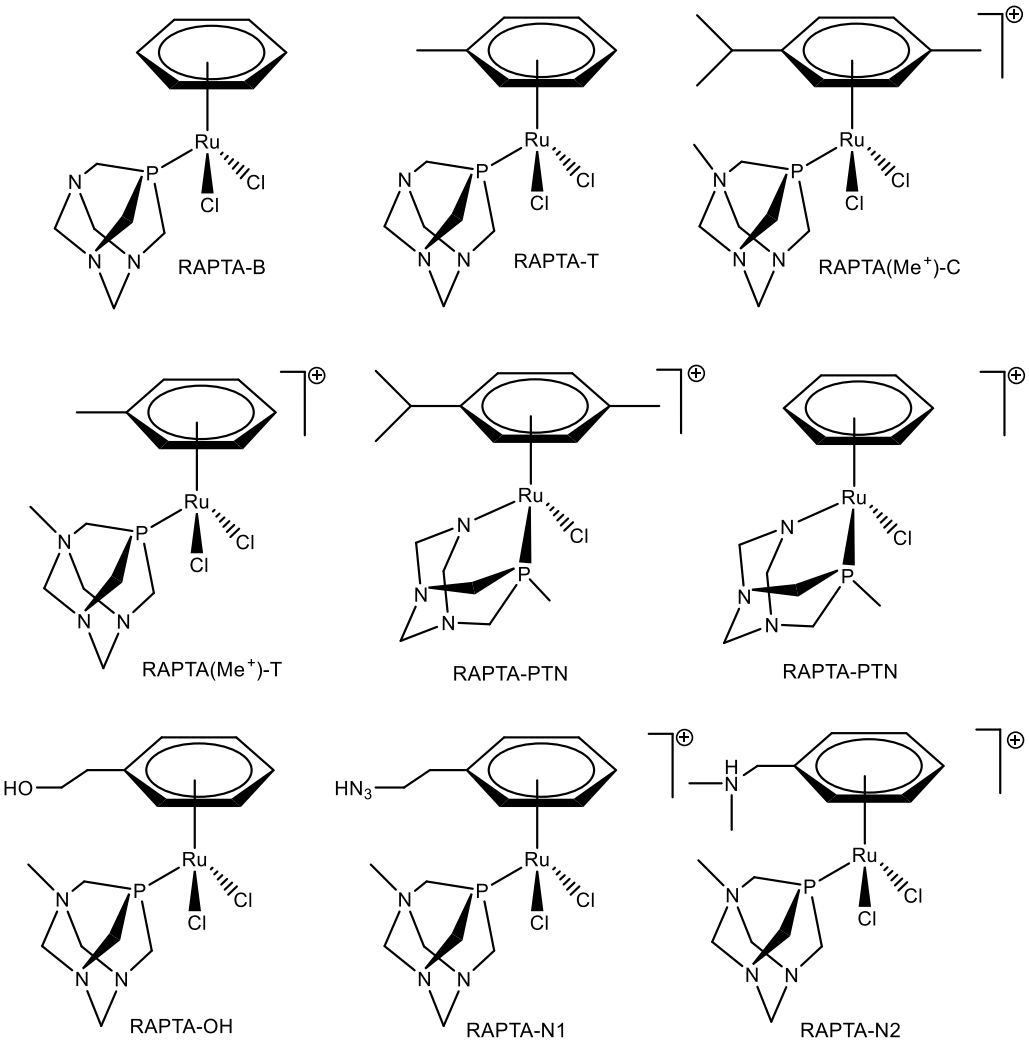

Figure 1.16: Family of RAPTA complexes.

To enhance drug efficacy and obtain more targeted compounds, facile functionalisation of the RAPTA structure has been exploited with ethacrynic acid, known as glutathione-S-transferases (GST) inhibitors (Figure 1.17). Ethacrynic acid is a biologically important molecule known to inhibit GSTs, which are expressed in certain chemoresistant tumors. GST is an enzyme that calalyses the conjugation of intracellular xenobiotics with glutathione, leading to the xenobiotic being expelled out the cells by the GS-export pump.[160]

The complexes were found to be competitive inhibitors with high cytotoxic activity against (A549, T47D, HT29), cell lines with high level of GST.[155, 160]

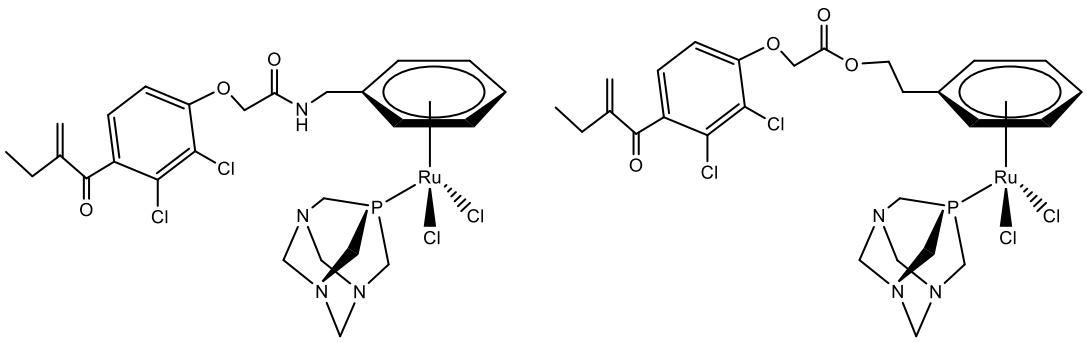

Figure 1.17: RAPTA complexes as glutathione transferase inhibitors.

A model RAPTA compound, for intracellular visualization by fluorescence microscopy, was developed by tethering some planar aromatic substituents (anthracene derivatives) to the arene ring of the RAPTA structure (Figure 1.18). The inclusion of anthracene derivatives also introduced a potential DNA intercalator into the structure. These complexes undergo aquation in aqueous solution and low toxicities were observed (IC_{50} > 200 μM) towards 12 cell lines (same as the parent RAPTA compounds). The intracellular localization in the A549 lung carcinoma cell line (24 h incubation, 50 μM, λ_{ex} 365 nm), was observed, but only weak fluorescence was monitored which prevented identification of precise intracellular localization of the complex.[161]

Further development in RAPTA complexes was done by incorporating cyclopentadienyl ligands and these complexes have been evaluated for their *in vitro* cytotoxicity. Recently, two new complexes have been developed with modified PTA ligand of acetylcholine and trimethylglycine containing quaternary ammonium groups (Figure 1.19).

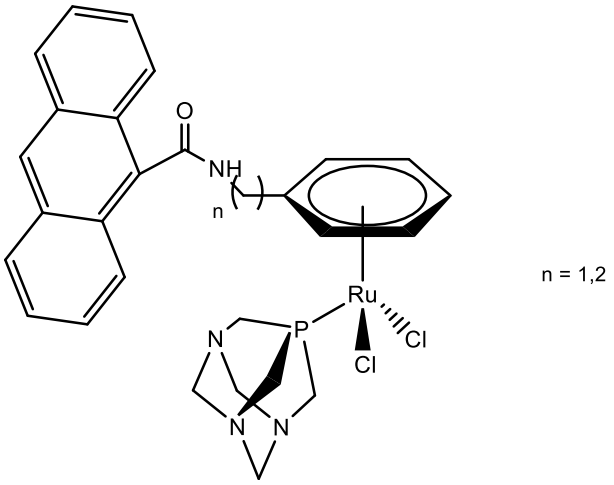

Figure 1.18: Functionalization of the arene ligand of RAPTA compounds with fluorescence anthracene for intracellular visualization purpose.

These complexes were highly cytotoxic against A2780, SKOV3 and K562 cell lines with IC_{50} values in the ranges of 4.7–5.1 and 5.5–8.3 μM, respectively. The structurally related PTA analogues were designed to contain naturally occurring quaternary ammonium groups, including the neurotransmitter acetylcholine.

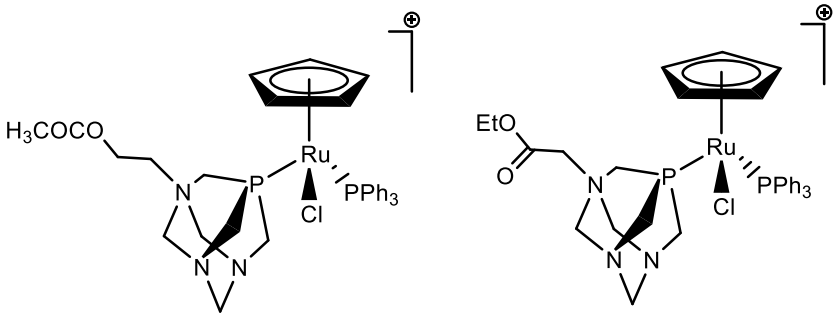

Figure 1.19: Ruthenium cyclopentadienyl complexes with modified-PTA ligands, acetylcholine (left) and trimethylglycine (right).

It was suggested to explore if the specific activity results from either the structural similarity of the modified-PTA ligands to these naturally occurring ammonium ions or if the high cytotoxicity is simply result from modulation of the amphiphilic nature of the ruthenium complex.[162]

Since then, RAPTA compounds have been expanded to include more than 80 complexes with promising anticancer properties and suggesting more study with advanced proteomics as effective target.[155]

1.5 Development of new ruthenium anticancer complexes

On the basis of the apparent necessity of a face-capping aromatic ligand for anticancer activity in RAPTA complexes and other organometallics, a RAPTA analogue was prepared by replacement of the aromatic fragment with a 1,4,7-trithiacyclononane ligand (ttcn) [Ru(ttcn)Cl_2(PTA)], (Figure 1.20).[157]

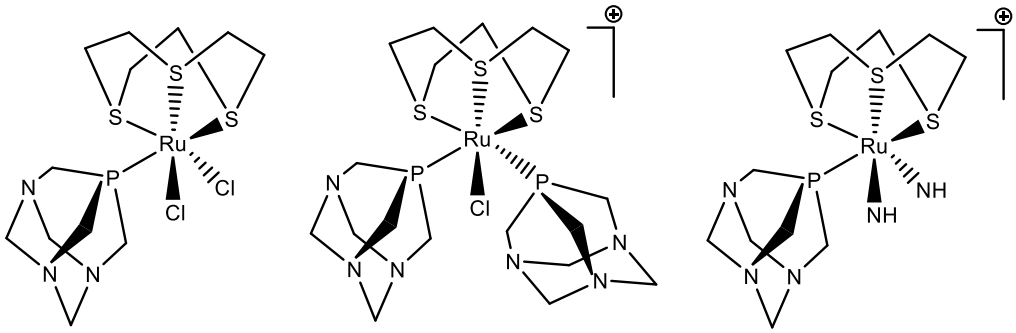

Figure 1.20: RAPTA analogues with replacement of the aromatic ligand with a ttcn.

The complex behaved in a similar manner to the RAPTA compounds in aqueous solution with slightly decreased cytotoxicity and selectivity in TS/A and HBL-100 cell lines. In contrast, when two coordinated PTA ligands were used,

$[Ru(ttcn)Cl(PTA)_2][OTf]$, the complex showed a selective mild cytotoxicity against the TS/A cell line with IC_{50} 388 µM whereas it became inactive towards the HBL-100 cell line (IC_{50} > 1000 µM).[163]

In the same study, the (ttcn) ligand was used to modify the ruthenium arene ethylenediamine complexes.The prepared complex [Ru(ttcn)Cl(en)][OTf], (Figure 1.20), was found to be generally more active, but lack of data for the leading complex in the same cell lines prevents direct comparison.[163] This study indicates the fact that the aromatic fragment may be effectively replaced by another face-capping ligand of similar steric demand without changing the compound activity.

Further study on the (ttcn) complexes was explored using novel chelating ligand 1-(2-picolyl)-4-phenyl-1*H*-1,2,3-triazole (ppt). The complex $[Ru(ttcn)Cl(ppt)][CF_3SO_3]$ aquates faster and exhibited higher cytotoxicity *in vitro* against human lung squamose carcinoma cell line (A-549) compared to cisplatin.[164]

An expansion of the structure-activity relationship of the ruthenium (ttcn) complexes was done using neutral *N*–*N*, and anionic *N*–*O* and *O*–*O* chelating ligands, *i.e.* dach (*trans*-1,2-diaminocyclohexane), pic^- (picolinate), and $acac^-$ (acetylacetonate) ligands, however the cytotoxicity was only evaluated for $[Ru(ttcn)(dach)Cl]PF_6$ which showed less activity than $[Ru(ttcn)(en)Cl]PF_6$. Moreover, this study also developed a new face-capping ligand, 1,4,7-triazacyclononane (tac), (Figure 1.21). The new half-sandwich complexes did not show any activity (up to 300 µM) against MDA-MB-231 human mammary carcinoma cells.[165]

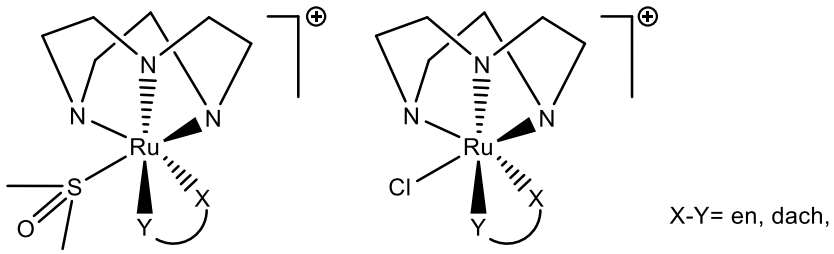

Figure 1.21: Ruthenium tac complexes with different chelating agent, en (ethylendiammine) and dach (trans-1,2-diaminocyclohexane).

On the basis of these results, many approaches to the design of anticancer drugs have been adopted and one of the strategies is to replace the arene ligand with new *fac*-ligands with hydrophobic properties to achieve highly active anticancer complexes.

1.5.1 New *facially-capping* ruthenium complexes

Developing a series of new ruthenium half sandwich complexes is still a key pathway to discovering more efficient anticancer drugs. Ru(II) coordination compounds in which the aromatic ligand is substituted by a neutral tridentate macrocycle that occupies three facial coordination sites, for instance, cis-1,3,5-triaminocyclohexane (tach), are an emerging class of compounds for the design of such active drugs.

1.5.2 The cis-1,3,5-triaminocyclohexane ligand

The face capping N_3, cis-1,3,5-triaminocyclohexane (tach) ligand forms the basis of many applications, particularly in bioinorganic chemistry,[166, 167] and in the modelling of metalloenzyme active sites.[168-170]

The tach ligand has been widely used due to its ability to provide three coordinating sites to different metals, similar to arene ligands, and many complexes have been reported.[171-173] One of the important features is the ability of tach to be a framework for further ready modification by condensation with aldehyde to form Schiff base derivatives.[168, 169, 172]

These derivatives have shown promising anticancer activity, for instance a novel metal chelator *N*,*N*′,*N*″-tris(2-pyridylmethyl)-1,3,5-*cis*,*cis*-triaminocyclohexane (tachpyr), (Figure 1.22), was mainly studied for its cytotoxic effect in both murine and human

bladder cancer cell lines.[171] Tachpyr exhibits an enhanced potency similar to desferrioxamine, an iron chelator known to treat acute intoxication by $FeSO_4$, in which both compounds were found to induce inhibition of ferritin synthesis.[174]

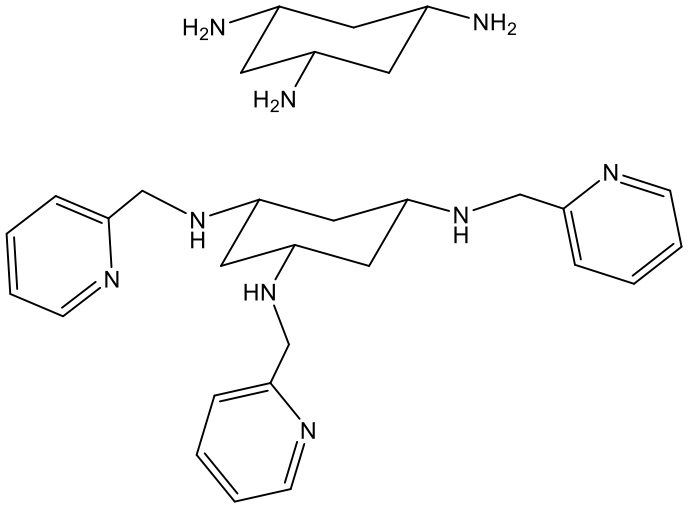

Figure 1.22: Structure of cis-tach (top) and N,N',N"-tris(2-pyridylmethyl)-1,3,5-cis,cis triaminocyclohexane (tachpyr) (bottom).

Several mechanisms have been proposed to describe the anti-tumor activity of tachpyr. One of the possible mechanisms is iron deprivation which is based on the ability of tachpyr to coordinate to biologically important divalent metal, Fe(II) to form a 1:1 complex. The ligand then undergoes dehydrogenation of one, two or three of its aminomethylene groups to form mono-, di- and triimino Fe(II) complexes (an inseparable mixture) and results in cytotoxicity, due to tachpyr's oxidation process.[171, 174]

On the other hand, to further elucidate tachpyr mechanism of action and better evaluate its potential applications, several novel metal complexes of tachpyr were synthesised and tested on MBT2 and T24 cultured bladder cancer cells. The Ca(II), Mn(II), and Mg(II) complexes were as cytotoxic as tachpyr itself, while the Zn(II), Fe(II), and Cu(II) complexes showed no cytotoxicity.[174] This initially supports the role of iron-

depletion in the cytotoxic mechanism of tachpyr. In order to obtain further support of this hypothesis, the sterically hindered tachpyr derivatives containing either methyl or ethyl groups at the three secondary amines were prepared. These nontoxic derivatives were demonstrated by the steric effect of the alkyl groups and also by the lengthening the bond distance between the metal and nitrogen atom.[175]

A second proposed mode of action is the activation of caspases via a mitochondrial mechanism that culminates in apoptosis, however the alkylated derivatives of tachpyr did not exhibit any activation of these enzymes.[176, 177]

As an ongoing effort to deduce the mechanism of action, recently, it was reported by Ciano [178] that DNA was found as a new possible target. The DNA-tachpyr binding was evaluated by linear dichroism (LD) that showed disruption in the linearity of the double helix, similar to the spermine derivative, which leads to suggest that tachpyr mimics spermine in binding to DNA in a non-intercalating fashion, probably with the phosphate backbone of DNA. Further evidence of this hypothesis was obtained by co-crystallising tachpyr with a short DNA oligonucleotide, two consecutive nucleobases (GC), that highlight the non-intercalation binding with DNA and presence of tachpyr in close proximity of the phosphate backbone of the DNA. These results support that the iron chelation is unlikely to be the mechanism of action of tachpyr.[178]

In the same study, a series of tach derivatives were synthesised to probe the structural effects in the cytotoxic activity. Different groups including heterocyclic, salicylaldehyde, and benzaldehyde derivatives were substituted on the three-amine nitrogen atom and two mono-substituents were also synthesised, illustrated in Figure 1.23 and the biological evaluation of activity were performed against A549 and A2780 cell lines by MTT assay. Some of the promising IC_{50} value are reported in Table 1.2.

As shown in Table 1.2, the change from basic nitrogen substituent, pyridine (pK_a = 5.2) to acidic nitrogen, pyrrole (pK_a = -3.8) leads to loss of activity, which indicates the influence of heteroatoms in increasing the cytotoxicity against cancer cell lines. The high activity obtained with benzaldehyde derivatives, in some derivatives even higher

than tachpyr, suggests that nitrogen atoms of the heterocyclic rings are not essential for high activity. This also supports the earlier hypothesis that iron chelation is not involved in mechanism of anticancer activity of tachpyr. On the other hand, changing the substituent in the 4-position of the phenyl ring doesn't correlate with changes to the IC_{50} value leading to the deduction that the steric of the substituent are not necessary for the high activity. The importance of the phenyl ring in the antiproliferative activity of tach derivatives was evaluated by the mono-substituted compound (cyclohexane and benzene ring) which both exhibited moderate activity with an IC_{50} value within the range (73-87 µM). Although the purity of the two derivatives was not confirmed by elemental analysis, the result still seems very promising.

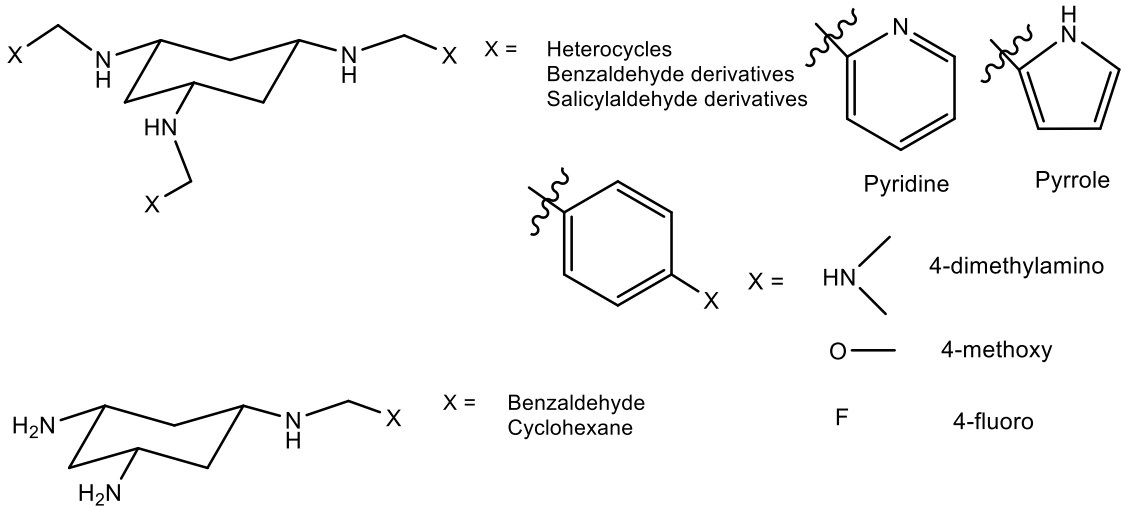

Figure 1.23: Structural modification of tach ligand synthesised by Ciano, tri-armed (top) with some example of the promising results, and mono-armed (bottom).[178]

The structure-activity relationship of the tach-based derivatives showed the necessary of the presence of one substituent to improve the lipophilicity and hence the activity of tach ligand.[178]

Table 1.2: IC_{50} values for tach derivatives tested against A549 and A2780 cells.

Compound	IC_{50} (μM – A549)	IC_{50} (μM – A549)
Tach	> 250	> 250
Tach-pyridine	4.99 ± 0.02	4.01 ± 0.03
Tach-pyrrole	188.2 ± 21.4	147.7 ± 7.1
Tach-benzene	6.65 ± 0.21	3.03 ± 0.10
Tach-4dimethylaminobenzene	1.03 ± 0.03	1.24 ± 0.02
Tach-4fluorobenzene	3.49 ± 0.06	2.62 ± 0.04
Tach-4methoxybenzene	2.42 ± 0.09	6.06 ± 0.07

On the basis of these results, the tach ligand has been modified with one phenyl ring (chapter two). to generate an anticancer Ru complex which, all of the investigations with the tach ligand suggest that it is a good candidate for the development of synergistic anticancer drugs. In accordance with the fact that little is known on the cellular uptake or interactions with biomolecules, more work is needed within this field.

1.5.3 Ruthenium tach complexes

Over the years, much research has looked at the synthesis and properties of tach complexes, particularly divalent transition metals, and they have been studied as a chemotherapeutic agent.[175]

The coordinating properties of cis-tach have been thoroughly investigated. A variety of metal species can be synthesised such as discrete complexes, molecular clusters and infinite architectures, where the three amine groups adopt an equatorial conformation in solution whilst the ring-flipped structure formed on coordination to a metal enforces an axial conformation of the three binding site in tridentate fasion,[169] or in

hexadentate fashion in case of functionalised tach that the arms can also coordinate to the metal.[175]

Mono-substituted tach complexes have been reported by Walton and co-workers in which the two arms have been cleaved upon coordination, (Figure 1.24), and this behaviour is limited only to benzaldehyde derivatives.[166] Then the cleavage of arms was overcome by using furfural or cinnamaldehyde to functionalise the tach structure and coordinate to Zn(II) to afford a model of the active site of enzymes (Figure 1.22).[167, 169]

Ruthenium tach complexes have attracted much attention since being reported by Gamble *et al* as promising anticancer agents.[179, 180] A wide range of ruthenium tach complexes have been synthesised as shown in Figure 1.25 and the biological activity of ruthenium(II) tach complexes was assessed by MTT colorimetric assay against the A549 lung adenocarcinoma and A2780 ovarian carcinoma cell lines. Some of the promising IC_{50} results are illustrated in Table 1.3.

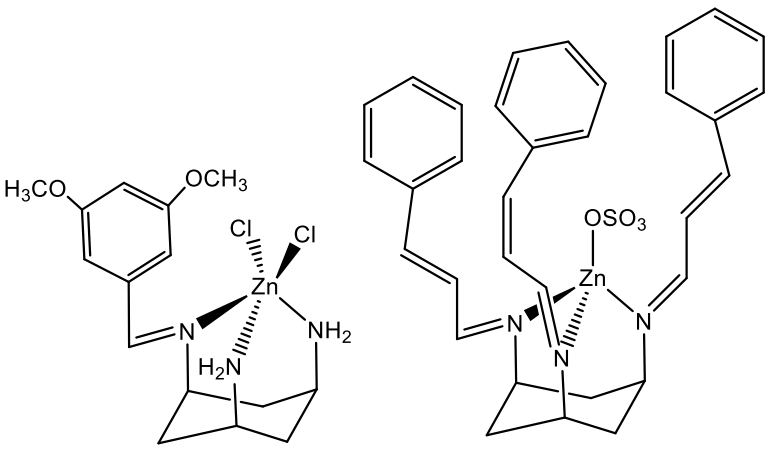

Figure 1.24: Cis-tach metal complexes with modified amine groups, monotach (left) and cinnamaldehyde tach (right).

As shown in Table 1.3, the triphenylphosphine complex $[Ru(tach)(PPh_3)(DMSO)Cl]^+$ displayed low activity in both cell lines while the DMSO complex $[Ru(tach)(DMSO)_2Cl]Cl$

was inactive. It is evident that the hydrophobic triphenylphosphine played a major part in obtaining moderate activity instead of DMSO ligand, and the poor lipophilic nature of the complex [Ru(tach)$(DMSO)_2Cl$] (in addition of slow aquation) are thought to be the main reason of their inactivity. The *N,N*-chelating complex was inactive as well, presumably due to the poorly labile DMSO ligand which remained complexed to Ru even when exposed to harsh conditions such as boiling solvent, therefore the activation of this complex did not proceed.

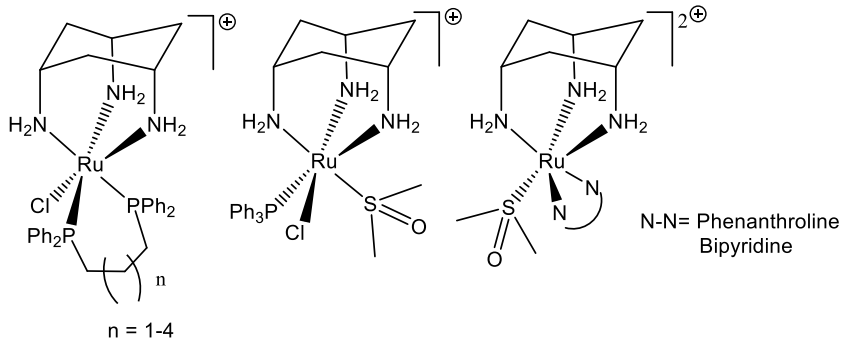

Figure 1.25: Ruthenium(II) tach complexes synthesised by Gamble.

The most promising results were obtained with complexes containing diphosphine chelating ligand [Ru(tach)(P-P)Cl]Cl, some which have cytotoxicity that exceeds that of cisplatin. This activity was attributed to lipophilicity and the flexibility of the chelating diphosphine in combination with the enhanced solubility and hydrogen bond donors provided by *cis*-tach ligand and the reactive chloride ligand.

Table 1.3: IC_{50} values for ruthenium(II) tach complexes tested against A549 and A2780 cells.

Compound	IC_{50} (μM – A549)	IC_{50} (μM – A549)
[Ru(tach)$(DMSO)_2$Cl]Cl	> 300	> 300
[Ru(tach)(PPh_3)(DMSO)Cl]Cl	194 ± 4	67.8 ± 10
[Ru(tach)(phen)DMSO]Cl	> 300	> 300
[Ru(tach)(dppp)Cl]Cl	1.02 ± 3	0.35 ± 1
[Ru(tach)(dppb)Cl]Cl	1.15 ± 2	0.39 ± 1
[Ru(tach)(dppe)Cl]Cl	9.88 ± 4	3.39 ± 12

1.6 Aims of the project

Ruthenium-tach complexes have repeatedly indicated promising anticancer activity, however the actual cellular target for these complexes and the mechanism underlying their biological effects has not been clarified. The aim of this project was firstly to design a series of complexes in which the tach ligand was structurally modified, and then to investigate the effects of these structural changes on the biological activity and cytotoxic properties.

The complexes were prepared by a structural modification to one of the nitrogen groups of the parent tach **[2]** in order to produce a mono-armed tach ligand. On incorporation of the mono-armed ligand into the ruthenium coordination sphere, shown in Figure 1.26, the activities of the new complexes were then compared to the non-toxic tach **[2]** in order to observe any differences in cytotoxicity. It was hoped that the structure activity relationships would provide further understanding of the mechanism of the anti-proliferative activity.

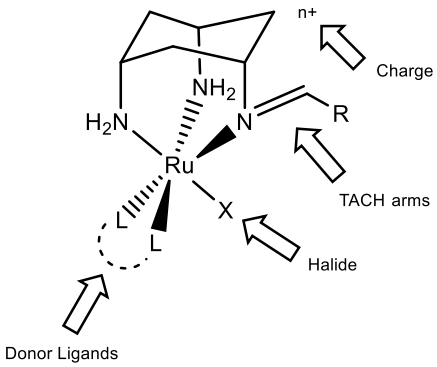

Figure 1.26: Proposed structural modification and development to ruthenium tach complexes.

To explore the cellular uptake and the fate inside cells of ruthenium tach complexes, the mechanism of action was probed by the synthesis of labelled ruthenium tach complexes with fluorescent tags. This study contributed significantly to the understanding of the possible intracellular targets of the complexes.

Another important aim is directed towards the interaction of Ru(II) tach complexes with biomolecules, in order to identify the main biological target for these complexes. This will be achieved by following the interaction of Ru tach complexes with both DNA and protein models using a range of spectroscopic methods including UV-Vis spectroscopy and fluorescence techniques. A range of modified tach ligands and complexes will be studied *in vitro* in order to examine their potential to inhibit tumour cell growth.

Chapter 2

Synthesis and characterisation of tachmonosubstituted ligands.

2 Synthesis and characterisation of tachmono-substituted ligands.

2.1 Introduction

Schiff bases, named after Hugo Schiff,[181, 182] are nitrogen analogues of an aldehyde or ketone in which the C=O group is replaced by a C=N-R group, (Figure 2.1). They are sometimes referred to as imines, azomethanes, aniles, aldimines or ketamines etc.[183-185]

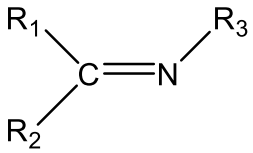

R_1, R_2, and/or R_3= alkyl or aryl

Figure 2.1: General structure of a Schiff base.

Schiff bases that contain aryl or aromatic substituents are more stable and more readily synthesised due to their extra stability through conjugation effects, while those with aliphatic substituents are unstable and readily polymerize or decompose.[186]

The classical method to prepare Schiff base compounds is by condensation of an aldehyde or ketone with a primary amine under specific conditions.[187] The modification of tach is usually performed using aldehydes as the resulting Schiff base is more readily formed than ketone,[186] therefore the general mechanism shown in Figure 2.2 is for reaction with an aldehyde. In general, the Schiff base formation is a two-step sequence: addition and elimination.[183, 188] In the first part of the reaction, the electrophilic carbon atom can be attacked by the nucleophile amine which causes a proton transfer to produce an unstable product known as a carbinolamine. The

formation is generally driven to completion by elimination of water and then the final neutral Schiff base is form by deprotonation of the imine product.[189]

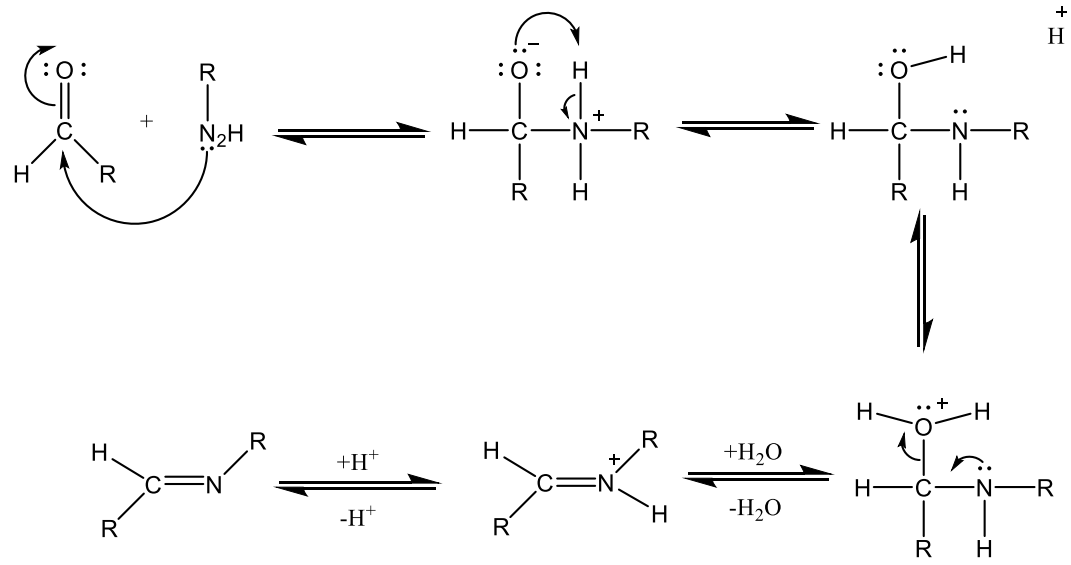

Figure 2.2: General mechanism of Schiff base formation.

The mechanism of Schiff base formation is a reversible reaction as protonation of the imine causes hydrolysis of the Schiff base and conversion back to the aldehyde or ketone and amine starting materials. This backward reaction is catalysed by aqueous acid or base and, for this reason, imine formation should be performed under mildly acidic conditions (pH = 4.5).[190] Additionally, imine compounds are rapidly hydrolysed by water and so the reactions have to be carried out under vigorously anhydrous condition such as via azeotropic distillation,[183, 191, 192] or using molecular sieves to completely remove water formed in the system.[193]

Schiff bases have a wide variety of applications in many fields including organic, analytical, biological, and inorganic chemistry. They have also gained importance in medicinal and pharmaceutical fields due to a broad range of biological properties, including anti-inflammatory,[185, 194-196] antimicrobial,[185, 197] anticancer,[198, 199] antiviral,[200] and antioxidant[201] behaviour. The azomethane linkage makes Schiff bases

good chelating molecules due to their ability to provide a lone pair of electrons on a nitrogen atom.[186]

Although Schiff base molecules have a lot of applications especially in biological areas, the imine bond does have some limitations such as low water solubility and low stability in acidic media. The reduction of imines to amines is considered to be the best strategy to overcome these problems.[202] The rapidly growing interest in these ligands resulted in enhanced research activity in the field of their coordination chemistry, leading to complexes of high stability, good solubility and very interesting hydrogen bond donor qualities which enhance the possibility of biomolecule interaction.[202, 203]

The imine double bond of a Schiff base is readily reduced by complex metal hydrides.[204] Reduction of this type is probably the most efficient and convenient method for the conversion of C=N into amino compounds. Thus, lithium aluminium hydride[205] and sodium borohydride[206] can be used, the latter being a more effective reducing agent because of its inertness to a wider range of solvent media and because of its greater specificity.[207] Therefore in this work the reduction for the Schiff bases was performed with sodium borohydride.

2.1 Synthesis and characterisation of tach [2]:

Cis-tach was obtained by following the procedure reported in the literature.[178, 179] This method comprises of reacting *cis*-1,3,5-cyclohexanecarboxylic acid with diphenylphosphoryl azide (DPPA) in the presence of triethylamine, with benzene as a solvent. The tachcarbamate **[1]** was formed in good yield as a cream coloured precipitate. The benzyl protecting group was then cleaved by using strongly acidic conditions such as hydrobromic acid to give the hydrobromide salt of cis-tach, **[2]**HBr, summarized in Figure 2.3.

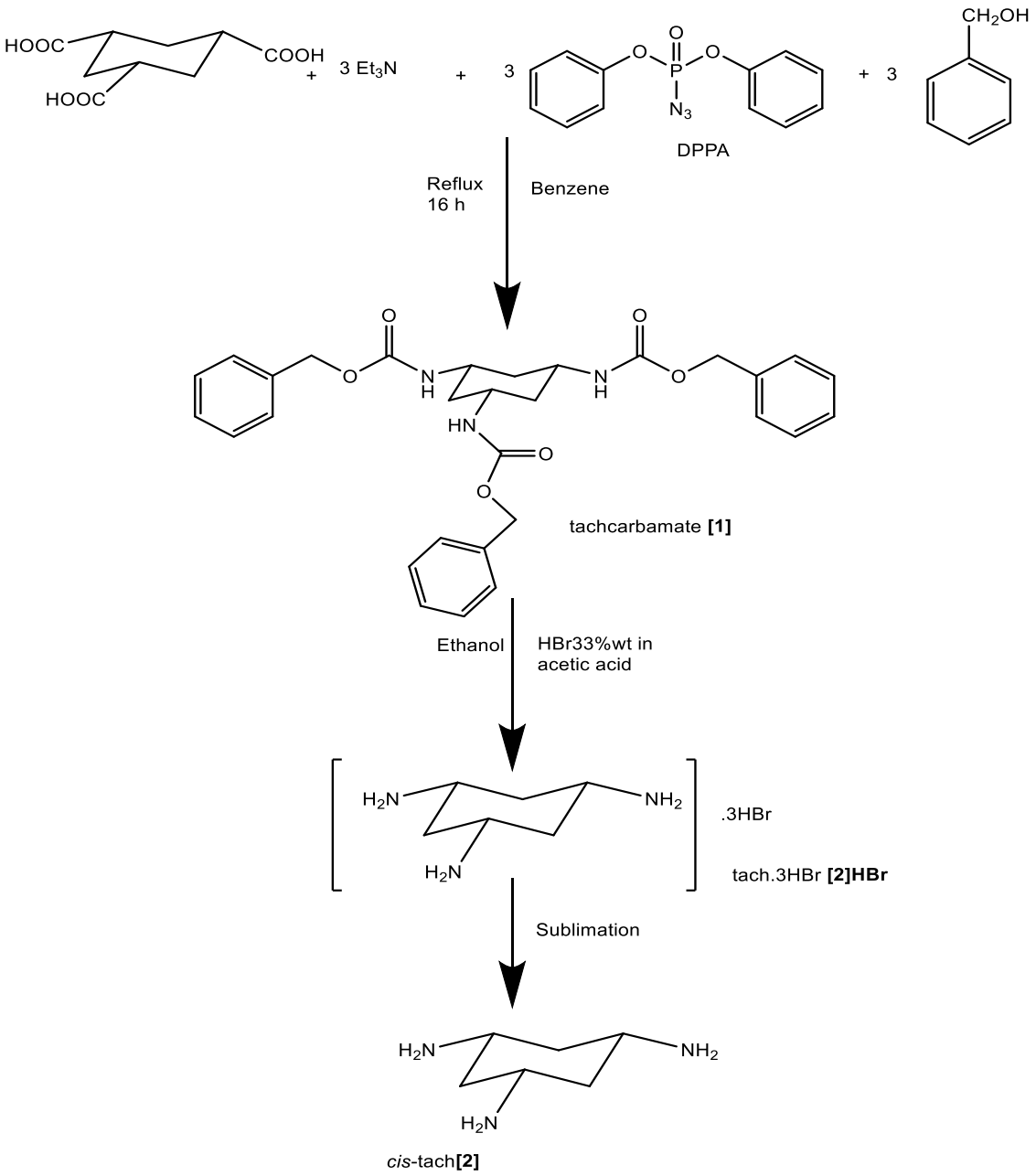

Figure 2.3: Synthesis scheme for cis-tach [2]. [178, 208]

Base-free *cis*-tach **[2]** was isolated after removing the hydrogen bromide by passage down an ion exchange column followed by sublimation, and was collected as a bright white solid.[209]

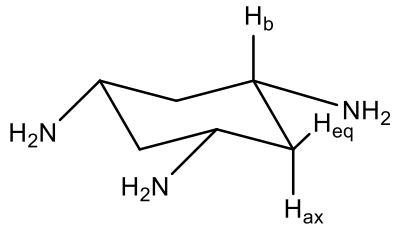

Figure 2.4: Free tach [2] structure.

It is possible to identify the symmetry of the cis-tach ligand from the nature of the resonances in the ^{1}H NMR spectrum. Both the number of signals and the magnitude of the coupling constants can be explained by an analysis of the structure**.** The symmetry environment of the cis-tach can be identified from the ^{1}H NMR resonances, (Figure 2.5).

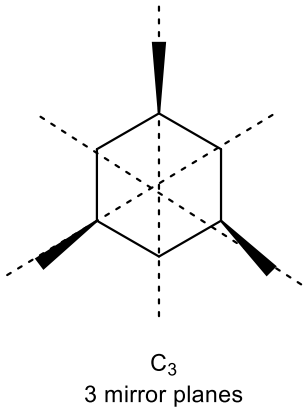

Figure 2.5: The possible symmetry environments for free tach [2] ligand.

The ^{1}H NMR spectrum of the tach molecule shows only three environments, while the amine protons resonances are not observed due to fast exchange with the solvent. The non-equivalent proton resonances suggest a C_3 symmetry centre, (Figure 2.4). The most deshielded proton is *b* due to its two-bond proximity to the electronegative nitrogen atom of the amine. The signal appears as triplet of triplets at 2.78 ppm, with a large coupling constant (ca. 12 Hz) to the two equivalent axial protons $\mathbf{a_{ax}}$ and the small coupling constant (ca. 4 Hz) to the two equivalent equatorial protons $\mathbf{a_{eq}}$.

The two other signals at 1.95 and 0.9 ppm are for geminal protons $\mathbf{a_{eq}}$ and $\mathbf{a_{ax}}$ respectively. The $\mathbf{a_{eq}}$ proton has a large *J* geminal coupling of ≈12 Hz with the $\mathbf{a_{ax}}$ proton. Proton $\mathbf{a_{ax}}$ appears as a quartet signal due to both axial-axial and geminal couplings being similar in magnitude.

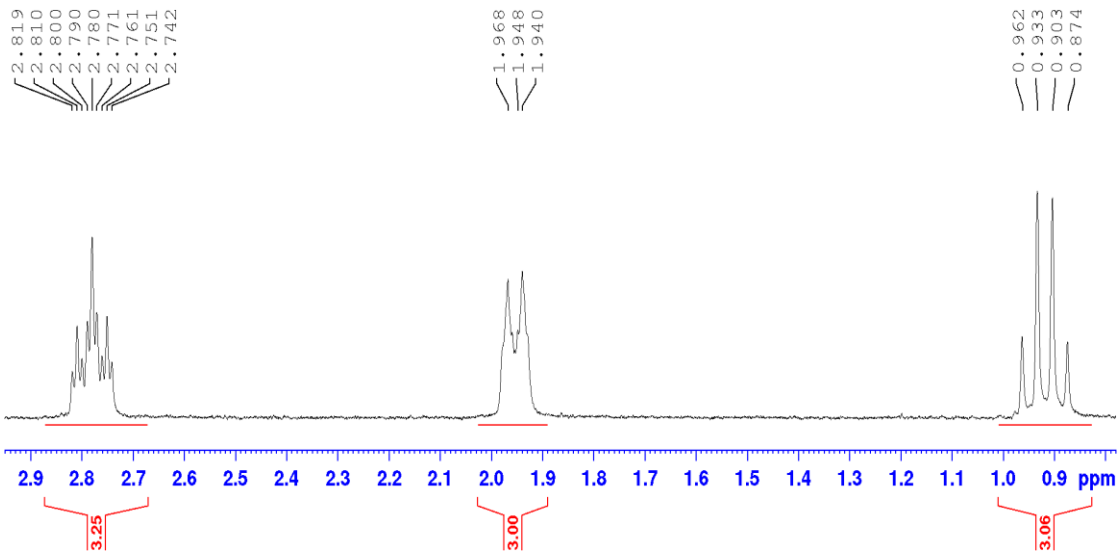

Figure 2.6: ^{1}H NMR spectrum of free tach [2] in D_2O.

It was clear from the ^{1}H NMR spectrum and multiplicities that the tach protons have an equatorial conformation in solution.

2.2 Synthesis and characterisation of tachmb [3] ligand

The synthesis of the mono-substituted tach compound was targeted in order to understand the importance of the monofunctionalised substituents on the biological activity. The presence of substituents may either alter the level of solubility or affect

hydrogen bond interactions, which are by far the most important specific interactions in biological recognition processes.[210] Several SAR (structure-activity relationship) examples from medicinal chemistry research illustrate the points made above.[211] The structure of *cis*-tach opens the possibility of adding different substituents on all of the three amines, however, the trisubstituted tach possesses high cytotoxicity compared to the non-substituted ligand which has much lower biological activity. This result provides support for synthesis of the monosubstituted analogue and benzaldehyde was chosen because the aromatic rings can act as acceptors of hydrogen bonds and interact with biomolecules. Furthermore, the varying biological activity between the mono-armed tach with the free-tach could be investigated, providing a comparison between their different complexes.

For the preparation of modified tach, the two amine groups in the tach **[2]** first needed to be protected. Therefore, the first synthetic step was the protection of two out of three tach nitrogen atoms by reaction with di-*tert*-butyl dicarbonate (Boc_2O), (Figure 2.7).

The tach.diBoc **[3-a]** was prepared following the reported literature procedures.[178] Here, two equivalents of triethylamine were added to one equivalent of tach.3HBr in methanol solvent. A dilute solution of Boc anhydride in methanol solution was then slowly added drop wise overnight to the tach.3HBr solution.

The reason for adding the Boc_2O very slowly was to prevent as much as possible the formation of tri-substituted tach. The solvent was then evaporated and the residue dissolved in water (pH=10). The tach.diBoc was extracted with ethyl acetate, leaving the unreacted tach and triethylamine in the aqueous layer. The organic layers were dried over $MgSO_4$ and the di-protected product **[3-a]** was isolated as a white solid in good yield. The NMR spectrum showed complete selectivity for the tach.diBoc **[3-a]** due to the presence of characteristic signals in the ^1H NMR spectrum. These resonances include the signal of an NH proton that appeared at low field region (6.9 ppm) due to coordination to the carbonyl group, and the appearance of a signal corresponding to the tert-butyl protons (1.4 ppm integrating for 18 protons) indicating

the presence of two protecting groups. Furthermore, a peak at m/z 330.2388 was observed in the ESI-MS for the di-protected compound [M] + H^+. It is worth noting that a small peak for the tri-protected tach was usually also present in the positive mode high-resolution ESI-MS at m/z 430.2898. However, the presence of a small amount of this compound was not considered to be a problem, as in the next synthetic step it cannot react with the benzaldehyde, and in the deprotection step it will be hydrolysed from the Boc group releasing free tach.

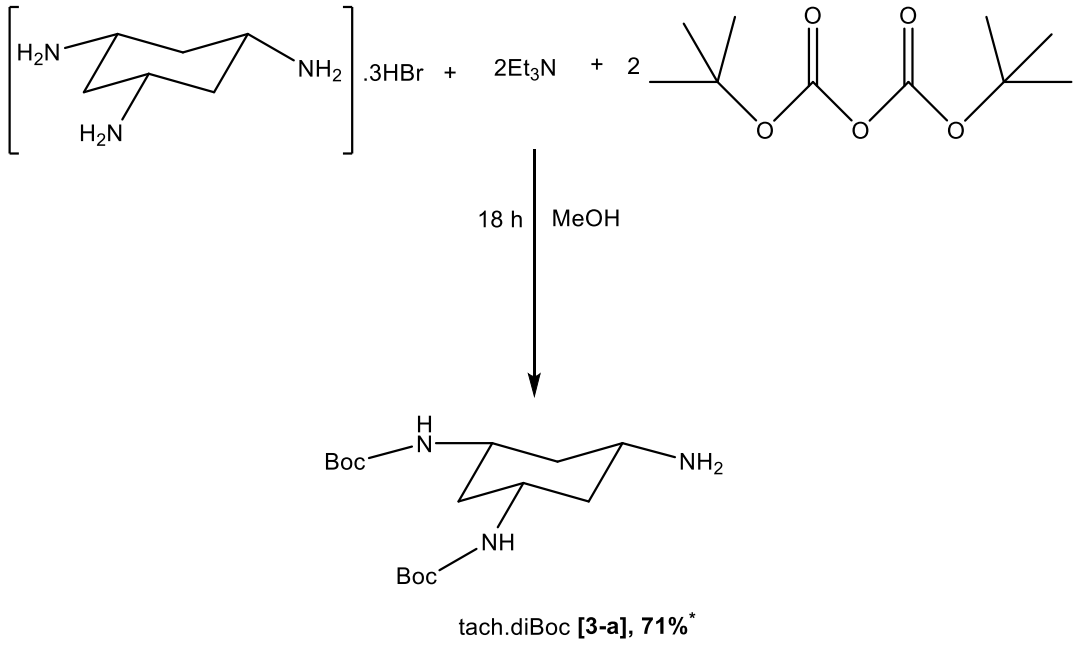

Figure 2.7: Synthetic scheme for tach.diBoc [3-a]. *Isolated yield.

One equivalent of benzyldehyde was added to the tach.diBoc **[3-a]** in methanol as a solvent and the reaction mixture was stirred at room temperature for 24 hours. The ^1H NMR spectrum showed the presence of unreacted aldehyde which implied the reaction was not complete. The reaction was therefore heated at reflux in toluene, with a Dean–Stark apparatus used to remove the water which was produced as a by-product (as the removal of water minimises the reverse hydrolysis reaction). After 18 hours, only a small peak for the desired compound was observed in the ESI-MS, in

addition to another unexpected peak for disubstituted compound at m/z 405.25. Due to this signal, it was suggested that heating may cause a cleavage of one Boc group. Therefore, the reaction was repeated at room temperature in methanol solution and molecular sieves were added to drive the reaction forward (by removal of water that is produced during the formation of Schiff base). The ESI-MS spectrum showed clear evidence for the Schiff base compound **[3-b]** at m/z 418.27. In the final step, the solvent was evaporated to leave a white solid which was washed three times with diethyl ether.

The presence of the Schiff base compound **[3-b]** was indicated by the appearance of a characteristic singlet signal for the imine proton in the ^{1}H NMR spectrum at low field, typically at 8.26 ppm in $CDCl_3$, and the emergence of the benzyl protons resonances in the aromatic region at 7.6 ppm. Each of these signals implies the successful coordination of a benzyl substituent, while the presence of the tert-butyl and coordinated NH protons are clear evidence of the existence of the protecting groups.

The imine bond in **[3-b]** was reduced with sodium borohydride, which was slowly added to a solution of tachmonoimbenz.diBoc **[3-b]** in methanol with stirring at room temperature for 16 hours, (Figure 2.8). An extraction with chloroform gave tachmonobenz.diBoc **[3-c]** in high yield (78%) and high purity.

The resulting ^{1}H NMR spectrum of **[3-c]** showed the disappearance of the imine signal with the corresponding appearance of the methylene signal at 3.72 ppm.

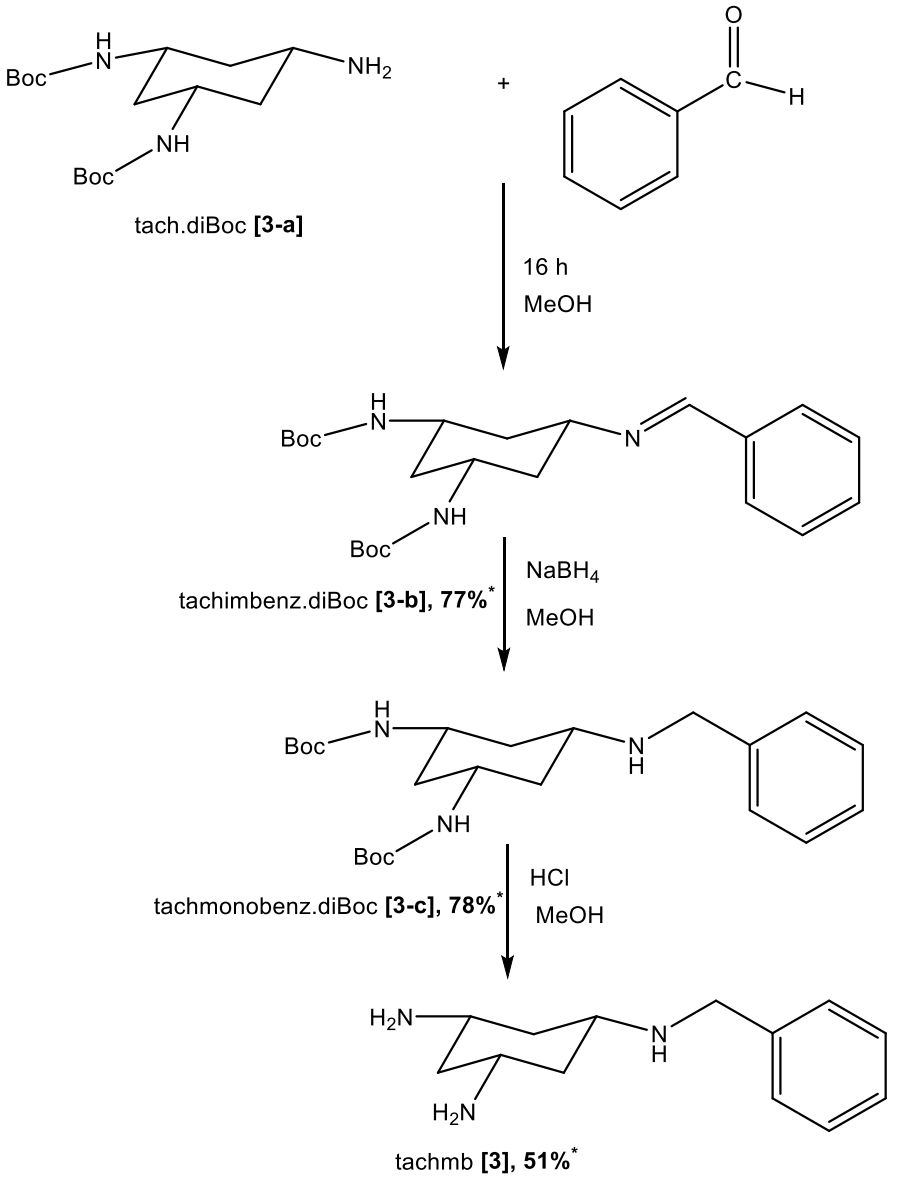

Figure 2.8: Synthetic scheme of tachmb [3]. *Isolated yield.

The last step for the synthesis of tachmb **[3]** was the deprotection step of the tachmonobenz.diBoc **[3-c]**. The hydrolysis of Boc was performed using concentrated HCl which was added to the solution of tachmonobenz.diBoc **[3-c]** in methanol and stirred for 3 hours. The solvent was then evaporated and the residue was taken up in

to acidic water (pH=2) and extracted with ethyl acetate. The organic layers were discarded, and the pH of the aqueous layers was modified to pH 14 and then extracted with dichloromethane.

The final yields were usually low (approx. 45%). The ESI-MS showed evidence for the tachmonobenz **[3]** at m/z 220.18 and no peaks for the di-substituted compound were present.

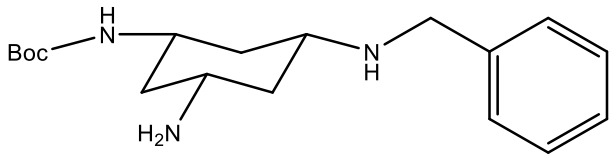

Tachmonobenz.monoBoc [3-I]

Figure 2.9: Structure of Tachmonobenz.monoBoc [3-I].

When the deprotection reaction with HCl was performed on a large scale (0.6 mmol) the ESI-MS showed a peak for **[3-I]** compound, (Figure 2.9), at m/z 320.23 implying that the reaction was not complete. For this reason, the reaction was repeated again but it was left to stir for 18 hours in an ice-bath. Increasing the reaction time caused problems due to the hydrolysis of the benzyl arm of the ligand. However, the yield increased slightly to 51 % and full characterization showed clear evidence for the tachmb **[3]**. The ^{1}H NMR spectrum showed the characteristic mono-substitution pattern (Figure 2.10). Using ^{1}H NMR spectroscopy, it is possible to demonstrate the difference between tach signals, **[2]**, to the benzyl substituted ligand, **[3]**. The benzyl-arm of ligand **[3]** causes the loss of C_3 symmetry and introduces a new C_s symmetry to the molecule. This leads to two sets of signals for each of the tach protons contained in the mirror plane and one for the others. The aromatic protons of the phenyl ring appeared at 7.26 ppm (Figure 2.10), and the COSY NMR spectrum (Figure 2.11), highlights the coupling between the tach protons.

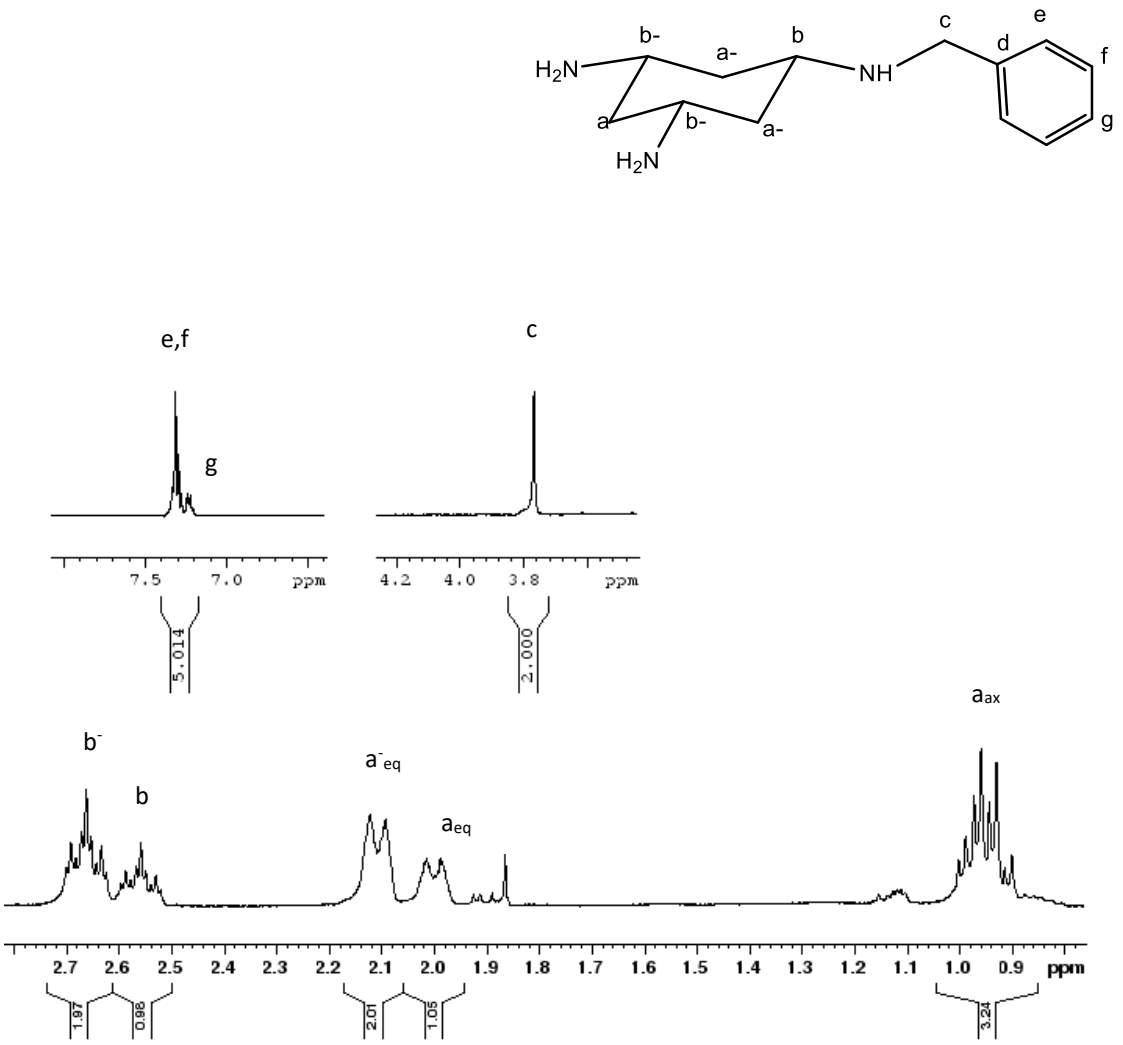

Figure 2.10: ^{1}H NMR spectrum of tachmb [3] in d_4-MeOH.

It is possible to explain the splitting pattern of the aliphatic signals observed. The most deshielded protons **b** and **b**$^-$ at 2.7 and 2.5 ppm respectively, appear as triplet of triplets due to large geminal coupling (12.2 Hz) with the two axial protons $\mathbf{a_{ax}}$, $\mathbf{a^-_{ax}}$ and small coupling (4 Hz) with the two equatorial protons $\mathbf{a_{eq}}$, $\mathbf{a^-_{eq}}$, while the broad doublet of equatorial protons is a result of having the same coupling constant to both $\mathbf{a_{ax}}$ and **b**. Proton $\mathbf{a_{ax}}$ has two different coupling constants ($^3J_{ax\text{-}ax}$ = 12 Hz; $^3J_{ax\text{-}eq}$ = 4 Hz).

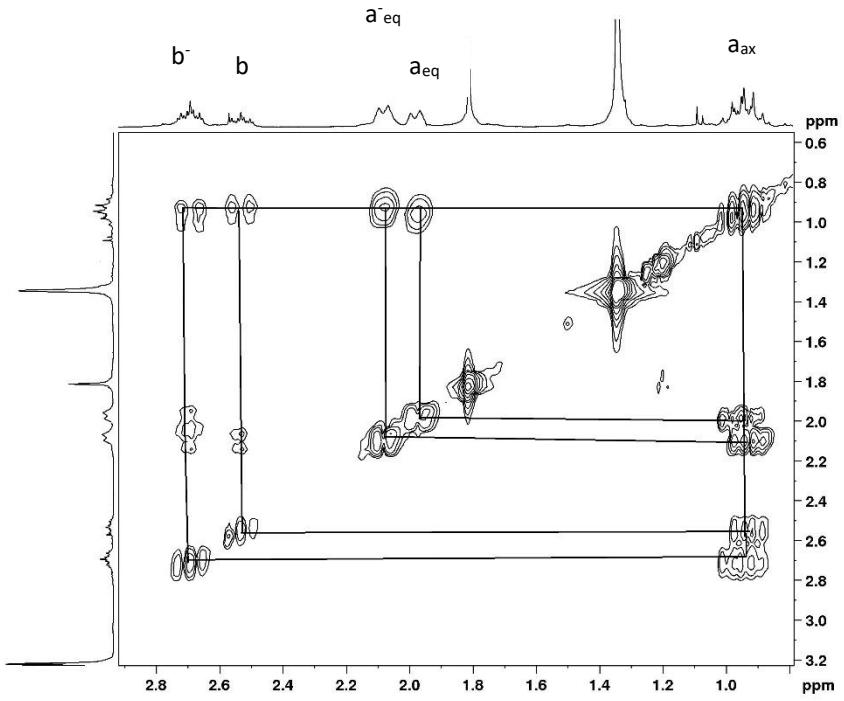

Figure 2.11: COSY NMR of tachmb [3](showing details of the aliphatic region only, recorded in d_4-MeOH).

The ^{13}C NMR spectrum, along with the DEPT 135 helped to assign the carbons bound to two protons (**a**,**a**$^-$) at 40.6 and 42.5 ppm for **a** and **a**$^-$ respectively. The carbon attached to only one proton, **b**, appeared at 43.5 ppm while **b**$^-$ resonated at lower field, 52.3 ppm, due to the proximity of the highly electronegativity amine groups. The most deshielded of the protons was for the quaternary carbon **d** which appeared at 140.3 ppm. The identity of this signal was confirmed by the disappearance of the peak in DEPT spectra (although the DEPT is quite weak) as shown in Figure 2.12.

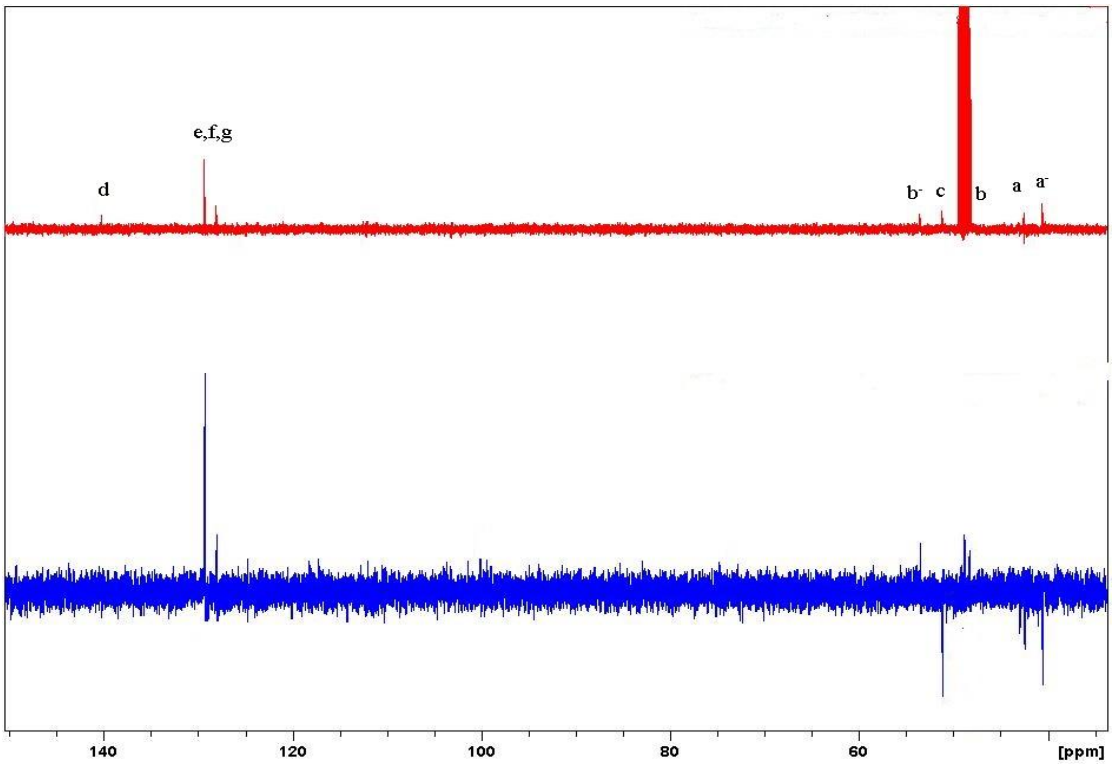

Figure 2.12: $^{13}C\{^{1}H\}$ NMR (top) and DEPT 135 (bottom) spectra for tachmb [3], recorded in d_4-MeOH.

A long-range correlations ^{1}H-^{13}C heteronuclear experiment HMBC, (Figure 2.13), then assigned proton **c** from its correlation with carbons **e** and **f** and quaternary carbon **d** in the benzyl substituent, and also highlights the coupling between proton and carbon atoms in the aromatic ring (**e**, **f**, **g**). The HMQC allowed to complete and confirm the assignment of the ^{1}H and ^{13}C spectra and illustrates the direct, one-bond coupling between each of the protons and carbon atoms, (Figure 2.14).

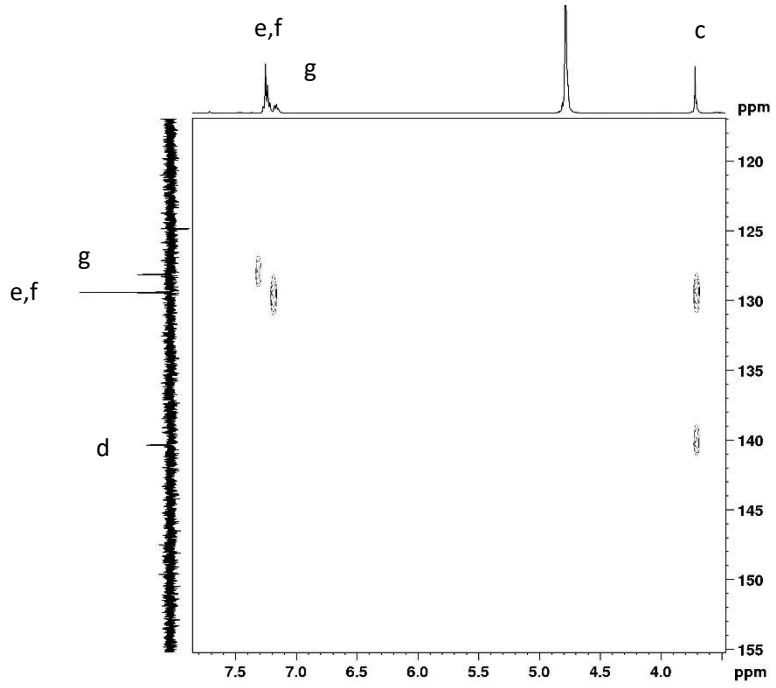

Figure 2.13: HMBC spectrum of tachmb [3], recorded in d_4-MeOH.

An ATR spectrum was recorded which showed all the stretching and bending of the secondary amine at 3340 and 736 cm^{-1} respectively and the bending at 1570 cm^{-1} assigned to the primary amine. The CH stretching and bending of the aromatic ring could be observed at 3059 and 698 cm^{-1} respectively.

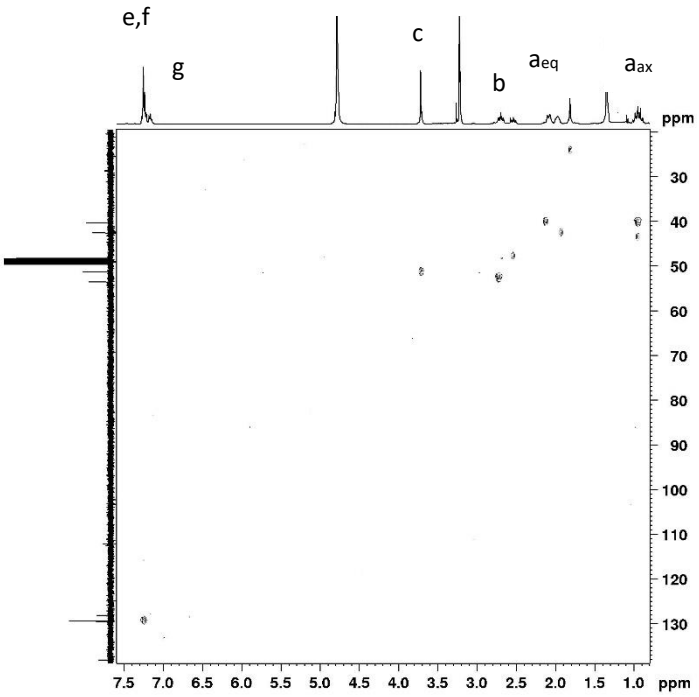

Figure 2.14: HSQC spectrum of tachmb [3], recorded in d_4-MeOH.

Several crystallisation methods were attempted to obtain single crystals suitable for X-ray diffraction, such as slow evaporation from methanol or water and methanol/ether diffusion, but all the attempts were un successful. The purity of the new ligand tachmb **[3]** was investigated by elemental analysis, which indicated the presence of water within the structure (also highlighted by ^{1}H NMR spectroscopy). As mentioned previously, the aim of the benzyl modification was to explore the contribution of the one-armed tach ligands such as **[3]** to antiproliferative activity. In order to perform this study, the high purity and good water solubility of **[3]** were essential qualities. The effect of compound **[3]** in two cancer cell lines was investigated by MTT assay (Chapter 5), and a study of the coordination of ligand **[3]** to ruthenium metal precursors can be found in (Chapter 3).

2.3 Conclusion

Developing the structure of *cis*-tach ligand **[3]** has been achieved by using benzaldehyde and following the Schiff base methodology. In order to selectively achieve a mono-substituted ligand, two of the three amine moieties were first protected using di-*tert*-butyl dicarbonate (Boc_2O) to obtain a tach-diBoc **[3-a]**. Further reaction with the aldehyde under anhydrous conditions allowed the formation of imine compound-tachimben **[3-b]** which has been reduced to mono-amine compound **[3-c]** using sodium borohydride. Reduction to the amine compound increases both the stability and solubility of the molecule. To achieve the final target, the Boc deprotection has been performed and the tachmben **[3]** has been isolated with 51% yield and high solubility in water. The new ligand has been characterized by NMR spectroscopy, mass spectrometry and IR spectroscopy and the purity was indicated by CHN analysis.

Chapter 3

Synthesis and characterization of

Ru(II)tachmonosubstituted complexes.

3 Synthesis and characterization of Ru(II)tachmonosubstituted complexes.

3.1 Introduction

Metal complexes consist of a coordination centre (which is a metal ion) and surrounding bound molecules or ions (known as ligands).[212] Coordination or metal chelation is an outstanding method to increase the lipophilicity of a ligand and hence the bioactivity profile might improve.[213, 214] On coordination to a metal, the inactive ligand may achieve pharmacological properties that turn it into a structure-selective binding agent for biomolecules or nucleic acids. Much research indicates that the pharmacological and medicinal activity depends strongly on the nature of the metal ion,[214] as metal complexes offer many possibilities for the design of different varieties of drugs which are not available to organic compounds.[215, 216] This versatility is due to a wide range of possible coordination numbers, geometries and oxidation states of the metal centre.[217, 218] Furthermore, the ability of metals to undergo ligand exchange reactions allows them to coordinate to, and interact with, biological molecules.[219] All of these properties have stimulated the research in medicinal chemistry field since the accidental discovery of cisplatin in the 1960s.[220, 221] Platinum-and ruthenium-based complexes are the most commonly studied transition metals in this field.[83, 222, 223]

Ruthenium metal complexes have attracted considerable attention in the pharmaceutical field, as they may overcome the negative aspects of platinum-based drugs.[92] Different Ru(II) and Ru(III) complexes have been prepared with amine, imine, dimethyl sulfoxide, diphosphine, and N-heterocyclic ligands that exhibit interesting DNA binding properties,[92, 99] however the main disadvantage of these complexes were their limited solubility in aqueous solution, hence the solubility of metal complexes are very important in administration and transport.[92] The most soluble, and most

successful, ruthenium-based anticancer complex is [*trans*-$RuCl_4$(DMSO)Im][ImH], NAMI-A, (Chapter 1) whose solubility is increased by presence of dialkyl sulfoxide ligands.[216, 224]

On the other hand, previous studies suggest that the presence of hydrophobic PPh_3 ligand in the complex sphere of Ru compounds such as RAPTA[tpp]-C and RAPTA[tpp]-O1, (Figure 3.1), results in more cytotoxic and less selective bioactivity, perhaps due to increased drug uptake.[99] Recent study of the influence of the triphenylphosphine moiety on several η^6-arene ruthenium (II) complexes of the type [Ru(p-cymene)Cl(PPh_3)(L)] (where L are pyridine derivatives), showed that the PPh_3 ligand leads to increased ruthenium complex antiproliferative activity in comparison to complexes lacking a PPh_3 ligand.[225]

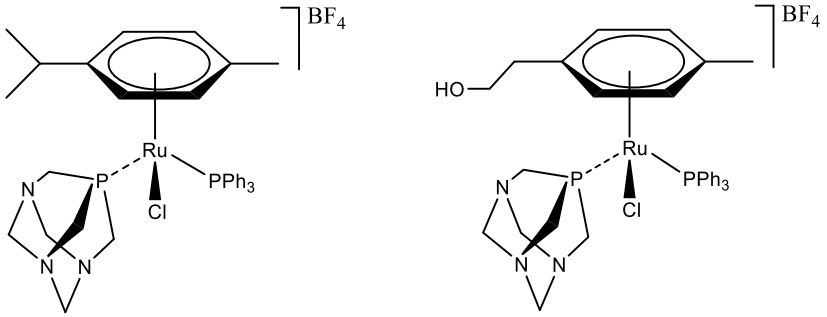

Figure 3.1: Structure of two RAPTA complexes, RAPTA[tpp]-C (left) and RAPTA[tpp]-O1 (right).

The use of phosphine ligands in anticancer complexes is favourable as these ligands have both σ-donor and π-acceptor character and are therefore able to stabilize metals in both high and low oxidation states.[226] Furthermore, biphosphine (P–P) ligands also play an important role in catalysis and in bioinorganic chemistry (which first started with gold(I) complexes).[227, 228] Ruthenium(II) piano stool complexes incorporating a chelating diphosphine ligand showed high activity in several human cancer cell lines,

(Figure 3.2), and have been investigated in several studies[229-232] ([(*p*-cymene)RuCl(p-p)], where p-p = dppm and dppe).[233]

Most recently, three new ruthenium complexes with general formula [Ru(Spym)(bipy)(P–P)]PF_6, [Spym = pyrimidine-2-thiolate; bipy = 2,2'-bipyridine; P–P = 1,2-*bis*(diphenylphosphino)ethane, 1,3-*bis*(diphenylphosphino)propane or 1,1'-*bis*(diphenylphosphino)ferrocene)] were synthesized and their *in vitro* antitumor activity was tested using the MDA-MB-231 human tumor cell line. All three complexes displayed a high degree of cytotoxicity, even higher than that of cisplatin at the same concentration.[234]

Furthermore, several ruthenium(II) *cis*-tach complexes have been prepared using different precursors with promising *in vitro* cytotoxicity against two cell lines: A549 and A2780 mentioned in Chapter 1. Two complexes with diphosphine ligands showed activity higher than cisplatin in the A549 cell line.

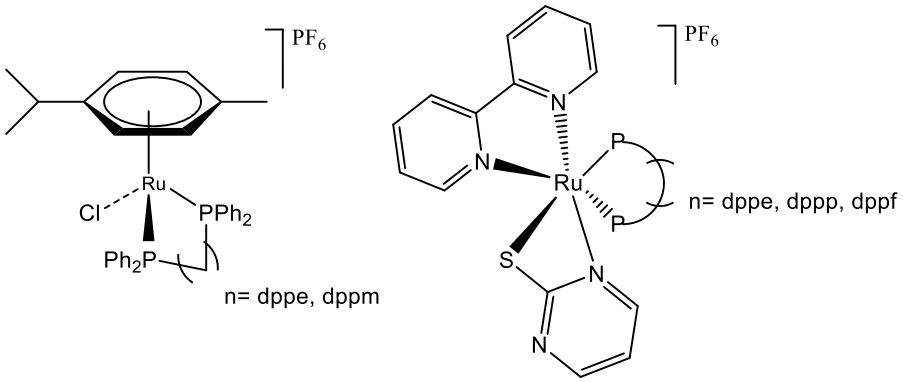

Figure 3.2: Structures of different ruthenium(II) diphosphine complexes exhibited anti-tumour activity [RuCl(p-cymene)(p-p)]PF_6 (left) and [Ru(Spym)(bipy)(P–P)]PF_6 (right)

In view of the facts above, it was thought worthwhile to explore the coordination chemistry of tachmonoben **[3]** to expand the library of this promising set of ruthenium complexes containing the tach ligand.

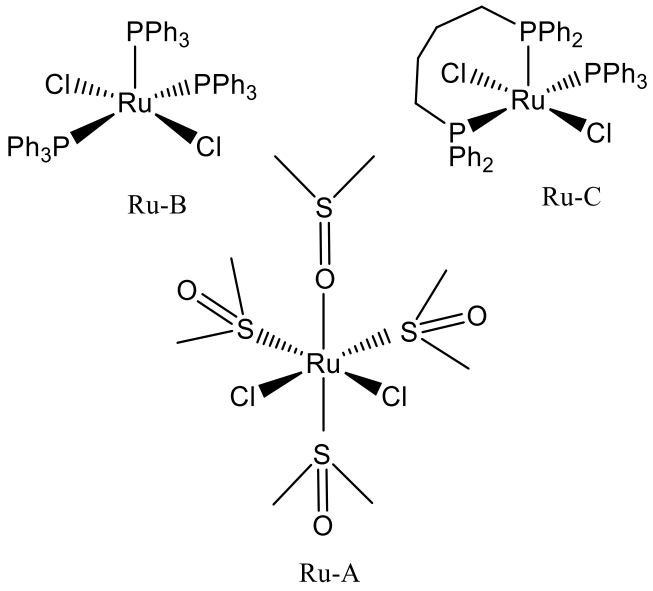

Figure 3.3: Three precursor Ru-A, Ru-B, and Ru-C used to synthesise new ruthenium(II)tachmb complexes.

With the aim of developing a potent complex with the modified tach ligand **[3]**, several ruthenium tachmb **[3]** complexes have been synthesised using different ruthenium precursors (Figure 3.3). Each of the metal precursors was chosen for a different reason. The well-known [*cis*-$Ru(DMSO)_4Cl_2$], **Ru-A**, had already shown *in vivo* activity against metastases and binding affinity to DNA.[102, 235] The formally sixteen electron complex [$Ru(PPh_3)_3Cl_2$], **Ru-B**, has a relatively labile ligand (triphenylphosphine) that allowes for additional donors to coordinate[236] (Figure 3.3). This precursor can coordinate different facially capping ligands such as tris(pyrazolyl)borate (Tp) and η^6-cyclopentadienyl (Cp) to produce [$RuCl(PPh_3)_2(X)$] (X = Tp and Cp),[237] and therefore was selected to coordinate with **[3].** Due to the background of promising biological activity for

ruthenium complexes containing diphosphine ligands mentioned earlier, the chemistry of **Ru-C** (containing a dppb ligand) was also investigated with modified tach ligand **[3]**. Upon coordination of ligand **[3]** to each of the ruthenium precursors, the resulting complexes were then studied in antitumor activity (Chapter 6).

3.2 Reaction of tachmonoben [3] with $[Ru(DMSO)_4Cl_2]$, Ru-I

The preparation of tach-containing ruthenium(II)DMSO complexes employs a widely used starting material [*cis*-$RuCl_2$(DMSO-O)(DMSO-S)$_3$], which is prepared directly from the reaction of $RuCl_3.3H_2O$ with DMSO as a solvent .[238] This strategy has been improved by Alessio to overcome the main drawback and achieve Ru(II) DMSO complexes in high yield (approx. 80%) and excellent purity.[102]

Gamble prepared [RuCl(cis-tach)(DMSO-S)$_2$]Cl by heating [cis-$RuCl_2$(DMSO-O)(DMSO-S)$_3$] with tach in DMSO at 130˚C for 30 minutes (Figure 3.4).[179, 180] It was proposed that the reaction of tachmonoben **[3]** with [cis-$RuCl_2$(DMSO-O)(DMSO-S)$_3$] would follow a similar route, so identical conditions to those of Gamble were employed for the reaction. After 30 minutes of heating at 130 °C, ethyl acetate was added to the reaction mixture in DMSO with cooling to -20˚C, however no precipitate was observed (as was seen in Gamble's preparation). Therefore, all of the solvent was evaporated to leave a yellow solid.

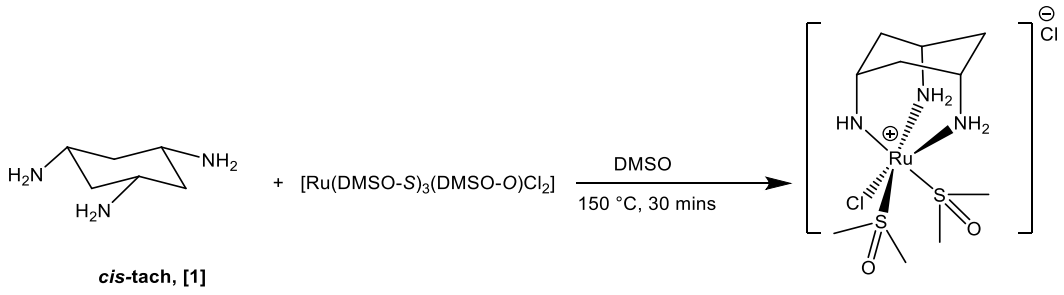

Figure 3.4: Synthesis of [RuCl(cis-tach)(DMSO-S)$_2$]Cl, [4] by Gamble.

The ^{1}H NMR spectra of the solid in deuterated DMSO solution did not appear to confirm that coordination of the ligand to the metal had occurred; the spectrum still exhibited the aromatic signals due to the benzyl ring of **[3]**, and also only a slight shift in the position of the tach protons signals was observed. Furthermore, the complexation was evidenced by the observation of small peak of the molecular ion peak in ESI mass spectrum (at m/z 512) with the expected ruthenium and chlorine isotope pattern.

Several crystallisation methods were attempted in order to isolate the complex and to obtain single crystals suitable for X-ray diffraction. Slow evaporation of a methanol solution of [RuCl(tachmonobenz)(DMSO-S)$_2$]PF$_6$ (obtained from chloride metathesis with sodium hexafluorophosphate) twice produced ruthenium-containing crystals. However, the crystals that appeared from both attempts were not those of the expected Ru(II) complex, but instead belonged to the starting material [cis-RuCl$_2$(DMSO-O)(DMSO-S)$_3$], **Ru-A**.

As these results were inconclusive, the complexation reaction between tachmb **[3]** and [*cis*-RuCl$_2$(DMSO-O)(DMSO-S)$_3$] was repeated in an NMR tube using deuterated DMSO solvent, so that the formation of the product could be monitored by NMR spectroscopy. The reaction was heated at 50 ˚C for two hour intervals, and the ^{1}H NMR spectrum was recorded every two hours to follow the reaction. The NMR spectrum showed noticeable change after the first two hours, but heating for more than two hours did not cause any further change. Full characterisation of the compound was performed by NMR and MS spectroscopy. The ^{1}H NMR spectrum showed two sets of signals for all the protons, (Figure 3.5).

As shown in Figure 3.5, the axial proton $\mathbf{a_{ax}}$ and the aromatic protons **e**, **f**, and **g** have two signals. The coordinated DMSO signals were too complicated to assign and again have more than two signals. Methylene proton **c** was expected to appear as a singlet but instead it existed as two singlet resonances. Moreover, the total integration of the protons gave more than the expected number of protons of only one complex, so it is

expected that two of the tach amine groups were coordinated with the ruthenium metal which leads to the presence of two or three isomers in solution.

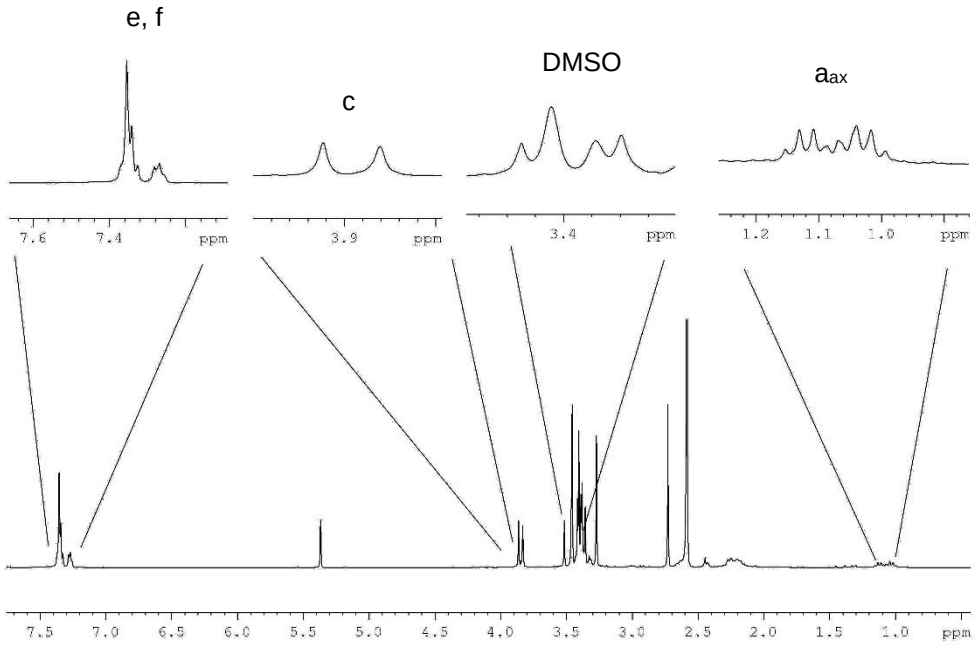

Figure 3.5: ^{1}H NMR spectra of the reaction mixture of [Ru(DMSO)$_4$Cl$_2$] and tachmb [3] in DMSO solvent after 2 hours at 50˚C.

Clear evidence for the isomer formation was given by ESI-MS. A peak was observed at m/z 565.12 (rather than at the expected m/z of 512) which corresponds to the [RuCl$_2$(tachmb)(DMSO-S)$_2$] compound. Therefore, it was presumed that these isomers were an intermediate for the reaction (Figure 3.6).

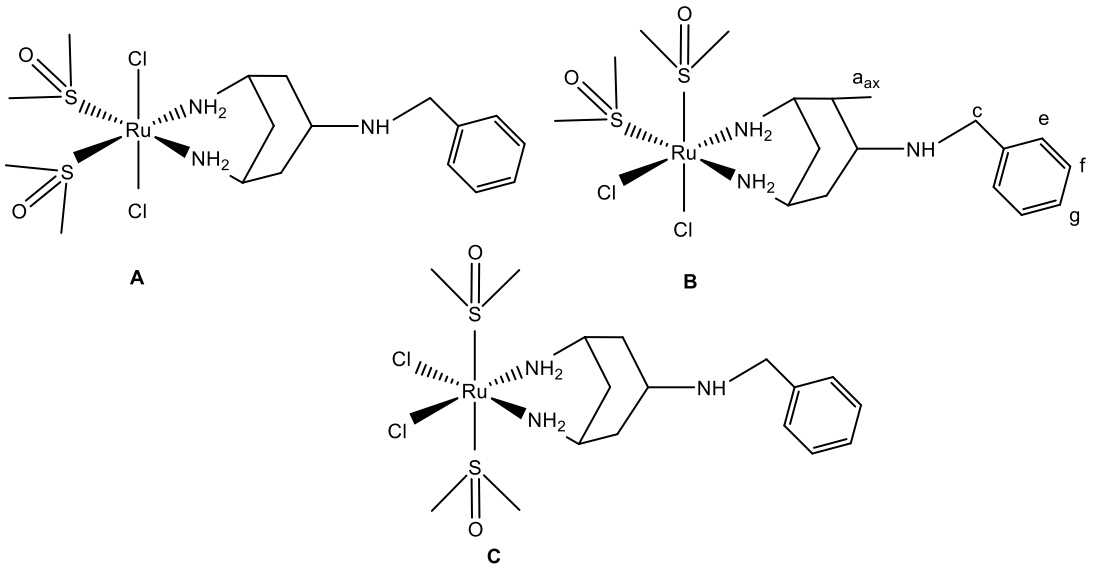

Figure 3.6: Proposed structure of [RuCl$_2$(tachmonoben)(DMSO-S)$_2$] isomers.

The complexation reactions were repeated again with the same solvent (deuterated DMSO) in an NMR tube but the temperature was increased to 130°C for 30 min in order to drive the reaction to completion. The ^{1}H NMR showed the disappearance of the two sets of the signals with small shift in proton signal and the appearance of a DMSO peak near 3.36 and 2.50 ppm but the integration showed more protons than expected. Furthermore, the ESI-MS showed an unexpected result. The peak with the greatest mass to charge ratio in the spectrum at m/z 538.6 was assigned to a dimer along with a small peak of the deuterated Ru-tachmonoben complex, so the protonated DMSO was used but the same result was found in both NMR and ESI-MS spectrum. Several crystallisation methods were tried in order to isolate the complex, slow evaporation of a methanol solution of the reaction mixture obtained from chloride metathesis with sodium hexafluorophosphate followed by filtration, gave crystals suitable for X-ray diffraction analysis. The obtained crystals did not belong to the expected ruthenium tachmb complexes, but to the ruthenium dimer shown in Figure 3.7.

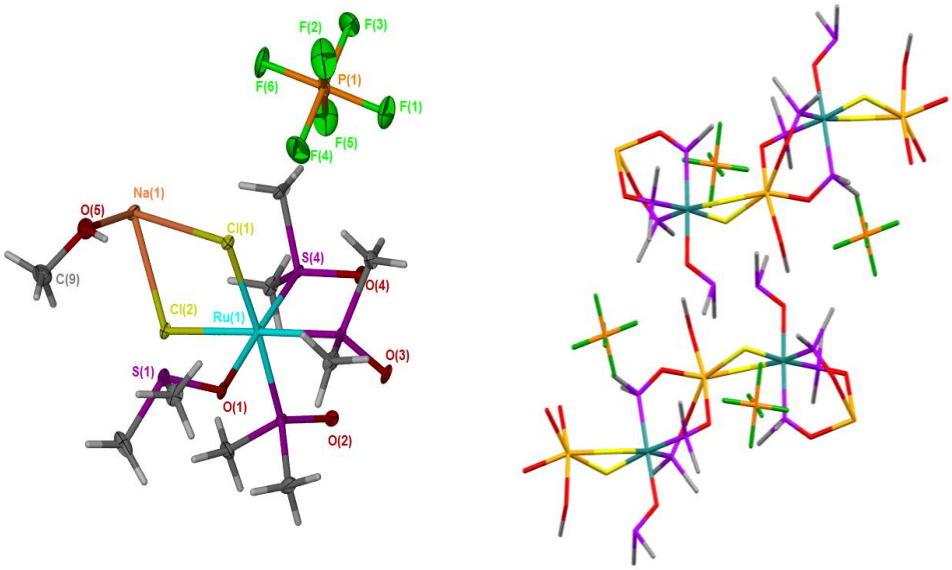

Figure 3.7: the asymmetric unit of Ruthenium dimer (thermal elipsoids are at 50 %) (Left) , and the unit cell which shows the packing in the crystal (right).

On the basis of these results, it was concluded that DMSO was not a suitable solvent for this reaction and choosing another solvent would be preferable.

The complexation reaction has been performed in different solvents (MeOH, THF and H_2O) and water was found to be the best solvent for the reaction of tachmonoben **[3]** and $[Ru(DMSO)_4Cl_2]$ as clearly evidenced by the ^1H NMR spectrum shown in Figure 3.8.

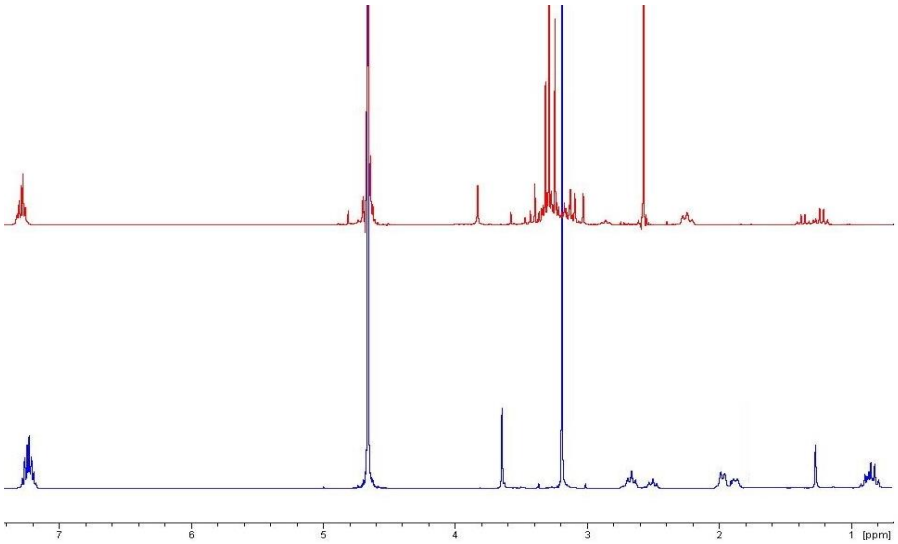

Figure 3.8: *^{1}H NMR spectra of the reaction mixture of Ru(II)tachmonoben,* ***[5]*** *(top) and tachmonoben,* ***[3]*** *(bottom) in D_2O solvent after heating for two hours.*

When both reagents were dissolved in D_2O, the ^{1}H NMR spectrum showed a small downfield shifting in the tachmb **[3]** resonances, while the ESI-MS spectrum did not show any peaks for the complex or Ru-fragmentations (only the free ligand was observed). Therefore, the reaction mixture was heated for 2 hours at 50 °C and followed by ^{1}H NMR spectroscopy. The heating was stopped when the colour changed to deep yellow. The NMR spectra showed that the axial and equatorial (**a**) tach protons had been shifted to 1.24 and 2.26 ppm respectively with a high ^{2}J coupling (14 Hz) between them. A resonance for coordinated DMSO at 3.2 and 2.3 ppm and the presence of the aromatic resonance suggested the coordination of tachmb **[3]** to ruthenium, so the solvent was evaporated to leave an oily residue which was recrystallized from methanol and diethyl ether and gave a brownish- yellow precipitate, dried under high vacuum in 66% yield. Clear evidence for the presence of the Ru-complex was given by LIFDI spectrum which showed the presence of [Ru(tachmonobenz)(DMSO)Cl_2], **[5]** at m/z 469.04 with the expected ruthenium and

chlorine isotope pattern (Figure 3.9) along with unknown small peaks at m/z 335.05 which leds to presume the presence of impurities.

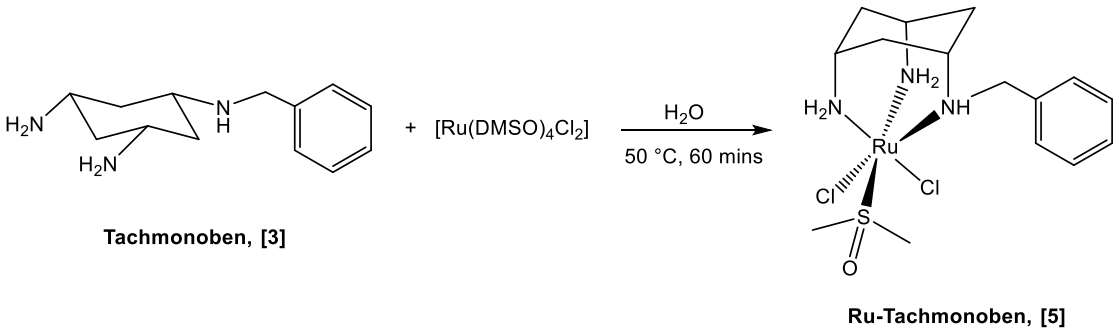

Figure 3.9: Preparation of [Ru(tachmonobenz)(DMSO)Cl₂], [5] in H₂O solvent

The ATR-IR spectrum provided further evidence for the presence and the coordination mode of the dimethylsulfoxide, in which the band appears at 1092 cm^{-1} at the same boundary for S-DMSO (1070-1233).[224]

In the ^{1}H NMR spectrum, the protons for the tachmb ligand exhibited resonances expected for a species in a C_1 symmetry environment around ruthenium metal (the symmetry was discussed in Chapter 2) which is different from the symmetry of the starting ligand that has a C_S symmetry, therefore it was hypothesised that a complex has been formed. In addition, the presence of two resonance for the DMSO methyl groups confirmed a C_1 symmetry. The C_1 symmetry possesses a one-fold axis so it is expected to present of all the ^{1}H environments illustrated in Figure 3.10.

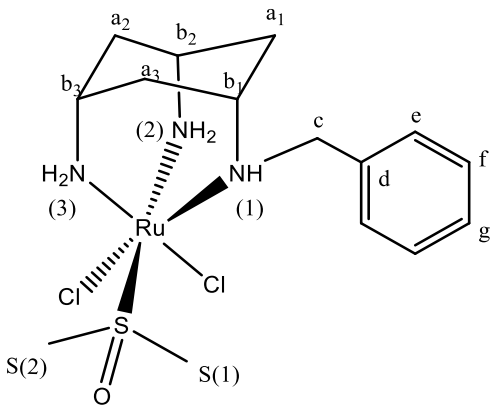

Ru-Tachmonoben, [5]

Figure 3.10: Scheme used for the characterization of Ru-tachmonoben , [5]

Although there is some overlap in the signal peaks, particularly in the regions from 3.0 to 3.5 ppm, the use of 2D NMR spectroscopy can improve this considerably. In the aliphatic region, the signal can be assigned by using the correlation spectroscopy (COSY) NMR that highlight the coupling between *CH* and CH_2 protons. Furthermore, it was possible to assign the coupling between amine groups which are also partially overlapping with other signals.

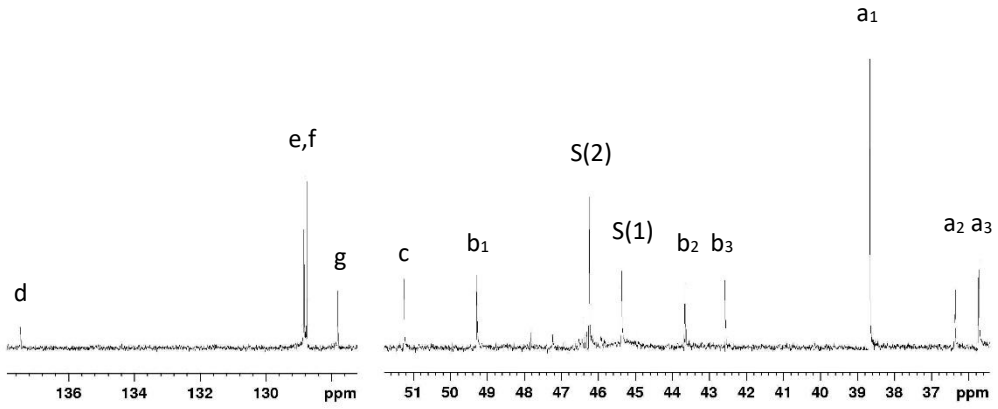

Figure 3.11: Part of the $^{13}C\{^{1}H\}$ NMR for compound [5] recorded in D_2O

The $^{13}C\{^{1}H\}$ NMR spectrum in Figure 3.11 presents, as expected, six signals to the *CH* and CH_2 protons for tachmb resonance and the CH_2 signals were confirmed by DEPT 135. The two inequivalent DMSO methyl groups and methylene proton **c** were assigned on the basis of HSQC NMR spectrum that highlights the $^{1}J_{H\text{-}C}$ couplings, correlating the protons to the carbon which they are bound to. The higher deshielding region shows three signals for the aromatic protons and the most deshielded signal at 137.4 ppm was assigned to **d** proton.

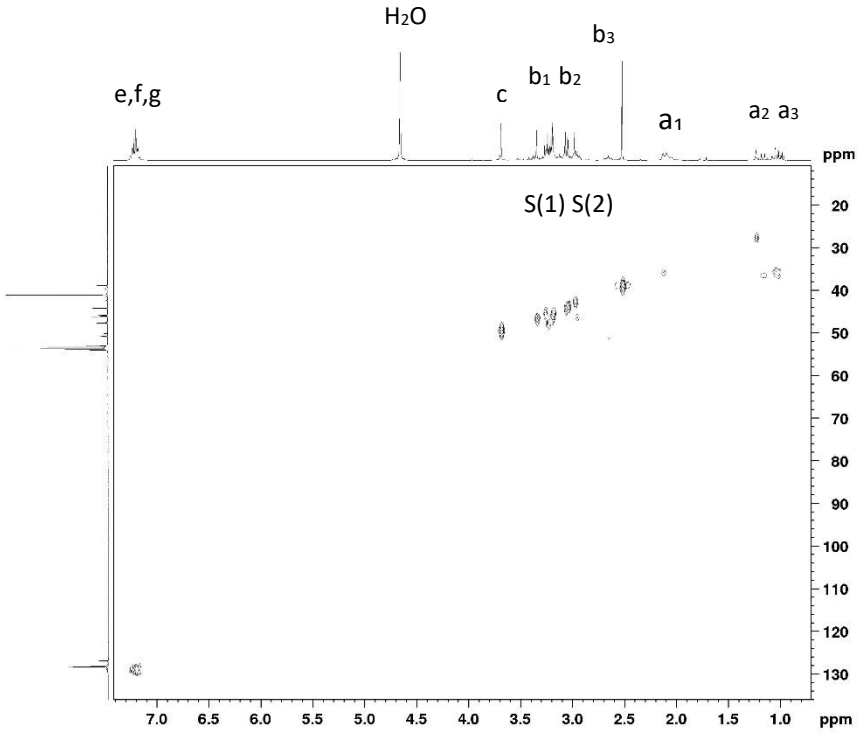

Figure 3.12: HSQC spectrum of [5] recorded in D_2O

Although the assignment for the resonance in **[5]** can be performed, the integration of the resonance in the crowded area was more than actual number of proton within the complex. This indicates that there are some impurities as highlighted before in MS spectrum and it was further confirmed by unsuccessful elemental analysis.

The complex could not be isolated with analytical purity, and a suitable crystal could not be obtained. Therefore complex **[5]** was excluded from biological evaluation carried out in Chapter 5, and also an alternative synthetic method must be explored.

3.3 Synthesis of Ru(II)tachmb triphenylphosphine complexes

As the preparation of a pure Ru(II)tachmb precursor was not achieved with $[Ru(DMSO)_4Cl_2]$, **Ru-B**, as precursor, the use of another ruthenium complex was required. Dichlorido-tris(triphenylphosphine) ruthenium(II) is a preferable complex as the electron deficiency around the ruthenium centre (16 electrons) induced ligand binding. Furthermore, the triphenylphosphine ligand is relatively labile which allows for coordination to another electron donor.[236]

In order to explore the reaction of the modified ligand tachmb **[3]** with $[RuCl_2(PPh_3)_3]$, the reaction was performed using the same conditions as for the corresponding reaction with cis-tach.[179] In a sealed NMR tube, one equivalent of tachmb **[3]** was added to $[RuCl_2(PPh_3)_3]$ in CD_2Cl_2 solvent. The colour changed from brown to orange then, after 10-15 min, a yellow solution was formed.

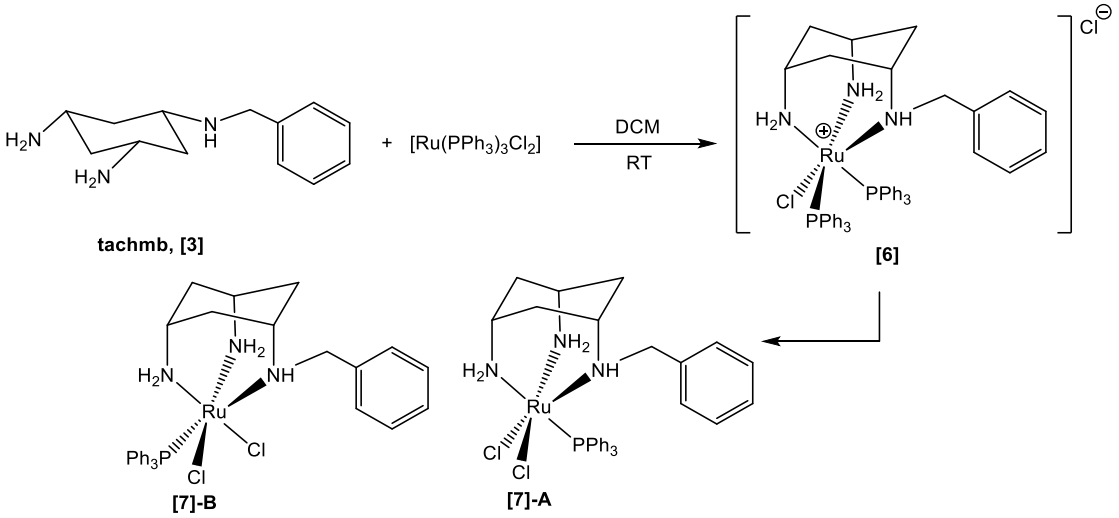

Figure 3.13: Synthesis of [Ru(tachmb)Cl₂(PPh₃)] [7] from the reaction of tachmb[3] and [Ru(PPh₃)₃Cl₂] in DCM.

The complex formation was monitored by ^{31}P $\{^1H\}$ spectroscopy and spectra were recorded every half hour (Figure 3.14). The first spectrum showed two doublet resonances at δ_p 36.3 and 46.7 ppm ($^2J_{pp}$ of 30 Hz), with two small singlet peaks at δ_p

61.5 and 67.4 ppm. In addition to a single sharp resonance at δ_p -11 ppm for the liberated triphenylphosphine, these spectra are distinctly different to the starting material spectrum which exhibits a broad resonance at δ_p 45ppm. The integrations showed a ratio of 1:2 for the liberated triphenylphosphane to the two doublets, suggesting two phosphine ligands remain coordinated to the metal as expected for $[Ru(tachmb)(PPh_3)_2Cl]^+$, **[6]**$^+$. After one hour, the intensity of the two doublet resonances decreased with a corresponding increase of the small single peaks, at 61.5 and 67.4 ppm suggesting that $[Ru(tachmb)(PPh_3)_2Cl]^+$ is an intermediate in the reaction and a new product was formed. After several hours the peaks for $[Ru(tachmb)(PPh_3)_2Cl]^+$, **[6]**$^+$ were no longer observed with the presence of the two single peaks in a ratio of half that of the liberated triphenylphosphine suggesting the displacement of a triphenylphosphine group of **[6]**$^+$and $[Ru(tachmb)Cl_2(PPh_3)]$, **[7]** is the product from the charge-neutralization occurring between the chloride anion and $[Ru(tachmb)(PPh_3)_2Cl]^+$, **[6]**$^+$ yielding the neutral complex $[Ru(tachmb)Cl_2(PPh_3)]$,**[7]** **(**Figure 3.14 and 3.15) and free PPh_3.

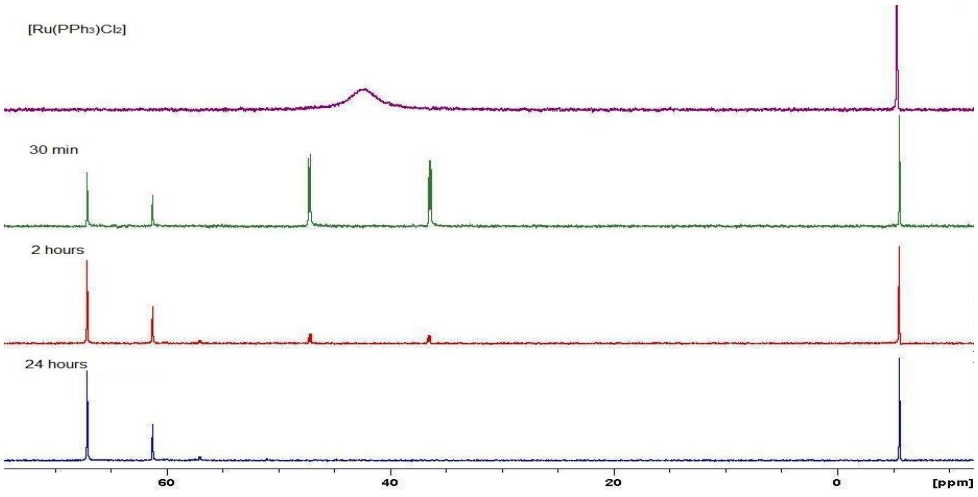

Figure 3.14: $^{31}P\{^1H\}$ spectra for the reaction progress of $[Ru(PPh_3)_3Cl_2]$ and tachmb[3] in CD_2Cl_2.

The identity of **[7]** was assigned by cross-peaks in the 2D ^{1}H-^{31}P correlation spectrum (HMBC) that show long range correlations (from ^{2}J to ^{4}J coupling) (Figure 3.10). The first singlet peak at δ_p 67.4 ppm has four cross peaks two with ortho and meta protons of phenylphosphine and the other two with amine protons of the tachmb ligand and the adjacent *CH* proton (**b**), while the second singlet peak at δ_p 61.5 ppm also has two cross peaks with phenylphosphine (ortho and meta protons) while the two others were assigned to substituted amine *NH* and methylene proton (**c**) bound to it. The 2D NMR confirms the presence of structural isomers of **[7]** depending on the orientation of the triphenylphosphine relative to benzyl and based on the cross peaks, the two isomers **A** and **B** were presumed. Isomer **A** is the main product based on the intensity of the phosphorus peak and the integration that shows 1:0.5 for the two peaks. Also, the trans isomer shows high coupling than cis isomer (Figure 3.15). It was possible to explain the different intensities based on the statistical distribution expected for **A** over **B** is 2 to 1 since there were a possibility to couple to two different NH_2 groups.

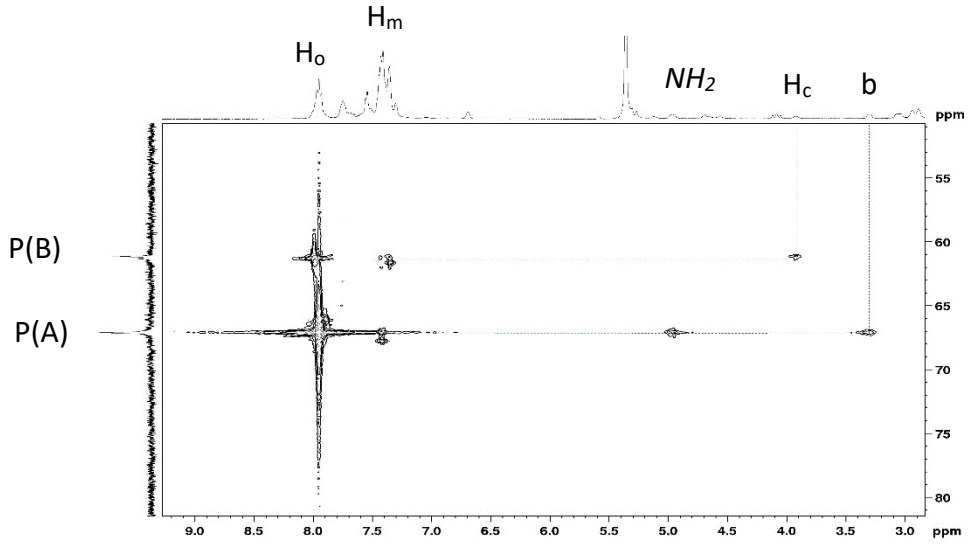

Figure 3.15: $^{31}P\{^{1}H\}$ spectra for the reaction progress of $[Ru(PPh_3)_3Cl_2]$ and tachmb [3] in CD_2Cl_2.

The conversion of complex **[6]** to **[7]** is further supported by LIFDI spectrum which exhibit high intensity peaks at m/z 880.24 immediately after mixing, with the expected ruthenium and chlorine isotope pattern assigned to **[6]**. Then, after 3 hours, one peak for [Ru(tachmb)Cl_2(PPh_3)], **[7]**, was observed at m/z 653.24.

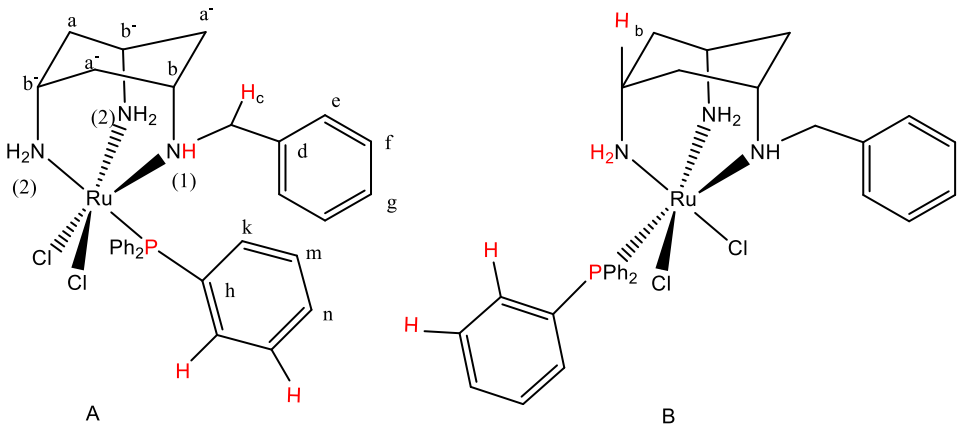

Figure 3.16: The two isomers A and B for [Ru(tachmb)Cl_2(PPh_3)],[7] with scheme used for the characterization for [7].

This assignment is in accordance with that reported for a similar reaction with cis-tach,[180] but the reaction with tachmb **[3]** was faster than cis-tach as the conversion from **[6]** to **[7]** was happened within 6 hours while [[Ru(*cis*-tach)Cl_2(PPh_3)] has formed after 2 weeks which may be a consequence of the bulkier tachmb **[3]** ligand assisting phosphine dissociation.

The tachmb **[3]** protons in ^{1}H NMR spectrum exhibited different resonances when interacting with [Ru(PPh_3)$_3$$Cl_2$]. The absence of axial-axial coupling ($^3J_{HH}$ = 10 Hz) with the existence of large coupling ($^2J_{HH}$ = 16.8 Hz), confirmed that the expected ring-flip on coordination to metal has occurred causing the appearance of a doublet for both $\mathbf{a_{ax}}$ and $\mathbf{a_{eq}}$ protons, suggest that the ring-flip has occurred and all amine groups are adopting an axial conformation. This is confirmed by the appearance of the amine

resonance at higher field (4.5-6.5 ppm) and this would occur only when amine groups coordinated to ruthenium metal in a K^3 fashion.

The ^1H NMR spectrum of **[7]** exhibited two sets of resonance belonging to the two isomers **A** and **B** that were presumed from the 2D ^1H-^{31}P NMR. The set of stronger signals indicates the formation of isomer **A** (major product) while the weaker one is assigned to isomer **B** (minor). The proton resonances from tachmb **[3]** or aliphatic groups were observed with considerable overlap in the high-field region from 1 to 3.5 ppm. By considering the heteronuclear (HMBC and HMQC) spectra and DEPT 135 spectrum this problem can be resolved (Figure 3.17), proton signals in this region were assigned to the resonance of *CH_2* and *CH* protons, while the signal observed at 3.8 ppm belongs to methylene proton **c** due on the observed cross peaks to **d** and **f** protons in phenyl arm in HMBC spectrum. The signals from 4.5 to 6.3 ppm were assigned to amine groups by disappearance of the cross peaks in 2D HMQC spectrum in comparison to the ^1H NMR spectrum. Nine resonances were observed for the tachmb ligand in the ^1H NMR spectrum **[7]** which suggests C_s symmetry around ruthenium metal. Furthermore, the single resonance for the coordinated phosphorus nuclei at 67.4 and 61.5 ppm indicates a C_s symmetry and free rotation of phenyl rings for each isomer.

The signals in the low-field region below 6.5 ppm were attributed to protons of aromatic rings. The assignment of carbon signals in this region were doublets for the carbon of the phenyl ring in (PPh_3) which is due to the ^{13}C nucleus coupling to a single ^{31}P nucleus and this confirmed the presence of only one triphenylphosphine ligand coordinated to the metal complex.

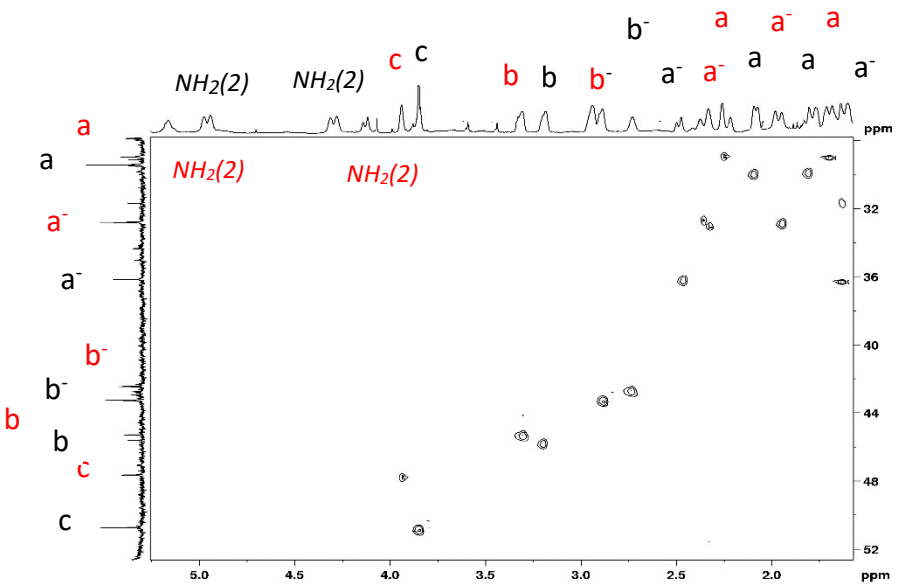

Figure 3.17: HSQC spectrum of aliphatic region [7] recorded in CD_2Cl_2, black (A), red (B).

Complex **[7]** was isolated by precipitation on addition of pentane to a dichloromethane solution (×3), giving a brown powder in good yield 64% and high purity as shown by elemental analysis.

3.4 Synthesis of Ru(II)tachmb diphosphine complex

To further develop ruthenium(II)tachmb complexes it was proposed to explore the coordination chemistry of [Ru(tachmb)Cl_2(PPh_3)], **[7]** with chelating diphosphine ligands. Therefore, a solution of **[7]** with an excess of dppp in CD_2Cl_2 was heated at 50°C in a sealed NMR tube and monitored by $^{31}P[^1H]$ NMR spectroscopy. The spectrum showed a new species with two doublet resonance at -20.5 ppm and δ_p 48.6 ppm and these resonances are coupled to each other by a $^2J_{pp}$ of 31 Hz. The resonance at -20.5

ppm is evidence of the coordination of the dppp in a κ^1 fashion (Figure 3.18). Further heating of the solution for two days in an attempt to obtain the target complex [Ru(tachmb)(dppp)Cl]Cl, resulted in no further change.

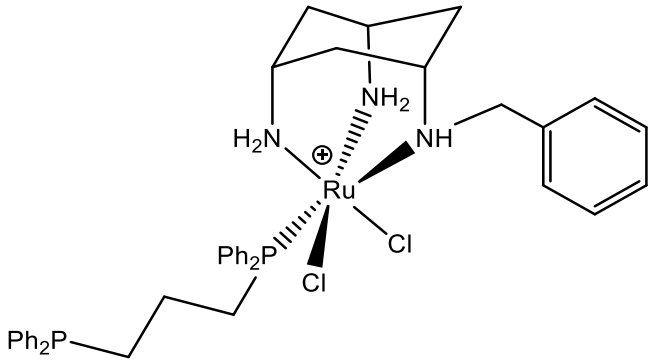

Figure 3.18: Proposed structure of the complex formed in the reaction between [Ru(tachmb)Cl$_2$(PPh$_3$)], [7] and dppp.

Due to problematic displacement of the chloride described above, an alternative synthetic method was sought to expand the library of Ru(II)-tachmb complexes, therefore it was suggested to prepare [RuCl$_2$(PPh$_3$)(P-P)] first then coordinate with tachmb **[3]**.

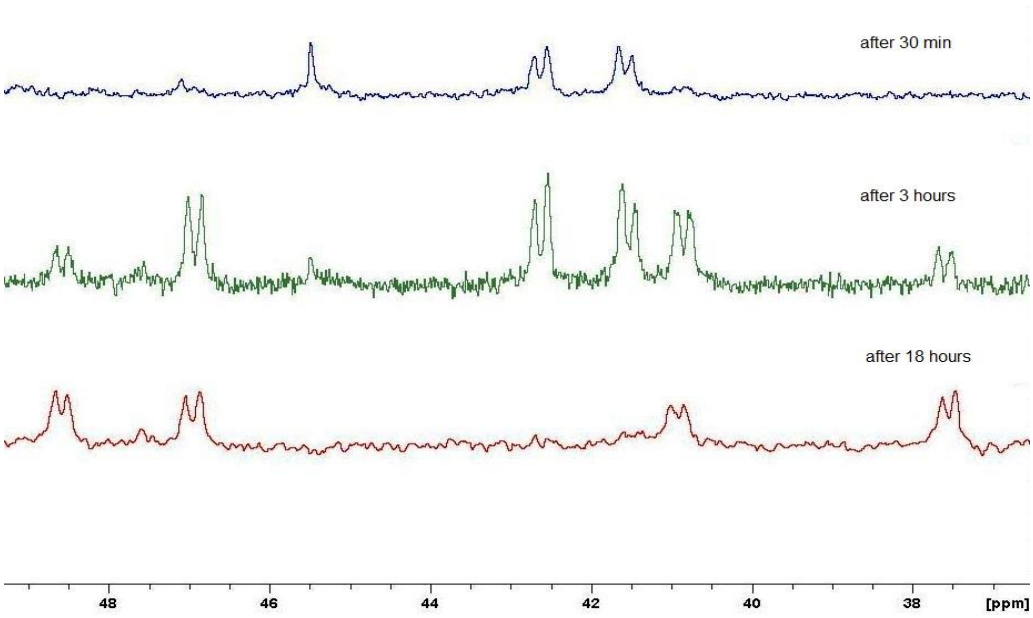

Figure 3.19: ^{31}P [^{1}H] spectra for the reaction progress of [RuCl$_2$(PPh$_3$)(dppb)], [8] and tachmb[3] in CD$_2$Cl$_2$.

The preparation of [$RuCl_2(PPh_3)$(dppb)], **Ru-C** was previously reported.[240] Reaction of two equivalents of tachmb**[3]** was performed with **Ru-C** in a sealed NMR tube in CD_2Cl_2, resulted in a colour change of the solution from deep green to yellowish-green. As illustrated in Figure 3.15 the $^{31}P\{^1H\}$ NMR spectrum of the solution exhibited two doublet peaks initially, then several doublet peaks in the region (35-50) ppm appeared that changed with time. After standing for one day the reaction appeared to reach completion and a yellow solution was formed. Spectroscopic evidence demonstrated the tachmb**[3]** has been incorporated within the coordination sphere by two of the nitrogen groups forming an intermediate **[8]** first (the same behaviour indicated previously), then transforming to **[9]**; the $^{31}P\{^1H\}$ NMR spectrum showed four characteristic doublet resonances at 35-50 ppm, in addition to singlet resonance at -4.90 ppm assigned to liberated triphenylphosphane, suggesting the coordination of (dppb) to the ruthenium(II) metal (Figure 3.19). These resonance were mutually coupled ($^2J_{pp}$ of 35.2 Hz), demonstrating inequivalent phosphorus nuclei within the complex and the presence of two structural isomers of $[Ru(tachmb)(dppb)Cl]^+$ [**9**] with respect to the phenyl arm (Figure 3.20). Further evidence for this compound was given by LIFDI spectrum that exhibited a peak for [Ru(tachmb)(dppb)Cl]Cl **[9]** at *m/z* 782.20 without any fragmentation or other signal, and with the expected ruthenium and chlorine isotope pattern.

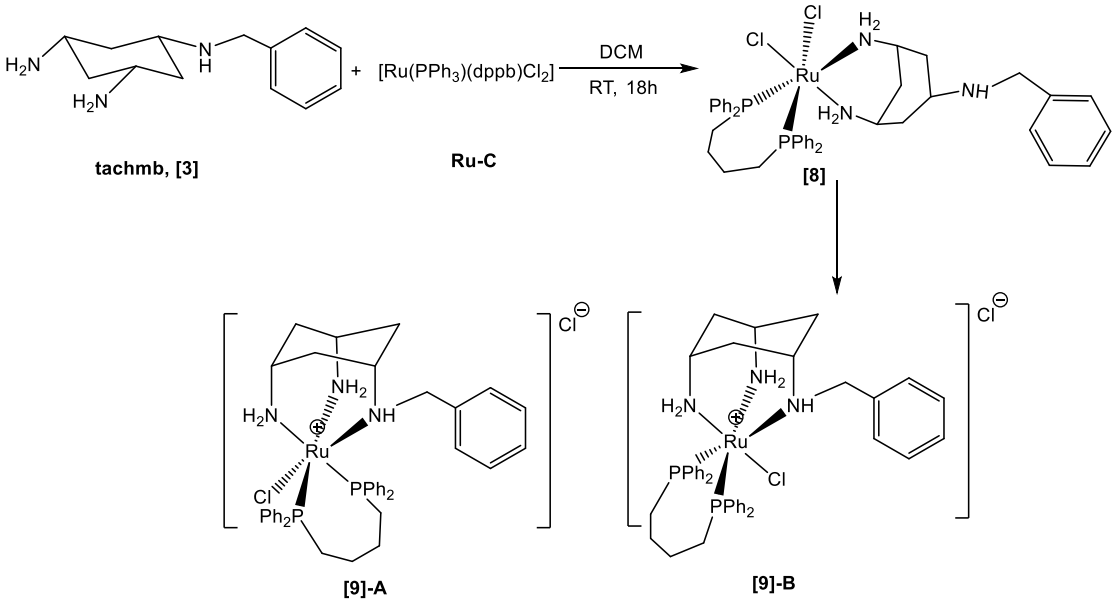

Figure 3.20: Synthesis of [Ru(tachmb)(dppb)Cl]Cl, [9]Cl from tachmb[3] and [Ru(PPh$_3$)(dppb)Cl$_2$] [8] in DCM solution

Although the ^{1}H NMR spectrum was very complex (Figure 3.21), it was able to provide an indication of the existence of the complex due to the presence of different resonance compared to the tachmb **[3]**. The spectrum showed the existence of the ligand signals and dppb signal, the presence of the coordinated amine resonances that appeared at low field region and the integration of the protons give the exact number of protons in aliphatic and aromatic regions. The assignment for each proton was difficult due to the decomposition of compound in solution thus 2D NMR did not give any helpful information.

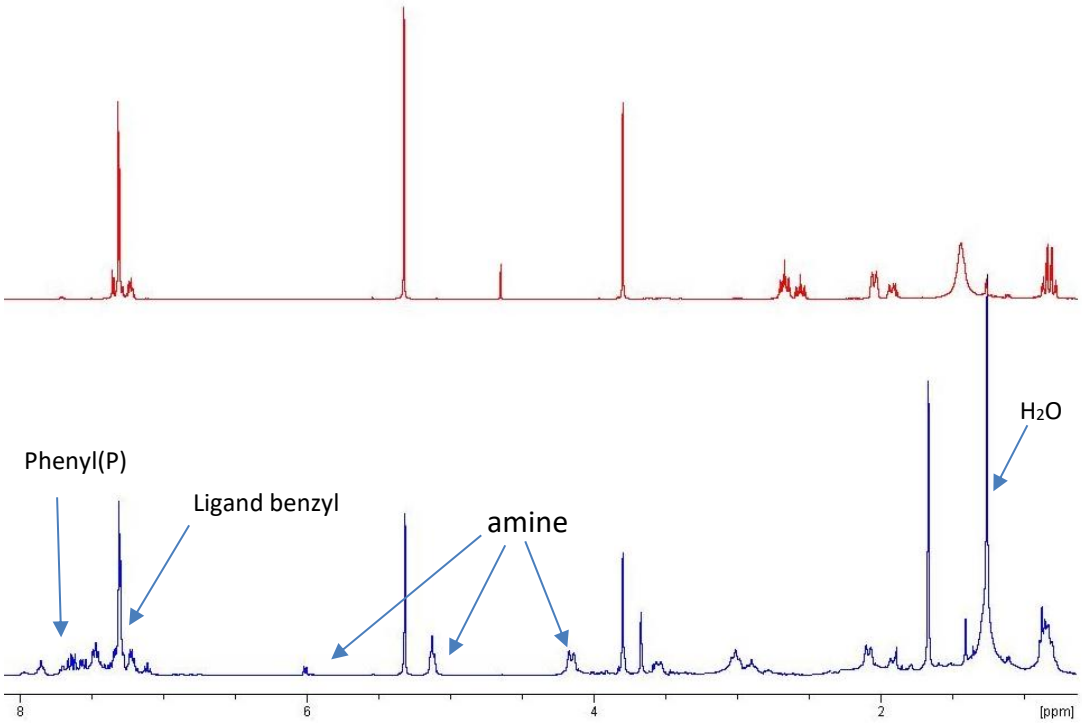

Figure 3.21: ^{1}H NMR spectra of Ru(II)tachmonoben, [9] (bottom) and tachmonoben, [3] (top) in CD_2Cl_2 solvent.

The cationic species for **[9]** is readily obtained without chloride metathesis with weakly coordinating anions such as hexafluorophosphate and this will provide extra advantage in clinical preparation and avoids incorporation of potentially toxic species. The complex was isolated with good yield 71% and the purity was indicated by CHN analysis with three water of crystallization. The solvent composition was also verified by the ^{1}H NMR spectrum.

3.5 Conclusions

The coordination chemistry of modified ligand **[3]** with ruthenium metal has been performed using different ruthenium complexes as coordination centres:

$[Ru(DMSO)_4Cl_2]$, $[RuCl_2(PPh_3)_3]$, and $[Ru(dppb)(PPh_3)Cl_2]$. Three complexes were obtained: **[5]**, **[7]** and **[9]** respectively.

Complex **[5]** was prepared and it was found that water was the best solvent for this reaction. This complex was isolated and fully characterized by a range of spectroscopic techniques but the purity could not be confirmed by elemental analysis.

Complex **[7]** was readily obtained in DCM solvent after charge neutralisation reaction for $\mathbf{[6]^+}$ within two hours. This complex was isolated with high purity and full characterization has been done that showed the presence of pairs of isomer **A** and **B** which are attributed to the different types of coordination modes between the metal and ligand. This behaviour was also observed for **[9]** and confirmed by ^{31}P NMR spectroscopy. Although this complex purity was approved by elemental analysis the characterisation could not be done due to the decomposition of the compound in solution.

Chapter 4

Biomolecule interaction of Ru(II)tach complexes

4 Biomolecule interaction of Ru(II)tach complexes

4.1 Introduction

Numerous ruthenium (II) complexes have been utilized in chemo and photodynamic therapy and have been certified by *in vitro* and *in vivo* studies,[92] since the discovery of two ruthenium(II) complexes $[Ru(bpy)_2(dppz)]^{2+}$ and $[Ru(phen)_2(dppz)]^{2+}$ that intercalate into DNA with the ability to act as a "light switch".[241, 242]

Anticancer compounds have a myriad of targets (DNA, proteins, membranes, etc.) and in fact the true potential mechanism responsible for the biological activity of any given compound is often difficult to determine.[243]

DNA represents a fertile target for metal complexes.[32, 243] In cancer cells, DNA can be preferentially damaged either through interactions with the sugar-phosphate backbone or coordination to the bases. Furthermore, non-covalent interactions with DNA lead to additional targets and more specificity by three modes of action (Figure 4.1): intercalation, groove binding and static electronic interactions.[244, 245] In static electronic interactions, the molecules interact with the negatively charged DNA double helix externally through a non-specific interaction. Groove binding refers to molecules that bind DNA in the base edges of the major groove or minor groove.[5]

The most commonly studied mode of action is intercalation, which is another DNA binding mode that is closely related to the antitumor ability of many anticancer compounds.[246] Intercalative binding is the non-covalent stacking interaction with the DNA double helix in a reversible manner resulting from the insertion of a planar heterocyclic aromatic ring between the base pairs of the DNA double helix.[247, 248]

Early work focused on intercalation by octahedral complexes containing at least one aromatic heterocyclic ligand for stacking, or partial intercalation, in between base

pairs.[249] One of the first classes of ruthenium complexes that was shown to interact with DNA included Ru(II) tris(phenanthroline) complexes and derivatives; these complexes had good chemical stability, high luminescence and an intense metal-to-ligand charge transfer (MLCT) band in the visible spectrum.[10] Many ruthenium(II) complexes with phenazine derivatives have shown promising results as DNA-linkers and interact with nucleobase pairs of the DNA, as the 1,10-phenanthroline presents a rigid and planar structure with a highly conjugated electron cloud.[250] In addition to all the properties noted above, Ru(II) complexes with a phenanthroline ligand display high redox potential, photo physical and photochemical properties.[249]

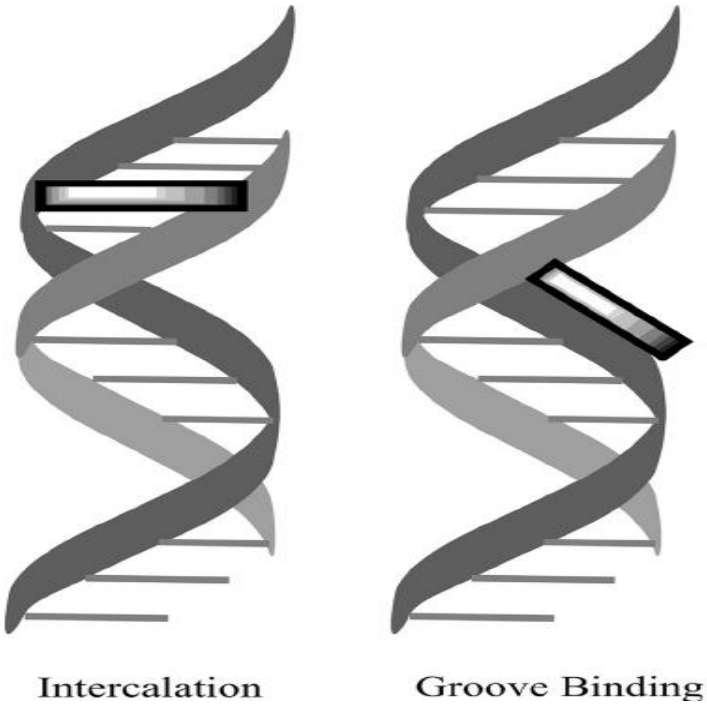

Figure 4.1: Non covalent interaction with a double helical DNA.

The polypyridyl ligands initially used were 2,2'-bipyridine (bpy), 1,10-phenanthroline (phen) and 4,7-diphenyl-1,10-phenanthroline (DIP)[251] (Figure 4.2). By studying the

difference in photophysical properties in the presence of DNA, it was observed that $[Ru(bpy)_3]^{2+}$ has little or no binding to the nucleic acid, while results for $[Ru(phen)_3]^{2+}$ and $[Ru(DIP)_3]^{2+}$ suggested that binding could occur by two possible modes: intercalative or electrostatic interaction depending on the chirality of the enantiomer of the complex, where the Δ isomer was able to intercalate, while the Λ isomer could only bind electrostatically, through interactions to DNA.

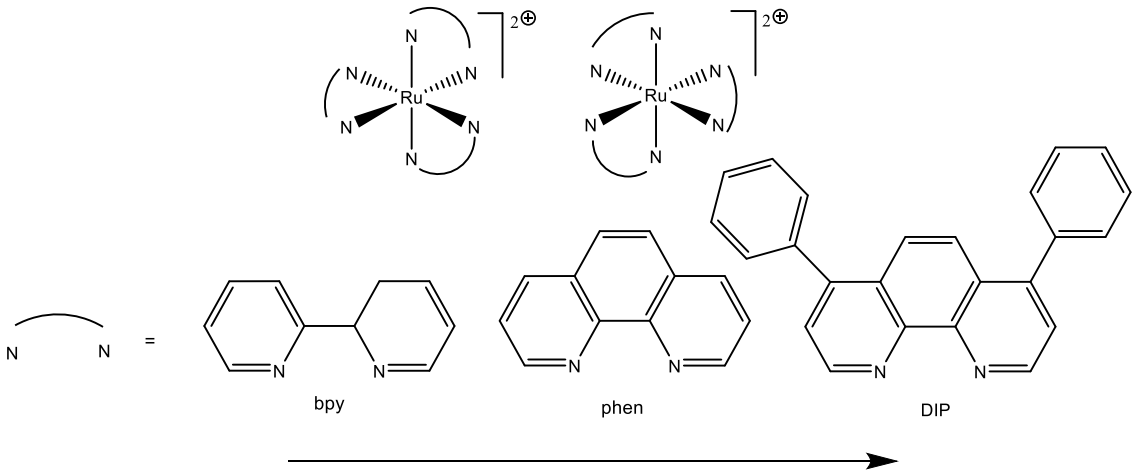

Figure 4.2: Ru (II) polypyridyl complexes.

The results suggest that the interactions with these nucleic acids are enantioselective, with the Δ enantiomer of the complex binding more favourably than the Λ enantiomer. This shows that the twist of the Δ enantiomer is a better fit to the right-handed helix sense of the DNA backbone,[249] and could therefore intercalate more effectively. Barton suggested an increase in ligand surface area would enhance the low binding affinity for these complexes for DNA (equilibrium binding constant K_b ~10^3 M^{-1}) (Figure 4.2).[252] Recently the synthesis of Ru(II) complexes that have ligands possessing a large aromatic surface area for intercalation such as dipyrido[3,2-a:2',3'-c] phenazine (dppz) and [2,3-h] dipyrido [3,2-a:2',3'-c] phenazine (pdppz) have been developed. Their ability to interact with oligonucleotides has been studied since the discovery of two ruthenium complexes by Barton and co-workers $[Ru(bpy)_2(dppz)]^{2+}$ and

$[Ru(phen)_2(dppz)]^{2+}$. It was reported that the dppz-based complexes bind to DNA with a high affinity (K_b~10^6 M^{-1})[241] and in the presence of DNA the luminescence was switched on, a property known as the "*light switch"* effect which is assigned to intercalation[253, 254] (Figure 4.3). A DNA light-switch compound is a compound that is non-luminescent in water but is able to luminesce in the presence of DNA. This property makes the complexes interesting as probes for cell studies using fluorescence microscopy.[255]

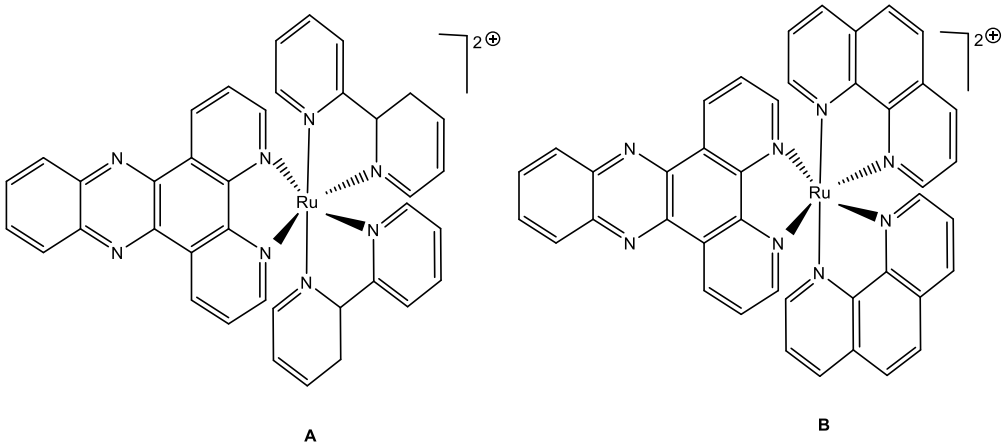

Figure 4.3: Structure of $[Ru(bpy)_2(dppz)]^{2+}$(A) and $[Ru(phen)_2(dppz)]^{2+}$(B).

Polypyridyl ruthenium complexes have also been used as intercalating photodynamic agents (Chapter 5).[256] To better understand the cellular behaviour of ruthenium(II) arene complexes, which are promising anticancer compounds, their luminescent behaviour was developed by coordination of the dppn ligand (dppn = 4,5,9,16-tetraaza-dibenzo[*a*,*c*]naphthacene) to produce [(*p*-cymene)Ru(dppn)(py)]$^{2+}$, (py = pyridine). This complex displays emission enhancement behavior and photocleavage activity towards DNA as it can emit fluorescence from the dppn-based singlet excited state and generate singlet oxygen from the dppn-based triplet excited state.[257]

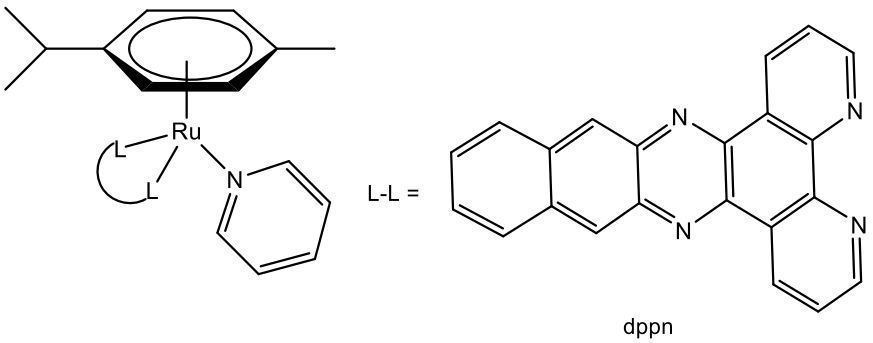

Figure 4.4: Structure of [(p-cymene)Ru(dppn)(py)]$^{2+}$, (dppn = 4,5,9,16-tetraaza-dibenzo[a,c]naphthacene py = pyridine).

These results inspired us to make different variations in the structure of the Ru(II)tach complex and determine how such changes affect their properties. The new ligand with extended aromatic groups, fluorescent diphosphine ligand FL-I represents a useful model for the synthesis of a new family of ruthenium tach complexes and the investigation of the cellular DNA binding.

As part of ongoing investigations on the biological potential of the ruthenium tach complexes, an exploration of the possible transport mechanisms should be carried out. In particular, serum albumin has been one of the most extensively studied proteins for many years, as albumin proteins represent the first possible targets for metallodrugs after intravenous administration.[258, 259] Among various serum albumin, bovine serum albumin (BSA) is the most extensively studied owing to its structural homology with human serum albumin (HSA).[260, 261]

Ruthenium complexes of known anticancer activity have been shown to interact with serum albumin.[259, 262] For instance, the interactions between Ru-based drug candidate KP1019 and plasma proteins (serum albumin and serum transferrin) were investigated by UV–vis spectroscopy and showed a higher degree of binding to serum proteins (80-90%) than transferrin.[263] The binding strengths of NAMI-A toward human serum albumin and other biomolecules (such as DNA) were examined by electrochemical and

biochemical methods and all the results confirm the preferential interaction of NAMI-A with proteins as compared with nucleotides.[264, 265] Indeed, recently RAPTA-T was considered to be more reactive and could also bind selectively to serum proteins albumin and transferrin, while cisplatin was found to be moderately reactive towards the protein without any selectivity.[157]

Although it is widely known that binding to DNA nucleobases, resulting in the distortion of the biomolecule and causing the inhibition of cell proliferation, is the main mechanism responsible for cytotoxicity,[54] protein targets have moved into the centre of attention for ruthenium-based complexes.[157] However, the dual-targeting function of ruthenium compounds inside cells has remained unverified,[266] and following entry of the drugs into cancer cells is valuable for drug discovery.[267] Different methods have been used to localize metallodrugs in tumour cells and, in case of ruthenium complexes, this fields still needs exploration.[268] Complexes with a DNA switch behaviour are considered as suitable models for DNA imaging. This is only done by the formation of lipophilic compounds, as the classical DNA switch $[Ru(bpy)_2(dppz)]^{2+}$ was unable to permeate into cells due to its poor lipophilicity.[269]

For all of these reasons, the development of anticancer complexes targeting both DNA and protein is highly desirable. In this chapter, the ruthenium tach complexes were expanded by the incorporation of a fluorescent probe into the coordination sphere, and then the investigation of the biological properties of the Ru(II)tach complexes have focused on both the binding ability towards calf thymus (CT-DNA) (performed with UV spectrometry, fluorescence spectrometry and competitive binding studies with ethidium bromide (EB)), and the affinity with bovine serum albumin BSA protein (performed with fluorescence spectrometry).

4.2 Synthesis of new Ru-Tach complexes

Adding a fluorescent probe to the coordination sphere of ruthenium has provided much information about the properties of metal compounds in biological environments *via* cellular localization studies.[270] Indeed, the added functional utility of inserted fluorescent probes has provided the capability to track and observe the distribution, influx, and efflux of metal−fluorophore compound in cells.[271]

New fluorescent diphosphine ligand FL-I, (Figure 4.5), was chosen to interact with Ru(II)tach complexes in order to visualize the site of accumulation in cells using confocal microscopy.

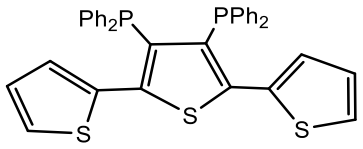

FL-I

Figure 4.5: Structure of new fluorescent ligand FL-I.

The fluorescent diphosphine ligand FL-I (provided by Prof. Paul Pringle) was coordinated to the metal by reaction with [Ru(*cis*-tach)$(DMSO)_2$Cl]Cl, **[4]** which is readily synthesised from the reaction of *cis*-tach **[1]** and $[RuCl_2(DMSO)_4]$ in DMSO solvent (Chapter 3).[179] The same conditions employed for synthesis of [Ru(*cis*-tach)(P-P)Cl] complexes (Figure 4.6) were performed.[179] Two equivalents of FL-I were added to a solution of one equivalent [Ru(*cis*-tach)$(DMSO)_2$Cl] **[4]** in CH_3OH and heated at reflux under nitrogen for 18 hours. After filtration to remove unreacted phosphine, the complex [Ru(*cis*-tach)(FL-I)Cl]Cl, **[10]** was isolated by addition of diethylether to a saturated dichloromethane solution giving a yellow powder with good yield, 68% (Figure 4.7).

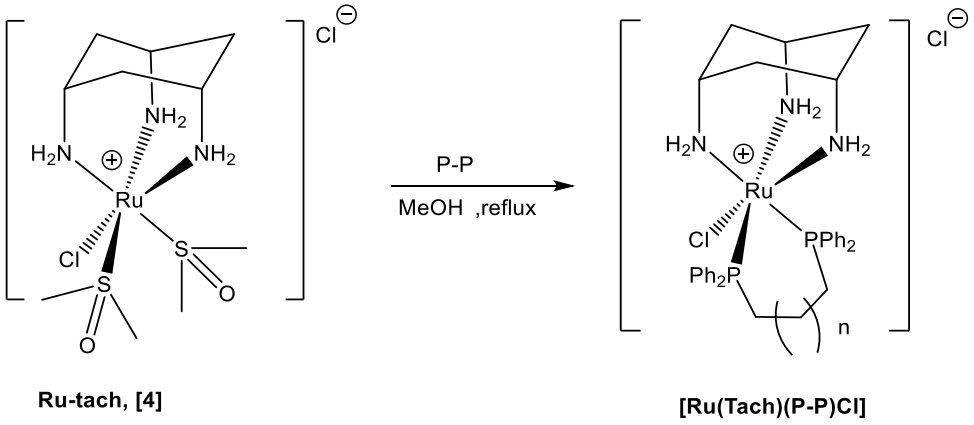

Figure 4.6: Synthesis of [Ru(cis-tach)(P-P)Cl]Cl, from [Ru(cis-tach)(DMSO)$_2$Cl] [4] and (P-P = dppe, dppm, dppp, dppv and dppb) ligand in CH_3OH as a solvent.

The successful coordination of the diphosphine ligand was evidenced by $^{31}P\{^1H\}$ NMR which exhibited a single resonance for the two coordinated phosphorus nuclei at δ_p 55.24 ppm, suggest the equivalent phosphorus nuclei for [Ru(tach)(FL-I)Cl]Cl, **[10]**, (Figure 4.8).

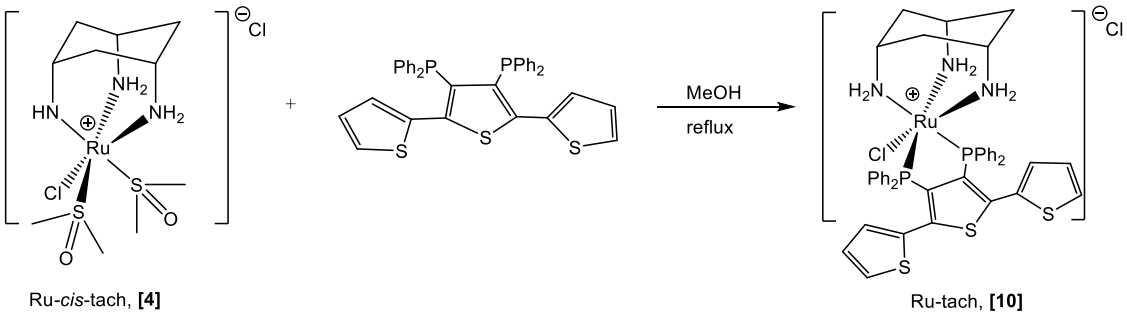

Figure 4.7: Synthesis of [Ru(cis-tach)(FL-I)Cl]Cl, [10] from [Ru(cis-tach)(DMSO)$_2$Cl] [4] and FL-I ligand in CH_3OH as a solvent.

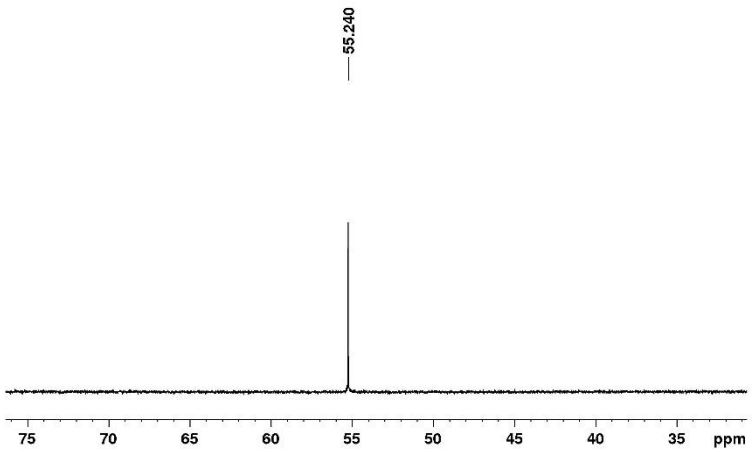

Figure 4.8: $^{31}P\{^{1}H\}$ NMR spectrum of Ru-tach [10] in CD_2Cl_2.

The ^{1}H NMR spectrum showed both the *cis*-tach and aromatic protons of FL-I. In the high field region (1.0-4.3ppm) of the spectrum, nine proton resonances were identified, two of which are coincidentally overlapping and appear as a quartet, indicating the same symmetry C_S as the starting compound **[4]**. The observation of a large ^{2}J-geminal coupling (15.7 H_Z) and absence of axial-axial cyclohexane *J* couplings confirms that the amine groups are coordinated to a metal centre in an axial conformation.

The disappearance of a DMSO resonance in the ^{1}H NMR spectra, with observation of singly charged **[10]** at 882.72 in the ESI-MS with expected ruthenium and chlorine isotope patterns, was indicative of the presence of a chloride ligand within the coordination sphere of the metal to complete the eighteen-valence electron count.

The ^{1}H NMR spectrum assignment for the tach protons was aided by the use of 2D homonuclear chemical shift correlation, COSY. According to the COSY spectrum (Figure

4.10), the *CH* (**b,b**$^{-}$) and *CH*$_2$ (**a,a**$^{-}$) protons were coupled to each other and give rise to the doublets (^{2}J = 16.5 Hz), but the two broad peaks were observed for protons **b** and **b**$^{-}$ due to their location next to the electronegative NH_2 groups. Two of the amine groups appear as a doublet (^{2}J = 12.1 Hz) due to coupling to **b**$^{-}$ while one appears at 1.49 ppm. This is outside of the typical 'coordinated amine region' between 2-5 ppm, but this resonance is consistent with many other ruthenium(II) tach complexes of this type[179] and indicates that the amine groups are coordinated to ruthenium metal in a k^3 manner.

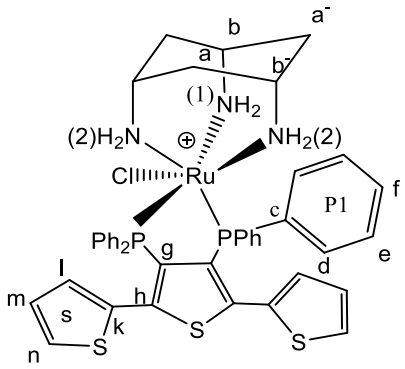

Figure 4.9: Numbering scheme for [10].

The aromatic region protons present eight signals, two of which are overlapping. Due to C_s symmetry present within the complex, only one half of the resonances for these aromatic protons were identified in the spectrum (Figure 4.9). The assignment of low field peaks can be achieved by the cross peaks in COSY spectrum (Figure 4.11) which can be used to differentiate between the phenyl substituent and heterocyclic protons (in conjunction with one bond heteronuclear chemical shift correlated ^{1}H-^{13}C NMR spectra when necessary). The heterocyclic protons appear in the higher field region than phenyl protons. Protons **l** resonate at 6.4 ppm and appear as a doublet of doublets due to the coupling to both **m** (^{3}J = 5.9 Hz) and **n** (^{4}J = 1.5 Hz). Protons **m**, which resonate at 7.2 ppm, are coupled to both **l** (^{3}J = 5.9 Hz) and **n** (^{3}J = 3.8 Hz) which

produces a doublet of doublets. The same multiplicity is observed for protons **n** (6.5 ppm) that couple to both **m** (^3J = 3.8 Hz) and **l** (^4J = 1.5 Hz), giving rise to a doublet of doublets.

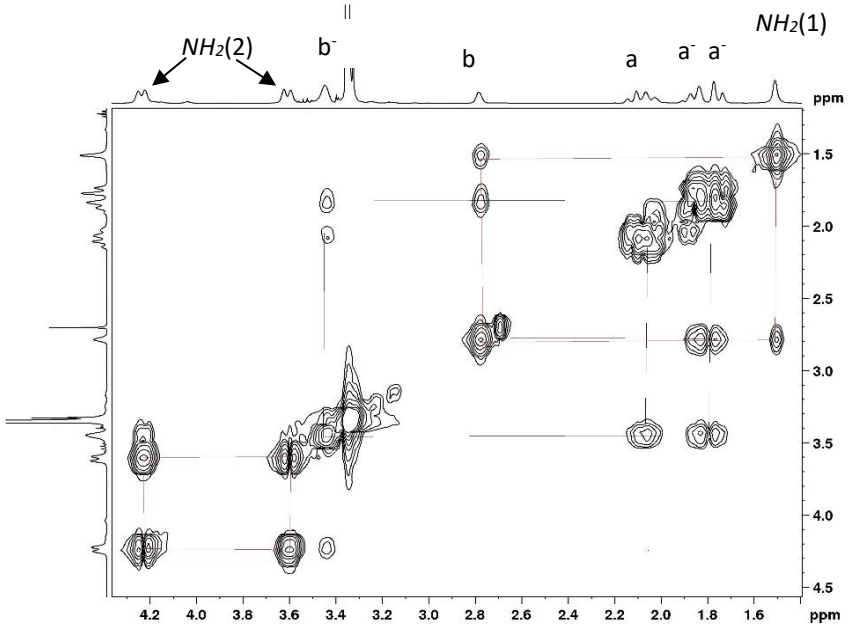

Figure 4.10: COSY NMR of Ru-tach [10], detail of the aliphatic region, recorded in CD_2Cl_2.

The other protons were assigned to phenyl rings, with the more deshielded protons **d** (in the ortho position) appearing as a virtual triplet, due to the coupling to protons **e** and phosphine with the same coupling constant (^3J = 7.9 Hz). The other aromatic protons appeared as a multiplets and overlapped so the assignments were completed using HMQC spectroscopy (Figure 4.12).

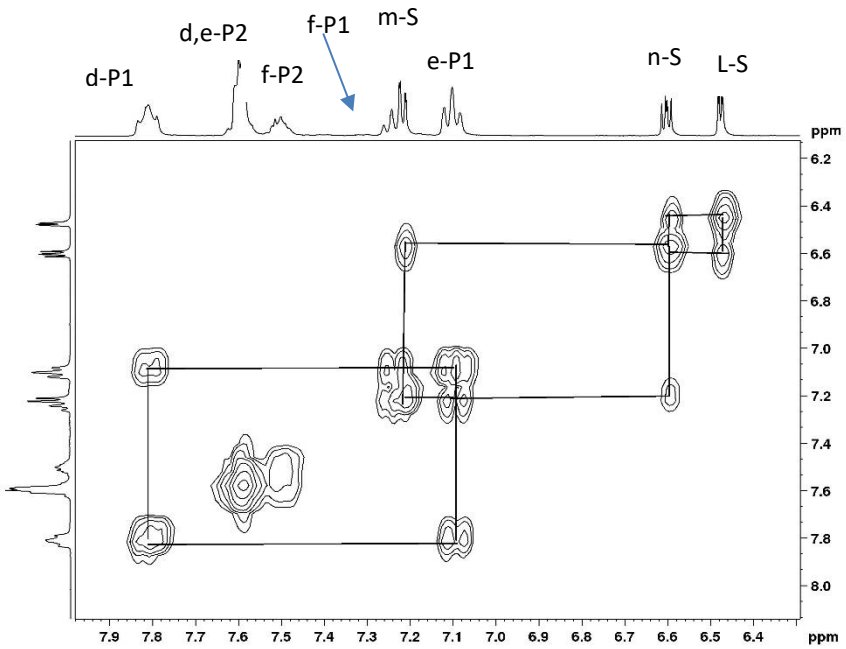

Figure 4.11: COSY NMR of Ru-tach [10], detail of the aromatic region, recorded in CD_2Cl_2, S is for the thiophene ring, P is for the phenyl protons).

The carbon signals were identified by both HMQC (Figure 4.12) and DEPT spectra that can provide additional information to complete the assignment. The *CH_2* groups have the opposite phase to *CH* groups, and also identify the quaternary carbon resonances by the disappearance of the signals. The *ipso* carbons are observed as triplets due to virtual coupling with two ^{31}P nuclei, confirming the coordination of the two equivalent phosphorus nuclei. This was demonstrated earlier by the single resonance in $^{31}P\{^{1}H\}$ NMR spectrum.

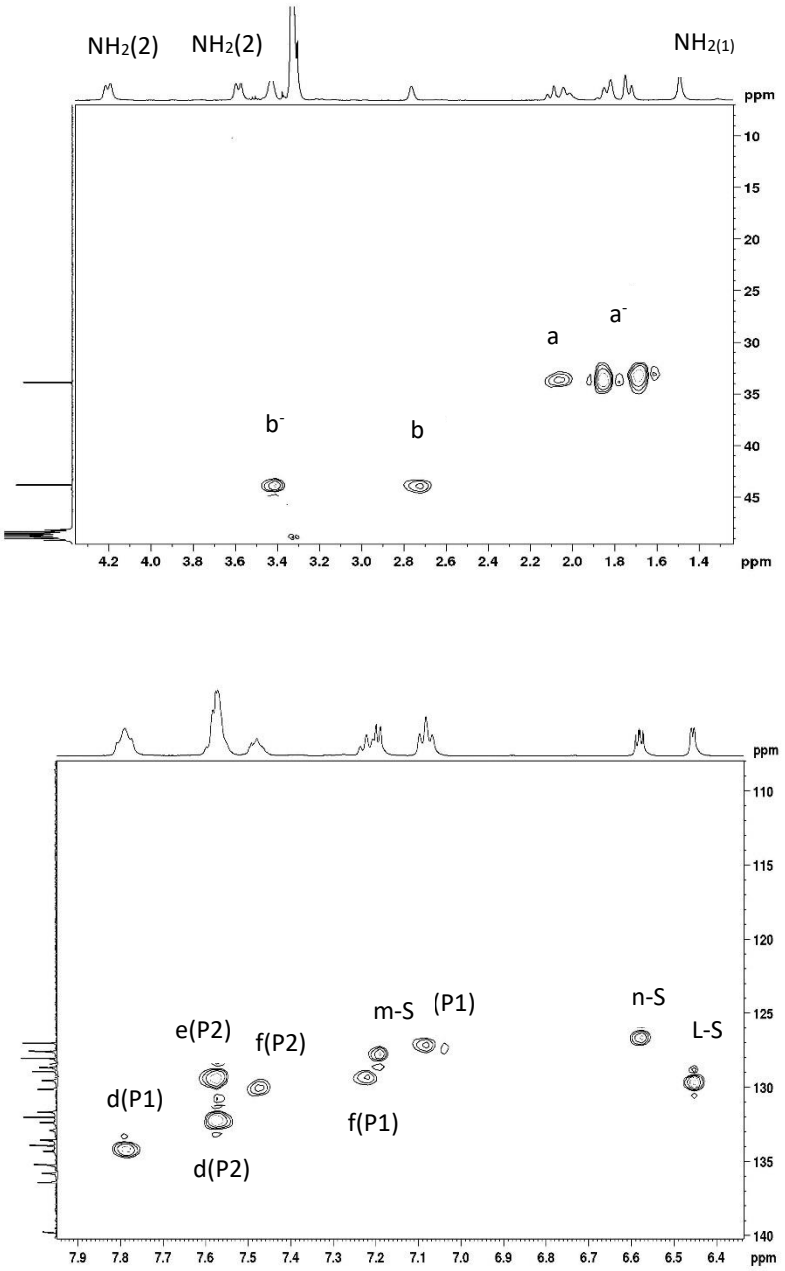

Figure 4.12: HMQC spectrum of [10] in CD_2Cl_2, aliphatic region (top) and aromatic region (bottom).

All the attempts to obtain single crystals of **[10]** were unsuccessful, however the complex was isolated with analytical purity without any anion metathesis. The purity was confirmed by elemental analysis.

The good solubility of **[10]** in water, and the fluorescent behaviour further discussed later, make the complex a good candidate for a biomolecule interaction study. The successful synthesis and promising properties of complex **[10]** also inspired the coordination of another fluorescent probe FL-II to the ruthenium tach complex.

4.3 Synthesis of Ru-tach [13]

To expand the range of promising diphosphine tach complexes of type [Ru(tach)(P-P)Cl]Cl, a new fluorescent ligand FL-II with an extended aromatic ring (Figure 4.13) was coordinated to Ru-tach complex **[4],** following a similar route and conditions as the previous complex, to give a yellow product. The $^{31}P\{^{1}H\}$ NMR spectrum exhibits two doublets centred at 69.5 and 74.1 ppm with a coupling constant ($^{2}J_{pp}$ of 8.77 Hz), suggesting inequivalent phosphorus nuclei for [Ru(tach)(FL-II)Cl]Cl, **[13]** (Figure 4.14), which may be due to different arrangements of the phenyl and pyrenyl group.

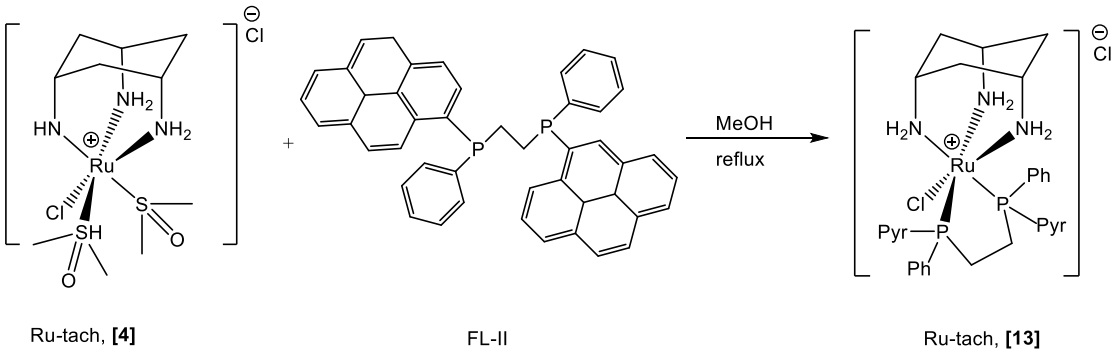

Ru-tach, **[4]** FL-II Ru-tach, **[13]**

Figure 4.13: Synthesis of [Ru(cis-tach)(FL-II)Cl]Cl, [13] from [Ru(cis-tach)(DMSO)$_2$Cl] [4] and FL-II ligand in CH_3OH as a solvent.

The ^{1}H NMR could not be used to give further indication of the complexes identity but the tach and aromatic protons could still be observed. The ESI mass spectrum supported the formation of complex **[13]** by the observation of the expected molecular ion at 912.21 m/z with ruthenium and chlorine isotope patterns, shown in Figure 4.14.

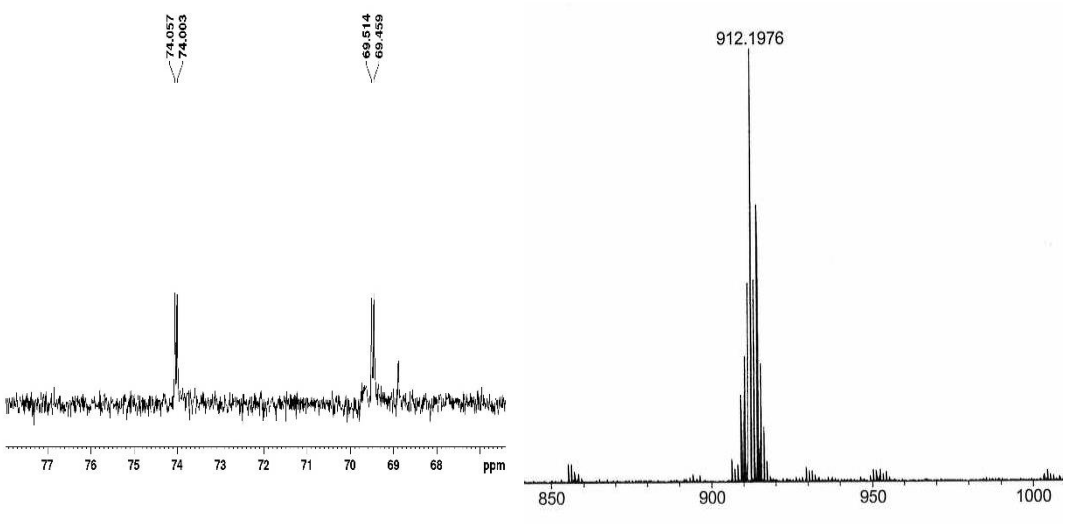

Figure 4.14: $^{31}P\{^{1}H\}$ NMR spectrum of Ru-tach [13] in CD_2Cl_2 (left) and ESI spectrum (right).

The new complex **[13]** was isolated in low yield (45%) therefore it could not be used for biological evaluation performed later.

On the other hand, two previously synthesised Ru-tach complexes were chosen to explore the *in vitro* evaluation of biomolecular interaction with new complex **[10]** to gain an understanding of how the structural characteristics affect their *in vitro* activities with CT-DNA and BSA (Sections 4.6 and 4.7) and *in vivo* potencies in the A2780 and A549 cell lines (Chapter 5). One complex was chosen due to the higher cytotoxicity in anticancer cells, [Ru(tach)(dppp)Cl]Cl **[11],** while the other was inactive [Ru(tach)(phen)(DMSO)]Cl_2, **[12]**.

4.4 UV-Vis absorption-fluorescence emission based studies for Ru-tach complexes

The electronic absorption spectra and emission spectra of the Ru(II) tach complexes are presented in Figure 4.15. All of the complexes show long tail absorption bands that occur in the lower energy region (340–550 nm) due to metal-to-ligand charge transfer (MLCT) and lie in the typical range of MLCT transitions found in other octahedral ruthenium complexes.[272-274] The very intense bands in the UV region between 230-310 nm can be assigned to ligand-centred $\pi \rightarrow \pi^*$ transitions.[275, 276]

Upon excitation at 350 nm, the emission spectra for **[11]** at room temperature showed a broad emission band with maximum emission at 430 nm. On addition of the new ligand FL-I to the coordination sphere of the Ru-tach complex, a red shift was observed for the emission wavelength of **[10]** to 440 nm and the emission was of higher intensity. Excitation of the free ligand (at 350 nm at room temperature) showed a broad emission band with a maximum emission at 465 nm. The emission observed for these complexes can be assigned to intra-ligand $\pi \rightarrow \pi^*$ transition mixed with metal-to-ligand charge transfer. Complex **[12]** showed a broad emission band with a maximum at 600 nm upon excitation at 450 nm shown in Figure 4.15. This emission is caused by a radiative process from the MLCT state to the ground state.[277]

Complex **[10]** and its corresponding ligand L **[1]** have different emission intensities and therefore the fluorescence quantum yield (Q_y) of the complexes **[10]** and L**[1]** with **[11]** and **[12]** could be determined using the comparative method**.**[278, 279] This method involves the use of different references with known fluorescence quantum-yield.[280]

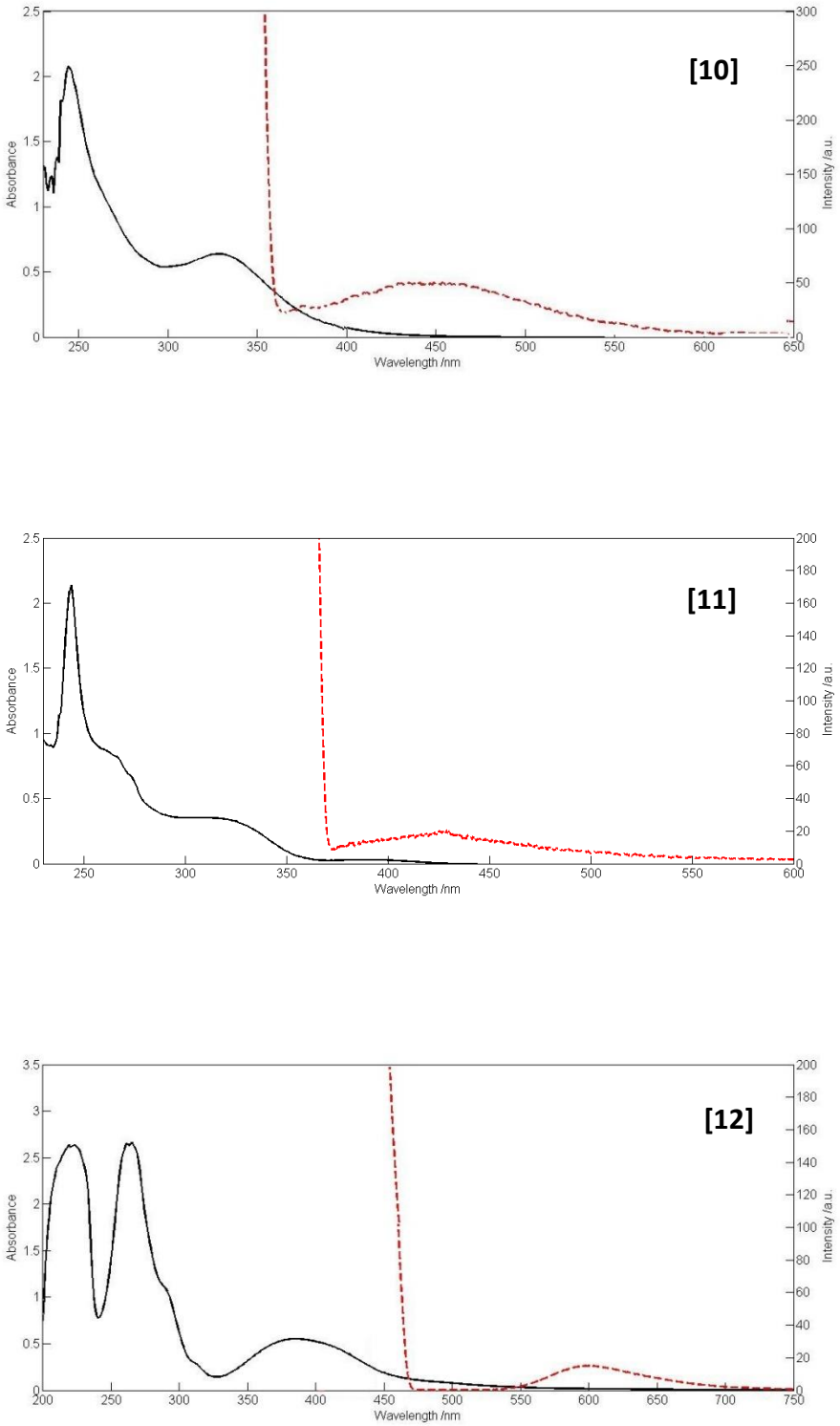

Figure 4.15: UV-Vis spectra (solid line) and fluorescence spectra (dash line) for [10], [11], and [12] excited with 350 nm for [10] and [11] and 450 nm for [12].

Anthracene (R_1), phenanthrene (R_2) and rhodamine 6G (R_3) were chosen as the references and the quantum yield (Q_y) of each reference sample was calculated relative to each other. The area of emission spectra was integrated using a/e-UV-VIS-IR spectral analysis software, and the quantum yield was calculated by using the equation:

$$Q = Q_R \left[\frac{Grad}{Grad_R}\right]\left[\frac{n^2}{n_R^2}\right]$$

Equation 4.1: Quantum yield equation.

Where the subscripts *R* denote reference, *Q* is the fluorescence quantum yield, *Grad* the gradient from the plot of integrated fluorescence intensity *vs* absorbance, and *η* the refractive index of the solvent.[281]

Table 4.1: Quantum yield for FL-I and Ru-tach complexes [10], [11], [12] and the references R_1, R_2.

compound	λ_{ex} (nm)	Solvent	Emission range (nm)	Quantum yield	Molar absorptivity($M^{-1}cm^{-1}$)
Ru-tach **[10]**	350	Chloroform	360-600	0.080 ± 0.012	8546.0
FL-I	350	Chloroform	360-600	0.160± 0.109	8625.9
Ru-tach **[11]**	350	Chloroform	360-550	0.047± 0.122	
Ru-tach **[12]**	450	Water	550-700	0.062± 0.214	7442.3
R_1	350	Ethanol	360-480	0.270± 0.081	-
R_2	310	Ethanol	345-500	0.125± 0.092	-
R_3	460	Ethanol	500-700	0.511± 0.021	-

The quantum yield of **[10]** was approximately half when compared to the related ligand FL-I. This suggests that the fluorescence of FL-I was quenched when coordinated to [Ru(tach)(DMSO)$_2$Cl]Cl. In addition, **[11]** and **[12]** have lower quantum yields (Q_y 0.047 and 0.06) than the free ligand FL-I.

These good fluorescent behaviours and quantum yields allow these complexes to be ideal candidates for further study in the field of biomolecules interaction, in order to open a window into their mechanism of action.

4.5 Stability of the investigated Ru-tach complexes.

Stability is the major requirement for the biological evaluation of a DNA/BSA binding interaction study, therefore checking the stability of the complexes in the same buffer solution used for study is very important.[282] The stability of **[10]**, **[11]**, and **[12]** complexes in 5 mM Tris-HCl was measured over 24 h using a scanning kinetic program on a UV-Vis spectrophotometer. The UV-Vis spectra recorded directly after dilution of complexes **[10]** and **[11]** did not show any appreciable changes in either the intensity or the position of the absorption bands after 24 h, which indicates the stability of the complexes in aqueous solution, while the spectra of complex **[12]** showed a remarkable decrease in the absorption band intensities. In particular, the MLCT band at 370 nm gradually weakened, and new bands started to appear near 500 nm with the presence of an isobestic point at 430 nm. Equilibrium was reached within 180 seconds (Figure 4.16).

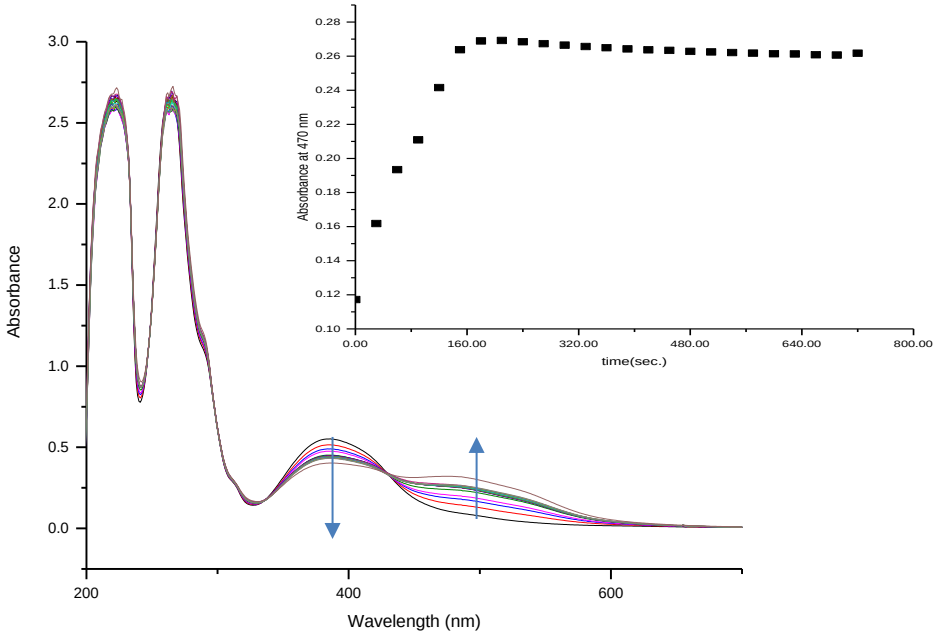

Figure 4.16: Photoreaction of [12] (0.15mM) in 5mM Tris-HCl buffer, pH 7.2, irradiated with normal laboratory light followed by UV/Vis absorption. Insert: photo ejection kinetics for [12] in 12 hours.

Complex **[12]** is indefinitely stable in the dark conditions. However, exposure of such solution to normal laboratory light causes a distinctive colour change from light yellow to a deep orange colour in water and to a red colour in methanol. Thus, this complex is considered to be a light sensitive compound. The presence of an isobestic point at 430 nm noted in the absorption spectra of the solution undergoing photolysis, (Figure 4.16), confirms clean conversion of **[12]** to its photoproduct.

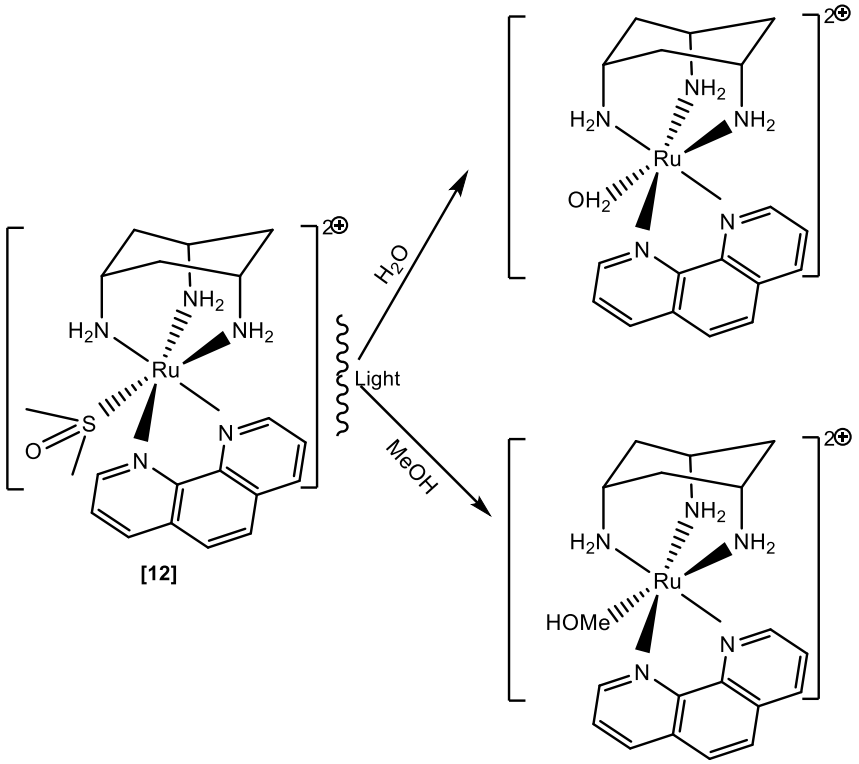

Figure 4.17: Photoejection of DMSO ligand of [12] in H_2O and MeOH solvent after irradiation with white light.

The nature of the photoproduct was further confirmed by electrospray ionization mass spectrometry (ESI) which indicated the ejection of DMSO ligand with the formation of $[Ru(tach)(phen)(H_2O)]^{2+}$ at *m/z* 214.32 in water and formation of $[Ru(tach)(phen)(MeOH)]^{2+}$ at *m/z* 221.55 in methanol solvent. This indicates the replacement of the DMSO ligand with a solvent molecule (Figure 4.17). The photo substitution reaction is clean and gives only a single photoproduct, as confirmed by the NMR photolysis experiment reported for **[12]** (Figure 4.18). Indeed, new sets of NMR signals are formed upon light excitation which correspond to free DMSO, while the coordinated DMSO signal decreased in intensity and integration accordingly.

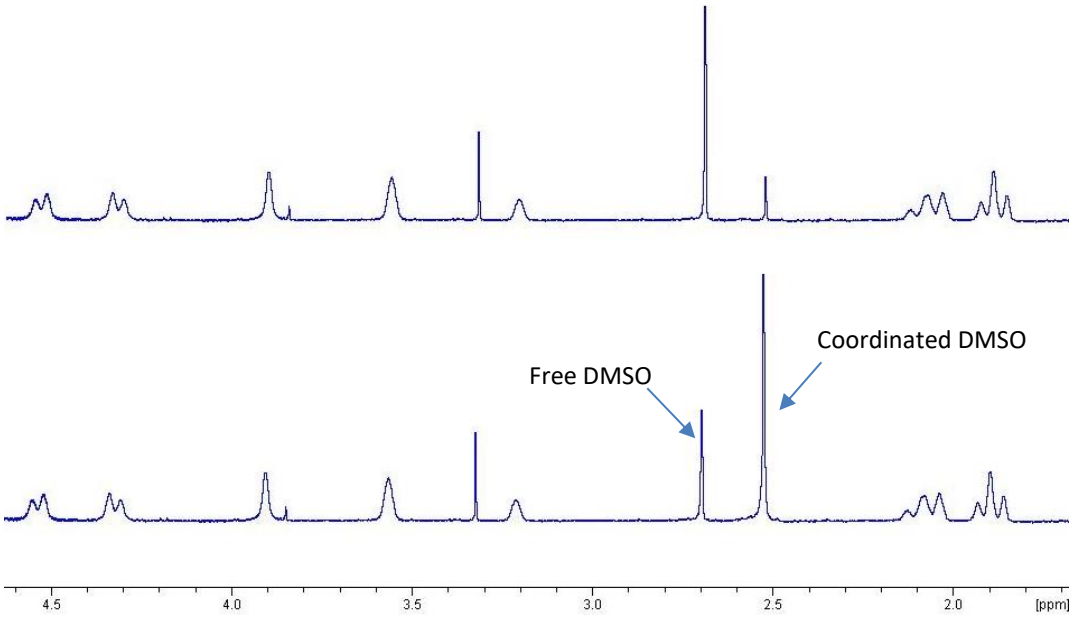

Figure 4.18: ^{1}H NMR spectra for [12] in D_2O (bottom) and after irradiated with white light after 3 hours (top).

This new behaviour for **[12]** as a light sensitive complex stimulated the screening of its interaction with biomolecules in dark and light environment and checking its cytotoxicity within the same conditions (Chapter 5).

4.6 DNA binding studies

DNA binding with small molecules is very important in the field of designing of new and efficient anticancer drugs.[283] Thus, the interaction between DNA and metal complexes is important for understanding the mechanism of action. Therefore, the types of binding of the new ruthenium (II) tach complex [Ru(tach)(L1)Cl]Cl **[10]** as well the two previously prepared Ru(II)tach complexes[Ru(tach)(dppp)Cl]Cl **[11]** and [Ru(tach)(phen)(DMSO)]Cl **[12]** with CT-DNA were studied by using UV-Vis spectroscopy and the fluorescence quenching techniques.

4.6.1 Electronic Absorption Titration

Electronic absorption spectroscopy is the most common technique used to examine the binding affinity of metal complexes with DNA.[284] This technique is based on monitoring the changes that occur in the UV-Vis spectrum of the metal complex or the UV-Vis spectrum of DNA upon their interaction. The binding ability of the complexes to CT-DNA can be easily determined by examining the modifications of the maximum of one of the absorption bands, either in the UV region or in the visible region, when the nucleic acid is present in different concentrations.[253, 284, 285]

"Hyperchromic" and "hypochromic" effects are the two spectroscopic features of DNA regarding its double helical structure.[286] The hyperchromic effect has been attributed to electrostatic interactions, hydrogen bonding or groove (minor or major) binding along the outside of the DNA helix. This increase in the absorption intensity is attributed to the decrease in base-base interactions and lowering of the hydrogen bond strength, which is a result of the change in the structure and conformation of DNA. The disruption of the double helix leads to separation of the double helix to two single strands that cause the hyperchromism.[287, 288] Observation of hypochromism (with or without bathochromism) is indicative of an intercalative binding mode that involves a strong stacking interaction between an aromatic chromophore and the base pair of DNA. This causes a decrease in the distance between the complex and the DNA bases and leads to a combination of the π electrons from both components. Therefore, the energy level of the π-π^* electron transition decrease and causes a red shift. Furthermore, the coupling π orbital is partially filled with electrons that decrease the transition and the absorbance as well.[289]

An absorption titration experiment was carried out to study the DNA interaction with Ru(II)tach complexes. The intense absorption band around 340 nm observed for **[10]** was used to characterize the interaction of the complexes with calf thymus DNA in 5 mM Tris-HCl (30 mM NaCl) buffer at pH 7.2. As the CT-DNA concentration is increased

(0-50 µM), the MLCT bands of the **[10]** complex exhibit a hypochromic shift from 0.48 to 0.30 with a small red shift of 2 nm for the band centred at 340 nm (Figure 4.19).

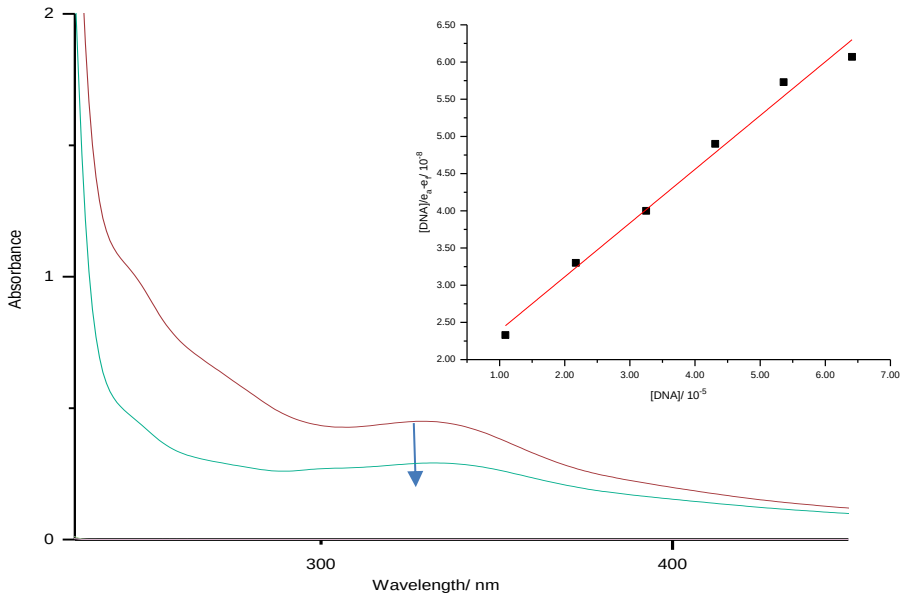

Figure 4.19: Absorption titration spectra of [Ru(tach)(L1)Cl]Cl, [10] with increasing concentrations (0-10 µM) of CT-DNA (5 Mm Tris-HCl buffer, pH 7.2, 30 mM NaCl), Insert: plot of [DNA] versus [DNA]/ε_a-ε_f with R^2=0.998.

However, complex **[11]** showed a very weak decrease in the absorbance around 320 nm and this change was attributed to a dilution effect only. The change in the absorption spectra of [Ru(tach)(phen)(DMSO)]Cl_2 **[12]**, with increasing concentration of CT-DNA is shown in Figure 4.20. At constant concentration of **[12]** (7 µM) in the dark, the presence of increasing concentration of DNA (0-10 µM) led to a gradual decrease in the intra ligand (π-π*) absorption band around 262 nm (16 %) and the MLCT band around 370 nm showed hypochromism (32%).

In contrast, when the same titration was repeated for complex **[12]** in the presence of normal laboratory light, the hypochromism around 268 nm and 364 nm increased significantly to 30% and 41%, respectively (Figure 4.20). The more significant decrease

in the absorbance observed for **[12]** compared to **[10]** can be explained by a stronger intercalation between the chromophore of the extended aromatic moiety and the chromophore of the base pair in DNA in the form of π-π stacking. This is common for complexes which contain phenanthroline as ancillary ligand.[253] The results suggested that complexes **[10]** and **[12]** bind to DNA by intercalation in a manner similar to known intercalators such as [Ru(IP)(DPPZ)].[290]

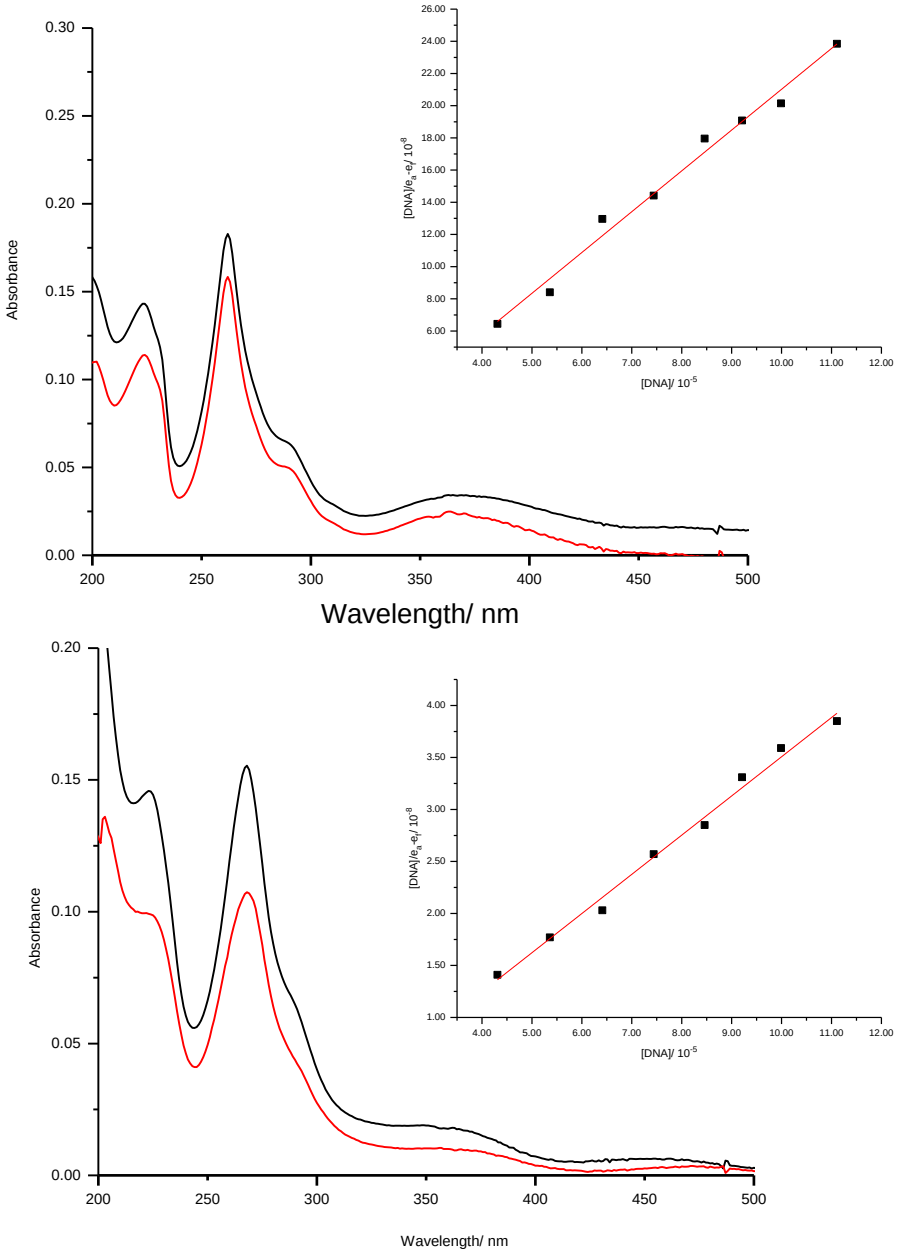

Figure 4.20: Absorption titration spectra of [Ru(tach)(phen)DMSO]Cl, [12] in the dark (top) and light (bottom) with increasing concentrations (0-10 µM) of CT-DNA (5 Mm Tris-HCl buffer, pH 7.2, 30 mM NaCl). Insert: plot of [DNA] versus [DNA]/ε_a-ε_f with R^2=0.966 (top) and 0.987 (bottom).

To compare quantitatively the binding strength of the complexes **[10]** and **[12]** with CT-DNA, the intrinsic binding constant or association constants (K_b) have been

calculated based on the variation in absorption at MLCT band for complex **[10]** and **[12]** with increasing concentration of DNA according to the Benesi-Hildebrand equation, modified by Wolfe *et al*:[291, 292]

$$\frac{[DNA]}{(\varepsilon_a - \varepsilon_f)} = \frac{[DNA]}{(\varepsilon_b - \varepsilon_f)} + \frac{1}{K_b(\varepsilon_b - \varepsilon_f)}$$

Equation 4.2: Benesi-Hildebrand equation.

where [DNA] is the concentration of DNA base pairs, ε_a, ε_f and ε_b correspond to $A_{observed}$/[complex], the extinction coefficient of the complex in its free form, and the extinction coefficient of the complex in the fully bound form, respectively; K_b represents the binding constant in M^{-1}. When each set of data were fitted to Equation 4.2, a straight line with a slope of $1/(\varepsilon_a-\varepsilon_f)$ and a y-intercept of $1/ K_b (\varepsilon_b- \varepsilon_f)$: K_b is obtained by the ratio of the gradient to intercept.

The K_b values of these complexes are $(3.42\pm0.23)x10^4$, $(9.98\pm0.13)x10^4$ and $(7.52\pm0.12)x10^5$ M^{-1} for **[10]** and **[12]** in dark and light respectively. These results suggest that the size and the shape of the plane area (intercalated ligand) has a significant effect on the binding affinity to DNA and the most suitable intercalating ligand, phenanthroline, leads to the highest binding affinity. This finding is further conformed by other techniques below, while the difference in activity in dark and light is attributed to the presence of the water ligand in the light complex. Since this is smaller than DMSO this leads to higher insertion than there parent DMSO complex.

4.6.2 Fluorescence titration

Fluorescence titrations have been widely used to study interactions between small molecules and DNA. The fluorescence emission of interacting compounds can be quenched (decrease of fluorescence emission) or in some compounds, the

fluorescence intensity increases as the compound-DNA interactions can prevent the compound fluorescence emission from being quenched by polar solvent. The hydrophobic environments inside the DNA helix reduces the accessibility of polar solvent molecules and the compounds mobility is restricted at the binding site, which leads to decrease of relaxation and hence fluorescence intensity increase.[293]

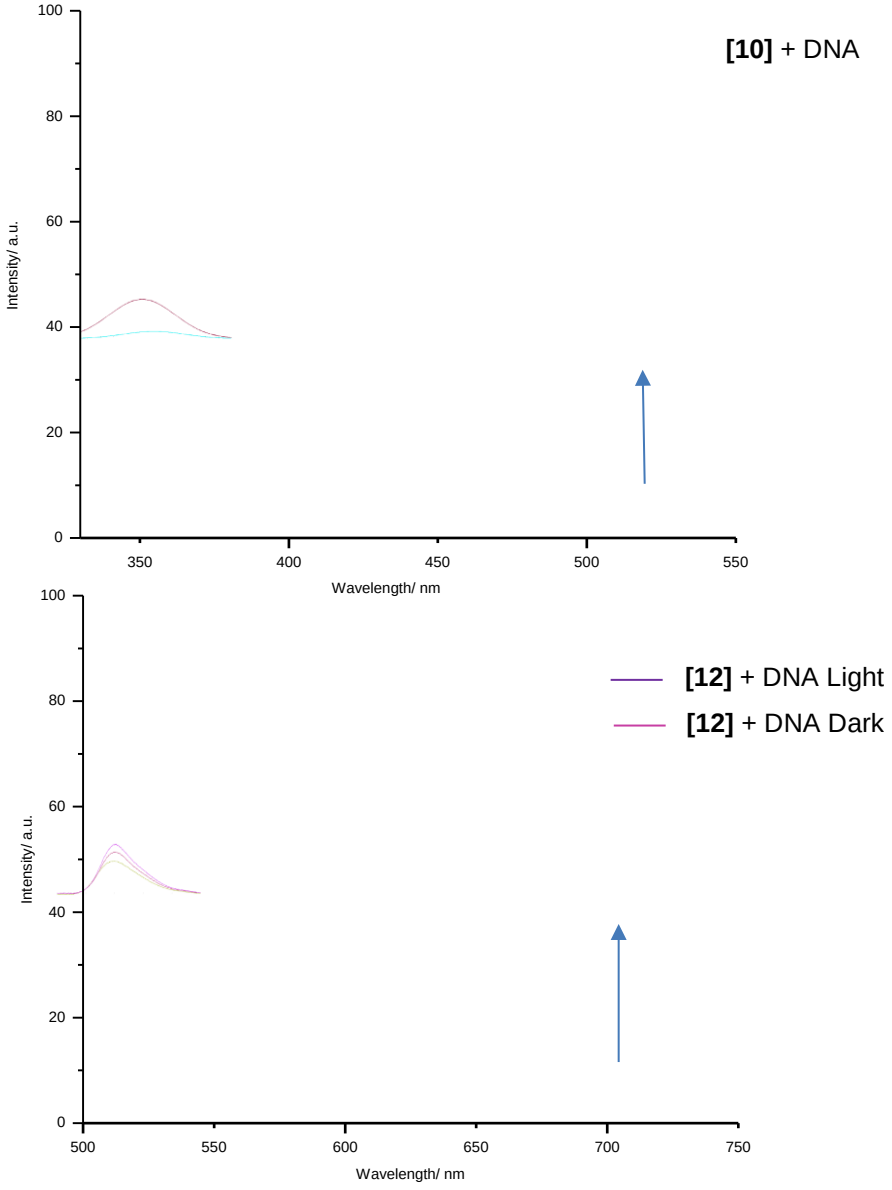

Figure 4.21: Emission spectra of complex [10] (top), and [12] (bottom) with increasing concentrations (0-10 µM) of CT-DNA (5 Mm Tris-HCl buffer, pH 7.2, 30 mM NaCl).

The intensity of emission from MLCT exited states from Ru(II)tach complexes **[10]** and **[12]** around 440 nm for **[10]** and 600 nm for **[12]** was found to depend on the DNA concentration. In the absence of CT-DNA, the emission for complex **[10]** was fully quenched in Tris-HCl buffer, but the complex becomes highly emissive upon binding to CT-DNA with a blue shift of 6 nm. However, Ru(II)tach complex **[12]** emission in Tris-HCl buffer increased remarkably with a red shift of 3 nm. The emission intensity was higher with light than the dark condition as shown in Figure 4.21. This behaviour further confirmed the findings of the UV-vis results and this enhancement is believed to be due to removal of the water molecules surrounding the complexes due to the intercalation of the complexes between DNA base pairs. [241, 294]

4.6.3 Competitive DNA binding studies

UV-Vis and fluorescent titration studies clearly indicated effective binding of **[10]** and **[12]** complexes with CT-DNA.

The competitive binding experiment based on the displacement of the intercalating dye, ethidium bromide (EB), from CT-DNA was carried out to obtain further proof for the binding of the Ru(II)tach complexes to DNA.

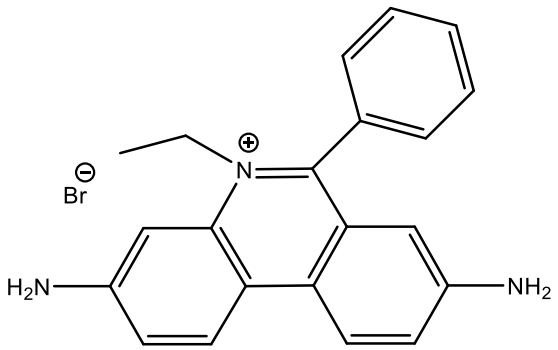

Figure 4.22: Ethidium bromide structure (EB).

Ethidium bromide (3,8-diamino-5-ethyl-6-phenyl phenanthridium bromide, EB) (Figure 4.22) is a planar cationic dye, known to be a carcinogen, mutagen and antimicrobial agent because of its ability to inhibit DNA synthesis, translation and gene transcription.[295] EB is a very useful sensitive fluorescent probe for DNA, which shows high fluorescence intensity when bound to the nucleic acid. The emission of free EB molecule is quenched in buffer solution and it shows a significant enhancement in fluorescence when intercalating to the base pair of CT-DNA.[284, 296] However, the enhanced fluorescence can be decreased or quenched when there is another species that can replace the EB or break the secondary structure of DNA.[297]

The affinity of Ru(II)tach complexes towards DNA can be measured by an EB competition assay, which is a measure of the extent of the fluorescence intensity reduction of the EB-DNA adduct. The competitive binding experiments have been undertaken following the emission spectra of the species in the wavelength range of 530-750 nm with an excitation wavelength at 518 nm, which is chosen to selectively excite EB only as none of the Ru(II) tach complexes exhibit fluorescence when excited at 518 nm.

Upon addition of the complexes (0-60 µM) to CT-DNA (10 µM) pre-treated with EB(µM) ([DNA]/[EB]=5) in 5mM Tris-HCl, 30 mM NaCl buffer at pH 7.2, the emission intensity of DNA-bound EB at 584 nm decreased significantly with the increase of the concentration of **[10]**, while **[12]** (irradiated with normal light) showed a higher decrease in emission intensity around 584 nm compared with the dark condition (Figure 4.23). These results indicate that the complexes **[10]** and **[12]** substitute DNA-bound EB and emphasize interaction *via* intercalation.

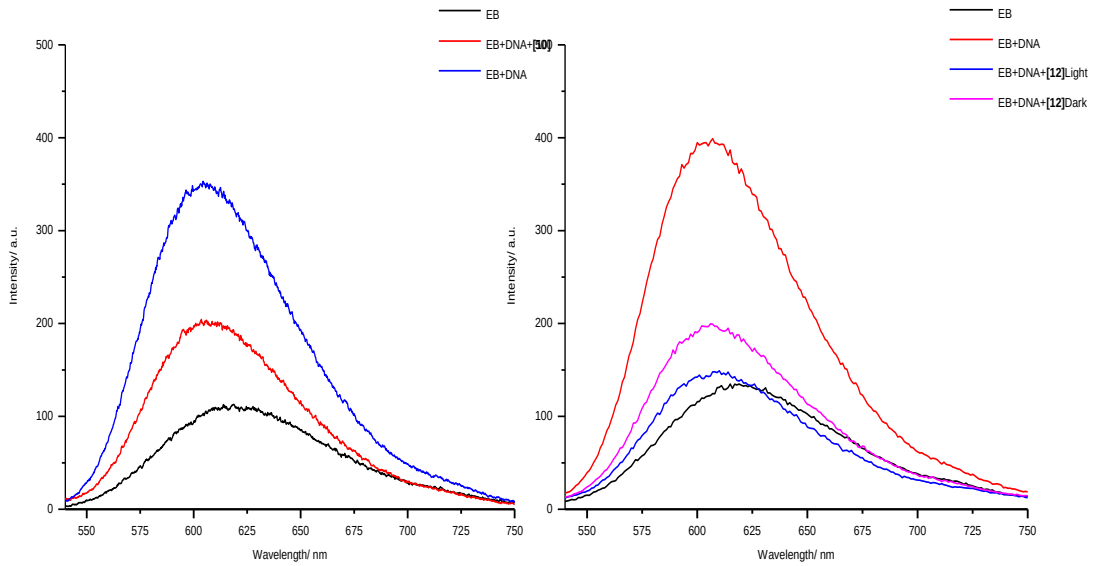

Figure 4.23: Effect of addition of [10] (left) and [12] (right) on the emission of the CT-DNA-bound EB at different concentration titrations (0-60 µM) in (5 Mm Tris-HCl buffer, pH 7.2, 30 mM NaCl).

The fluorescence quenching can be well described by the Stern-Volmer equation:[284]

$$\frac{I_\circ}{I} = 1 + K_{sv}\,[Q]$$

Equation 4.3: the Stern-Volmer equation.

where I_o and I are the fluorescence intensities of the EB-DNA adduct in the absence and presence of the quencher respectively, K_{sv} is the Stern-Volmer quenching constant and [Q] is the quencher concentration. The Stern-Volmer plots of I_o/I versus [Q] are shown in Figure 4.24. These illustrate that the quenching of EB bound to CT-DNA by **[10]** and **[12]** are in good agreement with the linear Stern-Volmer equation. The K_{sv} values were given by the ratio of the slope to intercept. The K_{sv} values for the tested Ru(II)tach complexes are listed in Table 4.2.

Furthermore, the EB displacement study provides information about the strength of the complex-DNA interaction through the apparent binding constant (K_{app}) by using the following equation:

$$K_{EB}[EB] = K_{app}[complex]$$

Equation 4.4: Equation to calculate the apparent binding constant.

where K_{EB} = 1x10^7 M^{-1}, [EB] is the concentration of EB used in this experiment which it was [5µM] for all complexes and [complex] is the concentration of the Ru(II)tach complexes **[10]** and **[12]** used to obtain a 50% reduction in the initial emission intensity of EB. Metal complexes that show a strong interaction with DNA give K_{app} values with magnitudes in the order of 10^5-10^6 M^{-1}.[284, 287, 298]

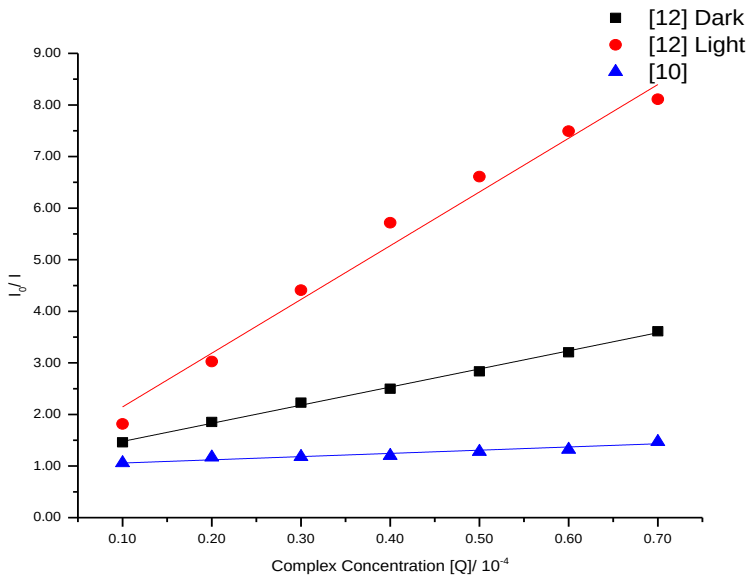

Figure 4.24: The Stern-Volmer plot of I_o/I versus [Q] for [10] and [12] complexes with CT-DNA, R^2 0.98([12] light), 0.99([12] dark, 0.93([10]).

From Equation 4.4, the apparent binding constants at room temperature have been calculated to be in the order shown in Table 4.1. The data suggest that the binding

ability of complex **[12]** is greater than complex **[10]**, which is in good agreement with the conclusion drawn from the absorbance titration (Section 4.2.1). The small difference between the two sets of binding that were obtained from fluorescence and absorbance titration is due to differences in the error between the two spectroscopic techniques and different calculation method, but they are comparable. The K_b, K_{sv} and K_{app} values for complex **[12]** in the light are 10-fold higher than **[10]**, and this strongly supports the intercalative mode of phenanthroline ligand,[241, 253, 294] presumably due to the plane area and hydrophobicity.[299] There is a difference in activity of **[12]** under light and dark conditions as the flat aromatic structures are known to intercalate between two DNA bases so place the metal in close proximity to the bases and facilitate direct photo-induced oxidation of guanines or DNA cleavage.[300] Moreover, complex **[10]** shows a lower binding strength to DNA due to the presence of diphenyl phosphine groups at the heterocyclic ligand which cause steric hindrance. The phenyl groups may come into close proximity of the base pairs at the intercalation site and lead to only partial insertion of the heterocyclic group in complex **[10],**[301] shown in Figure 4.25.

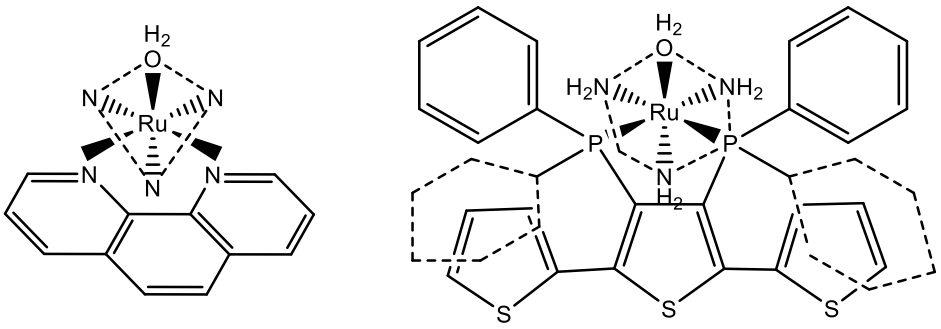

Figure 4.25: Schematic representation of the two intercalation Ru(II) tach complexes [10] (right) and [12] (left).

Table 4.2: Intrinsic binding constant values (K_b), (K_{sv}) and (K_{app}) from absorption and fluorescence spectroscopy.

Complex	K_b (M^{-1})	K_{sv} (M^{-1})	K_{app} (M^{-1})
[Ru(tach)(L1)Cl]Cl, **[10]**	$(3.42\pm0.23)\times10^4$	$(3.84\pm0.31)\times10^4$	$(2.04\pm0.05)\times10^6$
[Ru(tach)(phen)DMSO]Cl, **[12]** Dark	$(9.98\pm0.13)\times10^4$	$(2.16\pm2.32)\times10^5$	$(1.65\pm1.12)\times10^6$
[Ru(tach)(phen)DMSO]Cl, **[12]** Light	$(7.52\pm0.12)\times10^5$	$(9.68\pm2.02)\times10^5$	$(2.05\pm2.11)\times10^7$

4.7 Protein binding studies

Interactions between bovine serum albumin BSA and metal complexes have attracted interest due to BSA's structural homology with the most abundant human blood protein, human serum albumin. Bovine serum albumin (BSA) is usually preferred over other proteins in the protein binding studies because of its abundance, low cost, stability, medical significance, ligand binding properties and ease of purification.[302-304]

The highly fluorescent properties of BSA are related to the presence of aromatic amino acids tryptophan, phenylalanine and tyrosine residues.[305, 306] The emission behaviour of BSA is mainly contributed to by tryptophan alone, due to the fluorescence quenching of tyrosine when it is ionized and the very low quantum yield of phenylalanine (Q_y).The relative ratio of fluorescence intensity for the three amino acids (tryptophan, tyrosine, and phenylalanine) residues is (100:9:0.5) and thus, the emission intensity of BSA mainly comes from two tryptophan residues (Figure 4.26).[307]Trp-212 is located within the hydrophobic binding pocket in sub-domain IIA and Trp-134 is located on the surface of sub-domain IB.[308, 309]

The fluorescence behaviour of BSA can provide significant information about the dynamics, structure and protein folding. Also, it is an efficient approach for evaluating the interaction with metal complexes. In the case of an interaction with the metal complex, the fluorescence emission of the protein at 345 nm decreases regularly as the concentration of the compound increases, and in the case of a red or blue shift of the emission maximum in the fluorescence spectrum of the BSA suggests an increase in the hydrophobicity of the microenvironment around the tryptophan residues.[308, 310]

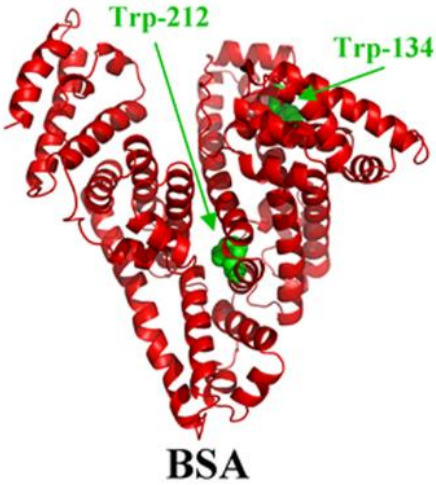

Figure 4.26: BSA structure with tryptophan residue Trp-212 and Trp-134 in green. Image adapted from Belatik et al.[311]

Fluorescence quenching experiments have been performed using a solution of BSA (5µM) in buffer (5 mM Tris-HCl,30 mM NaCl buffer at pH 7.2) and the concentration of complexes **[10]**, **[11]** and **[12]** (dark and light environment) were varied (from 0 to 50 µM). In the absence of any Ru complex, BSA has a strong emission peak at 345 nm (when excited at 295 nm). An intrinsic fluorescence decrease at 345 nm, within the range of 33% to 12% hypochromism was observed when BSA was titrated with the test Ru(II)tach complexes shown in Figure 4.27. These changes in emission indicate the interaction of all the tested complexes with BSA protein. The different hypochromism suggests the binding affinity of the free complexes is in the order **[11]**> **[10]**> **[12]**.

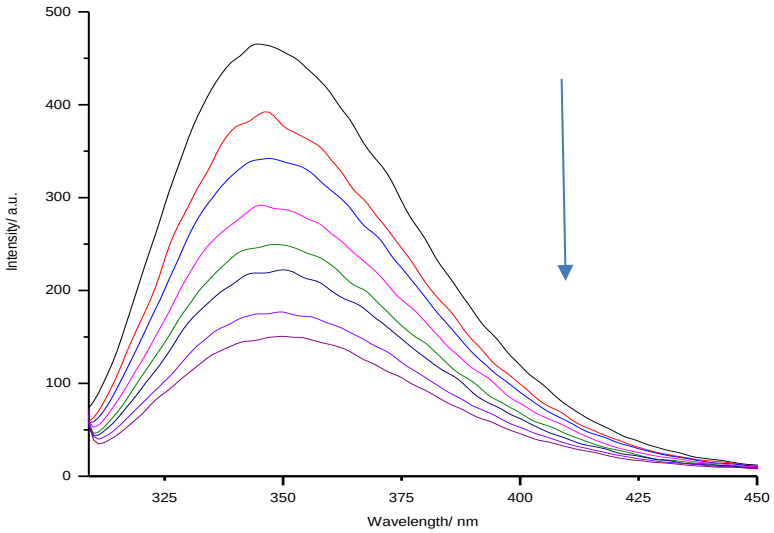

Figure 4.27: Flurescence spectra of BSA in the absence and presence of complex [11] in (5 mM Tris-HCl buffer, pH 7.2, 30 mM NaCl).

The fluorescence quenching is illustrated by the Stern-Volmer equation:[308]

$$\frac{I_\circ}{I} = 1 + K_{sv}\,[Q]$$

Equation 4.5: the Stern-Volmer quenching constant for BSA.

where I_o and I are the fluorescence intensities of BSA in the absence and presence of a quencher (i.e. the metal complex), K_{sv} is the Stern-Volmer quenching constant and [Q] is the concentration of the quencher.

A linear I_o/I *vs* [Q] plot indicates that a single type of quenching mechanism is involved, whereas a deviation from linearity indicates a mixed quenching mechanism.[312] The K_{sv} values for Ru(II)tach complexes were obtained as a slope from the plot I_o/I *vs* [Q], (Figure 4.28). The values of K_{sv} were in order of 10^4 and the K_{sv} with a magnitude order

of 10^4 M^{-1} are indicative of moderate to strong interaction between BSA and the Ru(II)tach complexes.[308, 313, 314]

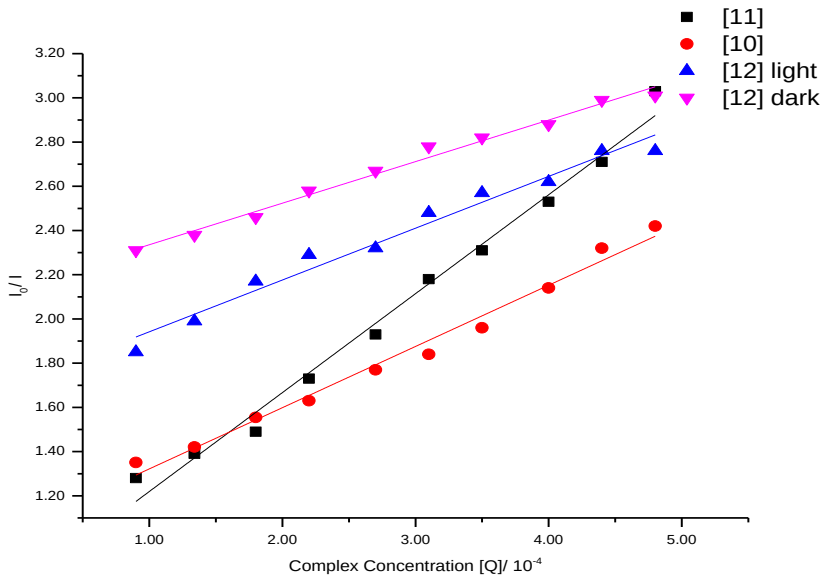

Figure 4.28: The Stern-Volmer plot of I_o/I versus [Q] for [11], [10] and [12] complexes with BSA, R^2 0.98([11]), 0.98([10]), 0.97[12] light, 0.99[12] dark.

In addition, according to the well-known connection between the K_{sv} and the K_q

$$K_q = \frac{K_{sv}}{\tau_\circ}$$

Equation 4.6: Quenching rate constant.

the quenching rate constant K_q can be calculated. Taking in to account the value of the fluorescence lifetime of protein in the absence of quencher is 10^{-8} s.[313] The K_q values for the Ru(II)tach complexes are shown in Table 4.2 and they fall in the order of 10^{11} L mol^{-1} S^{-1}. These values are higher than the maximum value for dynamic quenching (2.0 x 10^{10} L mol^{-1} S^{-1}) which suggests the involvement of a static quenching mechanism by the Ru(II)tach complexes.[285]

Further confirmation of the quenching mechanism type can obtained by UV-Vis absorption spectroscopy which is a simple method used to distinguish between the type of quenching.[306] The absorption spectra were recorded in the absence and presence of increasing amount of the Ru(II)tach complexes. The BSA absorbance shows two characteristic bands; one around 210 nm is due to the α-helix structure of the protein while the other band at 278 nm is assigned to the aromatic amino acid residues.[313] A marked decrease in the 210 nm absorbance is indicative of the perturbation of the secondary structure of the BSA, whereas the changes remarked in the 278 nm band are more subtle, and point out, to some extent, the environment of the aromatic amino acid residues is altered.[308, 313, 315]

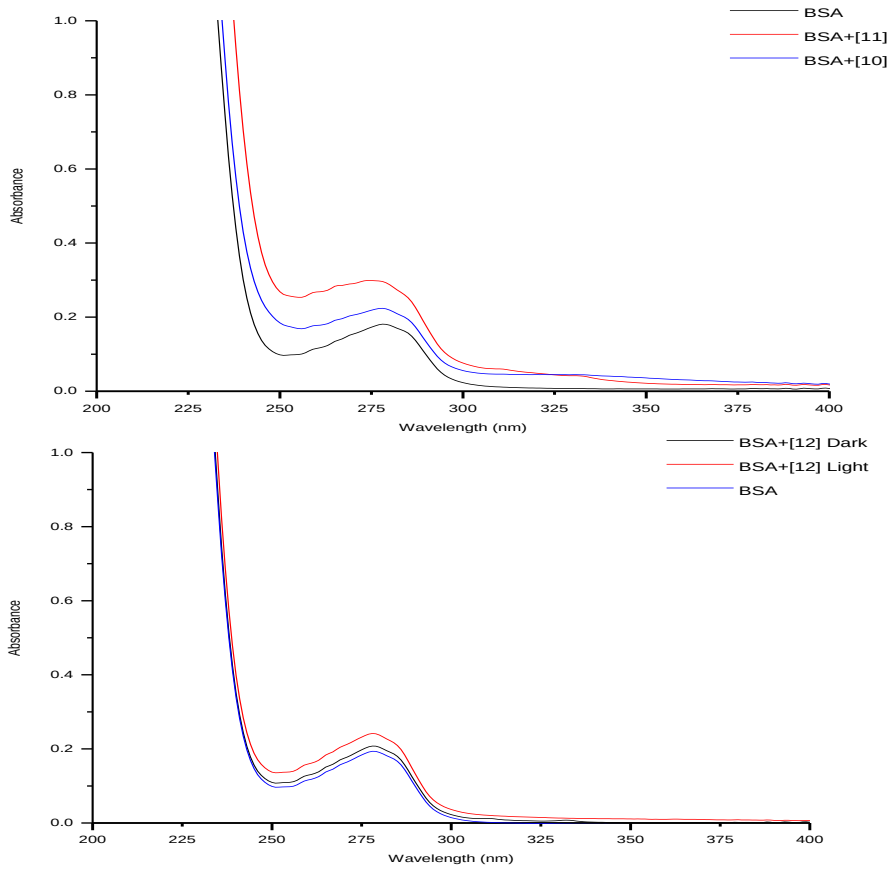

Figure 4.29: Absorption spectra of BSA in the presence of complexes [10] and [11] (top), [12] within dark and light (bottom) in (5 mM Tris-HCl buffer, pH 7.2, 30 mM NaCl).

For dynamic quenching, the absorption spectrum of the fluorophore is not changed or modified as only the excited-state fluorescence molecule is influenced by the quencher. Alternatively, static quenching refers to a new species formed between the ground-state of the fluorophore and a quencher which leads to significant changes in the absorption band at 278nm.[316]

The absorption spectra of a fixed concentration of BSA (5 µM) and an increasing concentration of the Ru(II)tach complexes are shown in Figure 4.29. As can be seen in Figure 4.29, addition of Ru(II)tach complexes to BSA leads to an increase in the absorption maximum at 278 nm with a small blue shift.

These results revealed the static quenching mechanism occurred during the interaction between BSA and Ru(II) tach complexes and these are in good agreement with the observation made from the fluorescence titration of the Ru(II)tach complexes against BSA protein.[305, 306]

To analyse the binding constant (K_b) and binding sites when a small molecule binds independently to a set of equivalent sites on a macromolecule, the equilibrium between free and bound molecules can represented by the Scatchard equation[298, 303, 308]

$$\log\left[\frac{I_\circ - I}{I}\right] = \log K_b + n\log[Q]$$

Equation 4.7: Scatchard equation for binding constant (K_b) calculation.

where I_o and I are the fluorescence intensities of the protein in the absence and presence of quencher respectively, K_b is the binding constant, [Q] is the concentration of the quencher and n is the number of binding sites.

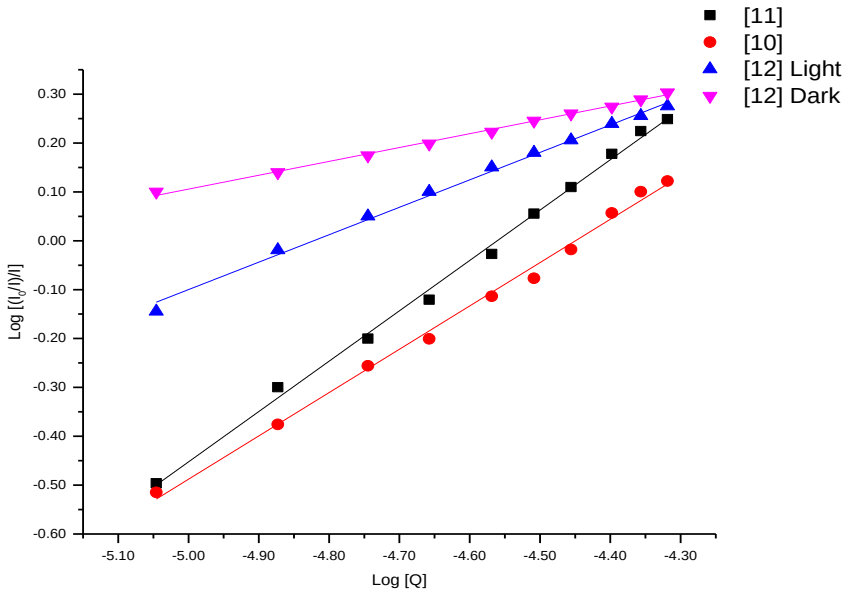

Figure 4.30: Plot of log(I_o-I)/I vs log [Q] for Ruthenium(II)tach complexes [10], [11], [12](in dark and light condition, R^2 0.99 (for all complexes).

Figure 4.30 shows the double-logarithm curve log(I_o-I)/I *vs* log [Q]. The double-logarithm plot yields a straight line and the binding constant K_b and n can be calculated from the slope and the intercept of the linear plot respectively. The binding constant (K_b) and n values for the Ru(II)tach complexes are given in Table 4.3.

Table 4.3: The quenching constants(K_{sv}) (K_q), binding constants (K_b), number of binding sites (n) of BSA-[10], [11], [12] complexes.

Complexes	K_{sv} (M^{-1})	K_q (M^{-1} S^{-1})	K_b (M^{-1})	n
[Ru(tach)(L1)Cl]Cl, **[10]**	$(2.78\pm0.17)10^4$	$2.78x10^{11}$	$(7.94\pm0.09)10^4$	(0.88±0.02)
[Ru(tach)(dppp)Cl]Cl, **[11]**	$(4.47\pm0.11)10^4$	$4.47x10^{11}$	$(5.01\pm0.08)10^5$	(1.03±0.02)
[Ru(tach)(phen)DMSO]Cl, **[12]** Light	$(2.24\pm0.13)10^4$	$2.34x10^{11}$	$(6.31\pm0.06)10^3$	(0.67±0.01)
[Ru(tach)(phen)DMSO]Cl, **[12]** Dark	$(1.88\pm0.07)10^4$	$1.88x10^{11}$	$(4.02\pm0.03)10^2$	(0.55±0.01)

From the value of K_b and n, it can be concluded that the complexes bind to BSA in a 1:1 molar ratio as the value of n is nearly 1 for all the complexes (except **[12]** which has a considerably lower value than others), and they show strong to moderate binding affinity for BSA in the order of **[11]**>**[10]**>**[12]**. K_b values with a magnitude order in the range 10^3-10^6 M^{-1} are reported as being indicative of an efficient interaction with protein.[298, 308, 314] It is known that the binding constant of a compound to serum albumin should be sufficiently high to ensure that a significant amount gets transported and distributed through the organism, but also low enough so that the compound can be released once it achieves its target. Generally, an ideal range is thought to be 10^4-10^6 M^{-1}.[308]

The higher affinity of Ru(II)tach complexes **[11]** and **[10]** compared to **[12]** can be attributed to the hydrolysis of chloride ligand in the case of complexes **[10]** and **[11]** and the subsequent formation of aqua adducts. The aqua adducts provide active coordination centres which increase the reactivity towards the BSA protein target shown in Figure 4.31. The hydrolysis of the chloride ligand in **[11]** is so fast that the reaction rate cannot be calculated (as stated by Gamble).[179] Furthermore, the presence of diphenyl phosphine group has been shown to increase the affinity toward

albumins as previously reported for platinum complex [Pt(2-phenylpyridine)(dppm)Cl], dppm=bis(diphenylphosphinomethane), that has K_{sv} $1.27x10^5$ M^{-1}.[313] As a result, the interactions between **[11]** and **[10]** with albumins can be mainly attributed to the interaction of hydrophobic ligand and whole complex with tryptophan site. The activity of **[12]** in the dark and laboratory light that showed a very low activity towards BSA $(4.02\pm0.23)10^2$ M^{-1} due to the presence of DMSO ligand which is resistance to substitution while their reactivity has increased to $(6.31\pm0.06)10^3$ M^{-1} within light due to the formation of aqua complex.

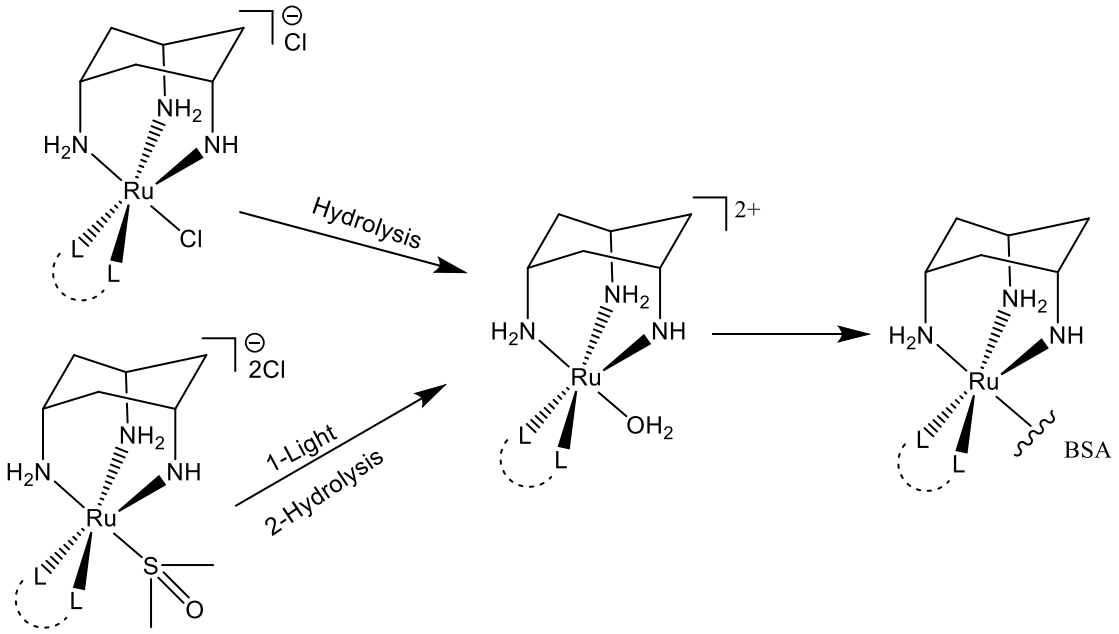

Figure 4.31: Possible interaction between BSA and [10], [11], (top) and [12], (bottom) where L-L (dppp, L1 and phen).

4.8 Conclusion

New Ru-tach complexes **[10]** and **[13]** incorporating fluorescent chelating diphosphine ligands L **[1]** and **[2]** were prepared. Complex **[10]** was fully characterized by NMR spectroscopy, mass spectrometry and UV-Vis spectroscopy and shown to be analytically pure. The obtained complexes **[10]** and **[13]** possess high fluorescent properties when excited at 350 nm in comparison to **[11]** and **[12]**, which is valuable for further applications of these complexes. The biological potential of the complexes will also be explored (Chapter 5).

The binding affinities of Ru(II)tach complexes **[10]**, **[11]**, and **[12]** with CT-DNA have been investigated by UV absorption and fluorescence spectrometry. The results obtained suggested an intercalative mode of interaction for both **[12]** and **[10]** due to the presence of aromatic heterocyclic ligand for stacking, or partial intercalation, in between base pairs. Instead, complex **[11]** does not show any reactivity to CT-DNA and these findings is in agreement with previous reports that **[11]** did not alter the mobility of the plasmid DNA in gel electrophoresis assays.[179]

The complexes' affinities to protein were investigated and BSA was selected as a relevant model. This study was monitored by UV-vis spectrometry and fluorescence spectroscopy. The experimental results indicated that **[11]** has a higher binding affinity than the other complexes tested and that the quenching of the fluorescence intensity of serum albumin operated via a static quenching mechanism.

Chapter 5

Biological evaluation of Ru-tach complexes

5 Biological evaluation of Ru-tach complexes

5.1 Introduction

A number of common chemotherapy drug compounds in clinical use are unselective for cancer cells. Cisplatin and its derivatives, carboplatin and oxaliplatin, which are widely used chemotherapeutic agents for cancer treatment, are typical examples of this class of unselective compounds.[317] The lack of selectivity is the main reason for their severe side effects (toxicity, nephrotoxicity, vomiting, nausea, etc.).[318]

In the attempt of overcoming the problem of side effects, a prodrug can be used[319, 320] which means that the compound is administered to the patient in a non-active form, and subsequent activation must occur to transform the prodrug into the active species when it has localized in specific tissue. To activate the prodrugs, two kinds of stimuli can be employed; either an internal or an external one. An example of the first case, the stimulus can be provided by chemical reduction (cellular condition, enzymatic reaction, hypoxia, etc.). The disadvantage of this approach is that there is no control on the activation process, as it relies on intracellular parameters. On the contrary, this drawback can be overcome when an external stimulus (such us temperature, magnetic field or light irradiation) is employed.[321-323] By using such approach, complete spatial and temporal control on the generation of the actual toxic molecule can be done by a physician. Light activation of a prodrug is the most commonly applied technique in the clinic for the treatment of certain age related macular degeneration, skin-related diseases and cancer.[324] In the field of anticancer study, the light mediated activation of prodrugs can be divided in to two main classes: photodynamic therapy (PDT) and photoactivated chemotherapy (PACT).[300, 323, 325-327]

PDT relies on the combination of a non-toxic photoactive compound known as a photosensitiser (PS), light and molecular oxygen to induce cell death using an oxygen-dependent mechanism. More precisely, the (PS) is irradiated with light at specific wavelength to reach its singlet excited state, (PS^*), which must then undergo an

intersystem crossing (ISC) to achieve a triplet character ($^3PS^*$). At this point, a proton or electron transfer to the surrounding biological substrate can take place to form radicals that can further react with molecular oxygen to generate reactive oxygen species (ROS, type I). In parallel, an energy transfer from ($^3PS^*$) to oxygen in its triplet ground state ($^3O_2$) can occur which leads to the formation of oxygen in its singlet state ($^1O_2$, type II) shown in Figure 5.1.[324]

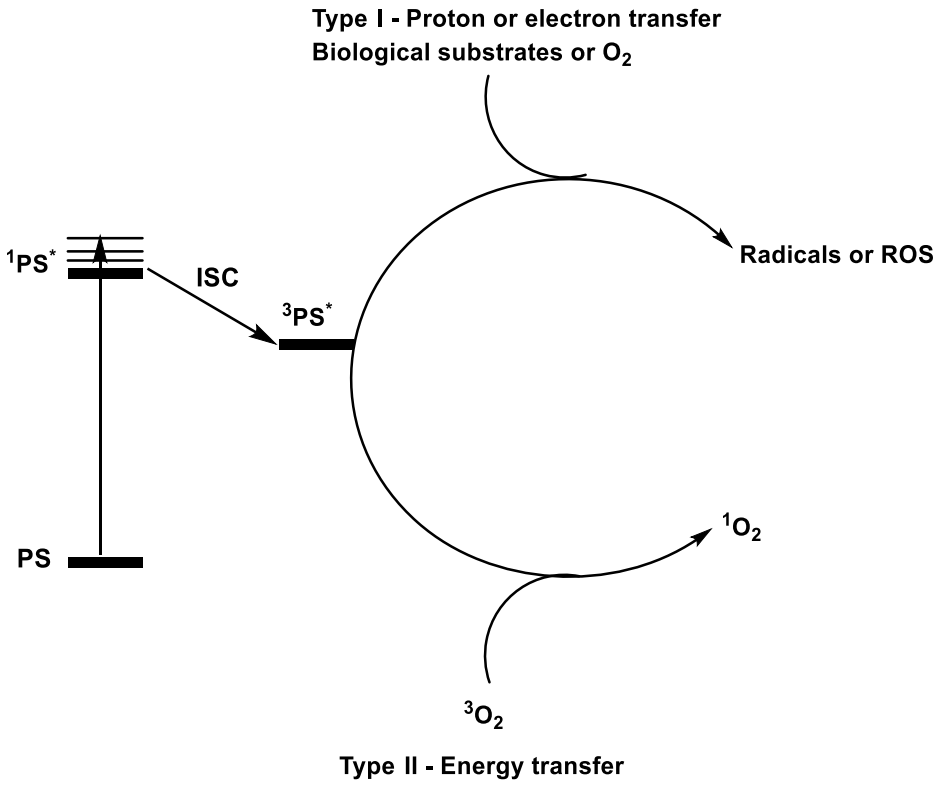

Figure 5.1: Mechanisms of action of PDT.[300]

The $^1O_2$ is a very reactive and toxic form of oxygen and this high reactivity leads to a short diffusion distance 0.02 µm with an estimated half-life of 40 ns in a biological

environment, generating cellular damage that leads to cell death.[328, 329] As a consequence, PDT induces cell death with spatial and temporal control, and the most approved PSs act *via a* type II mechanism.[330] The most extensively studied complexes as potential photosensitizers in photodynamic therapy (PDT) are porphyrin derivatives,[331] however a drawback or disadvantage of PDT is its lack of efficiency on cancers as most tumours are hypoxic (low oxygen tension) in their internal core.[16] To overcome this drawback, researchers have developed novel photo-activation strategies that do not depend on an oxygen-dependent mechanism. Such strategies are known as photoactivated chemotherapy (PDAT), which has several activation pathways to produce the toxic species and induce cell death such as ligand ejection, DNA crosslinking and caging pathways.[300]

Over the past few years, considerable research has been focused on using transition metal complexes in the fields of PDT and PACT,[332, 333] with a particular focus on ruthenium complexes as attractive alternatives to platinum anticancer drugs.[92] Ruthenium (II) complexes have shown to be well suited as novel agents for photodynamic therapy (PDT) and photoactivated chemotherapy (PACT) due to their interesting features as DNA intercalating probes[241, 334, 335] and their $^1O_2$ production near the genetic material.[336, 337] Furthermore, these complexes are good PS candidates due to the existence of triplet excited states. The main drawback of these compounds is the presence of MLCT absorption maximum in the range 450-500 nm, while the PDT relies on the excitation at higher wavelengths (>600 nm) that allow for deep tissue penetration.[338] Therefore, focus on the other mechanism of PDAT is required to overcome the limitations mentioned above. The PACT has different photo-activation strategies either by metal-based DNA photobinder acting or photo activated release approaches. Glazer and coworkers have developed a new series of Ru(II) polypyridyl complexes shown in Figure 5.2,[339] which photoeject a methylated ligand followed by the formation of an aqua species that can bind either to DNA or protein. The *in vitro* study showed no toxicity (IC_{50} > 100 µM) under dark conditions in HL60 leukemia and A549 cell lines and after irradiation at > 450 nm, their cytotoxicity was enhanced within the range of 2.6-1.1 µM. The activity of the photoproduct has been confirmed by using

plasmid DNA pCU19 in which complex **A** showed DNA photobinding whilst complex **B** showed DNA damage and photobinding.[339]

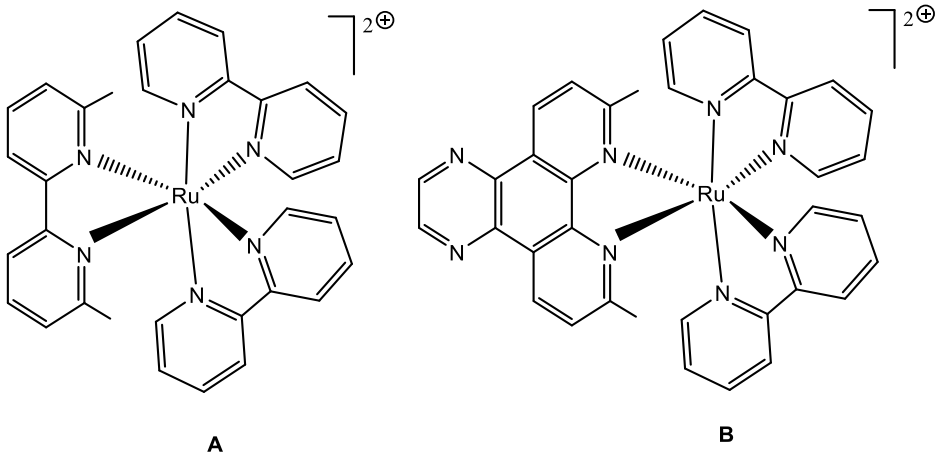

Figure 5.2: Structure of the photolight activated complexes A and B synthesized by Glazer and coworkers.[339]

As long as the covalent bonding to DNA is not the only target for ruthenium complexes, Feyter's and Wang's groups highlight the intercalation in DNA that nicking the activity upon visible light irradiation (Figure 5.3).[340, 341]

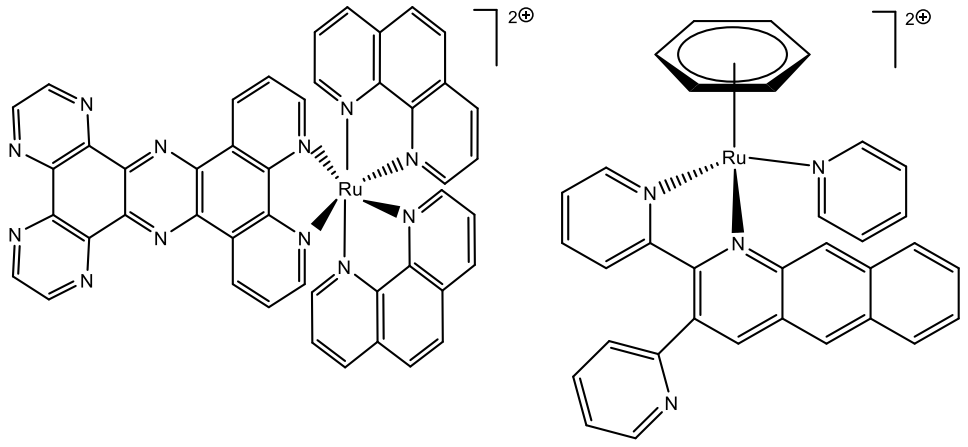

Figure 5.3: Intercalating ruthenium complexes that absorb visible light.[300]

Driven by these promising *in vitro* results with ruthenium polypyridyl complexes as PDT and PACT agents, and in combination with the high binding affinity of Ru(II) tach complex **[12]** with CT-DNA reported in Chapter 4, this complex was tested in A2780 and A549 cell lines both in the dark and under light irradiation.

5.1.1 In vitro evaluation of activity via MTT assay: Principle and procedure

An important aspect in the development in cancer therapies is ultimately drug discovery. To achieve this aspect new compounds with potential anticancer activity are continuously prepared.[342] The cytotoxicity of natural products and drugs is a very important factor to assay in order to determine how toxic these compounds or complexes are to cells and tissues. Many studies and assays have been adopted to screen the cytotoxicity of chemicals and drug compounds and even plants. The 3-(4, 5-dimethylthiazolyl-2)-2, 5-diphenyltetrazolium bromide (MTT) assay has been widely used as a reliable method to examine cell viability as evidenced by thousands of published articles.[343-345]

The MTT assay relies on the reduction of a tetrazolium salt to formazan by a colouring agent or enzyme called dehydrogenase, which are found in the mitochondria of living (viable) cells (Figure 5.4). The yellow, water soluble tetrazolium salt is reduced to the non-soluble purple formazan, which crystallises as needle-like crystals from the medium containing viable cells. The insoluble formazan product can be solubilized with organic solvent like DMSO, SDS (sodium dodecyl sulfate), and isopropanol.[346, 347]

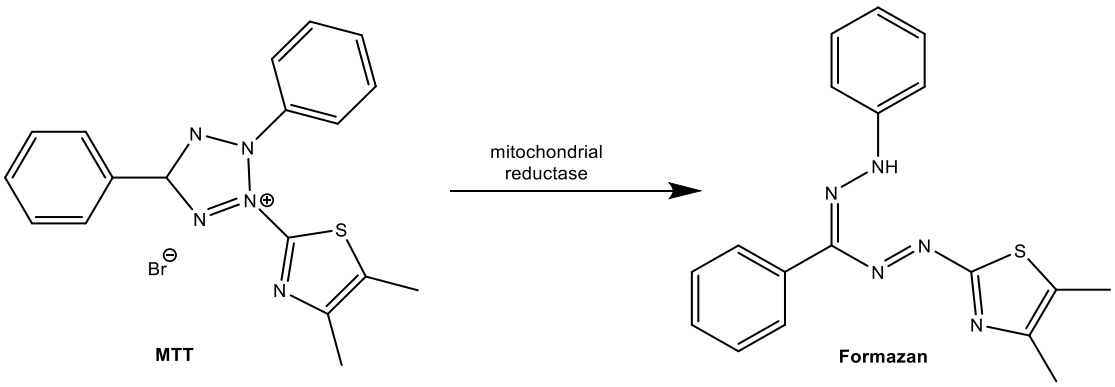

Figure 5.4: The reduction of MTT bromide to formazan product.

The formazan product has a distinct absorbance maximum at wavelength 540 nm and this absorbance is directly proportional to the number of viable cells within the population and inversely proportional to the degree of cytotoxicity.[348]

The absorbance values of wells with cells incubated with the test compound are compared to the absorbance values of wells with untreated cells. The decrease in cell number indicates cell growth inhibition, and the complex or drug activity is then defined as the concentration of the compound that is required to obtain 50% growth inhibition in comparison to the growth of untreated cells, which represents 100% growth.[345, 349]

The 50% inhibitory concentration (IC_{50}) can be expressed as a molar concentration (micromolar concentration) or mass per volume, so the IC_{50} is the concentration of test compound that produce 50% decrease in the control level of viable cells 100% (positive control) in comparison to the blank control 0% (negative control).

Since the reading obtained in MTT assay is absorbance (A), the base line for IC_{50} values calculation is the absorbance (A) value of the control wells in the MTT plate, and this value should be identical for the dilution that used to prepare the stock solution. By using the absorbance of control wells, the absorbance values of the blank control were subtracted from all other values then the percent value of inhibition at each concentration can be calculated using the following equation:

$$\%\ Inhibition\ = 1 - \left(\frac{A_{obs}}{A_{control}}\right) \times 100$$

Equation 5.1: Equation of the percent inhibition calculation from the absorbance of the 96 well plate.

where $A_{obs.}$ is the observed absorbance value for the treated cells at different concentration, while $A_{control}$ is the absorbance values for the untreated cells, a positive control that represent 100% viability.[350]

Then the percent inhibition of each concentration can be plotted to allow for the calculation of the IC_{50} value. % cell viability is plotted against the log of the compound concentration and fitted as a sigmoidal curve, and the IC_{50} value extrapolated from the graph as the concentration which gives 50% growth inhibition.[349, 350]

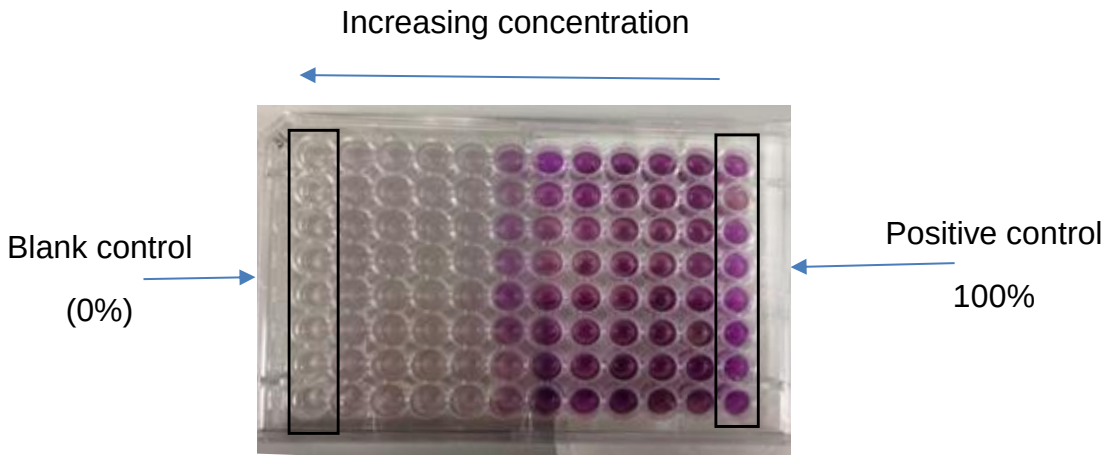

Figure 5.5: Picture of a 96-well plate used in MTT assay.

5.2 MTT assay for Ruthenium(II)tach complexes

5.2.1 *In vitro* evaluation of tachmonoben

In an effort to comprehend the mechanisms of action of a compound, a series of modified target compounds that differ structurally from the 'traditional' can help to evaluate structure activity relationships (SARs).[351,352]

Cis-tach **[1]** does not inhibit the growth of two cell lines, A549 and A2780 up to concentration of 250 μM, and is considered as an inactive compound, while the previously prepared trisubstituted tach ligand, tachben,[178] exhibited a high level of toxicity (IC_{50} 6.65±0.21 and 3.03±0.10 in A549 and A2780, respectively).

These differences in the final IC_{50} highlight the effect of the tach 'arms' in cytotoxicity and show the enhancement of activity of the tri-armed tach ligand. This is presumably due to increasing lipophilicity which leads to an increase in the ability to cross membranes or actively interact with the target (as the aromatic arm is a hydrogen bond donor).[178]

The results mentioned above in combinations with the SARs hypothesis by Ciano, that one arm on the tach moiety is a main requirement to have at least mild toxicity, prompted us to modify the structure of tach and synthesise tachmonoben **[3]** (Chapter 2). Importantly for the biological evaluation, the purity of **[3]** was confirmed by elemental analysis and NMR spectroscopy and the solubility in media was checked to at least 450 μM prior to use in both cancer cell lines.

The cytotoxic activity of **[3]** against A549 and A2780 cell lines has been investigated by using the MTT assay according to general procedure (Chapter 7). In both cell lines, tachmonoben **[3]** showed a moderate toxicity in comparison with the widely-used drug cisplatin as a positive control (Figure 5.6), with an average IC_{50} value of (66.42±1.32) μM against A549 and (64.1±1.9) μM against A2780 cells. The observed IC_{50} revealed

that cytotoxicity depends on the presence of the arm, which seems to support the hypothesis discussed earlier relating to the comparison between the nontoxic tach and higher toxicity tri-substituted tachben (Table 5.1). The hydrophobic π-donating substituent within the tach structure could also enhance the intercellular accumulation of tachmb **[3].** It may play an additional important role in biomolecular interactions and recognition processes.

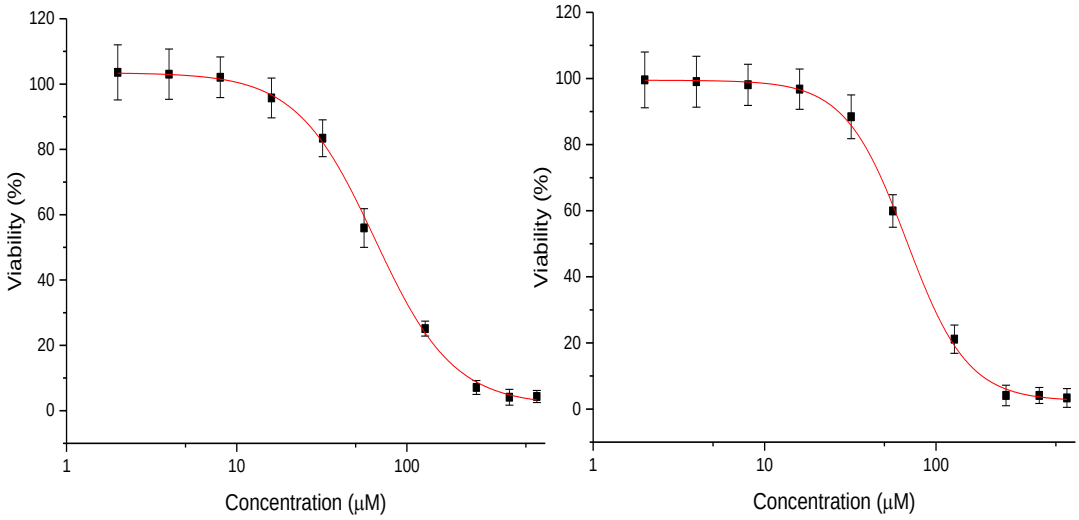

Figure 5.6: IC_{50} graphs of tachmonoben [3] against A2780 (left) and A549 (right) cells.

These results are consistent with previous observations on ruthenium arene complexes that showed enhanced cytotoxicity of the complexes with increasing the size of the arene ring system.[126]

There is a difference between the cytotoxicity of the two cell lines and this attributed to the different biological conditions within each system that cause difference in the IC_{50} value for the test compounds.

Table 5.1: IC_{50} and power values for tachmonoben [3] and cisplatin, tach, and tachben for comparison.(a) IC_{50} of Cisplatin and tachben were obtained with the same medium and condition for other compounds.[178]

Compound	A549		A2780	
	IC_{50} (µM)	*Power*	IC50 (µM)	Power
Cisplatin[a]	2.85±0.24	1.3±0.1	0.40±0.01	1.0±0.1
Tach **[1]**	>300	-	>300	-
Tachben[a]	6.65±0.21	-	3.03±0.10	-
Tachmonoben**[3]**	66.42±1.32	2.4±0.17	64.14±1.9	1.88±0.15

5.2.2 In vitro evaluation of Ru-tachmonoben complexes

Although tachmonoben was not very active against A549 and A2780 cell lines, it still acts as a promising ligand which prompted us to improve the activity of the modified ligand by preparation of the new ruthenium(II) tachmonoben complexes presented in Chapter 3.

Three complexes were synthesised [Ru(tachmb)(DMSO)Cl_2] **[5]**, [Ru(tachmb)(PPh_3)Cl_2] **[7]**, [Ru(tachmb)(dppb)Cl]Cl **[9]** - but only two complexes **[7]** and **[9]** passed the purity check by elemental analysis (±0.35 % deviation from the calculated values) therefore **[5]** was not tested.

These two complexes were only slightly soluble in culture medium; thus they were initially dissolved in DMSO then diluted with medium. The IC_{50} values and *power* values for **[7]** and **[9]** are given in Table 5.2. The complexes display high activity in comparison to cisplatin. In particular, **[9]** possesses potent activity exceeding that of cisplatin in the A549 and A2780 cell lines.

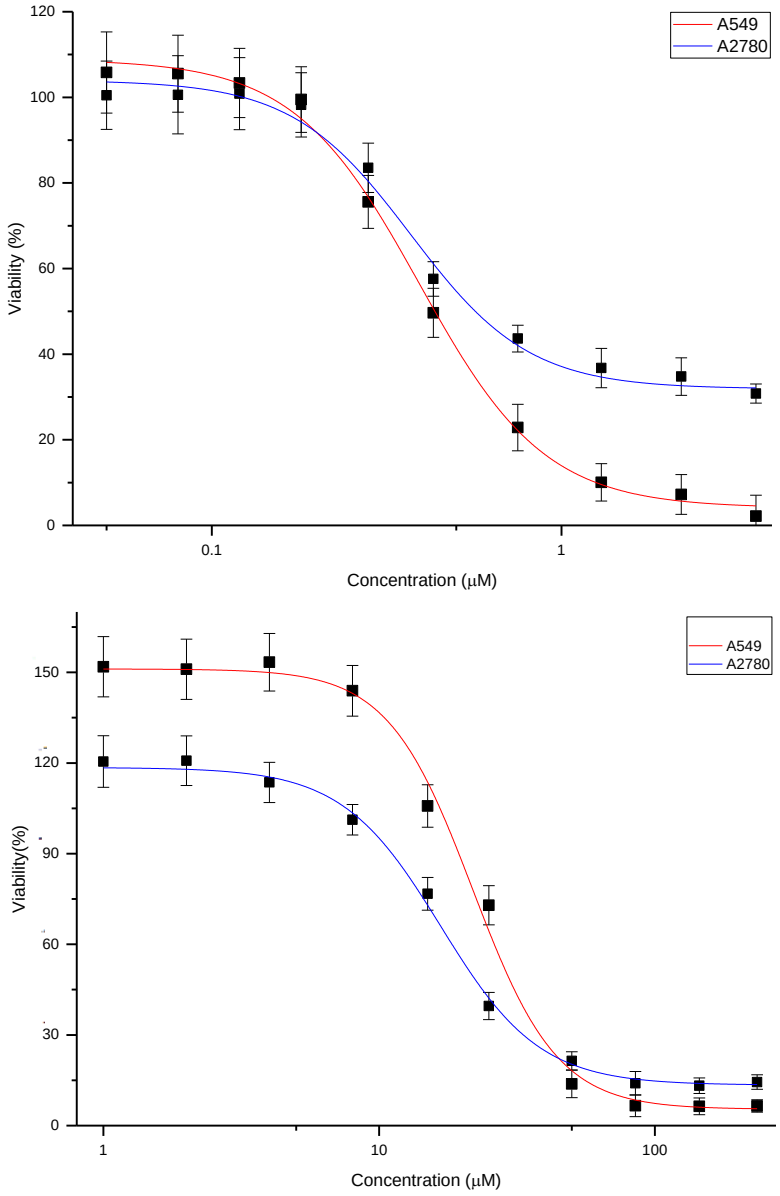

Figure 5.7: Logarithmic dose-response curve of [Ru(tachmb)(PPh$_3$)Cl$_2$] [7] (bottom) and [Ru(tachmb)(dppb)Cl]Cl [9] (top) against A549 and A2780.

As highlighted before, the higher activity of the two ruthenium(II) modified-tach complexes **[7]** and **[9]** compared to the non-modified tach complexes supports the hypothesis of increased cytotoxic activity by the presence of the benzyl substituent

within the tach structure. This is evident by comparison with the ruthenium tach complexes previously prepared and their biological activity, which was evaluated by MTT assay (values are shown in Table 5.2).[179]

As shown in the table, the tachmonoben ligand has notably increased the anti-proliferative action of the complexes compared to the complex reported by Gamble. In particular, especially complex **[7]** has higher cytotoxicity in both cell lines than [Ru(tach)(PPh_3)(DMSO)Cl]Cl. This behaviour can be explained by the effects of the steric hindrance of the phenyl ring, which promotes the incorporation of a chloride ligand in to the coordination sphere of the metal rather than the large DMSO molecule. In turn, this results in increasing the rate of activation of the compound within a cell and nucleus; DMSO is resistant to exchange with water, the important activation step for complexes in biological systems, due to a strong Ru-S bond. The slow exchange of DMSO was the main reason for the weak anti-proliferative of [Ru(tach)(PPh_3)(DMSO)Cl]Cl. Such behaviour appears to parallel that of ruthenium arene complex [(η^6-arene)Ru(en)Cl]$^+$ in which the hydrolysis provides a pathway for activation. Again, the aqua ligands are much more reactive, for example, toward substitution by guanine bases on DNA.[136] Another example of the effect of the leaving groups in the activity of complex is given by Alessiao's complex, [Ru(tacn)en(DMSO)] where tacn=1,4,7-triazacyclononane, which it was nonactive due to weak hydrolysis.[165] On the other hand, the tachmonoben **[3]** increase the lipophilicity of **[7]** while [Ru(tach)(PPh_3)Cl_2]Cl was poorly soluble which prevent their assessment by MTT assay.

Table 5.2: IC_{50} and p values for [9] and [7] with in comparison to tach complexes in both A549 and A2780.

Compound	A549		A2780	
	IC_{50} (μM)	*Power*	IC_{50} (μM)	*Power*
[Ru(tachmb)(PPh_3)Cl_2]**[7]**	21.82±1.16	2.82±0.3	16.73±0.7	2.41±0.20
[Ru(tachmb)(dppb)Cl]Cl **[9]**	0.39±0.01	2.4±0.18	0.34±0.03	2.50±0.38
[Ru(tach)(PPh_3)(DMSO)Cl]Cl	149.0±4	2.00±5	67.8±10	1.95±6
[Ru(tach)(dppb)Cl]Cl	1.15±2	1.76±3	0.39±1	2.27±4

5.2.3 *In vitro* evaluation of Ru-cis tach complexes

The cytotoxicity of the ruthenium-tach complexes described in Chapter 4 was evaluated with the MTT assay against the A549 and A2780 cell lines.

On the basis of their IC_{50} values, [Ru(tach)(dppp)Cl]Cl, **[11]** is more cytotoxic than [Ru(tach)(FL-I)Cl]Cl **[10]** and is more cytotoxic than cisplatin (Table 5.3). All previously prepared ruthenium(II) tach diphosphine complexes showed similar activity, and from the structure activity relationships it has been proposed that phenyl rings are capable of forming hydrogen bonds to the amine groups thus protecting the cis-tach amine groups when passing through the cell membrane. They create steric bulk around the reactive coordination site of the complex as shown in Figure 5.8 and it was proven by the X-ray structure for the complexes.[179] The flexibility and hydrophobicity have a great influence on increasing cytotoxicity as it proved previously,[126, 133, 353] thus the more flexible ligand dppp has higher cytotoxicity than FL-I.

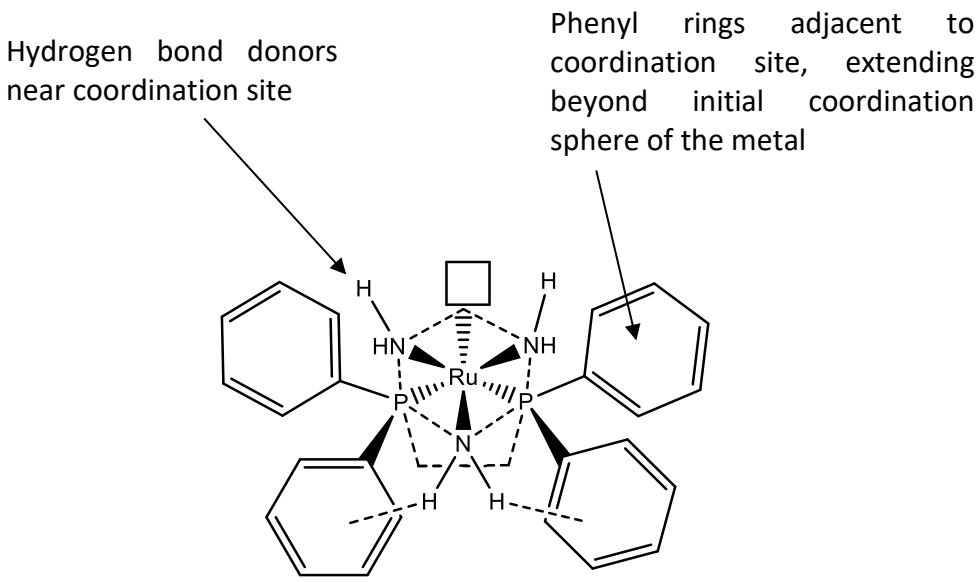

Figure 5.8: Schematic representation of the diphosphine complexes.[179]

Table 5.3: IC_{50} values and power values of [10] and [11] against A549 and A2780.

Compound	A549		A2780	
	IC_{50} (μM)	*Power*	IC_{50} (μM)	*Power*
[Ru(tach)(FL-I)Cl_2]Cl**[10]**	20.61±1.08	2.32±0.2	18.03±0.74	3.21±0.30
[Ru(tach)(dppp)Cl]Cl **[11]**	1.12±0.03	1.98±0.13	0.37±0.02	2.97±0.56

The interaction of **[10]** and **[11]** with biomolecules provides potential insight into the anti-proliferative activity. Although **[10]** showed an intercalative mode of interaction with DNA models under physiologically relevant conditions, there is not a strong correlation between this reactivity and cytotoxicity towards cancer cell lines. This bound correlation led to the investigation of proteins as potential targets of ruthenium tach complexes, which is supported by the low binding affinity of **[10]** with BSA protein in comparison to **[11]** that leads to low efficient distribution. These results prompted

us to presume non-classical mechanism of action in comparison to cisplatin; a hypothesis which was further confirmed by *in vitro* evaluation of **[12]** performed in the following section.

5.2.4 *In vitro* evaluation of photochemistry of Ru [12]

The photochemical reaction of [Ru(tach)(phen)(DMSO)]Cl, **[12]** was monitored by absorption spectroscopy (Figure 4.9) and it exhibited selective photo ejection of the DMSO ligand when irradiated with laboratory white light. The kinetics of this photo ejection in Tris-HCl buffer at pH 7.2 were monitored using a wavelength of 470 nm previously described in Section 4.5. Electrospray ionization mass spectrometry (ESI) indicates the ejection of DMSO ligand and the formation of $[Ru(tach)(phen)(H_2O)]^{2+}$ at *m/z* 214.32, which was further conformed by ^{1}H NMR.

To determine the potency of light sensitive complex **[12]**, cytotoxicity studies by MTT assay were performed in A549 and A2780 cell lines. Cells were incubated with complex **[12]** for 20 hours in the dark before irradiation with normal white light for 30 min and dark controls were run in parallel.

The MTT assay indicated that under dark conditions, **[12]** exhibited weak to no activity in both A2780 and A549 cell lines respectively, while on irradiation the cytotoxicity was enhanced to 61.22 ± 3.52 µM in A2780 and up to 302.36 ± 5.33 µM in A549.

These differences in the light and dark IC_{50} values prompted us to irradiate the cells for longer time periods in order to estimate the effect of light over several time points. Therefore, the cells were incubated with LED for 30 minutes, 24 hours and 48 hours in the two cell lines, in addition to one dark plate as control.

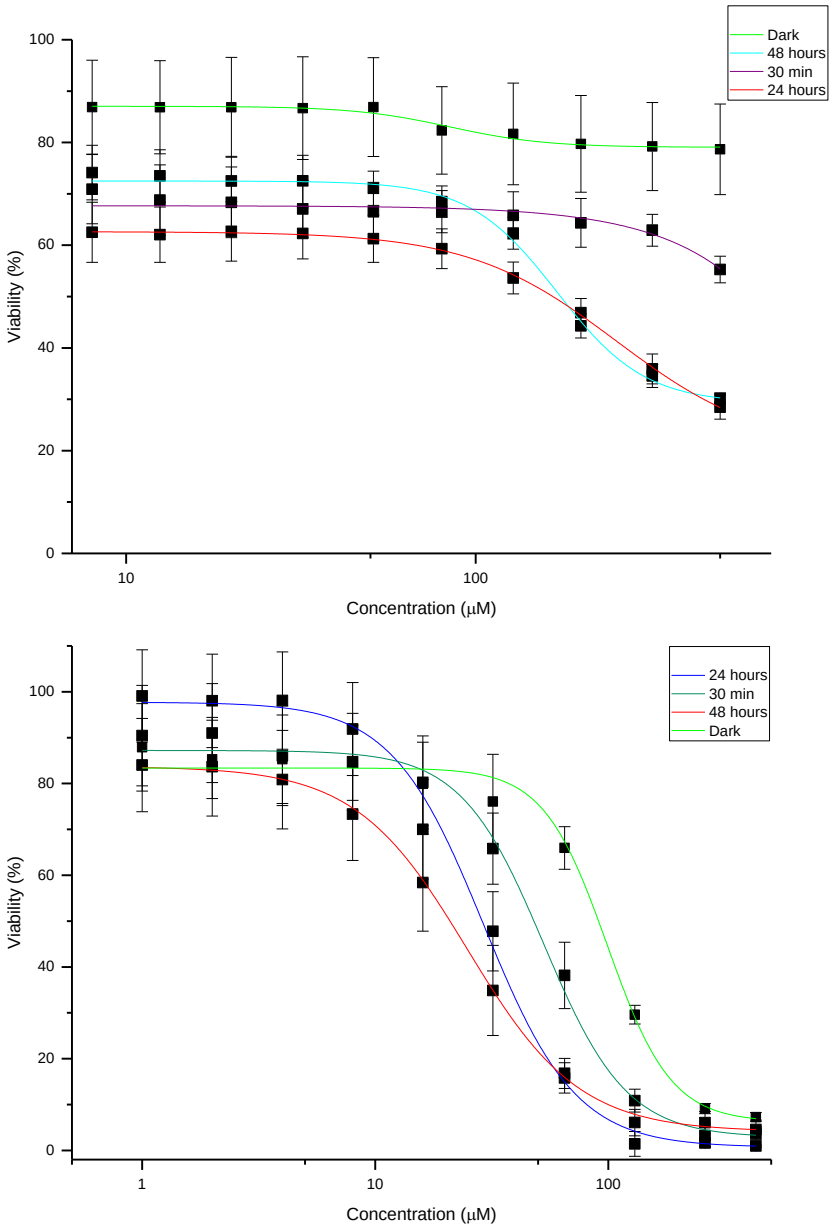

Figure 5.9: Viability graph of [12] against A549 (top) and A2780 (bottom), time shown are irradiation times.

As expected, the compound displayed an enhancement of cytotoxicity upon increasing time of light irradiation and shows higher toxicity within 48 hours (Figure 5.10).

This enhancement of IC_{50} value upon incubation with LED light (Figure 5.11) can be explained by photo ejection of the DMSO ligand upon light activation. This is quickly followed by the formation of an aqua complex which can bind to DNA in an intercalative manner (as supported in Chapter 4) with a higher binding affinity in the light condition rather than dark condition.

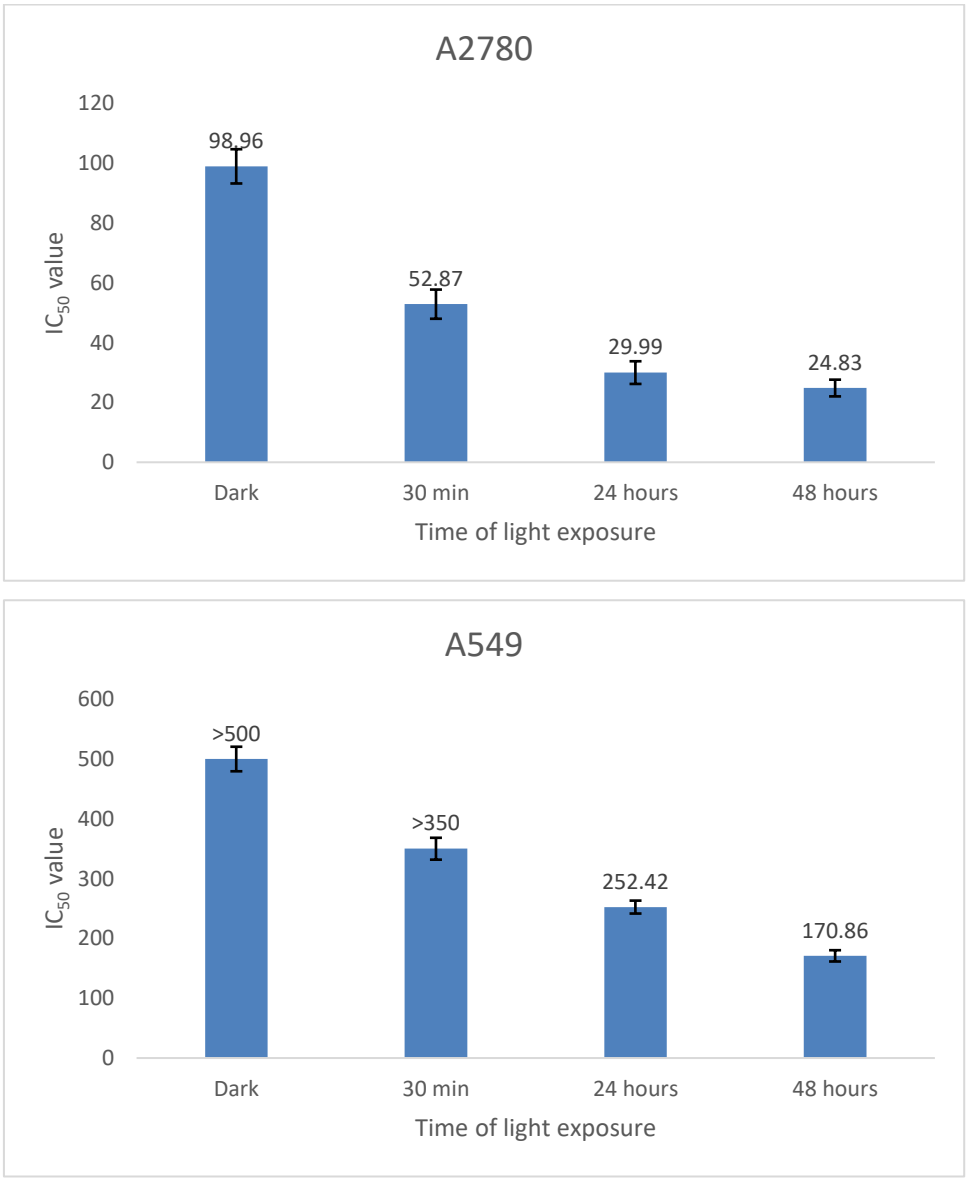

Figure 5.10: IC_{50} values of [12] in the dark and upon light irradiation against A2780(top) and A549 (bottom).

Although complex **[12]** exhibited significantly higher binding strength to DNA compared to other ruthenium tach complexes, the low cytotoxicity demonstrates that there is no significant correlation between this reactivity and toxicity in cancer cells. This conclusion is in good agreement with previous presumptions for **[10]** and **[11]**, therefore it is presumed that these complexes behaved like RAPTA compounds which are more reactive towards proteins than cisplatin, and even bind to protein in the presence of DNA.[156, 354, 355]

5.3 Structure-Activity Relationship

In an attempt to analyse the activity of ruthenium tach complexes and modified tach, there are some features that should be highlighted for further development and increased activity of ruthenium tach complexes.

A structural modification of the cis-tach ligand is a main requirement for increasing the activity. Any modification of the tach ligand which leads to a increased susceptibility of the complex to form the chloride analogue will lead to higher cytotoxicity of the complex. Chloride is a good leaving group inside cells which may be exchanged with biological targets such as DNA or protein.

The diphosphine ligand provides good to excellent activity for ruthenium tach complexes and also with arene complexes,[216] by providing flexibility and hydrophobicity.

On the basis of IC_{50} values for **[10]**, **[11]** and **[12]**, it is apparent that DNA is not the main target of these complexes and, instead, protein might be the primary target of these molecules. This is clearly evidenced by the study of interaction of these complexes with DNA and BSA protein which show that **[12]** and **[10]** process a higher intercalative potency than **[11]** but they have lower cytotoxicity. Therefore, their stronger binding to DNA does not correlate with increased biological activity. This

inconsistent correlation between cytotoxicity and DNA affinity was shown previously in dinuclear ruthenium(II) polypyridyl complexes containing three and ten methylene chains in their bridging linkers, indicating that the cytotoxicity may not originate from DNA targeting.[356]

In general, it seems that the DNA does not play important rule in the mechanism of action of tach-based complexes, as the decorating of the ruthenium tach compound with an intercalating group is not favoured.

The evidence presented from this study (and others) strongly suggests that the presence of more hydrophobic areas within the tach structure, a chloride group as an exchange site, and a diphosphine chelating ligand, results in highly active ruthenium tach complexes (as shown in the complexes with the general formula [Ru(tach)(P-P)Cl]Cl[179] and [Ru(tachmb)(dppb)Cl]Cl).

5.4 Conclusion

The MTT assay is a quantitative, and reliable colorimetric method when used to measure the efficacy of cytotoxic compounds. Two different cell lines were used in the study: A549 and A2780. The new ligand tachmonoben **[3]** and its Ru(II) complexes **[7]** and **[9]** were assessed using the MTT assay and they have shown very promising activity, with complex **[9]** surpassing the activity of cisplatin in the A2780 line.

The chelating diphosphine complexes **[10]** and **[11]** exhibited high cytotoxicity, as expected from the high hydrophobicity of diphosphine ligands. The fluorescent tag on **[10]** and the 'light switch' feature with DNA would be useful to follow the subcellular localization in future.

The lightsensitive complex **[12]** was weakly to non-toxic in the dark on A2780 and A549 cell lines respectively, however upon irradiation it showed a remarkable phototoxicity. The phototoxicity of **[12]** was performed by pre-treatment of the anticancer cell lines

with **[12]** followed by incubation with an LED to provide the light to the complex. The observed increase in activity is due to the activation of the complex by the formation of aqua product [Ru(tach)(phen)(H_2O)] after irradiation with light, which is proved by UV-VIS and mass spectroscopy (Chapter 4). The aqua product then interacts with the biomolecules more easily and leads to an increase in the activity.

Chapter 6

Conclusion and future work

6 Conclusion and future work

6.1 Conclusion

The primary objective of this research was to expand the ruthenium tach framework by structural modification to one of the amine groups. The incorporation of a benzyl functional group *via* condensation with benzaldehyde followed by reduction of a C=N bond was achieved to produce tachmb **[3]** ligand. The new ligand exhibited a moderate effect on cytotoxicity potency in both A549 and A2780 cell lines compared to the non-active behaviour of free tach and the high cytotoxicity of the tri-substituted tach (tachben). This finding supports the hypothesis that the presence of at least one tach 'arm' is required to tune the activity of the tach ligand.

To introduce the tachmb **[3]** ligand into the coordination sphere of the ruthenium, the easily prepared precursor $[Ru(DMSO)_4Cl_2]$ was used firstly to produce the highly water soluble complex $[Ru(tachmb)(DMSO)Cl_2]$ **[5]**. However, the cytotoxicity of this complex was not quantified as a pure sample could not be obtained (as confirmed by elemental analysis). Therefore, two other starting materials, $[Ru(PPh_3)_3Cl_2]$ and $[Ru(dppb)(PPh_3)Cl_2]$, were then used and resulted in the formation of two new complexes, $[Ru(tachmb)(PPh_3)Cl_2]Cl$, **[7]**, and $[Ru(tachmb)(dppb)Cl]Cl$, **[9]**, respectively. The presence of benzyl substituted tach (tachmb, **[3]**) within the coordination sphere of ruthenium tach complexes promoted the existence of two structural isomers of each complex which were identified by NMR spectra. Furthermore, the steric demand of the ligand enforces the lability of DMSO and increased the exchange of DMSO with a chloride ligand. The presence of a more labile chloride ligand within the coordination sphere of metal may be the explanation for the increase in the activity of the complexes. As expected, complexes **[7]** and **[9]** showed high activity against the A549 and A2780 cell lines while **[9]** possesses even higher cytotoxicity than cisplatin (which exhibited IC_{50} values of 0.39±0.01 μM A549 and 0.34±0.03 μM A2780).

The library of ruthenium tach complexes were extended further by addition of fluorescent probes FL-I and FL-II to visualize the sites of accumulation in the cell. This produced complexes **[10]** and **[13]** complexes were characterized by NMR and MS while the low yield of **[13]** prevented further study.

With the goal of gaining deeper insight in to the mode of action of the ruthenium tach complexes, fluorescent [Ru(tach)(L1)Cl]Cl **[10]**, highly active [Ru(tach)(dppp)Cl]Cl **[11]** and light sensitive [Ru(tach)(phen)DMSO]Cl_2 **[12]** were chosen to examine their interaction with biomolecules (DNA and protein). Absorption fluorescence spectroscopy was used to investigate the binding constant of CT-DNA and BSA to the ruthenium tach complexes. The results reveal that **[11]** did not show any activity towards CT-DNA while **[10]** and **[12]** bind to CT-DNA by an intercalating mode due to the planarity of the chelating FL-I and phenanthroline. The light sensitive **[12]** exhibited strong nuclease activity in the presence of light. The binding constant (K_b) values are in the range of 3.42×10^4 to 7.52×10^5 M^{-1}, and the apparent binding constants (K_{app}) in the range from 2.04×10^6 M^{-1} to 2.05×10^7 M^{-1}, as measured by UV and fluorescence spectroscopy. On the other hand, BSA binding properties of the complexes have been investigated and all the complexes bind in a 1:1 molar ratio through static mode. The high binding constant for BSA is obtained with **[11]** which is 5.01×10^5 M^{-1}.

The *in vitro* evaluation of the complexes showed high activity of complex **[11]** compared to **[10]** and **[12]** which supports the assumption that DNA is not the first target for ruthenium complexes.

Furthermore, the light sensitive complex **[12]** exhibited moderate to high phototoxicity upon irradiation with normal light while it was weak to non-active in the dark against A549 and A2780 cell lines. This reactivity occurs because complex **[12]** exhibits photo-ejection of the DMSO ligand which activates the complex through ligand exchange and formation of an aqua complex (as indicated by UV-VIS spectrum, MS spectroscopy and NMR spectroscopy). The aqua ligand is more labile than DMSO and therefore allows for enhanced coordination to biomolecules.

6.2 Future work

In general, the room for the development and future study of ruthenium tach complexes is spacious. The work in this thesis ends with two promising complexes; fluorescent analogues of ruthenium tach complexes **[10]** can be used as models for intracellular visualization by fluorescence microscopy or confocal microscopy as this complex possesses the 'light-switch' property which is an important feature when designing a molecular probe for cellular imaging. The other promising complex for further study is **[12]**, which is a good candidate to be a photoactive compound. These complexes have only been evaluated against two cancer cell lines therefore they could be evaluated to other tumour types such as A2780cis and $A2780^{AD}$ (drug-resistant variants). The evaluation of activity in non-cancerous cells should be performed to investigate the selectivity profile.

The interaction of these complexes with biomolecules can be further studied by NMR spectroscopy and mass spectrometry. Furthermore, some crystallization experiments of the complexes with DNA sequences and proteins could be performed to obtain a deeper understanding of the complex binding.

Furthermore, density functional theory (DFT) and molecular dynamics (MD) may also be used to examine the interaction with nucleic acids and proteins.

Chapter 7

Experimental

7 Experimental

7.1 General

Materials and solvents used were purchased from Sigma-Aldrich UK or from Fisher Scientific without further purification. *Cis*-*cis*-1,3,5-Cyclohexanetricaboxylic acid was purchased from TCI UK and ruthenium trichloride hydrate from Precious Metals Online, propane-1,3-diylbis(diphenylphosphane) from Strem Chemicals and butane-1,4-diylbis(diphenylphosphane) from Lancaster Synthesis. *Cis*,*cis*-1,3,5-triaminocyclohexane (*cis*-tach) was synthesised acoording to literature procedure,[168, 180, 357] dichlorido*tris* (triphenylphosphane)ruthenium(II),[358] dichlorido[*fac*-tris(dimethylsulfoxide-κ*S*)] (dimethylsulfoxide-κ*O*)ruthenium(II),[102] [Ru(dppb)(PPh_3)Cl_2],[240] [Ru(tach)(dppp)Cl]Cl, **[11]**,[179] [Ru(tach)(phen)(DMSO)]Cl_2, **[12]**[179] were prepared according to literature procedures, and FL-I and FL-II were kindly donated by Prof. Paul Pringle (University of Bristol).

NMR spectra were obtained using either a Jeol ECS 400, Jeol EXC 400 (^{1}H 399.78 MHz, ^{31}P 161.83, ^{13}C 100.52) at 293 K or a Bruker Avance 500 spectrometer (^{1}H 500.23 MHz, ^{31}P 202.50, ^{13}C 125.78) at 295 K. ^{31}P and ^{13}C spectra were recorded with proton decoupling. The CD_2Cl_2 used for NMR experiments was dried over CaH_2 and degassed with three freeze-pump-thaw cycles. All other solvents were used as received. IR spectra were recorded on a Unicam Research Series FTIR using SensIR Technologies ATR equipment. High resolution mass spectrometry was performed by the University of York mass spectrometry service using the ESI technique on a Bruker Daltronic microTOF instrument(ESI-MS). Elemental analyses (CHN) were performed using an Exeter Analytical Inc. CE-440 analyser. pH measurements were recorded using a MeterLab ION 450 calibrated with Aldrich standard solutions of pH 4, 7 and 10.

7.2 Chapter 2 Experimental

7.2.1 Synthesis of *cis* tach

7.2.1.1 *Cis,cis*-1,3,5-cyclohexanetris(benzyl carbamate), [1]

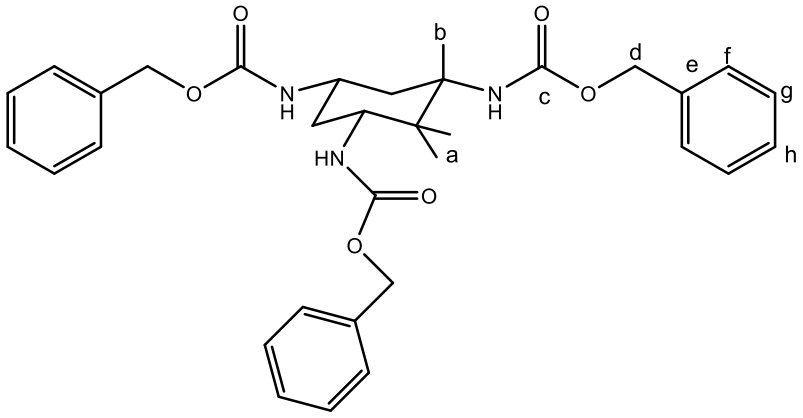

Triethylamine (7.02 g, 9.67 mL, 69.38 mmol) and diphenylphosphorylazide (DPPA) (19.09 g, 15 mL, 69.38 mmol) were added to a mixture of *cis,cis*-1,3,5-cyclohexane tricarboxylic acid (5.0 g, 23.13 mmol) in 125 mL of benzene as a solvent. The mixture was heated at reflux until all the solid had dissolved. Benzyl alcohol (7.50 g, 7.2 mL, 69.38 mmol) was added and the reaction mixture was heated at reflux for 18 h. The resulting cream suspension was filtered and the white solid washed with small amounts of cold diethyl ether. The compound was used without further purification.

Yield: 8.5 g, 15.9 mmol, 69%

^{1}H NMR: (d_6-DMSO) δ 7.35 (15H, m, **f**+**g**+**h**), 5.00 (6H, s, **d**), 3.41 (3H, m, **b**), 1.89 (3H, bd, $\mathbf{a}_{eq}$), 1.07 (3H, ap.q, $\mathbf{a}_{ax}$).

7.2.1.2 *Cis,cis*-1,3,5-triaminocyclohexane trihydrobromide, tach·3HBr, [2]HBr.

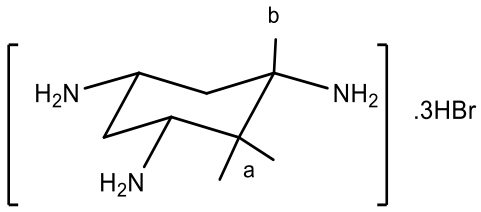

A solution of HBr 33% wt in acetic acid (60 mL) was added to tach(benzylcarbamate) (6 g, 11.28 mmol) and the mixture was left stirring at room temperature for 16 h. Ethanol (100 mL) was then added and the mixture was left stirring for a further 24 h. The white precipitate formed was isolated by filtration and washed with chilled ethanol, then dried under vacuum.

Yield: 3.4 g, 9.14 mmol, 80%

^{1}H NMR: (d_6-DMSO) δ 3.53 (3H, tt, $^3J_{ax\text{-}ax}$ = 12.3 Hz, $^3J_{ax\text{-}eq}$ = 4.0 Hz, **b**), 2.48 (3H, bd, ^2J = 12.3 Hz, $\mathbf{a_{eq}}$), 1.62 (3H, ap.q, $^3J = {}^2J$ = 12.3 Hz, $\mathbf{a_{ax}}$).

7.2.1.3 *Cis,cis*-1,3,5-triaminocyclohexane, tach, [2]

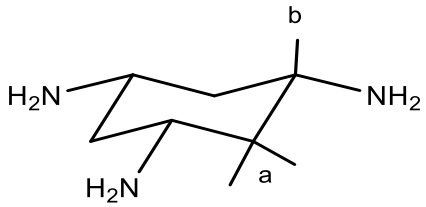

Cis,cis-1,3,5-triaminocyclohexane trihydrobromide, tach·3HBr, (1.0 g, 2.68 mmol) was dissolved in the minimum amount of water and loaded on to a Dowex 1X4-50 (300 g) ion exchange column, which had previously been prerinsed with water, 1 M HCl, 1 M NaOH and finally with water again till neutral pH. The fractions with basic pH were collected and the solvent evaporated. The residue was sublimed at 10^{-2}mbar at 70 °C

using a liquid nitrogen cold finger, a bright white solid were obtained and stored under inert gas.

Yield: 0.21 g, 0.63 mmol, 46%.

^{1}H NMR: (D_2O) δ 2.76 (3H, tt, $^3J_{ax\text{-}ax}$ = 11.6 Hz, $^3J_{ax\text{-}eq}$ = 3.6 Hz, **b**), 1.95 (3H, ap.d, ^2J = 11.6 Hz, $\mathbf{a_{eq}}$), 0.89 (3H, ap.q, ^3J = ^2J = 11.6 Hz, $\mathbf{a_{ax}}$).

7.2.2 Synthesis of tachmonobenze, tachmb [3]

7.2.2.1 *Cis,cis*-1,3-di-tert-bythylcarbamate-5-aminocyclohexane, tach-diBoc, [3-a]

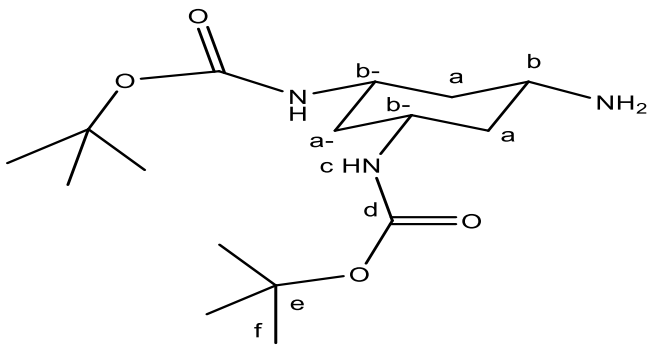

Tach·3HBr (200 mg, 0.54 mmol) was dissolved in 40 mL methanol then triethylamine (109 mg, 150 µL, 1.08 mmol) was added to the mixture. Boc_2O (236 mg, 248 µL, 1.08 mmol) was diluted with 40 mL of MeOH and the resulting solution was slowly added dropwise (one drop every 10-12 sec) to the tach solution. The reaction was stirred for 16 h. The solvent was evaporated and the white solid was dissolved with basic water pH 10 (NaOH solution in water) (12 mL) and ethyl acetate (12 mL). The layers were separated and the aqueous layer was extracted with ethyl acetate (3×12 mL). An emulsion was usually formed during the extraction, which was left with the organic layer during the extraction. The organic layers were dried over MgSO4, filtered and the solvent was evaporated, leaving a white solid.

Yield: 126 mg, 0.38 mmol, 71%.

^{1}H NMR: (d_6-DMSO) δ 6.84 (2H, m, **c**), 3.46 (3H, s, **b**+**b'**), 1.75 (3H, bt, $\mathbf{a_{eq}}$+ $\mathbf{a'_{eq}}$), 1.33 (18H, s, **f**), 0.98 (3H, m, $\mathbf{a_{ax}}$,$\mathbf{a'_{ax}}$).

ESI-MS: positive ion m/z 330.2391 ($[M+H]^+$, error 0.8 mDa).

7.2.2.2 *Cis,cis*-1-benzylamino-3,5-diaminnocyclohexane, tachmonoimbenz.diBoc [3-b].

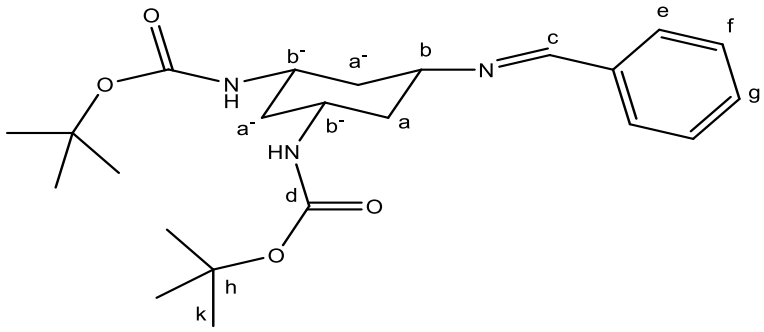

Tach-diBoc (126 mg, 0.40 mmol, 1 eq.) was dissolved in methanol (24 mL) and benzaldehyde (40 mg, 42 µL, 0.40 mmol, 1 eq.) was added to the solution. The mixture was stirred at room temperature for 16 h and water was removed by adding molecular sieves (3 A˚). After cooling to room temperature, the mixture was filtered and solutionwas evaporated, leaving a cream solid. The mixture was extracted with chloroform (3×15 mL) and the organic layers combined were dried over $MgSO_4$, filtered and the solvent removed by rotary evaporation, leaving a white solid. which was washed with pentane and diethyl ether.

Yield: 122 mg, 0.30 mmol, 77%.

^{1}H NMR:(CD_3OD) δ 8.30 (1H, s, **c**), 7.66 (2H, dd, ^3J = 5.9 Hz, ^4J = 2.5 Hz, **e**), 7.32(3H, m, **f**+**g**), 3.42(1H, m, **b**), 2.27 (2H, tt, $\mathbf{b^-}$), 2.02 (3H, ap.d, ^2J = 11.6 Hz, $\mathbf{a_{eq}}$+$\mathbf{a^-_{eq}}$), 1.34 (18H, s, k), 0.97 (3H, m, $\mathbf{a_{ax}}$+$\mathbf{a^-_{ax}}$).

ESI-MS: positive ion m/z 418.2838 ($[M+H]^+$, error 1.4 mDa).

7.2.2.3 *Cis,cis*-1-(benzylamino)cyclohexane, tachmonobenz.diBoc [3-c]

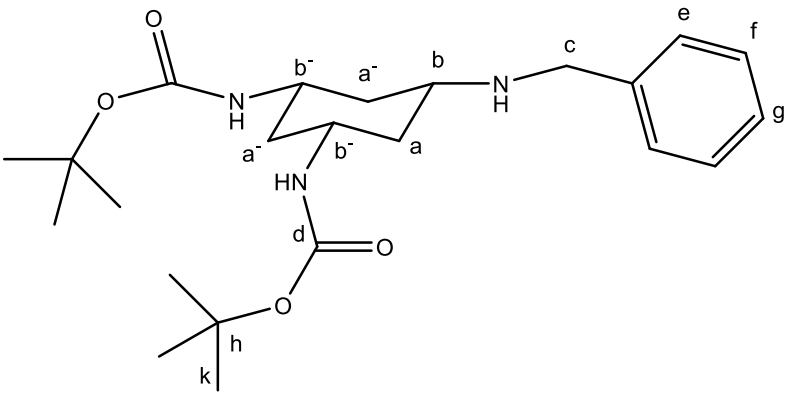

Cis,cis-1-(benzylidenamino)cyclohexane, tachmonoimbenz.diBoc (122 mg, 0.30 mmol, 1 eq.) was dissolved in methanol (20 mL) and sodium borohydride (23 mg, 0.60 mmol, 2 eq.) was slowly added in portions. The solution was leaved to stirrer at room temperature for a further 16 h. The solvent was evaporated and the residue was taken with water (15 mL) and extracted with chloroform (4×15 mL). The organic layers combined were dried over $MgSO_4$, filtered and the solvent evaporated, leaving a white solid that was used without further purification.

Yield: 98 mg, 0.24 mmol, 78 %.

^{1}H NMR: (CD_3OD) δ 7.23 (5H, m, **e**+**f**+**g**), 3.74 (2H, s, **c**), 2.68 (2H, tt, **b**$^-$), 2.13 (1H, m, **b**), 2.02 (3H, d, $\mathbf{a}_{eq}$+$\mathbf{a}^-_{eq}$), 1.33 (18H, s, **k**), 0.97 (3H, m, $\mathbf{a}_{ax}$+$\mathbf{a}^-_{ax}$).

ESI-MS: positive ion m/z 420.2838 ($[M+H]^+$, error 1.1 mDa).

7.2.2.4 *Cis,cis*-1-benzylamino-3,5-diaminocyclohexane, tachmb [3]

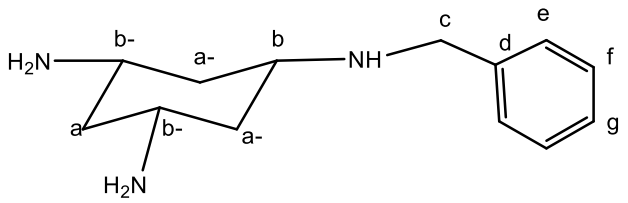

Compound **[3-c]** (98 mg, 0.24 mmol) was suspended in 20 mL of MeOH and 4 mL of conc. HCl were added. To dissolve the compound, 8 mL of chloroform were added to the mixture, which was left stirring in an icebath for 16 h. The solvent was concentrated down to about 5 mL and 20 mL of water were added. The mixture was extracted with ethyl acetate (2×20 mL) and the organic layers were discarded. The pH of the solution was adjusted with NaOH (pH 14) and extracted with ethyl acetate (4×20 mL). The organic layers combined were dried over $MgSO_4$, filtered and the solvent evaporated, leaving a colourless oil.

Yield: (27 mg, 0.12mmol, 51%). Found: C 67.66; H 9.42; N 17.96%. Calcd for $C_{13}H_{21}N_3.0.7H_2O$: C 67.32; H 9.73; N 18.12%.

^{1}H NMR: (CD_3OD) δ 7.23 (5H, m, **e**+**f**+**g**), 3.71 (2H, s, **c**), 2.75 (2H, tt, $^3J_{ax\text{-}ax}$ = 12.2 Hz, $^3J_{ax\text{-}eq}$ = 4.0 Hz, **b'**), 2.52 (1H, m, **b**), 2.11 (2H, d, ^2J = 12.2 Hz, $\mathbf{a_{eq}}$), 2.01 (1H, m, $\mathbf{a'_{eq}}$), 0.97 (3H, m, $\mathbf{a_{ax}}$+ $\mathbf{a^-_{ax}}$).

^{13}C{^{1}H} NMR (D_2O 100.5 MHz, 293K): 140.3 (**d**), 129.4, 128.2 (**e**+**f**+**g**), 52.3 ($\mathbf{b^-}$), 51.4 (**c**), 43.5 (**b**), 42.5 ($\mathbf{a^-}$), 40.6 (**a**).

ATR-IR (cm^{-1}): 3340 (w), 3059 (w), 2926(m), 1570 (m), 1453 (m), 1223 (m), 1168 (w), 736 (m), 698 (m).

ESI-MS: positive ion m/z 220.1810 ($[M+H]^+$, error -0.4mDa).

7.3 Chapter 3 Experimental

All reactions were performed under an atmosphere of dry nitrogen using standard Schlenk line and glove box techniques. Dichloromethane and pentane were purified with an Innovative Technologies anhydrous solvent engineering system. Diethyl ether was dried over sodium, and d_2-dichloromethane over calcium hydride and vacuum transferred prior to use. All other chemicals were purchased from Sigma-Aldrich UK.

7.3.1 [Ru(tachmb)(DMSO-*S*)(Cl)$_2$], [5]Cl

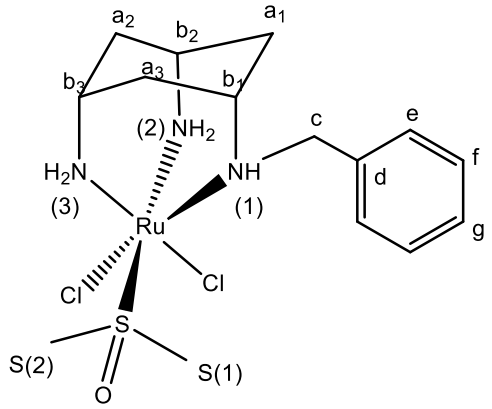

Tachmb **[3]** (25.0 mg, 0.114 mmol) was added to a solution of dichloro[*fac*-tris(dimethylsulfoxide-κ*S*)](dimethylsulfoxide-κ*O*)ruthenium(II) (55.3 mg, 0.114 mmol) in water (15 mL). The resulting yellow suspension was heated at 50°C for 60 minutes. The pale yellow solution was allowed to cool, then the solvent removed *in vacuo*. The residue was taken up in the minimum volume of methanol, and addition of diethyl ether (50 mL) resulted in precipitation of the product, which was isolated by filtration under reduced pressure, washed with diethyl ether (2 x 20 mL) and dried *in vacuo*.

Yield: 35.3 mg (66%, 0.075 mmol of [Ru(tachmb)(DMSO)Cl_2], Found: C 30.58; H 6.12; N 3.96%. Calcd for $C_{15}H_{27}Cl_2N_3ORuS$: C 38.38; H 5.80; N 8.95%.

^{1}H NMR (D_2O): δ 7.26(5H, m, **e**+**f**+**g**), 3.82 (2H, s, **c**), 3.53 (s, 2H, C*H*, **C2**), 3.62(1H, m, **b_1**), 3.28 (3H, s, **S(2))**, 3.13 (1H, s, **b_2**), 2.57 (1H, d, ^2J = 14 Hz, **b_3**),2.32(3H, s**, S(1))**, 2.26

(2H, m, **a_1**), 1.24 (2H, m, ^2J = 14 Hz, **a_2**), 1.12 (2H, m, ^2J = 14 Hz, **a_3**); **$^{13}C\{^1H\}$NMR** (D_2O): δ 137.4(**d**), 128.3, 128.2, and 127.7 (**e**+**f**+**g**), 51.2(**c**), 49.1(**b_1**), 46.2 (**S(2)**), 45.3 **(S(1))**, 43.5 (**b_2**), 42.4 (**b_3**), 38.6 (**a_1**), 36.2(a_2), 35.8(**a_3**). **LIFDI**: *m/z* 469.0421 **[5]** and 335.05 unknown**. ATR-IR** (cm^{-1}): 3003 (w), 2918 (m), 1532 (m), 1400 (m), 1313 (m), 1092 (s, S–O), 1016 (m), 681 (m).

7.3.2 [Ru(tacmb)Cl_2(PPh_3)] [7]

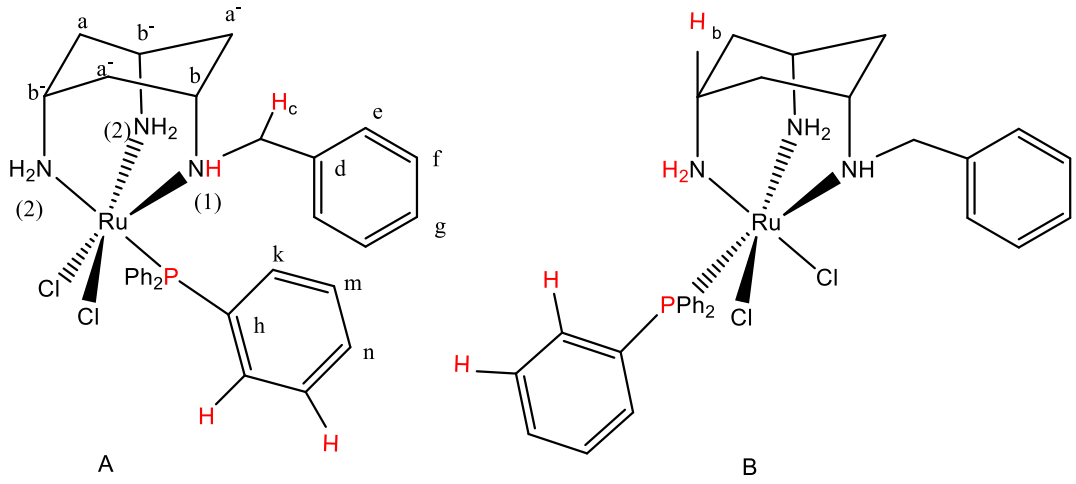

Tachmb **[3]** (25 mg, 0.114 mmol) was added to a Schlenk tube charged with dichloridotris(triphenylphosphane)ruthenium(II) (110 mg, 0.114 mmol) in dichloromethane (15 mL) a red solution was formed and stirred for 3 hours, during which time the solution changed colour to orange then finally to yellow solution. The unreacted solid was removed by filtration and the filtrate reduced in volume to approximately 1 mL *in vacuo*. The product was precipitated by addition of pentane (15 mL) as brown powder, and washed twice with pentane (20 mL).

Yield: 47.6 mg (64%, 0.077 mmol of [Ru(tachmb)(PPh_3)Cl_2]. Found: C 56.14; H 5.53; N 5.72%. Calcd for $C_{31}H_{36}Cl_2N_3PRu$: C 56.97; H 5.55; N 6.43%.

^{1}H NMR (CD_2Cl_2) for **A** isomer:δ 7.95 (6H, *app.* t, $^{3}J_{HH}$ = 7.3 Hz, $^{4}J_{HH}$ = 1.5 Hz, **k**), 7.75 (6H, m, **n**), 7.55 (tt, $^{3}J_{HH}$ = 7.3 Hz, $^{4}J_{HH}$ = 1.5 Hz, **m**), 7.42 (5H, m, **e**+**f**+**g**), 6.39 (1H, d, $^{2}J_{HH}$ = 10.8 Hz, **N1**), 5.21 (2H, d, $^{2}J_{HH}$ = 10.8 Hz, **N2**), 4.15 (2H, d, $^{2}J_{HH}$ = 10.8 Hz, **N2**), 3.91 (2H, s, **c**), 3.22 (1H, s, **b**), 2.80 (2H, bs, **b**$^{-}$), 2.45 (1H, d, $^{2}J_{HH}$ = 16.8 Hz, **a**$^{-}$), 2.35(2H, d, $^{2}J_{HH}$ = 16.8 Hz, **a**), 2.05 (2H, d, $^{2}J_{HH}$ = 16.8 Hz **a**), 1.72(2H, d, $^{2}J_{HH}$ = 16.8 Hz, **a**$^{-}$); **^{31}P{^{1}H} NMR** (CD_2Cl_2) δ 67.4; **^{13}C{^{1}H}NMR** (CD_2Cl_2) δ 139.1 (d, $^{1}J_{PC}$ = 35 Hz, **h**), 133.68 (d, $^{2}J_{PC}$ = 10 Hz, **K**), 129.2 (d, $^{4}J_{PC}$ = 4.1 Hz, **n**), 128.7 (d, $^{3}J_{PC}$ = 8.9 Hz, **m**), 128,45, 128.19 (s, **e**+**f**+**g**), 50.7 (s, **c**), 45.2 (s, **b**), 43.2 (s, **b**$^{-}$), 36.3 (s, **a**$^{-}$), 32.8(s, **a**$^{-}$), 29.4(s, **a**).

^{1}H NMR (CD_2Cl_2) for **B** isomer: δ 7.99 (6H, *app.* t, $^{3}J_{HH}$ = 7.3 Hz, $^{4}J_{HH}$ = 1.5 Hz, k), 7.79(6H, m, n), 7.45 (tt, $^{3}J_{HH}$ = 7.3 Hz, $^{4}J_{HH}$ = 1.5 Hz, m), 7.32(5H, m, e+f+g), 6.29 (1H, d, $^{2}J_{HH}$ = 10.8 Hz, N1), 5.09(2H, d, $^{2}J_{HH}$ = 10.8 Hz, N2), 4.25(2H, d, $^{2}J_{HH}$ = 10.8 Hz, N2), 3.84 (2H, s, c), 3.42 (1H, s, b), 2.92 (2H, bs, b^{-}), 2.40 (1H, d, $^{2}J_{HH}$ = 16.8 Hz a^{-}), 2.37(2H, d, $^{2}J_{HH}$ = 16.8 Hz a), 2.25(2H, d, $^{2}J_{HH}$ = 16.8 Hz a), 1.80(2H, d, $^{2}J_{HH}$ = 16.8 Hz a^{-}); **^{31}P{^{1}H} NMR** (CD_2Cl_2) δ 61.5; **^{13}C{^{1}H}NMR** (CD_2Cl_2) δ 139.9 (d, $^{1}J_{PC}$ = 35 Hz, h), 133.08 (d, $^{2}J_{PC}$ = 10 Hz, K), 129.1(d, $^{4}J_{PC}$ = 4.1 Hz, n), 128.2 (d, $^{3}J_{PC}$ = 8.9 Hz, m), 128,05, 127.6 (s, e+f+g), 47.6 (s, c), 45.6 (s, b), 42.4 (s, b^{-}), 35.6 (s, a^{-}), 31.9 (s, a^{-}), 28.2(s, a). **LIFDI**: 653.24.

7.3.3 [Ru(tachmb)(dppb)Cl]Cl, [9]

A solution of [Ru(dppb)(PPh_3)Cl_2], **[8]** (98 mg, 0.114 mmol) in CH_2Cl_2 (15 mL) was stirred with tachmb **[3]** (25 mg, 0.114 mmol) for 18 hours. The solution was filtered to remove unreacted phosphane, and the filtrate reduced in volume to approximately 1 mL *in vacuo*. (1 mL) and pentane (10 mL) was added and the product collected by filtration, and the process repeated. The pale green product was dried *in vacuo*. The ^{1}H NMR could not achieved as the product was easily decomposed in solution.

Yield: 63 mg (55%, 0.0805 mmol of [Ru(tachmb)(dppb)Cl]Cl.3H_2O). Found: C 60.10; H 6.41; N 5.68%. Calcd for $C_{41}H_{49}N_3P_2ClRu$(3 H_2O): C 60.22; H 6.04; N 5.14%. **^{31}P{^{1}H} NMR**

(CD_2Cl_2) δ 37.1(d, 1P,$^2J_{pp}$ = 35), 41.3(d, 1P,$^2J_{pp}$ = 35), 46.8(d, 1P,$^2J_{pp}$ = 35),48.6(d, 1P,$^2J_{pp}$ = 35).**ESI-MS**: *m/z* 782.213 ([M+H]$^+$, error 0.8mDa).

7.4 Chapter 4 Experimental

7.4.1 [Ru(*cis*-tach)(FL-I)Cl]Cl, [10]

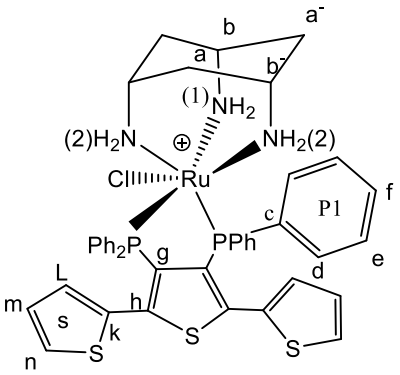

A solution of [Ru(cis-tach)(DMSO)$_2$Cl]Cl, **[4]** (50 mg, 0.118 mmol) in methanol (10 mL) was heated under reflux with L [1] (146 mg, 0.237 mmol) for 18 h. The solution was filtered to remove unreacted L [1] and the solvent was removed *in vacuo*, recrystallised three times in dichloromethane/diethyl ether, collected by filtration and the yellow product dried *in vacuo*. Yield: 72 mg, 68%, 0.0815 mmol of [Ru(*cis*-tach)(FL-I)Cl]Cl.2H_2O). Found: C 52.65; H 5.80; N 5.39%. Calcd for $C_{33}H_{41}N_3P_2Cl_2Ru(2H_2O)$: C 52.87; H 6.05; N 5.61%. **^{1}H NMR** (CD_2Cl_2) δ 7.81 (4H, m, **d(P1))**, 7.58 (8H, m, **d,e(P2))**, 7.47 (2H, m,**f(P2)**, 7.24 (2H, m, **f(P1)**, 7.21 (2H, dd, $^3J_{HH}$= 3.8 Hz, $^4J_{HH}$ = 1.5 Hz, **m(S)**, 7.10 (4H,t, **e(P1))**, 6.58 (2H, dd, $^3J_{HH}$= 5.9 Hz, $^4J_{HH}$ = 3.8 Hz, **n(S))**, 6.48 (2H, dd, $^3J_{HH}$= 5.9 Hz, $^4J_{HH}$ = 1.5 Hz, **L(S))**, 4.22 (2H, d, $^2J_{HH}$ = 12.06 Hz, **N2**), 3.59 (2H, d, $^2J_{HH}$ = 12.06 Hz, **N2**), 3.43 (2H, s, **b**$^-$), 2.77 (1H, s, **b**), 2.11 (1H, d, $^2J_{HH}$ = 15.35 Hz, **a**), 2.03 (1H, d, $^2J_{HH}$ = 15.35 Hz, **a**), 1.84 (2H, d, $^2J_{HH}$ = 15.35 Hz, **a**$^-$), 1.74(2H, d, $^2J_{HH}$ = 15.35 Hz, **a**$^-$), 1.49 (2H, s, **N1**); **^{31}P{^{1}H}NMR** (CD_2Cl_2) δ 55.24 (s, 2P); **^{13}C{^{1}H} NMR** (CD_2Cl_2) δ 140.7 (s, **c**), 135.8 (t, **d(P1))**, 133.2 (t, **d(P2))**, 132.6 (t, **f(P2))**, 131.4 (dd, **L(S))**, 130.9 (s, **f(P1))**, 130.8 (s, **d,e(P2))**,

129.3(dd, **m(S))**, 128.8 (s, **e(P1))**, 128.02(dd, **n(S)**, 44.5 (s, **b**+**b**$^-$), 34.4 (s, **a**+**a**$^-$)**ESI-MS**: *m/z* 882.7231 ([M+H]$^+$, error 1.1mDa).

7.4.2 [Ru(cis-tach)(FL-II)Cl]Cl, [13]

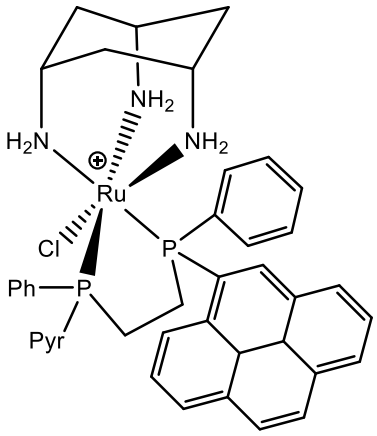

A solution of **[4]** (45 mg, 0.106 mmol) in methanol (10 mL) was heated under reflux with L **[2]** (137.7 mg, 0.213 mmol) for 18 hours. The solution was filtered to remove unreacted ligand, and the solvent removed *in vacuo*. Small amount of CH_2Cl_2 was added to the residue, followed by diethyl ether (10 mL) and the product collected by filtration, and the process repeated. The yellow product was dried *in vacuo*. Yield: 44 mg (45%, 0.048 mmol of [Ru(cistach)(FL-II)Cl]Cl. **^{31}P{^{1}H} NMR** (CD_2Cl_2) δ 74.45 (d, 1P,$^2J_{pp}$ = 8.77 Hz), 69.48(d, 1P,$^2J_{pp}$ = 8.77 Hz)

ESI-MS: *m/z* 912.2134 ([M+H]$^+$, error 0.8mDa).

7.4.3 Absorption spectroscopy

UV-Vis spectra were recorded on a spectrophotometer. Samples were analysed in a quartz cuvette with a path length of 1 cm with a spectral range of 200 – 600 nm, all the spectra were recorded in Tris-HCl buffer 5mM, pH 7.2, unless otherwise stated. The

background was corrected for blank solvent absorbance prior to every measurement and was collected at room temperature.

7.4.4 Fluorescence Spectroscopy

Emission spectra were recorded on a fluorescence spectrophotometer with an excitation slit width of 10 nm and an emission slit width of 10 nm, PMT detector voltage was 700 V and 240 nms^{-1} scan speed. All experiments were performed using a 1 cm path length quartz cuvette. All the spectra were recorded in Tris-HCl buffer 5mM, pH 7.2, unless otherwise stated. The background was corrected for blank fluorescence before each measurement and was collected at room temperature.

7.4.5 Quantum yield calculation

The quantum yield value were measured for ruthenium tach complexes **[10]**, **[11]**, **[12]** and the ligand L **[1]** by using comparative method,[359] and it is calculated using the slope of the line determined from the plot of the absorbance against the integrated fluorescence intensities, which it was integrated using the software a/e-UV-VIS-IR spectral analysis software, and the quantum yield can be calculated using equation (4.1).

For emission quantum yields, reference molecules were chosen to have similar absorption and emission spectra as the sample molecule, to minimize errors arising from the wavelength dependence of the apparatus. Anthracene (R_1), Phenanthrene (R_2) and Rhodamine 6G (R_3) were chosen as a reference and the quantum yield (Q_y) of each reference sample was calculated relative to each other. At least 5 data points were used in the construction of each graph.

7.4.6 DNA binding studies

The chemicals and solvents were of analytical reagent grade and were used as received unless otherwise noted. Tris–HCl and CT-DNA were purchased from Sigma–Aldrich chemicals except Ethidium bromide (EB) donated by York Structural Biology Laboratory, Department of Chemistry, University of York. Millipore water was used for preparing buffer.

All the experiments involving with the interaction of complexes with CT DNA were carried out buffer containing 5 mM Tris-HCl. The purity of DNA in the buffer was determined by UV absorbance ratio A260/A280 of about 1.8/1.9 indicating that the DNA was sufficiently free from protein.[360] The stock solution of Calf thymus DNA (CT-DNA) was dissolved in aqueous buffer (30 mM NaCl, 5 mM Tris, pH = 7.2), it was stored at 4 °C and used within 4 days.

7.4.6.1 Electronic absorption titration

Absorption titration experiment were performed with fixed concentrations of the complexes. The complexes were dissolved in Tris–HCl buffer (5 mM Tris–HCl, 30 mM NaCl, pH 7.2). Absorption titration experiments were performed in the absence and presence of DNA with increasing concentration of CT-DNA and keeping the concentration of complex constant. While measuring the absorption spectra, an appropriate amount of CT-DNA was added to both compound solution and the blank solution to eliminate the absorbance of CTDNA itself, before measurements, the mixture was mixed well and incubated at room temperature for 5 min. From the absorption titration data, the binding constant (K_b) was determined using equation 4.2.[291, 292]

7.4.6.2Fluorescence titration

All fluorescence measurements were carried out by keeping concentration of complex constant while varying the DNA concentration from 0 to 10 µM. The fluorescence spectra of the complexes were recorded by using the excitation wavelength of 350 nm for **[10]** and **[11]**, and 450 nm for **[12]**. Before measurements, the mixture was mixed well and incubated at room temperature for 5 min.[241, 294]

7.4.6.3 Competitive DNA binding studies

In the ethidium bromide (EB) fluorescence displacement experiment, 5 µL of the EB Tris solution (1 mM) was added to 1 mL of DNA solution (1×10^{-4} mol/L, at saturated binding level), followed by a 1 h incubation in the dark. The complex was then titrated into the EB/DNA mixture. Before measurements, the solution was well mixed and incubated at room temperature for 5 min. Fluorescence spectra of EB bound to DNA were obtained at an excitation wavelength of 520 nm and an emission wavelength of 584 nm. Triplicate titrations were performed and the apparent binding constants were calculated using equation 4.3.[297]

7.4.7 Protein binding studies

BSA was purchased from Sigma. The concentrations of the stock solutions of BSA in Tris–HCl buffer (5 mM Tris–HCl, 30 mM NaCl, pH 7.2) are determined from absorption spectroscopy by dividing absorbance at 280 nm by the molar extinction coefficients of BSA ($\varepsilon 280 = 66{,}000\ M^{-1}cm^{-1}$).

7.4.7.1 Absorption studies

The absorption spectra of BSA in the presence of different concentrations of **[10]**, **[11]** and **[12]** were recorded in the range of 200-400 nm. The concentration of BSA was kept at 5 µM while the concentrations of complexes were varied from 0.0–5.0 × 10^{-5} M.

7.4.7.2 Fluorescence quenching experiment

The fluorescence quenching experiment was performed with an excitation slit width of 5 nm and an emission slit width of 5 nm, PMT detector voltage was 700 V and 240 nms^{-1} scan speed, using bovine serum albumin. The quenching of emission intensity of the tryptophan residues of BSA at 343 nm was monitored in the presence of increasing concentrations of complexes. The quencher was added in equal increments with concentration increasing from 0-50 µM to a fixed concentration of BSA 5 µM. For every addition, the mixture solution was shaken and allowed to stand for 5 min and then fluorescence spectra were recorded from 300 to 500 nm at an excitation wavelength of 296 nm. Triplicate titrations were performed and the quenching constants were calculated using equation 4.5.[308]

7.5 Chapter 5 Experimental

Human lung adenocarcinoma A549 cells were donated by the Department of Biology, University of York. Human ovarian carcinoma A2780 cells were purchased from the European Collection of Cell Cultures (ECACC), Salisbury, UK. All materials were purchased from Gibco/Fisher Scientific, except PBS from Sigma. The experiments were achieved in an Envair class II Laminar flow microbiological safety hood BIO 2+ under sterile conditions. Cells were counted using a Beckman Coulter Vi-Cell® Analyser and the MTT assay result visualised with a Hidex Plate Chameleon™V plate reader. Plates were centrifuged with a Beckman Coulter Allegra™25R Centrifuge using a S5700 rotor.

Cells were centrifuged with a Thermo scientific megafuge 40R centrifuge. Plates were shaken with an Eppendorf Thermomixer® compact. Dulbecco Modified Eagle Medium (DMEM) were used to grow A549 cells in the presence of 10% FBS; A2780 cells were grown in RPMI 1640 medium enriched with 10% FBS and 1% LGlutamine. All cell lines were kept in 25 cm^2 cell culture flasks at 37°C in a 90% RH, 5% CO2 Binder BF56 Steri-Cult incubator. Cells were subcultured when 70-80% confluent with 0.25% EDTA-trypsin.

7.5.1 *In vitro* biological evaluation

The colourmetric assay was first described by Mosmann,[343] it proceeded in a 96-well plate format. The cells were incubated in the wells at a density of 1000 (A549) or 3500 (A2780) for 18 hours before the addition of tested complexes in a humidified atmosphere (37^{o}C, 5% CO_2). The tested compound should be solubilize first using culture medium or DMSO then medium in case of insoluble complex, the DMSO percent in wells containing the cells was never higher than 1% and the DMSO was added to the control wells as well. Each plate contains control wells, which is contain cells without complexes and blank wells that seeded with medium only.

Cells are usually exposed to testing compounds at different concentration for 72 hours then MTT solution (50µL, 2mg/Ml) was added to treated cells and incubated for two to three hours where the yellow MTT is reduced to purple formazan in the viable cells only while the dead cells did not reduce the MTT formazan.

After the three hour exposure to MTT solution, the plates were centrifuged at 500 RPM, 4˚C for 10 min then the growing medium was removed and the formazan was dissolved in an organic solvent DMSO (150 µL) to achieved a homogenous solution, then the absorbance at 570 nm was recorded using a plate reader, and analysis of the results were done by Orgin v8.5 to calculate the cytotoxicity (inhibition concentration,

50%) values.[344] All the compounds was tested in at least triplicate and an average IC_{50} with its standard deviation was calculated.

Appendix. X-Ray Crystallography Data

Crystal data and structure refinement for ruthenium dimer.

Identification code	jml1602_twin1_hklf4
Empirical formula	$C_9H_{28}Cl_2F_6NaO_5PRuS_4$
Formula weight	684.48
Temperature/K	110.05(10)
Crystal system	monoclinic
Space group	$P2_1/n$
a/Å	11.2512(5)
b/Å	14.1289(6)
c/Å	15.2670(7)
α/°	90
β/°	93.787(4)
γ/°	90
Volume/Å^3	2421.65(19)
Z	4
ρ_{calc}g/cm^3	1.877
μ/mm^{-1}	11.928
F(000)	1376.0
Crystal size/mm^3	0.114 × 0.06 × 0.044
Radiation	CuKα (λ = 1.54184)
2Θ range for data collection/°	8.536 to 134.332
Index ranges	-13 ≤ h ≤ 13, -16 ≤ k ≤ 16, -18 ≤ l ≤ 13

Reflections collected	6744
Independent reflections	6744 [R_{int} = ?, R_{sigma} = 0.0459]
Data/restraints/parameters	6744/0/276
Goodness-of-fit on F^2	1.216
Final R indexes [I>=2σ (I)]	R_1 = 0.0476, wR_2 = 0.1377
Final R indexes [all data]	R_1 = 0.0591, wR_2 = 0.1399
Largest diff. peak/hole / e $Å^{-3}$	1.60/-1.29

Abbreviation

◦	degree
˚C	degree Celsius
λ	wavelength
δ	chemical shift (NMR)
π	Pi
σ	sigma
μ	micro
η^6	C_6H_6
^{13}C	carbon
^{1}H	proton
A	adenosine
A549	Human lung adenocarcinoma
A2780	Human ovarian carcinoma
AgOTf	silver trifluoromethanesulfonate
$AgPF_6$	silver hexafluorophosphate
aq.	aqueous
Boc	*t*-butoxycarbonyl
BSA	bovine serum albumin
bpy	2,2'-bipyridine
cm	centimetres

cm^{-1}	wavenumber
CHN	carbon, hydrogen, nitrogen (elemental analysis)
cisplatin	cis – $[PtCl_2(NH_3)_2]$
COSY	correlation spectroscopy
Cp	η^5-cyclopentadienyl
CT	calf thymus
d	doublet
DCM	dichloromethane
dd	doublet of doublets
DEPT	distortionless enhancement by polarisation transfer
DMEM	Dulbecco's modified Eagle's Medium
DMF	dimethylformamide
DMSO	dimethylsulfoxide
DNA	deoxyribonucleic acid
dppb	1,4-bis(diphenylphosphino)butane
dppz	dipyrido[3,2-2',3'-c]phenazine
EDTA	ethylendiaminetetraacetic acid
en	1,2-ethylenediamine
eq	equatorial
ESI-MS	electrospray ionisation mass spectrometry
EtBr	ethidium bromide ($C_{21}H_{20}BrN_3$)

Et_2O	diethyl ether
fac	*facial*
FBS	foetal bovine serum
FTIR	fourier transform infrared
G	guanosine
G	grams
GSH	glutathione
h	hour(s)
HMBC	heteronuclear multiple bond correlation
HSQC	heteronuclear spin-quantum coupling spectroscopy
Hz	Hertz
IC_{50}	50% growth inhibition concentration
IR	infra-red
J	coupling constant
K	Kelvin
M	molar
m	multiplet
m/z	mass to charge ratio
MeOD	methanol-d4
MLCT	metal-to-ligand-charge-transfer
min	minutes

mL	millilitres
mmol	millimole
mol	moles
MS	mass spectrometry
MTT	3-(4, 5-dimethylthiazolyl-2)-2, 5-diphenyltetrazolium bromide
NMR	nuclear magnetic resonance
NOESY	nuclear overhauser effect spectroscopy
p-cymene	para-cymene
PDT	photodynamic therapy
PDAT	photoactivated chemotherapy
phen	1,10-phenanthroline
ppm	parts per million
Pt	platinum
RNA	ribonucleicacid
Ru	ruthenium
s	singlet
t	triplet
tt	triplet of triplets
UV	ultra-violet
Vis	visible

References

1. C. Blanpain, *Nat Cell Biol*, 2013, **15**, 126-134.
2. WHO Media centre, **http://www.who.int/cancer/en/**).
3. L. M. F. Merlo, J. W. Pepper, B. J. Reid and C. C. Maley, *Nat Rev Cancer*, 2006, **6**, 924-935.
4. J. Ferlay, H.-R. Shin, F. Bray, D. Forman, C. Mathers and D. M. Parkin, *Int. J. Cancer*, 2010, **127**, 2893-2917.
5. A. Kamb, N. A. Gruis, J. Weaver-Feldhaus, Q. Liu, K. Harshman, S. V. Tavtigian, E. Stockert, R. S. Day, B. E. Johnson and M. H. Skolnick, *Science*, 1994, **264**, 436-440.
6. D. Hanahan and R. A. Weinberg, *Cell*, 1987, **100**, 57-70.
7. M. A. Swartz, N. Iida, E. W. Roberts, S. Sangaletti, M. H. Wong, F. E. Yull, L. M. Coussens and Y. A. DeClerck, *Cancer Research*, 2012, **72**, 2473.
8. J. M. Rosen and C. T. Jordan, *Science*, 2009, **324**, 1670.
9. K. O. Hicks, F. B. Pruijn, T. W. Secomb, M. P. Hay, R. Hsu, J. M. Brown, W. A. Denny, M. W. Dewhirst and W. R. Wilson, *J. Natl. Cancer Inst.*, 2006, **98**, 1118-1128.
10. O. Trédan, C. M. Galmarini, K. Patel and I. F. Tannock, *J. Natl. Cancer Inst.*, 2007, **99**, 1441-1454.
11. L. A. Huxham, A. H. Kyle, J. H. E. Baker, L. K. Nykilchuk and A. I. Minchinton, *Cancer Res.*, 2004, **64**, 6537.
12. C. M. Lee and I. F. Tannock, *BMC Cancer*, 2010, **10**, 255.
13. R. J. Epstein, *Human Molecular Biology: An Introduction to the Molecular Basis of Health and Disease*, Cambridge University Press, 2002.
14. A. J. B. Alberts, J. Lewis, M. Raff, K. Roberts, and P. Walter., *Molecular Biology of the Cell*, New York: Garland Science, 4th edition. edn., 2002.
15. R. K. Jain, *Adv. Drug Deliv. Rev.*, 2001, **46**, 149-168.
16. A. L. Harris, *Nat. Rev. Cancer*, 2002, **2**, 38-47.
17. P. J. Dyson and G. Sava, *Dalton Trans.*, 2006, 1929-1933.
18. C. S. Allardyce, A. Dorcier, C. Scolaro and P. J. Dyson, *Appl. Organomet. Chem.*, 2005, **19**, 1-10.
19. M. Peyrone, *Justus Liebigs Annalen der Chemie*, 1844, **51**, 1-29.
20. B. Rosenberg, L. Van Camp and T. Krigas, *Nature*, 1965, **205**, 698-699.
21. S. P. Fricker, *Dalton Trans.*, 2007, 4903-4917.
22. D. J. Higby, H. J. Wallace, D. J. Albert and J. F. Holland, *Cancer*, 1974, **33**, 1219-1225.
23. Z. Abigail, *Emerg. Infect. Dis.*, 1999, **5**, 729.
24. G. Giaccone, *Drugs*, 2000, **59**, 9-17.
25. Y. Jung and S. J. Lippard, *Chem. Rev.*, 2007, **107**, 1387-1407.
26. S. Dasari and P. B. Tchounwou, *Eur. J. pharmacol.*, 2014, **0**, 364-378.
27. M. Sooriyaarachchi, A. Narendran and J. Gailer, *Metallomics*, 2011, **3**, 49-55.
28. R. A. Hromas, J. A. North and C. P. Burns, *Cancer Lett.*, 1987, **36**, 197-201.
29. D. P. Gately and S. B. Howell, *Br. J. cancer*, 1993, **67**, 1171.
30. S. Ishida, J. Lee, D. J. Thiele and I. Herskowitz, *Proc. Natl. Acad. Sci. U.S.A.*, 2002, **99**, 14298-14302.
31. K. Ohashi, K. Kajiya, S. Inaba, T. Hasegawa, Y. Seko, T. Furuchi and A. Naganuma, *Biochem. Biophys. Res. Commun.*, 2003, **310**, 148-152.
32. D. Wang and S. J. Lippard, *Nat. Rev. Drug Discov.*, 2005, **4**, 307-320.
33. A. Eastman, *Cisplatin. Chemistry and biochemistry of a leading anticancer drug*, 1999, 111-134.

34. R. P. Perez, *Eur. J. Cancer*, 1998, **34**, 1535-1542.
35. M. A. Fuertes, C. Alonso and J. M. Pérez, *Chem. Rev.*, 2003, **103**, 645-662.
36. A. M. Fichtinger-Schepman, J. L. van der Veer, J. H. den Hartog, P. H. Lohman and J. Reedijk, *Biochemistry*, 1985, **24**, 707-713.
37. D. J. Beck and R. R. Brubaker, *J. Bacteriol*, 1973, **116**, 1247-1252.
38. H. N. Fraval, C. J. Rawlings and J. J. Roberts, *Mutat. Res. Fund. Mol. Mech. Mut.*, 1978, **51**, 121-132.
39. V. Brabec, in *Platinum-Based Drugs in Cancer Therapy*, eds. L. R. Kelland and N. P. Farrell, Humana Press, Totowa, NJ, 2000, pp. 37-61.
40. R. C. Todd and S. J. Lippard, *Metallomics*, 2009, **1**, 280-291.
41. A. Eastman, *Pharmacol. Ther.*, 1987, **34**, 155-166.
42. P. M. Takahara, A. C. Rosenzweig, C. A. Frederick and S. J. Lippard, *Nature*, 1995, **377**, 649-652.
43. J.-M. Teuben, C. Bauer, A. H. J. Wang and J. Reedijk, *Biochemistry*, 1999, **38**, 12305-12312.
44. J. M. Malinge, M. J. Giraud-Panis and M. Leng, *J. Inorg. Biochem.*, 1999, **77**, 23-29.
45. J. S. Hoffmann, D. Locker, G. Villani and M. Leng, *J. Mol. Biol.*, 1997, **270**, 539-543.
46. B. A. Donahue, M. Augot, S. F. Bellon, D. K. Treiber, J. H. Toney, S. J. Lippard and J. M. Essigmann, *Biochemistry*, 1990, **29**, 5872-5880.
47. S. J. Brown, P. J. Kellett and S. J. Lippard, *Science*, 1993, **261**, 603-605.
48. G. Orphanides, W. H. Wu, W. S. Lane, M. Hampsey and D. Reinberg, *Nature*, 1999, **400**, 284-288.
49. D. Fink, S. Aebi and S. B. Howell, *Clin. Cancer Res.*, 1998, **4**, 1-6.
50. S. G. Chaney and A. Vaisman, *J. Inorg. Biochem.*, 1999, **77**, 71-81.
51. D. E. Szymkowski, K. Yarema, J. M. Essigmann, S. J. Lippard and R. D. Wood, *Proc. Natl. Acad. Sci. U. S. A.*, 1992, **89**, 10772-10776.
52. D. Mu, D. S. Hsu and A. Sancar, *J. Biol. Chem.*, 1996, **271**, 8285-8294.
53. K. M. Henkels and J. J. Turchi, *Cancer Res*, 1999, **59**, 3077-3083.
54. M. Groessl, O. Zava and P. J. Dyson, *Metallomics*, 2011, **3**, 591-599.
55. N. Mauro Coluccia and Giovanni, *Anticancer Agents Med. Chem.*, 2007, **7**, 111-123.
56. S. M. Aris and N. P. Farrell, *Eur. J. Inorg. Chem.*, 2009, **2009**, 1293-1302.
57. A. M. Basri, R. M. Lord, S. J. Allison, A. Rodríguez-Bárzano, S. J. Lucas, F. D. Janeway, H. J. Shepherd, C. M. Pask, R. M. Phillips and P. C. McGowan, *Chem. Eur. J.*, 2017, **23**, 6341-6356.
58. M. J. Cleare and J. D. Hoeschele, *Platinum Metals Rev.*, 1973, **17**, 2-13.
59. M. H. Hanigan and P. Devarajan, *Cancer Ther.*, 2003, **1**, 47-61.
60. R. Y. Tsang, T. Al-Fayea and H. J. Au, *Drug Saf.*, 2009, **32**, 1109-1122.
61. B. Desoize and C. Madoulet, *Crit. Rev. Oncol. Hematol.*, 2002, **42**, 317-325.
62. D.-W. Shen, L. M. Pouliot, M. D. Hall and M. M. Gottesman, *Pharmacol.Rev.*, 2012, **64**, 706-721.
63. J. Jassem, *Ann. Oncol.*, 1999, **10 Suppl 6**, 77-82.
64. L. R. Kelland, *Drugs*, 2000, **59 Suppl 4**, 1-8; discussion 37-38.
65. F. N. Santos, T. B. de Castria, M. R. Cruz and R. Riera, *Cochrane. Database Syst. Rev.*, 2015, **10**, 1361-6137.
66. R. B. Weiss and M. C. Christian, *Drugs*, 1993, **46**, 360-377.
67. M. A. Fuertes, J. Castilla, C. Alonso and J. M. Perez, *Curr. Med. Chem. Anticancer Agents*, 2002, **2**, 539-551.
68. D. S. Alberts and R. T. Dorr, *Oncologist*, 1998, **3**, 15-34.
69. R. S. Go and A. A. Adjei, *J. Clin. Oncol.*, 1999, **17**, 409-422.

70. M. Boisdron-Celle, A. Lebouil, P. Allain and E. Gamelin, *Bull.Cancer*, 2001, **88 Spec No**, S14-19.
71. J. Graham, M. Muhsin and P. Kirkpatrick, *Nat. Rev. Drug. Discov.*, 2004, **3**, 11-12.
72. C. R. Culy, D. Clemett and L. R. Wiseman, *Drugs*, 2000, **60**, 895-924.
73. T. Alcindor and N. Beauger, *Curr. Oncol.*, 2011, **18**, 18-25.
74. P. Soulie, E. Raymond, S. Brienza and E. Cvitkovic, *Bull. Cancer*, 1997, **84**, 665-673.
75. E. Raymond, S. G. Chaney, A. Taamma and E. Cvitkovic, *Ann. Oncol.*, 1998, **9**, 1053-1071.
76. N. J. Wheate, S. Walker, G. E. Craig and R. Oun, *Dalton Trans.*, 2010, **39**, 8113-8127.
77. I. Ali, W. A. Wani, K. Saleem and A. Haque, *Anticancer Agents Med. Chem.*, 2013, **13**, 296-306.
78. A. Bhargava and U. N. Vaishampayan, *Expert Opin. Investig. Drugs*, 2009, **18**, 10-15.
79. J. Welink, E. Boven, J. B. Vermorken, H. E. Gall and W. J. van der Vijgh, *Clin. Cancer Res.*, 1999, **5**, 2349-2358.
80. T. C. Johnstone, K. Suntharalingam and S. J. Lippard, *Chem. Rev.*, 2016, **116**, 3436-3486.
81. K. Gkionis, S. T. Mutter and J. A. Platts, *RSC. Advances*, 2013, **3**, 4066-4073.
82. T. Boulikas, *Expert Opin. Investig. Drugs*, 2009, **18**, 1197-1218.
83. M. Frezza, S. Hindo, D. Chen, A. Davenport, S. Schmitt, D. Tomco and Q. P. Dou, *Curr. Pharm. Des.*, 2010, **16**, 1813-1825.
84. C. Di, M. Vesna and Q. P. D. Michael Frezza and, *Curr. Pharm. Des.*, 2009, **15**, 777-791.
85. I. Ott and R. Gust, *Archiv. Der. Pharmazie.*, 2007, **340**, 117-126.
86. M. A. Jakupec and B. K. Keppler, *Curr. Top. Med. Chem.*, 2004, **4**, 1575-1583.
87. D. B. Lovejoy and D. R. Richardson, *Expert Opin. Investig. Drugs*, 2000, **9**, 1257-1270.
88. C. R. Chitambar, *Future Med. Chem.*, 2012, **4**, 1257-1272.
89. N. Kröger, U. R. Kleeberg, K. Mross, L. Edler and D. K. Hossfeld, *Oncol. Res. Treat.*, 2000, **23**, 60-62.
90. Y. Ellahioui, S. Prashar and S. Gómez-Ruiz, *Inorganics*, 2017, **5**, 4.
91. W. H. Ang and P. J. Dyson, *Eur. J. Inorg. Chem.*, 2006, **20**, 3993-3993.
92. C. S. Allardyce and P. J. Dyson, *Platin. Met. Rev.*, 2001, **45**, 62-69.
93. J. Reedijk, *Platin. Met. Rev.*, 2008, **52**, 2-11.
94. I. Kostova, *Curr. Med. Chem.*, 2006, **13**, 1085-1107.
95. J. B. Vincent and S. Love, *Biochim. Biophys. Acta.*, 2012, **1820**, 362-378.
96. G. Suss-Fink, *Dalton Trans.*, 2010, **39**, 1673-1688.
97. W. M. Motswainyana and P. A. Ajibade, *Adv. Chem.*, 2015, **2015**, 1-20.
98. F. P. Dwyer, E. C. Gyarfas, W. P. Rogers and J. H. Koch, *Nature*, 1952, **170**, 190-191.
99. W. H. Ang and P. J. Dyson, *Eur. J. Inorg. Chem.*, 2006, **2006**, 3993-3993.
100. M. J. Clarke, *Coord. Chem. Rev.*, 2003, **236**, 209-233.
101. M. J. Clarke, F. Zhu and D. R. Frasca, *Chem. Rev.*, 1999, **99**, 2511-2534.
102. E. Alessio, G. Mestroni, G. Nardin, W. M. Attia, M. Calligaris, G. Sava and S. Zorzet, *Inorg. Chem.*, 1988, **27**, 4099-4106.
103. I. Bratsos, A. Bergamo, G. Sava, T. Gianferrara, E. Zangrando and E. Alessio, *J. Inorg. Biochem.*, 2008, **102**, 606-617.
104. S. Kapitza, M. Pongratz, M. A. Jakupec, P. Heffeter, W. Berger, L. Lackinger, B. K. Keppler and B. Marian, *J. Cancer Res. Clin. Oncol.*, 2005, **131**, 101-110.
105. E. Alessio, G. Mestroni, A. Bergamo and G. Sava, *Curr. Top. Med. Chem.*, 2004, **4**, 1525-1535.
106. G. Sava, I. Capozzi, K. Clerici, G. Gagliardi, E. Alessio and G. Mestroni, *Clin. Exp. Metastasis*, 1998, **16**, 371-379.

107. J. M. Rademaker-Lakhai, D. van den Bongard, D. Pluim, J. H. Beijnen and J. H. Schellens, *Clin. Cancer. Res.*, 2004, **10**, 3717-3727.
108. A. Bergamo and G. Sava, *Dalton Trans.*, 2007, 1267-1272.
109. M. Bacac, A. C. G. Hotze, K. v. d. Schilden, J. G. Haasnoot, S. Pacor, E. Alessio, G. Sava and J. Reedijk, *J. Inorg. Biochem.*, 2004, **98**, 402-412.
110. B. Gava, S. Zorzet, P. Spessotto, M. Cocchietto and G. Sava, *J. Pharm. Exp. Ther.*, 2006, **317**, 284.
111. C. Casarsa, M. T. Mischis and G. Sava, *J. Inorg. Biochem.*, 2004, **98**, 1648-1654.
112. G. Sava, S. Zorzet, C. Turrin, F. Vita, M. Soranzo, G. Zabucchi, M. Cocchietto, A. Bergamo, S. DiGiovine, G. Pezzoni, L. Sartor and S. Garbisa, *Clin. Cancer Res.*, 2003, **9**, 1898.
113. A. Levina, A. Mitra and P. A. Lay, *Metallomics*, 2009, **1**, 458-470.
114. E. S. Antonarakis and A. Emadi, *Cancer Chemother. Pharmacol.*, 2010, **66**, 1-9.
115. C. G. Hartinger, S. Zorbas-Seifried, M. A. Jakupec, B. Kynast, H. Zorbas and B. K. Keppler, *J. Inorg. Biochem.*, 2006, **100**, 891-904.
116. C. G. Hartinger, M. A. Jakupec, S. Zorbas-Seifried, M. Groessl, A. Egger, W. Berger, H. Zorbas, P. J. Dyson and B. K. Keppler, *Chem. Biodivers.*, 2008, **5**, 2140-2155.
117. A. K. Bytzek, G. Koellensperger, B. K. Keppler and G. H. C, *J. Inorg. Biochem.*, 2016, **160**, 250-255.
118. S. Kapitza, M. A. Jakupec, M. Uhl, B. K. Keppler and B. Marian, *Cancer Lett.*, 2005, **226**, 115-121.
119. A. Levina, J. B. Aitken, Y. Y. Gwee, Z. J. Lim, M. Liu, A. M. Singharay, P. F. Wong and P. A. Lay, *Chem. Eur. J.* , 2013, **19**, 3609-3619.
120. M. J. Clarke, *Coord. Chem. Rev.*, 2002, **232**, 69-93.
121. G. Sava, S. Pacor, F. Bregant, V. Ceschia and G. Mestroni, *Anti-Cancer Drugs*, 1990, **1**, 99-108.
122. B. D. Palmer, W. R. Wilson, S. M. Pullen and W. A. Denny, *J. Med. Chem.*, 1990, **33**, 112-121.
123. J. L. Wike-Hooley, J. Haveman and H. S. Reinhold, *Radiother. Oncol.*, 1984, **2**, 343-366.
124. E. Reisner, V. B. Arion, B. K. Keppler and A. J. L. Pombeiro, *Inorg. Chim. Acta.*, 2008, **361**, 1569-1583.
125. M. J. Clarke, S. Bitler, D. Rennert, M. Buchbinder and A. D. Kelman, *J. Inorg. Biochem.*, 1980, **12**, 79-87.
126. A. Habtemariam, M. Melchart, R. Fernandez, S. Parsons, I. D. Oswald, A. Parkin, F. P. Fabbiani, J. E. Davidson, A. Dawson, R. E. Aird, D. I. Jodrell and P. J. Sadler, *J. Med. Chem.*, 2006, **49**, 6858-6868.
127. J. J. Soldevila-Barreda and P. J. Sadler, *Curr. Opin. Chem. Biol.*, 2015, **25**, 172-183.
128. Y. K. Yan, M. Melchart, A. Habtemariam and P. J. Sadler, *Chem. Commun.*, 2005, 4764-4776.
129. B. Therrien, *Coord. Chem. Rev.*, 2009, **253**, 493-519.
130. Y. N. V. Gopal, D. Jayaraju and A. K. Kondapi, *Biochemistry*, 1999, **38**, 4382-4388.
131. Y. N. Vashisht Gopal, N. Konuru and A. K. Kondapi, *Arch. Biochem. Biophys.*, 2002, **401**, 53-62.
132. D. S. Williams, G. E. Atilla, H. Bregman, A. Arzoumanian, P. S. Klein and E. Meggers, *Angew. Chem. Int. Ed.*, 2005, **44**, 1984-1987.
133. T. Bugarcic, O. Novakova, A. Halamikova, L. Zerzankova, O. Vrana, J. Kasparkova, A. Habtemariam, S. Parsons, P. J. Sadler and V. Brabec, *J. Med. Chem.*, 2008, **51**, 5310.
134. R. E. Aird, J. Cummings, A. A. Ritchie, M. Muir, R. E. Morris, H. Chen, P. J. Sadler and D. I. Jodrell, *Br. J. Cancer*, 2002, **86**, 1652-1657.

135. S. Grguric-Sipka, I. N. Stepanenko, J. M. Lazic, C. Bartel, M. A. Jakupec, V. B. Arion and B. K. Keppler, *Dalton Trans.*, 2009, **17**, 3334-3339.
136. F. Y. Wang, A. Habtemariam, E. P. L. van der Geer, R. Fernandez, M. Melchart, R. J. Deeth, R. Aird, S. Guichard, F. P. A. Fabbiani, P. Lozano-Casal, I. D. H. Oswald, D. I. Jodrell, S. Parsons and P. J. Sadler, *Proc. Natl. Acad. Sci. U.S.A.*, 2005, **102**, 18269.
137. A. Habtemariam, M. Melchart, R. Fernández, S. Parsons, I. D. H. Oswald, A. Parkin, F. P. A. Fabbiani, J. E. Davidson, A. Dawson, R. E. Aird, D. I. Jodrell and P. J. Sadler, *J. Med. Chem.*, 2006, **49**, 6858-6868.
138. S. J. Dougan and P. J. Sadler, *Chimia*, 2007, **61**, 704-715.
139. A. F. A. Peacock, A. Habtemariam, R. Fernández, V. Walland, F. P. A. Fabbiani, S. Parsons, R. E. Aird, D. I. Jodrell and P. J. Sadler, *J. Am. Chem. Soc.*, 2006, **128**, 1739-1748.
140. K. Ghebreyessus, A. Peralta, M. Katdare, K. Prabhakaran and S. Paranawithana, *Inorg. Chim. Acta.*, 2015, **434**, 239-251.
141. A. F. A. Peacock and P. J. Sadler, *Chem. Asian. J.*, 2008, **3**, 1890.
142. F. Wang, H. Chen, S. Parsons, I. D. Oswald, J. E. Davidson and P. J. Sadler, *Chem. Eur. J.*, 2003, **9**, 5810-5820.
143. O. Novakova, J. Kasparkova, V. Bursova, C. Hofr, M. Vojtiskova, H. Chen, P. J. Sadler and V. Brabec, *Chem. Biol.*, 2005, **12**, 121.
144. H. Chen, J. A. Parkinson, R. E. Morris and P. J. Sadler, *J. Am. Chem. Soc.*, 2003, **125**, 173.
145. H. Chen, J. A. Parkinson, S. Parsons, R. A. Coxall, R. O. Gould and P. J. Sadler, *J. Am. Chem. Soc.*, 2002, **124**, 3064.
146. A. Bergamo, A. Masi, A. F. Peacock, A. Habtemariam, P. J. Sadler and G. Sava, *J. Inorg. Biochem.*, 2010, **104**, 79-86.
147. C. Scolaro, A. Bergamo, L. Brescacin, R. Delfino, M. Cocchietto, G. Laurenczy, T. J. Geldbach, G. Sava and P. J. Dyson, *J. Med. Chem.*, 2005, **48**, 4161-4171.
148. P. Nowak-Sliwinska, J. R. van Beijnum, A. Casini, A. A. Nazarov, G. Wagnières, H. van den Bergh, P. J. Dyson and A. W. Griffioen, *J. Med. Chem.*, 2011, **54**, 3895-3902.
149. C. S. Allardyce, P. J. Dyson, D. J. Ellis and S. L. Heath, *Chem. Commun.*, 2001, 1396-1397.
150. A. K. Renfrew, A. D. Phillips, E. Tapavicza, R. Scopelliti, U. Rothlisberger and P. J. Dyson, *Organometallics*, 2009, **28**, 5061-5071.
151. A. Renfrew, *Chimia*, 2009, **63**, 217-219.
152. C. Gossens, A. Dorcier, P. J. Dyson and U. Rothlisberger, *Organometallics*, 2007, **26**, 3969-3975.
153. W. H. Ang, E. Daldini, C. Scolaro, R. Scopelliti, L. Juillerat-Jeannerat and P. J. Dyson, *Inorg. Chem.*, 2006, **45**, 9006-9013.
154. C. S. Allardyce, P. J. Dyson, D. J. Ellis, P. A. Salter and R. Scopelliti, *J. Organomet. Chem.*, 2003, **668**, 35-42.
155. B. S. Murray, M. V. Babak, C. G. Hartinger and P. J. Dyson, *Coord. Chem. Rev.*, 2016, **306**, 86-114.
156. M. V. Babak, S. M. Meier, K. V. M. Huber, J. Reynisson, A. A. Legin, M. A. Jakupec, A. Roller, A. Stukalov, M. Gridling, K. L. Bennett, J. Colinge, W. Berger, P. J. Dyson, G. Superti-Furga, B. K. Keppler and C. G. Hartinger, *Chem. Sci.*, 2015, **6**, 2449-2456.
157. M. Groessl, M. Terenghi, A. Casini, L. Elviri, R. Lobinski and P. J. Dyson, *J. Anal. At. Spectrom.*, 2010, **25**, 305-313.
158. C. Scolaro, T. J. Geldbach, S. Rochat, A. Dorcier, C. Gossens, A. Bergamo, M. Cocchietto, I. Tavernelli, G. Sava, U. Rothlisberger and P. J. Dyson, *Organometallics*, 2006, **25**, 756-765.

159. A. K. Renfrew, A. D. Phillips, A. E. Egger, C. G. Hartinger, S. S. Bosquain, A. A. Nazarov, B. K. Keppler, L. Gonsalvi, M. Peruzzini and P. J. Dyson, *Organometallics*, 2009, **28**, 1165-1172.
160. W. H. Ang, L. J. Parker, A. De Luca, L. Juillerat-Jeanneret, C. J. Morton, M. Lo Bello, M. W. Parker and P. J. Dyson, *Angew. Chem. Int. Ed. Engl.*, 2009, **48**, 3854-3857.
161. A. A. Nazarov, J. Risse, W. H. Ang, F. Schmitt, O. Zava, A. Ruggi, M. Groessl, R. Scopelitti, L. Juillerat-Jeanneret, C. G. Hartinger and P. J. Dyson, *Inorg. Chem.*, 2012, **51**, 3633-3639.
162. V. Ferretti, M. Fogagnolo, A. Marchi, L. Marvelli, F. Sforza and P. Bergamini, *Inorg. Chem.*, 2014, **53**, 4881-4890.
163. B. Serli, E. Zangrando, T. Gianferrara, C. Scolaro, P. J. Dyson, A. Bergamo and E. Alessio, *Eur. J. Inorg. Chem.*, 2005, **2005**, 3423-3434.
164. I. Bratsos, D. Urankar, E. Zangrando, P. Genova-Kalou, J. Kosmrlj, E. Alessio and I. Turel, *Dalton Trans.*, 2011, **40**, 5188-5199.
165. I. Bratsos, E. Mitri, F. Ravalico, E. Zangrando, T. Gianferrara, A. Bergamo and E. Alessio, *Dalton Trans.*, 2012, **41**, 7358-7371.
166. B. Greener, L. Cronin, G. D. Wilson and P. H. Walton, *J. Chem. Soc., Dalton Trans.*, 1996, 401-403.
167. B. Greener, M. H. Moore and P. H. Walton, *Chem. Commun.*, 1996, 27-28.
168. L. Cronin, S. P. Foxon, P. J. Lusby and P. H. Walton, *J. Biol. Inorg. Chem.*, 2001, **6**, 367-377.
169. L. Cronin and P. H. Walton, *Chem. Commun.*, 2003, 1572-1573.
170. B. Greener, S. P. Foxon and P. H. Walton, *New J. Chem.*, 2000, **24**, 269-273.
171. G. Park, F. H. Lu, N. Ye, M. W. Brechbiel, S. V. Torti, F. M. Torti and R. P. Planalp, *J. Biol. Inorg. Chem.*, 1998, **3**, 449-457.
172. R. Zhao, R. P. Planalp, R. Ma, B. T. Greene, B. T. Jones, M. W. Brechbiel, F. M. Torti and S. V. Torti, *Biochem. Pharmacol.*, 2004, **67**, 1677-1688.
173. M. L. Childers, F. Su, A. M. Przyborowska, B. Bishwokarma, G. Park, M. W. Brechbiel, S. V. Torti, F. M. Torti, G. Broker, J. S. Alexander, R. D. Rogers, K. Ruhlandt-Senge and R. P. Planalp, *Eur. J. Inorg. Chem.*, 2005, **2005**, 3971-3982.
174. S. V. Torti, F. M. Torti, S. R. Whitman, M. W. Brechbiel, G. Park and R. P. Planalp, *Blood*, 1998, **92**, 1384-1389.
175. G. Park, A. M. Przyborowska, N. Ye, N. M. Tsoupas, C. B. Bauer, G. A. Broker, R. D. Rogers, M. W. Brechbiel and R. P. Planalp, *Dalton Trans.*, 2003, 318-324.
176. M. R. Wilson, *Biochem. Cell Biol.*, 1998, **76**, 573-582.
177. B. T. Greene, J. Thorburn, M. C. Willingham, A. Thorburn, R. P. Planalp, M. W. Brechbiel, J. Jennings-Gee, J. t. Wilkinson, F. M. Torti and S. V. Torti, *J. Biol. Chem.*, 2002, **277**, 25568-25575.
178. L. Ciano, PhD Thesis, University of York, 2013.
179. A. Gamble, PhD Thesis, University of York, 2012.
180. A. J. Gamble, J. M. Lynam, R. J. Thatcher, P. H. Walton and A. C. Whitwood, *Inorg. Chem.*, 2013, **52**, 4517-4527.
181. E. Rotondo, R. Pietropaolo, G. Tresoldi, F. Faraone and F. Cusmano, *Inorg. Chim. Acta.*, 1976, **17**, 181-191.
182. H. Schiff, *Justus Liebigs Ann. Chem.*, 1864, **131**, 118-119.
183. E. Rotondo, R. Pietropaolo and F. Cusmano, *Inorg. Chim. Acta.*, 1978, **26**, 189-196.
184. H. Naeimi, J. Safari and A. Heidarnezhad, *Dyes Pigm.*, 2007, **73**, 251-253.
185. C. M. da Silva, D. L. da Silva, L. V. Modolo, R. B. Alves, M. A. de Resende, C. V. B. Martins and Â. de Fátima, *J. Adv. Res.*, 2011, **2**, 1-8.

186. A. Xavier and N. Srividhya, *J. Appl. Chem.*, 2014, **7**, 06-15.
187. E. H. Cordes and W. P. Jencks, *J. Am. Chem. Soc.*, 1963, **85**, 2843-2848.
188. E. Rotondo and F. C. Priolo, *J. Chem. Soc., Dalton Trans.*, 1982, 1825-1828.
189. H. Chen and J. Rhodes, *J. Mol. Med.*, 1996, **74**, 497-504.
190. K. C. Gupta and A. K. Sutar, *Coord. Chem. Rev.*, 2008, **252**, 1420-1450.
191. N. Rabjohn, *J. Pharm. Sci.*, 1964, **53**, 345.
192. Y. Zheng, K. Ma, H. Li, J. Li, J. He, X. Sun, R. Li and J. Ma, *Catal. Lett.*, 2009, **128**, 465-474.
193. F. H. Westheimer and K. Taguchi, *J. Org. Chem.*, 1971, **36**, 1570-1572.
194. C. Chandramouli, M. R. Shivanand, T. B. Nayanbhai, B. Bheemachari and R. H. Udupi, *J. Chem. Pharm. Res.*, 2012, **4**, 1151-1159.
195. S. M. Sondhi, N. Singh, A. Kumar, O. Lozach and L. Meijer, *Bioorg. Med. Chem.*, 2006, **14**, 3758-3765.
196. B. S. Sathe, E. Jaychandran, V. A. Jagtap and G. M. Sreenivasa, *Int. J. Pharm. Res. Dev.*, 2011, **3**, 164-169.
197. P. Venkatesh, *Asian J. Pharm. Hea. Sci.*, 2011, **1**, 8-11.
198. S. M. M. Ali, M. A. K. Azad, M. Jesmin, S. Ahsan, M. M. Rahman, J. A. Khanam, M. N. Islam and S. M. S. Shahriar, *Asian Pac. J. Trop. Biomed.*, 2012, **2**, 438-442.
199. R. Miri, N. Razzaghi-asl and M. K. Mohammadi, *J. Mol. Model.*, 2013, **19**, 727-735.
200. K. S. Kumar, S. Ganguly, R. Veerasamy and E. De Clercq, *Eur. J. Med. Chem.*, 2010, **45**, 5474-5479.
201. D. Wei, N. Li, G. Lu and K. Yao, *Sci. China Chem.*, 2006, **49**, 225-229.
202. L. Blackburn and R. J. K. Taylor, *Org. Lett.*, 2001, **3**, 1637-1639.
203. P. Purushottamachar, A. Khandelwal, T. S. Vasaitis, R. D. Bruno, L. K. Gediya and V. C. O. Njar, *Bioorg. Med. Chem.*, 2008, **16**, 3519-3529.
204. H. Li, P. Williams, J. Micklefield, J. M. Gardiner and G. Stephens, *Tetrahedron*, 2004, **60**, 753-758.
205. R. N. Castle, D. L. Aldous and M. Hall, *J. Am. Pharm. Assoc.*, 1953, **42**, 435-436.
206. J. H. Billman and A. C. Diesing, *J. Org. Chem.*, 1957, **22**, 1068-1070.
207. Y. H. Yang, S. X. Liu, J. Z. Li, X. Tian, X. L. Zhen and J. R. Han, *Synth. Commun.*, 2012, **42**, 2540-2554.
208. N. P. E. Barry and P. J. Sadler, *Chem. Commun.*, 2013, **49**, 5106-5131.
209. A. K. Nairn, S. J. Archibald, R. Bhalla, C. J. Boxwell, A. C. Whitwood and P. H. Walton, *Dalton Trans.*, 2006, 1790-1795.
210. R. Taylor, O. Kennard and W. Versichel, *J. Am. Chem. Soc.*, 1983, **105**, 5761-5766.
211. C. Bissantz, B. Kuhn and M. Stahl, *J. Med. Chem.*, 2010, **53**, 5061-5084.
212. I. Turel, *Molecules*, 2015, **20**, 1420-3049.
213. S. Tabassum, M. Zaki, F. Arjmand and I. Ahmad, *J. Photochem. Photobiol. B.*, 2012, **114**, 108-118.
214. K. Arora, A. Gupta and D. D. Agrawal, *Asian J. Chem.*, 2002, **14**, 1611.
215. W. Cai and X. Chen, *Nat. Protoc.*, 2008, **3**, 89-96.
216. P. C. A. Bruijnincx and P. J. Sadler, *Curr. Opin. Chem. Biol.*, 2008, **12**, 197.
217. S. M. Cohen, *Curr. Opin. Chem. Biol.*, 2007, **11**, 115-120.
218. C. Orvig and M. J. Abrams, *Chem. Rev.*, 1999, **99**, 2201-2204.
219. K. L. Haas and K. J. Franz, *Chem. Rev.*, 2009, **109**, 4921-4960.
220. P. C. Hydes and M. J. H. Russell, *Cancer Metastasis Rev.*, 1988, **7**, 67-89.
221. C. X. Zhang and S. J. Lippard, *Curr. Opin. Chem. Biol.*, 2003, **7**, 481-489.
222. M. A. Jakupec, M. Galanski, V. B. Arion, C. G. Hartinger and B. K. Keppler, *Dalton Trans*, 2008, 183-194.

223. G. Zhao and H. Lin, *Curr. Med. Chem.* , 2005, **5**, 137-147.
224. A. Bergamo, M. Cocchietto, I. Capozzi, G. Mestroni, E. Alessio and G. Sava, *Anti-Cancer Drugs*, 1996, **7**, 697-702.
225. R. Sáez, J. Lorenzo, M. J. Prieto, M. Font-Bardia, T. Calvet, N. Omeñaca, M. Vilaseca and V. Moreno, *J. Inorg. Biochem.*, 2014, **136**, 1-12.
226. C. A. McAuliffe and A. G. Mackie, *P-donor ligands IN Encyclpedia of Inorganic Chemistry*, 1994.
227. R. K. Johnson, C. K. Mirabelli, L. F. Faucette, F. L. McCabe, B. M. Sutton, D. L. Bryan, G. R. Girard and D. T. Hill, *Amer. Assoc. Cancer Res.*, 1985, **26**, 254-254.
228. C. K. Mirabelli, D. T. Hill, L. F. Faucette, F. L. McCabe, G. R. Girard, D. B. Bryan, B. M. Sutton, J. O. L. Barus, S. T. Crooke and R. K. Johnson, *J. Med. Chem.*, 1987, **30**, 2181-2190.
229. J. M. Walker, A. McEwan, R. Pycko, M. L. Tassotto, C. Gottardo, J. Th'ng, R. Wang and G. J. Spivak, *Eur. J. Inorg. Chem.*, 2009, **2009**, 4629-4633.
230. P. Kumar, R. K. Gupta and D. S. Pandey, *Chem. Soc. Rev.*, 2014, **43**, 707-733.
231. F. Aman, M. Hanif, W. A. Siddiqui, A. Ashraf, L. K. Filak, J. Reynisson, T. Söhnel, S. M. F. Jamieson and C. G. Hartinger, *Organometallics*, 2014, **33**, 5546-5553.
232. S. Doherty, J. G. Knight, R. K. Rath, W. Clegg, R. W. Harrington, C. R. Newman, R. Campbell and H. Amin, *Organometallics*, 2005, **24**, 2633-2644.
233. S. Das, S. Sinha, R. Britto, K. Somasundaram and A. G. Samuelson, *J. Inorg. Biochem.*, 2010, **104**, 93-104.
234. B. A. V. Lima, R. S. Corrêa, A. E. Graminha, A. Kuznetsov, J. Ellena, F. R. Pavan, C. Q. F. Leite and A. A. Batista, *J. Braz. Chem. Soc.*, 2016, **27**, 30-40.
235. G. Sava, S. Zorzet, T. Giraldi, G. Mestroni and G. Zassinovich, *Eur. J. Cancer Clin. Oncol.*, 1984, **20**, 841-847.
236. R. D. Ernst, R. Basta and A. M. Arif, *Z. Kristallogr.*, 2003, **218**, 49-51.
237. M. L. Man, J. Zhu, S. M. Ng, Z. Zhou, C. Yin, Z. Lin and C. P. Lau, *Organometallics*, 2004, **23**, 6214-6220.
238. I. P. Evans, A. Spencer and G. Wilkinson, *J. Chem. Soc., Dalton Trans.*, 1973, 204-209.
239. B. P. Hudson, C. M. Dupureur and J. K. Barton, *J. Am. Chem. Soc.*, 1995, **117**, 9379.
240. S. L. Queiroz, M. P. de Araujo, A. A. Batista, K. S. MacFarlane and B. R. James, *J. Chem. Educ.*, 2001, **78**, 87.
241. A. E. Friedman, J. C. Chambron, J. P. Sauvage, N. J. Turro and J. K. Barton, *J. Am. Chem. Soc.*, 1990, **112**, 4960-4962.
242. J. P. Hall, K. O'Sullivan, A. Naseer, J. A. Smith, J. M. Kelly and C. J. Cardin, *Proc. Natl. Acad. Sci. U.S.A.*, 2011, **108**, 17610-17614.
243. A. C. Komor and J. K. Barton, *Chem. Comm.*, 2013, **49**, 3617-3630.
244. P. B. Dervan, *Bioorg. Med. Chem.*, 2001, **9**, 2215-2235.
245. P. L. Hamilton and D. P. Arya, *Nat. Prod. Rep.*, 2012, **29**, 134-143.
246. I. Greguric, J. R. Aldrich-Wright and J. G. Collins, *J. Am. Chem. Soc.*, 1997, **119**, 3621-3622.
247. W. Bauer and J. Vinograd, *J. Mol. Biol.*, 1970, **54**, 281.
248. L. S. Lerman, *J. Mol. Biol.*, 1961, **3**, 18.
249. J. K. Barton, A. Danishefsky and J. Goldberg, *J. Am. Chem. Soc.*, 1984, **106**, 2172-2176.
250. H.-K. Liu and P. J. Sadler, *Acc. Chem. Res.*, 2011, **44**, 349-359.
251. C. V. Kumar, J. K. Barton and N. J. Turro, *J. Am. Chem. Soc.*, 1985, **107**, 5518.
252. J. K. Barton, *J. Biomol. Struct. Dyn.*, 1983, **1**, 621-632.
253. B. C. Poulsen, S. Estalayo-Adrian, S. Blasco, S. A. Bright, J. M. Kelly, D. C. Williams and T. Gunnlaugsson, *Dalton Trans.*, 2016, **45**, 18208-18220.

254. F. E. Poynton, J. P. Hall, P. M. Keane, C. Schwarz, I. V. Sazanovich, M. Towrie, T. Gunnlaugsson, C. J. Cardin, D. J. Cardin, S. J. Quinn, C. Long and J. M. Kelly, *Chem. Sci.*, 2016, **7**, 3075-3084.
255. C. G. Coates, J. J. McGarvey, P. L. Callaghan, M. Coletti and J. G. Hamilton, *J. Phys. Chem. B*, 2001, **105**, 730-735.
256. P. Kaspler, S. Lazic, S. Forward, Y. Arenas, A. Mandel and L. Lilge, *Photochem. Photobiol. Sci.*, 2016, **15**, 481-495.
257. Y. Chen, W. Lei, G. Jiang, Q. Zhou, Y. Hou, C. Li, B. Zhang and X. Wang, *Dalton Trans.*, 2013, **42**, 5924-5931.
258. B. P. Espósito and R. Najjar, *Coord. Chem. Rev.*, 2002, **232**, 137-149.
259. I. N. Stepanenko, A. Casini, F. Edafe, M. S. Novak, V. B. Arion, P. J. Dyson, M. A. Jakupec and B. K. Keppler, *Inorg. Chem.*, 2011, **50**, 12669-12679.
260. D. C. Carter and J. X. Ho, *Adv. Protein Chem.*, 1994, **45**, 153-203.
261. P. Qin, R. Liu, X. Pan, X. Fang and Y. Mou, *J. Agric. Food Chem.*, 2010, **58**, 5561-5567.
262. L. Messori, P. Orioli, D. Vullo, E. Alessio and E. Iengo, *Eur. J. Biochem.*, 2000, **267**, 1206-1213.
263. F. Piccioli, S. Sabatini, L. Messori, P. Orioli, C. G. Hartinger and B. K. Keppler, *J. Inorg. Biochem.*, 2004, **98**, 1135-1142.
264. A. R. Timerbaev, C. G. Hartinger, S. S. Aleksenko and B. K. Keppler, *Chem. Rev.*, 2006, **106**, 2224-2248.
265. I. Ascone, L. Messori, A. Casini, C. Gabbiani, A. Balerna, F. Dell'Unto and A. C. Castellano, *Inorg. Chem.*, 2008, **47**, 8629-8634.
266. J. Du, E. Zhang, Y. Zhao, W. Zheng, Y. Zhang, Y. Lin, Z. Wang, Q. Luo, K. Wu and F. Wang, *Metallomics*, 2015, **7**, 1573-1583.
267. C. T. Dollery, *Clin. Pharmacol. Ther.*, 2013, **93**, 263-266.
268. O. Zava, S. M. Zakeeruddin, C. Danelon, H. Vogel, M. Grätzel and P. J. Dyson, *Chem. Bio. Chem.*, 2009, **10**, 1796-1800.
269. B.-Z. Zhu, X.-J. Chao, C.-H. Huang and Y. Li, *Chem. Sci.*, 2016, **7**, 4016-4023.
270. J. D. White, M. M. Haley and V. J. DeRose, *Acc. Chem. Res.*, 2016, **49**, 56-66.
271. E. J. New, C. Roche, R. Madawala, J. Z. Zhang and T. W. Hambley, *J. Inorg. Biochem.*, 2009, **103**, 1120-1125.
272. A. A. Soliman, M. A. Amin, A. A. El-Sherif, C. Sahin and C. Varlikli, *Arabian J. Chem.*, 2017, **10**, 389-397.
273. C. Klein, M. K. Nazeeruddin, D. Di Censo, P. Liska and M. Grätzel, *Inorg. Chem.*, 2004, **43**, 4216-4226.
274. J. P. Sauvage, J. P. Collin, J. C. Chambron, S. Guillerez, C. Coudret, V. Balzani, F. Barigelletti, L. De Cola and L. Flamigni, *Chem. Rev.*, 1994, **94**, 993-1019.
275. W. F. Wacholtz, R. A. Auerbach and R. H. Schmehl, *Inorg. Chem.*, 1986, **25**, 227-234.
276. M. K. Nazeeruddin, A. Kay, I. Rodicio, R. Humphry-Baker, E. Müller, P. Liska, N. Vlachopoulos and M. Grätzel, *J. Am. Chem. Soc.*, 1993, **115**, 6382-6390.
277. A. Lewandowska-Andralojc and D. E. Polyansky, *J. Phys. Chem. A*, 2013, **117**, 10311-10319.
278. A. M. Brouwer, *Pure Appl. Chem.*, 2011, **83**, 2213-2228.
279. C. Wurth, M. G. Gonzalez, R. Niessner, U. Panne, C. Haisch and U. R. Genger, *Talanta.*, 2012, **90**, 30-37.
280. A. T. R. Williams, S. A. Winfield and J. N. Miller, *Analyst*, 1983, **108**, 1067-1071.
281. K. Rurack, in *Standardization and Quality Assurance in Fluorescence Measurements I: Techniques*, ed. U. Resch-Genger, Springer Berlin Heidelberg, Berlin, Heidelberg, 2008, pp. 101-145.

282. R. H. Fish and G. Jaouen, *Organometallics*, 2003, **22**, 2166-2177.
283. C. V. Kumar and E. H. Asuncion, *J. Am. Chem. Soc.*, 1993, **115**, 8547-8553.
284. T. Topala, A. Bodoki, L. Oprean and R. Oprean, *Farmacia*, 2014, **62**, 1049-1061.
285. M. Ganeshpandian, R. Loganathan, E. Suresh, A. Riyasdeen, M. A. Akbarsha and M. Palaniandavar, *Dalton Trans.*, 2014, **43**, 1203-1219.
286. S. Sathiyaraj, R. J. Butcher and C. Jayabalakrishnan, *J. Mol. Struct.*, 2012, **1030**, 95-103.
287. P. Kumar, S. Gorai, M. K. Santra, B. Mondal and D. Manna, *Dalton Trans.*, 2012, **41**, 7573-7581.
288. M. Sirajuddin, S. Ali and A. Badshah, *J. Photochem. Photobiol. B, Biol.*, 2013, **124**, 1-19.
289. C. S. Devi, D. A. Kumar, S. S. Singh, N. Gabra, N. Deepika, Y. P. Kumar and S. Satyanarayana, *Eur. J. Med. Chem.*, 2013, **64**, 410-421.
290. J. G. Liu, B. H. Ye, H. Li, L. N. Ji, R. H. Li and J. Y. Zhou, *J. Inorg. Biochem.*, 1999, **73**, 117-122.
291. M. Mudasir, N. Yoshioka and H. Inoue, *J. Inorg. Biochem.*, 1999, **77**, 239-247.
292. A. Wolfe, G. H. Shimer and T. Meehan, *Biochemistry*, 1987, **26**, 6392-6396.
293. A. Srishailam, N. M. Gabra, Y. P. Kumar, K. L. Reddy, C. S. Devi, D. A. Kumar, S. S. Singh and S. Satyanarayana, *J. Photochem. Photobiol. B.*, 2014, **141**, 47-58.
294. A. E. Friedman, C. V. Kumar, N. J. Turro and J. K. Barton, *Nucleic Acids Res.*, 1991, **19**, 2595-2602.
295. P. Karacan and O. Okay, *React. Funct. Polym.*, 2013, **73**, 442-450.
296. K. G. Strothkamp and R. E. Strothkamp, *J. Chem. Edu.*, 1994, **71**, 77-79.
297. J. Zhao, W. Li, R. Ma, S. Chen, S. Ren and T. Jiang, *Int. J. Mol. Sci.*, 2013, **14**, 16851-16865.
298. P. Krishnamoorthy, P. Sathyadevi, A. H. Cowley, R. R. Butorac and N. Dharmaraj, *Eur. J. Med. Chem.*, 2011, **46**, 3376-3387.
299. H. Xu, K.-C. Zheng, H. Deng, L.-J. Lin, Q.-L. Zhang and L.-N. Ji, *New J. Chem.*, 2003, **27**, 1255-1263.
300. C. Mari, V. Pierroz, S. Ferrari and G. Gasser, *Chem. Sci.*, 2015, **6**, 2660-2686.
301. A. Srishailam, N. M. Gabra, Y. P. Kumar, K. L. Reddy, C. S. Devi, D. A. Kumar, S. S. Singh and S. Satyanarayana, *J. Photochem. Photobiol. B, Biol.*, 2014, **141**, 47-58.
302. S. Mukhopadhyay, R. K. Gupta, R. P. Paitandi, N. K. Rana, G. Sharma, B. Koch, L. K. Rana, M. S. Hundal and D. S. Pandey, *Organometallics*, 2015, **34**, 4491-4506.
303. D. S. Raja, N. S. P. Bhuvanesh and K. Natarajan, *Eur. J. Med. Chem.*, 2011, **46**, 4584-4594.
304. D. S. Raja, G. Paramaguru, N. S. P. Bhuvanesh, J. H. Reibenspies, R. Renganathan and K. Natarajan, *Dalton Trans.*, 2011, **40**, 4548-4559.
305. R. K. Gupta, A. Kumar, R. P. Paitandi, R. S. Singh, S. Mukhopadhyay, S. P. Verma, P. Das and D. S. Pandey, *Dalton Trans.*, 2016, **45**, 7163-7177.
306. D. S. Raja, N. S. P. Bhuvanesh and K. Natarajan, *Dalton Trans.*, 2012, **41**, 4365-4377.
307. C. V. Dang, R. F. Ebert and W. R. Bell, *J. Biol. Chem.*, 1985, **260**, 9713-9719.
308. T. TopalĂ, A. Bodoki, L. Oprean and R. Oprean, *Clujul Med.*, 2014, **87**, 215-219.
309. M. Ehteshami, F. Rasoulzadeh, S. Mahboob and M. R. Rashidi, *J. Lumin.*, 2013, **135**, 164-169.
310. A. Ray, B. K. Seth, U. Pal and S. Basu, *Spectrochim. Acta Mol. Biomol. Spectrosc.*, 2012, **92**, 164-174.
311. A. Belatik, S. Hotchandani, R. Carpentier and H.-A. Tajmir-Riahi, *PLoS ONE*, 2012, **7**, 36723.
312. M. R. Eftink and C. A. Ghiron, *Anal. Biochem.*, 1981, **114**, 199-227.

313. F. Samari, B. Hemmateenejad, M. Shamsipur, M. Rashidi and H. Samouei, *Inorg. Chem.*, 2012, **51**, 3454-3464.
314. Y. L. Xiang and F. Y. Wu, *Spectrochim. Acta Mol. Biomol. Spectrosc.*, 2010, **77**, 430-436.
315. L. Q. Shen, Z. F. Yang and R. R. Tang, *Spectrochim. Acta Mol. Biomol. Spectrosc.*, 2012, **98**, 170-177.
316. M. R. Eftink and C. A. Ghiron, *J. Phys. Chem.*, 1976, **80**, 486-493.
317. T. Boulikas and M. Vougiouka, *Oncol. Rep.*, 2003, **10**, 1663-1682.
318. P. Kay, *Semin. Oncol. Nurs.*, 2006, **22**, 1-4.
319. V. Abet, F. Filace, J. Recio, J. Alvarez-Builla and C. Burgos, *Eur. J. Med. Chem.*, 2017, **127**, 810-827.
320. M. A. Lesniewska-Kowiel and I. Muszalska, *Eur. J. Med. Chem.*, 2017, **129**, 53-71.
321. J. B. Patrick and S. M. a. P. J. S. Fiona, *Anti-Cancer Agents Med. Chem.*, 2007, **7**, 75-93.
322. U. Schatzschneider, *Eur. J. Inorg. Chem.*, 2010, 1451-1467.
323. N. A. Smith and P. J. Sadler, *Phil. Trans. R. Soc. A*, 2013, **371**.
324. D. E. J. G. J. Dolmans, D. Fukumura and R. K. Jain, *Nat. Rev. Cancer.*, 2003, **3**, 380-387.
325. E. C. Glazer, *Isr. J. Chem.*, 2013, **53**, 391-400.
326. G. M. F. Calixto, J. Bernegossi, L. M. de Freitas, C. R. Fontana and M. Chorilli, *Molecules*, 2016, **21**.
327. C. Mari and G. Gasser, *Chimia*, 2015, **69**, 176-181.
328. A. P. Castano, T. N. Demidova and M. R. Hamblin, *Photodiagnosis Photodyn. Ther.*, 2004, **1**, 279-293.
329. J. Moan and K. Berg, *Photochem. Photobiol.*, 1991, **53**, 549-553.
330. K. Plaetzer, B. Krammer, J. Berlanda, F. Berr and T. Kiesslich, *Lasers Med. Sci.*, 2009, **24**, 259-268.
331. M. Ethirajan, Y. Chen, P. Joshi and R. K. Pandey, *Chem. Soc. Rev.*, 2011, **40**, 340-362.
332. P. M. Antoni, A. Naik, I. Albert, R. Rubbiani, S. Gupta, P. Ruiz-Sanchez, P. Munikorn, J. M. Mateos, V. Luginbuehl, P. Thamyongkit, U. Ziegler, G. Gasser, G. Jeschke and B. Spingler, *Chem. Eur. J.*, 2015, **21**, 1179-1183.
333. A. Leonidova, V. Pierroz, R. Rubbiani, Y. J. Lan, A. G. Schmitz, A. Kaech, R. K. O. Sigel, S. Ferrari and G. Gasser, *Chem. Sci.*, 2014, **5**, 4044-4056.
334. M. R. Gill, J. Garcia-Lara, S. J. Foster, C. Smythe, G. Battaglia and J. A. Thomas, *Nat. Chem.*, 2009, **1**, 662-667.
335. M. R. Gill, H. Derrat, C. G. W. Smythe, G. Battaglia and J. A. Thomas, *Chem. Bio. Chem.*, 2011, **12**, 877-880.
336. S. P. Foxon, C. Green, M. G. Walker, A. Wragg, H. Adams, J. A. Weinstein, S. C. Parker, A. J. H. M. Meijer and J. A. Thomas, *Inorg. Chem.*, 2012, **51**, 463-471.
337. H. J. Yu, S. M. Huang, L. Y. Li, H. N. Jia, H. Chao, Z. W. Mao, J. Z. Liu and L. N. Ji, *J. Inorg. Biochem.*, 2009, **103**, 881-890.
338. S. Bonnet, *Comments Inorg. Chem.*, 2015, **35**, 179-213.
339. B. S. Howerton, D. K. Heidary and E. C. Glazer, *J. Am. Chem. Soc.*, 2012, **134**, 8324-8327.
340. W. Vanderlinden, M. Blunt, C. C. David, C. Moucheron, A. Kirsch-De Mesmaeker and S. De Feyter, *J. Am. Chem. Soc.*, 2012, **134**, 10214-10221.
341. Y. Chen, W. Lei, G. Jiang, Y. Hou, C. Li, B. Zhang, Q. Zhou and X. Wang, *Dalton Trans.*, 2014, **43**, 15375-15384.
342. L. D. Mayer and A. S. Janoff, *Mol. Interventions*, 2007, **7**, 216-223.
343. T. Mosmann, *J. Immunol. Methods*, 1983, **65**, 55-63.
344. D. Gerlier and N. Thomasset, *J. Immunol. Methods*, 1986, **94**, 57-63.
345. D. A. Scudiero, R. H. Shoemaker, K. D. Paull, A. Monks, S. Tierney, T. H. Nofziger, M. J. Currens, D. Seniff and M. R. Boyd, *Cancer Res.*, 1988, **48**, 4827-4833.

346. R. F. Hussain, A. M. E. Nouri and R. T. D. Oliver, *J. Immunol. Methods*, 1993, **160**, 89-96.
347. L. Sliwka, K. Wiktorska, P. Suchocki, M. Milczarek, S. Mielczarek, K. Lubelska, T. Cierpial, P. Lyzwa, P. Kielbasinski, A. Jaromin, A. Flis and Z. Chilmonczyk, *Plos One*, 2016, **11**.
348. J. Carmichael, W. G. Degraff, A. F. Gazdar, J. D. Minna and J. B. Mitchell, *Cancer Res.*, 1987, **47**, 936-942.
349. J. L. Sebaugh, *Pharm. Stat.*, 2011, **10**, 128-134.
350. N. Ganot, S. Meker, L. Reytman, A. Tzubery and E. Y. Tshuva, *J. Vis. Exp.*, 2013.
351. K. S. Lovejoy and S. J. Lippard, *Dalton Trans.*, 2009, 10651-10659.
352. T. C. Johnstone, G. Y. Park and S. J. Lippard, *Anticancer Res.*, 2014, **34**, 471-476.
353. S. H. van Rijt, A. Mukherjee, A. M. Pizarro and P. J. Sadler, *J. Med. Chem.*, 2010, **53**, 840.
354. C. Scolaro, A. B. Chaplin, C. G. Hartinger, A. Bergamo, M. Cocchietto, B. K. Keppler, G. Sava and P. J. Dyson, *Dalton Trans.*, 2007, 5065-5072.
355. A. Casini, C. Gabbiani, F. Sorrentino, M. P. Rigobello, A. Bindoli, T. J. Geldbach, A. Marrone, N. Re, C. G. Hartinger, P. J. Dyson and L. Messori, *J. Med. Chem.*, 2008, **51**, 6773-6781.
356. P. Liu, B.-Y. Wu, J. Liu, Y.-C. Dai, Y.-J. Wang and K.-Z. Wang, *Inorg. Chem.*, 2016, **55**, 1412-1422.
357. T. Bowen, R. P. Planalp and M. W. Brechbiel, *Bioorg. Med. Chem. Lett.*, 1996, **6**, 807-810.
358. P. S. Hallman, T. A. Stephenson and G. Wilkinson, in *Inorganic Syntheses*, John Wiley & Sons, Inc., 1970, pp. 237-240.
359. C. Würth, M. Grabolle, J. Pauli, M. Spieles and U. Resch-Genger, *Anal. Chem.*, 2011, **83**, 3431-3439.
360. J. Marmur, *J. Mol. Biol.*, 1961, **3**, 208-218.